Investigating the role of *HDAC4* in *Drosophila* neuronal function

A thesis presented in partial fulfilment of the requirements for the degree of

Doctor of Philosophy (PhD)

in

Genetics

At Massey University, Manawatū, New Zealand

Wei Jun Tan

2022

ABSTRACT

HDAC4 plays an essential role in brain functions including neurodevelopment and memory formation, and increased levels of HDAC4 have also been associated with neurodegenerative disorders including Alzheimer's disease.

Histone deacetylases are enzymes that are traditionally known to regulate gene expression in the nucleus, however in neurons, HDAC4 shuttles between the nucleus and cytoplasm with a predominant distribution in the cytoplasm. Although studies have identified potential differences in subcellular function in which accumulation of nuclear HDAC4 has been shown to promote neurodegeneration, while cytoplasmic HDAC4 is neuroprotective, the mechanistic pathways through which it acts are still unknown. Therefore, this project aimed to determine the importance of nuclear and cytoplasmic pools of HDAC4 to the neurological functions of *Drosophila melanogaster*, as well as to determine the domains within the protein that are required for its function(s). This was carried out by expressing HDAC4 with mutations that resulted in altered subcellular distribution or carrying mutations in binding domain/motifs that have previously been shown to be important for HDAC4 function.

Increased expression of wild-type HDAC4 disrupted development of the retina and the mushroom body (MB, a brain structure derived from Kenyon cells which are crucial for learning and memory), and expression of each mutant revealed the importance of specific domains/motifs to HDAC4 function in these tissues. Of interest, impairments to MB formation were exacerbated by mutation of the ankyrin-binding site and by mutation of serine residues that promote nuclear exit when phosphorylated (i.e. resulting in restriction to the nucleus). Mutation of the MEF2-binding site ameliorated these phenotypes, suggesting that HDAC4 acts through MEF2 to regulate MB development. However, while deacetylase activity was found to be dispensable in the MB, an active deacetylase domain was required in order for the phenotype to manifest in the retina, and mutation of the MEF2-binding site had no impact on the deficits caused by nuclear restriction of HDAC4 and mutation of the ankyrin-binding domain. Together these data indicate that HDAC4 acts through varying mechanism(s) depending on the cell type.

Transcriptional changes in the *Drosophila* brain resulting from the expression of *HDAC4* or its mutant variants was also explored using RNA-Seq. However only wild-type *HDAC4* resulted in a large number of differentially expressed genes and the low level of differential gene expression in *HDAC4* variants suggests that non-transcriptional processes may be involved in the induction of phenotypes caused by expression of these mutants. Additionally, further analysis of genes that were differentially regulated revealed a number of processes related to mitochondrial energy production. These findings have provided new insights into the role of HDAC4 in *Drosophila* neurodevelopment which opens up additional research avenues to focus on in the future.

ACKNOWLEDGMENTS

Doing my PhD amidst a worldwide pandemic has been one that is full of self-discovery. Having been away from my home country for almost nine years, I have always thought I was never one to easily say that I miss home. However, it takes a pandemic to make me realise how much I have always taken things for granted. The travel restriction which prevented us or loved ones from visiting each other hits me harder than I thought and has definitely affected my focus at some point. Thankfully, I was fortunate enough to have the support and guidance of my primary supervisor, Dr Helen Fitzsimons. Her patience has really made me understand and appreciate the importance of having a supervisor being awesome at supervising. Aside from having to juggle teaching, supervising other students, writing manuscripts, and buried under tons other miscellaneous work, she has always managed to provide equal attention to everyone, and her words of encouragement have definitely helped me in my progress. Her depth of knowledge of the field is also inspiring and makes me want to do better for myself.

Other people who have aided me in this endeavour includes my co-supervisors, Dr Tracy Hale and Associate Professor Andrew Sutherland-Smith. Although we did not have much discussion in the later phase of my PhD, their inputs during my first year have been invaluable to my subsequent planning and direction. I would also like to thank the current and ex-members of our Neurogenetic Research Group, Sarah Wilson, Hannah Hawley, Andy Li, Ana Claasen, Madeleine Palmer and Dr Patrick Main, for their questions and suggestions regarding my experimental results. A thank you also goes out to the members of the biomedical lab groups that attended my presentations during our weekly lab meetings. Their questions have occasionally provided a fresh perspective in which we occasionally need for thinking out of the box.

I would also like to express my gratitude to Dr Matthew Savoian and Raoul Solomon of the Manawatu Microscopy and Imaging Centre (MMIC), without their role in maintaining the facility and training me for the usage of confocal microscopy and scanning electron microscopy, it would not have been possible to generate the majority of the data for this project.

To my Mom, Sofia Surya Sindhu, and Dad, Tan Chwee Seng, I would like to thank them for always supporting me on the things I pursue and also having provided for me during

my early years of education which has been essential to lead up to this stage. To my sister, Tan Wei Wei, although I do not express it, I am always grateful for her support and also being there for me to lend a listening ear or coming to me for one.

Lastly to my girlfriend Sarah Lew, our daily communication (thank you Skype) has been an important source of mental support for me to get through the day during this journey and I am looking forward to us reuniting once again.

This project was funded by the Royal Society of New Zealand Marsden Fund.

TABLE OF CONTENTS

LIST OF FIGURES

LIST OF TABLES

LIST OF SUPPLEMENTARY FIGURES

LIST OF SUPPLEMENTARY TABLES

LIST OF ABBREVIATIONS

3A	Mutations of three serine residues to alanine (nuclear-restricted)
AC	Adenyl cyclase
AD	Activating domain
ALH	After larval hatching
ALS	Amyotrophic lateral sclerosis
Ank1	Ankyrin 1
Ank2	Ankyrin 2
Ank3	Ankyrin 3
ANKRA2	Ankyrin repeat family A protein 2
APF	After puparium formation
BDMR	Brachydactyl-mental retardation syndrome
BDSC	Bloomington *Drosophila* Stock Center
BDGP	Berkeley *Drosophila* Genome Project
Ca	Calyx
CaMK	Calcium/calmodulin-dependent protein kinase
cAMP	Cyclic AMP
CBP	CREB binding protein
cVA	11-cis-vaccenyl acetate
CNS	Central nervous system
CRE	cAMP response element
CREB	cAMP response element-binding protein
CRISPR	Clustered regularly interspaced short palindromic repeats
CRIMIC	CRISPR-mediated integration cassette
CRISPR-TRiM	CRISPR-mediated tissue-restricted mutagenesis
dANK	Mutated ankyrin-binding
dMEF2	Mutated myocyte enhancer factor 2 binding
dNLS	Mutated nuclear localisation signal (cytoplasmic-restricted)

DAVID	Database for Analysis, Visualisation, and Integrated Discovery
DBD	DNA-binding domain
DHE	Dihydroethidium
DmHDAC4	*Drosophila* HDAC4
DmMEF2	*Drosophila* MEF2
DSCAM	Down syndrome cell adhesion molecule
EB	Ellipsoid body
Elav	Embryonic lethal abnormal vision
FADH2	Reduced flavin adenine dinucleotide
FDR	False Discovery Rate
$GAL80^{ts}$	Temperature-sensitive GAL80
GO	Gene Ontology
sgRNA	Single guide RNA
HAT	Histone acetyltransferase
HD	Huntington's disease
HDAC(s)	Histone deacetylase(s)
hHDAC4	Human HDAC4
KANK	Kidney ankyrin repeat-containing proteins
KCs	Kenyon cells
KD	Knock down
KEGG	Kyoto Encyclopaedia of Genes and Genomes
L1CAM	L1 cell adhesion molecules
LTM	Long-term memory
LTP	Long-term potentiation
MAPK	Mitogen-activated protein kinase
MARK	Microtubule affinity regulating kinases
MB	Mushroom body
MEF2	Myocyte enhancer factor 2
mtDNA	Mitochondrial DNA

NADH	Reduced nicotinamide adenine dinucleotide
NCoR	Nuclear receptor corepressor 1
NES	Nuclear export signal
NHL	Newly hatched larvae
NLS	Nuclear localisation signal
NMJ	Neuromuscular junction
Nrg	Neuroglian
PD	Parkinson’s disease
Pe	Peduncle
Pck2	Phosphoenolpyruvate carboxykinase 2-mitochondrial
Pepck2	Phosphoenolpyruvate carboxykinase 2
PKA	Protein kinase A
PKC	Protein kinase C
PKD	Protein kinase D
PP2A	Protein phosphatase 2A
PRSS12	Serine protease 12
PCA	Principal Component Analysis
PVIs	Parvalbumin-expressing inhibitory interneurons
RFXANK	Regulatory factor X associated ankyrin-containing protein
ROS	Reactive oxygen species
rRNA	Ribosomal RNA
RUNX2	Runt-related transcription factor-2
SEM	Scanning Electron Microscope
SMRT	Silencing mediator for retinoid and thyroid hormone receptors
SMA	Spinal muscular atrophy
SREBP	Sterol regulatory element binding protein
SRF	Serum response factor
STM	Short-term memory
SUMO	Small ubiquitin-like modifier

TARGET	Temporal and regional gene expression targeting
TCA	Tricarboxylic acid
TPM	Transcripts per million
TSA	Trichostatin A
UAS	Upstream activating sequence
VDRC	Vienna *Drosophila* Resource Center
WT	Wild-type
Y1142H	Mutation of tyrosine to histidine (catalytically-inactive)

1. BACKGROUND

1.1 Overview

The histone deacetylases (HDACs) are a family of enzymes that regulate transcription through the removal of acetyl groups from lysine residues in histones. This results in an enhanced attraction between the negatively charged DNA and positively charged histone tails and promotes chromatin packing, thus preventing access of transcription factors. This deacetylase activity is opposite to that of histone acetyltransferases (HATs) which acetylate histones to open chromatin and facilitate transcription factor accessibility. These processes of packing and unravelling of DNA are integral to the appropriate regulation of gene expression (Verdone, Caserta, & Di Mauro, 2005).

There are four classes of HDACs and of these, Class I & Class IIa have been implicated in regulation of long-term memory (LTM) via inhibition of plasticity-related gene transcription that is required for normal memory formation (Abel & Zukin, 2008). Preclinical drug trials of HDAC inhibitors carried out with the aim to enhance memory through alteration of memory-related gene expression profiles have shown the potential of these inhibitors in improving cognitive function in animal models of stroke and Alzheimer's disease (AD) (Chuang, Leng, Marinova, Kim, & Chiu, 2009). To date, most research on HDAC inhibitor drugs have focused primarily on Class I HDACs and there has been relatively little research on the role of Class IIa HDACs in learning and memory.

HDAC4 is a Class IIa HDAC that is widely expressed in the brain (Darcy, Calvin, Cavnar, & Ouimet, 2010). Unlike Class I HDACs which are largely nuclear, the subcellular distribution of HDAC4 is heterogenous across different brain areas and while it localises to some neuronal nuclei, it predominantly localises to the cytoplasm and shuttles in and out of the nucleus in response to physiological stimuli (Chawla, Vanhoutte, Arnold, Huang, & Bading, 2003). Disruption to the nucleocytoplasmic shuttling impairs cognitive function, with nuclear accumulation of HDAC4 impairing memory in mice (Sando et al., 2012). Increased nuclear abundance of HDAC4 also promotes neurodegeneration in a rodent model of Ataxia-telangiectasia, which involves neurodegeneration of the cerebellum, resulting in impairment of motor function (Li, Chen, et al., 2012). However, cytoplasmic HDAC4 appears to be neuroprotective as mice injected with cytoplasm-restricted HDAC4 performed better on the rota-rod which provides a measure of motor

learning (Li, Chen, et al., 2012). Additionally, cytoplasmic HDAC4 also improves memory in *C.elegans* (Wang, Cheng, et al., 2011). Therefore, the investigation into the activities of both nuclear and cytoplasmic HDAC4 will aid in understanding the involvement of *HDAC4* in memory and other neurological processes.

1.2 Neurodegenerative disorders: a global health burden

The human brain is a highly complex organ that requires precise regulated spatial and temporal developmental processes to organise its 100 billion neurons and form its network of synapses. It is the centre of the nervous system and requires structural maintenance and neuronal plasticity to coordinate complex processes such as learning and memory (van der Voet, Nijhof, Oortveld, & Schenck, 2014). Any dysregulation to these processes in terms of genetic or environmental factors can therefore potentially impede the brain's function or development, leading to neurodevelopmental or neurodegenerative disorders including dementia.

Dementia includes a wide category of brain diseases characterised by the decrease in ability to process and form memories, with AD being the most common form, affecting 50 million people worldwide. It is projected that by 2050, the number will increase to more than 152 million due to ageing population. This health issue has a huge impact on the economy with the current total estimated worldwide cost to be approximately a trillion US dollars per year and is forecast to double by 2030 (Patterson, 2018).

Dementia has also become a growing healthcare problem in New Zealand. In the last decade, it is estimated that approximately 50,000 people in New Zealand have been afflicted by dementia and the total financial cost on the healthcare system in 2011 was about $954.8 million (*New Zealand framework for dementia care*, 2013). It is estimated that the number of people living with dementia will triple by 2050 with a financial cost of approximately $5 billion (*Our Annual Story: The 2017 Report of Alzheimers NZ*, 2017).

The urgency to remedy the situation is preceded by the need to understand the fundamental molecular pathways that underlie these diseases. Studies on simple model organisms such as *Drosophila*, with a wide range of experimental tools and techniques

available are ideal for teasing apart complex molecular pathways to understand how the dysregulation of these processes leads to neurological disorders.

1.3 Learning and memory: the underlying mechanism

Learning is a process by which animals alter their behaviour based on experiences from their environment, and memory is the process through which this learned information is stored. Both learning and memory involve complex molecular mechanisms within specific neuronal circuits that are not yet fully understood. In the context of neuroscience, memory can be classified at a basic level into short-term memory (STM) and long-term memory (LTM), both, as the names imply, to allow the storage of information for a short period of time lasting for minutes to hours and long period lasting for days to a whole life time, respectively (Kandel, Schwartz, & Jessell, 2000).

The processes of learning and memory were proposed in the 1970s by Kandel (2001) to be conserved across the animal kingdom, based on his observations that simple organisms with evolved nervous system display rudimentary forms of learning. His early studies of invertebrate learning were carried out in the sea slug, *Aplysia californica*, where learned behaviour was correlated with the gill and siphon withdrawal, a defensive reflex by the animal in response to a weak tactile stimulus to its siphon. In general, this behaviour response is mild and lasts for only a brief moment after which the gill and siphon return back to their original states. However, when the stimulus is replaced with an electric shock to the tail, which is considered noxious, the slug becomes sensitised and subsequently elicits a much larger reflex response (i.e. further retraction of gill and siphon) when treated with only the weak tactile stimulus. This stronger sensitised response can last from several hours to a week and the duration correlates with the amount of shock training administered and demonstrates a basic form of non-associative learning (Hawkins, Kandel, & Bailey, 2006). In order to determine the molecular basis of the behavioural response, Kandel and colleague carried out a series of biochemical analyses and determined that memory formation involved the activation of cyclic AMP (cAMP) in the post-synaptic neuron in response to stimulation. This research, along with subsequent investigations in different model organisms led to the elucidation of basic

molecular pathways of learning and memory (Abel & Lattal, 2001) as briefly summarised below.

Following the release of the neurotransmitter, glutamate, from a pre-synaptic neuron in response to a stimulus, it binds to an AMPA receptor on a post-synaptic neuron to facilitate sodium influx, inducing depolarisation. This in turn stimulates the release of glutamate by the post-synaptic neuron which binds to AMPA receptors on the following post-synaptic neuron (Kandel, 2012) (**Figure 1.1**). However, the formation of STM requires a transient increase in synaptic strength. This is triggered when the neurotransmitter released by the pre-synaptic neuron also binds to an NMDA receptor which allows calcium influx (Kandel et al., 2000). Calcium binds to calmodulin to activate adenyl cyclase (AC), which results in the increase of cAMP. cAMP activates protein kinase A (PKA) which phosphorylates protein complexes at axon terminal and enhances the spontaneous release of neurotransmitter of the neuron (Cho et al., 2015; Ewert, 2013). The transition to LTM, however, requires the synthesis of new proteins. Following repetitive stimulation, cAMP levels increase and PKA activation reaches a threshold at which it recruits mitogen-activated protein kinase (MAPK). The two enzymes translocate into the nucleus where they phosphorylate transcription factors that induce expression of genes required for LTM. An example of a key transcription factor is the cAMP response element-binding protein (CREB). Phosphorylated CREB is able to trigger the expression of LTM related gene through binding to the CREB response element (CRE) in the promoter of genes required for synaptic plasticity such as *brain-derived neurotrophic factor* (*BDNF*) (Barco, Bailey, & Kandel, 2006; Kandel, 2012). BDNF has often been implicated in late-phase long-term potentiation (LTP), a process defined as an increase in synaptic strength between two neurons and is thought to be the cellular mechanism that underlies LTM. BDNF has been known to play a role in delivering AMPA receptors to the synaptic surface during neuronal strengthening (Caldeira et al., 2007; Pang & Lu, 2004). This is in addition to the AMPA phosphorylation by Ca^{2+}/calmodulin-dependent protein kinase II (CaMKII) which also leads to synaptic delivery of the receptor, thus enhancing the neuron sensitivity to neurotransmitter which leads to stronger depolarisation. BDNF has also been reported to promote neuronal growth and local protein synthesis at the synapse which are crucial for formation of new synapses and allows rapid synaptic modification in specific regions of cellular compartment respectively (Barco et al., 2006).

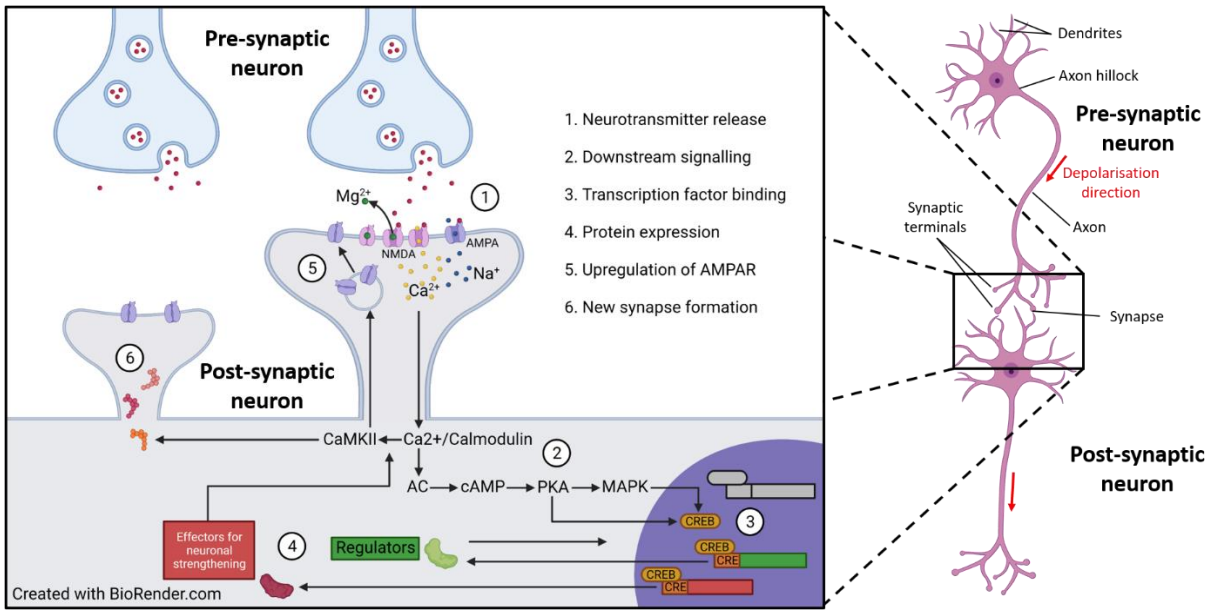

Figure 1.1: The underlying molecular mechanism for learning and memory
Diagrammatic representation of a pre-synaptic and post-synaptic neurons shown on the right. (1) The release of neurotransmitter such as glutamate from the pre-synaptic terminal binds to AMPA receptors to induce depolarisation which then allows the Mg^{2+} plugging the NMDA receptor to be repelled out into the extracellular space, thus allowing Ca^{2+} influx into the post-synaptic neuron. Ca^{2+} then forms a complex with calmodulin to activate adenyl cyclase (AC) to produce cAMP. (2) cAMP activates PKA which then allows the recruitment of MAPK. (3) PKA and MAPK translocate into the nucleus where it is able to phosphorylate transcription factor targets such as CREB. Phosphorylated CREB is able to bind to the CRE region on target DNA promoter. (4) CREB binding to CRE promotes the transcription of target genes and formation of proteins required for synaptic plasticity or transcription regulators. (5) Synaptic plasticity gene such as BDNF promotes neuronal growth and strengthening through upregulation of more AMPA to the membrane surface and (6) local protein synthesis which can result in the formation of new synapses. This figure is an original artwork created with referenced to Barco *et al*. (2006)

While research using simple model organisms has contributed a vast amount of knowledge to the understanding of the basic molecular mechanisms of learning and memory as described above, there are still many unanswered questions such as, in particular, how the expression of plasticity-related genes is regulated in specific neurons to facilitate memory formation and how these processes are dysregulated in disorders that affect cognition. Therefore, the study of the regulators of neuronal gene expression will help us to further understand the pathways involved in memory formation.

1.4 Neuroepigenetics

In recent decades, there has been an increasing focus on investigating the role of epigenetic machineries in the central nervous system (CNS) (Abel & Zukin, 2008; Alarcon et al., 2004; Lubin, Roth, & Sweatt, 2008; Miller & Sweatt, 2007; Petronis, 2010; Sweatt, 2013), which have led to the emergence of the neuroepigenetic sub-discipline.

The study of epigenetics focuses on features that are the level above the foundation of genetic inheritance (Sweatt, 2013), i.e., a heritable genetic alteration due to external or environmental changes affecting gene activity and expression. Many epigenetic mechanisms have been identified, however the two which have attracted the most focus are DNA methylation and regulation of chromatin structure through histone modification (Miller & Sweatt, 2007; Sweatt, 2013). The context of such research have mostly been on the role of epigenetic mechanisms in development, however, it is now known that experiences from stress, maternal behaviour, drug exposure or environmental toxins can influence the regulation of epigenetic machinery in the CNS (Borrelli, Nestler, Allis, & Sassone-Corsi, 2008; Champagne & Curley, 2009; Day & Sweatt, 2011; Dulac, 2010; Renthal & Nestler, 2008) and dysregulation of the machinery can lead to altered gene expression in neurons, which can impact on normal development and function. These multifactorial influences on epigenetic mechanisms have been proposed to be an important cause of diseases with low genetic penetrance (Petronis, 2010). Therefore, a better understanding of the role of epigenetic machinery in the CNS is essential in order to understand the causal effect of environment on epigenetic mechanisms.

1.4.1 Regulation of chromatin through histone modification

Within the nucleus of a cell, DNA is wrapped around histones and organised into chromatin, a dense and compact structure that allows for regulation of gene expression as well as protection of DNA from damage. Chromatin is made up of a DNA-histone complex which is the base unit of nucleosome, which comprises approximately 147 base pairs of double-stranded DNA wrapped around a histone octamer: two units of H2A, two units of H2B, two units of H3 and two units of H4. These nucleosome “beads” are held together by the histone H1 which also binds to the linker DNA that connects to the other

nucleosome, therefore it serves to stabilise the compact chromatin structure formation (**Figure 1.2**) (Kim, 2014; Li, Ding, & Zheng, 2014).

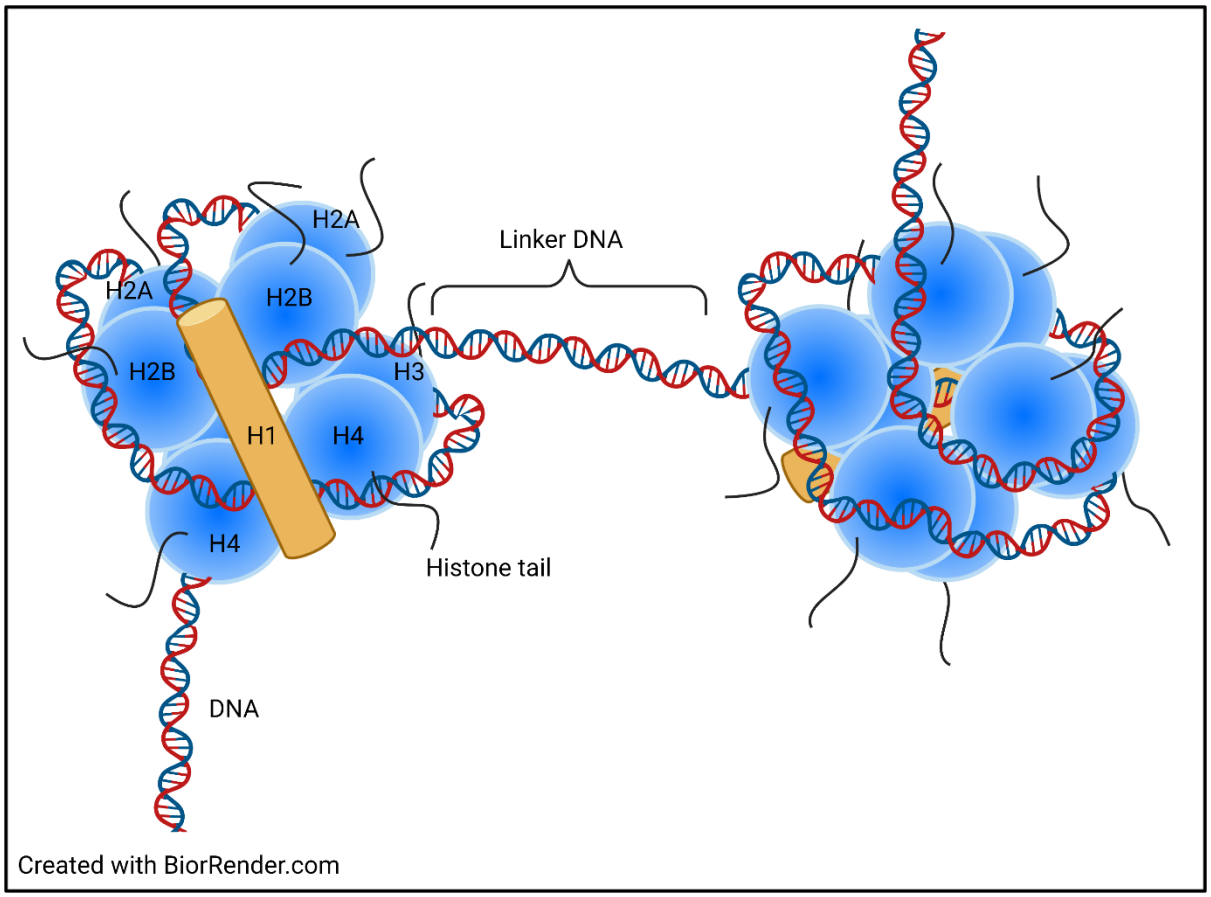

Figure 1.2: The nucleosomes are made up of DNA-histone complex
Each nucleosome is made up of approximately 147 bp of DNA wrapped around a histone octamer of H2A, H2B, H3 and H4. An H1 binds to the octamer and linker DNA to keep the DNA wrapped around the nucleosome and stabilise its arrangement between nucleosome that enables the compact formation in chromatin.

The histone proteins are directly responsible for the organisation of chromatin and are able to "pack" or "unpack" DNA and regulate its interaction with other nuclear proteins. These changes in chromatin structure are achieved through posttranslational modifications of histone tails by chromatin regulators via phosphorylation, methylation, ubiquitination, glycosylation, ribosylation, acetylation or deacetylation. Among the most studied regulators are the histone acetyltransferase (HAT) and histone deacetylase (HDAC) enzymes, which are involved in acetylation and deacetylation of the histone tails respectively (Volmar & Wahlestedt, 2015).

1.5 Histone acetylation and deacetylation

HAT activity has been associated with active gene expression via the catalytic transfer of an acetyl group from acetyl-CoA to the lysine ε-amino residue at the N-terminus of histone tail (Verdone et al., 2005). This modification affects gene transcription by neutralising the positive charge on the lysine and thus reducing the attraction between the histone and the DNA. This loosens the chromatin structure and also recruits other proteins to its binding surface to influence transcription (Josling, Selvarajah, Petter, & Duffy, 2012). Conversely, deacetylation of lysines by HDACs removes the acetyl group which results in the chromatin reverting back to its compact structure, preventing transcription factors from accessing the DNA. Therefore, HAT and HDAC activities are associated with the regulation of gene expression (Volmar & Wahlestedt, 2015) (**Figure 1.3**).

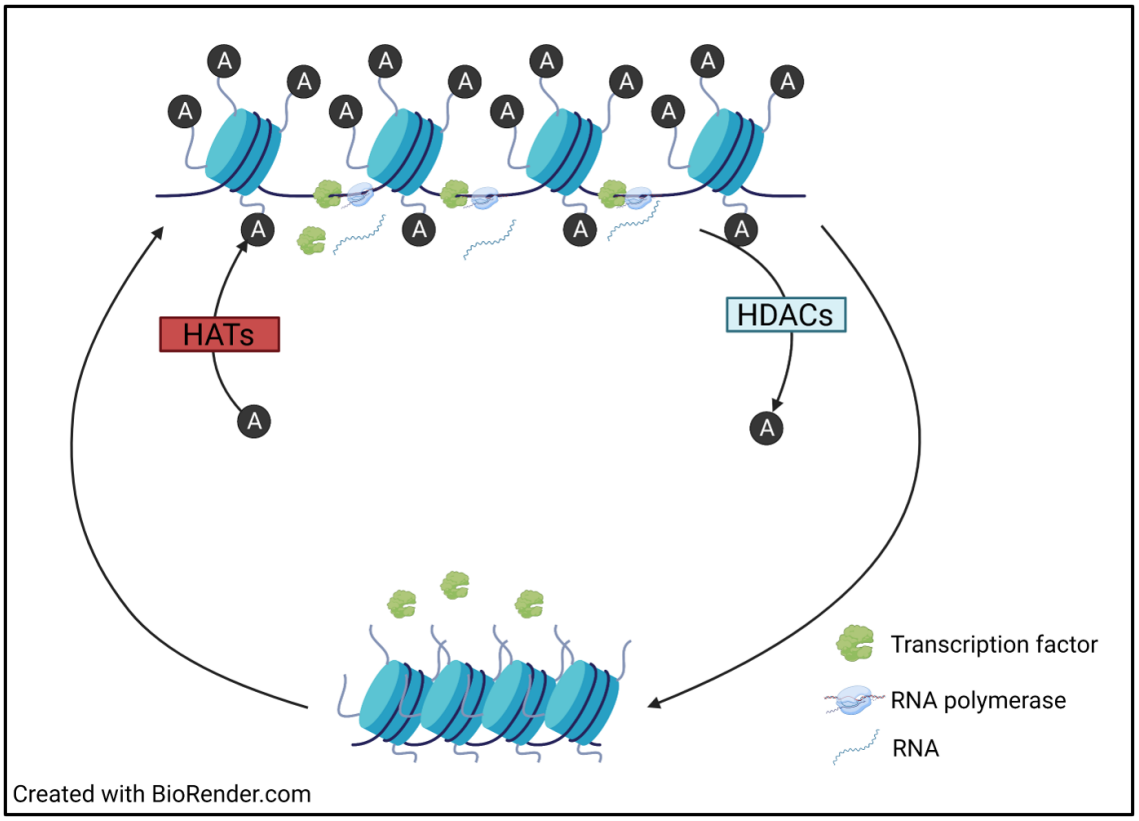

Figure 1.3: Acetylation and deacetylation of chromatin
HAT induces transcriptional activation of genes through its acetylation (black circle A) of histones which allow the chromatin structure to relax and allow transcription factors to access DNA and initiate transcriptions of target genes. Conversely, HDAC deacetylate histones which leads to chromatin condensation and prevents the access of transcription factors.

Despite the names HAT and HDAC implying that they target only histones, this is only the case because the first acetylated lysine residues were discovered in histones (Drazic,

Myklebust, Ree, & Arnesen, 2016). It has become clear that lysine acetylation and deacetylation is not limited to just histones but non-histone proteins including transcription factors, receptors and α-tubulin (Glozak, Sengupta, Zhang, & Seto, 2005), therefore HATs and HDACs are not only chromatin modifiers but have a much broader range of substrates and roles in non-transcriptional processes in the cell.

1.5.1 Histone acetylation and memory formation

In an early study conducted by Schmitt and Matthies (1979), radioactive-labelling of acetate showed a correlation between histone acetylation and learning in rats. They observed an increase in acetylation in the hippocampus (a brain region associated with learning and memory) of trained animals when compared to controls. This correlation was further confirmed by other studies showing the requirement of acetylation in memory-related activities (Alarcon et al., 2004; Korzus, Rosenfeld, & Mayford, 2004; Levenson et al., 2004). Mutation of the transcriptional coactivator CREB binding protein (CBP), which is also a HAT, leads to the impairment of chromatin acetylation and deficits in LTM in a mouse model of Rubinstein-Taybi syndrome (Alarcon et al., 2004). In addition, transgenic mice carrying a mutant variant of CBP that lacks HAT activity were not able to undergo memory consolidation (Korzus et al., 2004). Memory consolidation is the process of stabilising STM to LTM which requires the activation of CREB and CBP to trigger histone acetylation, after which CREB and CBP become dispensable for the subsequent steps of memory consolidation (Korzus et al., 2004). This demonstrates the requirement of HAT activity for LTM formation and furthermore, they were able to show rescue of the memory deficit through the suppression of the mutant CBP expression or administration of trichostatin A (TSA), an HDAC inhibitor. HDAC inhibitors were also used in a study by Levenson and colleagues (2004) to investigate the role of histone acetylation in LTP of rat hippocampal neurons. They discovered that the inhibition of HDAC activity increased acetylation of histone H3, which led to the enhancement of LTP in the hippocampus, thus, implicating HDACs in suppression of LTM.

1.6 The family of HDACs

The family of mammalian HDAC proteins are classified into four categories based on their sequence similarity to the yeast homolog: Class I, II, III and IV. Class I HDACs comprise of HDACs 1, 2, 3 and 8, which share sequence homology with the yeast gene, *Rpd3*, are restricted to the nucleus (Morrison, Majdzadeh, & D'Mello, 2007; Thul et al., 2017; Yao & Yang, 2011). HDACs 1, 2 and 3 are ubiquitously expressed in the body whereas HDAC8 is expressed mainly in the liver (Morrison et al., 2007).

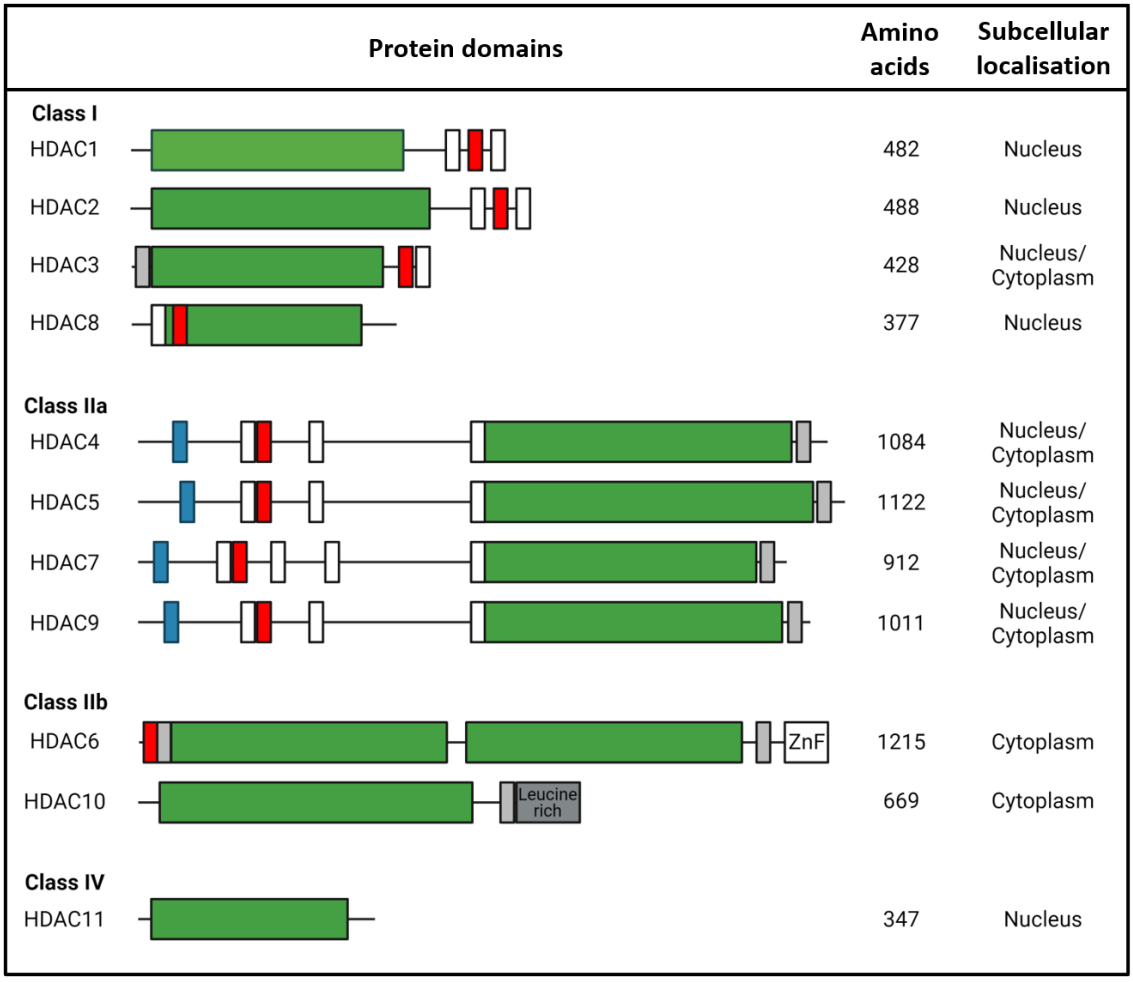

Figure 1.4: The HDAC domains and classifications
The four classifications of HDAC along with each of its protein domain diagram, protein size and subcellular distribution. Class III HDAC (sirtuin class) is not shown in this figure. Green boxes represent conserved deacetylase domain, white boxes represent serine phosphorylation sites, red boxes represent NLS, grey boxes represent NES and blue boxes represent MEF2-binding sites. Zinc finger motif and leucine rich domain is located in the C-terminal region of HDAC6 and HDAC10 respectively. This figure is an original artwork created with referenced to Chiaradonna, Cirulli, Palorini, Votta, and Alberghina (2015); Haberland, Montgomery, and Olson (2009); Liu, Peng, Seto, Huang, and Qiu (2012); Morris and Monteggia (2013); Park and Kim (2020); Yang and Grégoire (2005)

Class II HDACs are homologous to the yeast histone deacetylase *Hda1* and can be further categorised into two subgroups: Class IIa includes HDACs 4, 5, 7 and 9 which are highly expressed in the brain, heart and skeletal muscle and Class IIb, which consists of HDACs 6 and 10. HDAC6 is expressed mainly in the testis while HDAC10 is highly expressed in the liver, spleen and kidney (Verdin, Dequiedt, & Kasler, 2003). Class I and Class II HDACs differ in size and subcellular distribution: Class II HDACs are much larger in molecular weight and contain both a nuclear localisation signal (NLS) and a nuclear export signal (NES) sequences with the exception of HDAC10 which only has an NES. However, only Class IIa HDACs are localised to both the nucleus and cytoplasm and their subcellular localisation is dependent on activity-inducing chemical changes within the cell, which in turn regulate their distribution between compartments through nucleocytoplasmic shuttling (Chawla et al., 2003; Morrison et al., 2007; Thul et al., 2017). The way in which Class IIa HDACs shuttle between the nucleus and cytoplasm is dependent on the phosphorylation state of its conserved serine residues. These serine residues can be phosphorylated by kinases such as protein kinase C (PKC), protein kinase D (PKD), calcium/calmodulin-dependent protein kinase (CaMK) and microtubule affinity regulating kinases (MARK) which then allows the recruitment of the chaperone protein, 14-3-3ζ (Backs, Song, Bezprozvannaya, Chang, & Olson, 2006; Berdeaux et al., 2007; Chang, Bezprozvannaya, Li, & Olson, 2005; Dequiedt et al., 2006; Wang et al., 2000; Zhou et al., 2000). The binding of 14-3-3ζ to the phosphorylated serine allows it to usher the Class IIa HDAC out of the nucleus and into the cytoplasm, thus relieving its role as transcription repressor at the same time. Conversely, serine/threonine-protein phosphatase 2A (PP2A) in 3T3 fibroblast cells was shown to dephosphorylate the serine residues which then release 14-3-3ζ and allow nuclear re-entry of the Class IIa HDACs (Martin, Kettmann, & Dequiedt, 2007; Martin et al., 2008; Paroni et al., 2008; Weeks et al., 2017) (**Figure 1.4 & 1.5**).

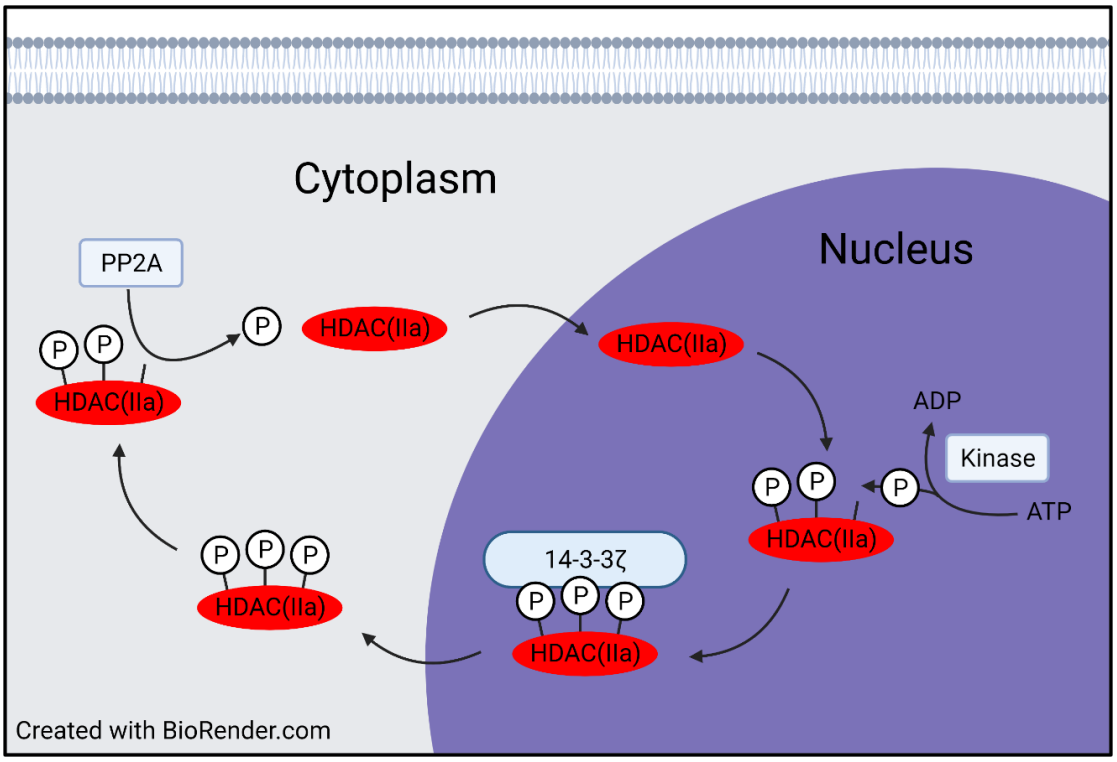

Figure 1.5: The nucleocytoplasmic shuttling of Class IIa HDACs
Phosphorylation of the Class IIa HDAC facilitates recruitment of the chaperone protein, 14-3-3ζ, which binds and translocates it to the cytoplasm. Entry into the nucleus requires dephosphorylation by PP2A.

Although vertebrate Class IIa HDACs have a conserved deacetylase domain, they are believed to be catalytically inactive, at least towards acetyl lysine, due to a key amino acid change from tyrosine to histidine within the domain (Haberland et al., 2009; Mihaylova et al., 2011). They also harbour an extended N-terminal region which contains a motif for interaction with proteins including the serine phosphorylation sites as well as binding domain for transcription factors such as CREB, myocyte enhancer factor 2 (MEF2) and serum response factor (SRF) (Davis, Gupta, Camoretti-Mercado, Schwartz, & Gupta, 2003; Haberland et al., 2009; Li, Chen, et al., 2012). On top of that, several other transcription factors have also been identified to interact with HDAC4 but their binding domains have not yet been characterised: Forkhead Box Class O (Wang, Moya, et al., 2011), activating transcription factor 4 (Zhang et al., 2014), hypoxia-inducible factor -1α (Seo, Kim, Na, & Lee, 2009), COOH-terminal-binding protein (Zhang, McKinsey, Lu, & Olson, 2001) and runt-related transcription factor-2 (RUNX2) (Vega et al., 2004). The two Class IIb HDACs differ in domain organisation to the Class IIa; HDAC6 possesses another conserved deacetylase domain on its extended N-terminal

while HDAC10 lacks the extended region (Morrison et al., 2007; Verdin et al., 2003) (**Figure 1.4**).

Class III consists of seven sirtuin proteins. The sirtuin class is distinct from all the other classes of HDACs in terms of its phylogenetics and functions and therefore will not be further introduced. Lastly, the single Class IV HDAC, HDAC11 is the smallest HDAC compared to the other classes of HDACs. HDAC11 is mainly present in smooth muscle, heart, kidney, brain, and gall bladder. It is localised primarily to the nucleus where it is reported to interact with HDAC6 in vivo despite HDAC6 having been reported to be cytoplasmic. This could perhaps underline the importance in understanding the complexity of subcellular translocation and distribution of HDACs. (Gao, Cueto, Asselbergs, & Atadja, 2002; Liu, Wu, Jin, Chang, & Xu, 2020; Morrison et al., 2007). Although HDAC11 has a conserved catalytic core region, it has also been recently discovered to possess a defatty-acylase activity which removes long chain fatty-acyl groups rather than acetyl groups (by deacetylase activity) from lysine H3K9. It is also reported to be 10,000 times more efficient than the conserved deacetylase activity (Cao et al., 2019).

The rapidly growing interest in Class II HDACs can be attributed to increasing evidence that they display other roles besides targeting histones for deacetylation. As mentioned earlier, it is known that lysine deacetylation is not limited to just histone targets, which has prompted some researchers to prefer using the term lysine deacetylase as the new nomenclature for the enzyme (Brandl, Heinzel, & Kramer, 2009; Drazic et al., 2016). However, the extended N-terminal region of Class IIa HDACs, particularly HDAC4, that contains transcription factor binding sites indicates that there are non-enzymatic roles to be explored.

1.6.1 The role of HDACs in neurological processes

Acetylation of chromatin has been associated with the formation of memory, therefore it is logical to assume deacetylation would suppress memory formation (Peixoto & Abel, 2013). Indeed, early studies have indicated that the application of HDAC inhibitors can enhance memory formation in several animal models of memory (Korzus et al., 2004; Levenson et al., 2004; Stefanko, Barrett, Ly, Reolon, & Wood, 2009; Vecsey et al., 2007).

In the last decade there has been focused research on the application of HDAC inhibitors for treatment against neurological disorders such as Parkinson's disease (PD), Huntington's disease (HD), AD, spinal muscular atrophy (SMA), Friedrich ataxia and amyotrophic lateral sclerosis (ALS) (Ziemka-Nalecz, Jaworska, Sypecka, & Zalewska, 2018).

At present, there are four main chemical classifications of HDAC inhibitor: the short-chain fatty acids, hydroxamic acids, cyclic peptides and benzamides (Abel & Zukin, 2008; Zhao et al., 2016; Ziemka-Nalecz et al., 2018) (**Figure 1.6**). Among these, the short-chain fatty acid, consisting of butyric acid and valproic acid and the hydroxamic acid, consisting of TSA and vorinostat have been used in studies of neurodegenerative disease models such as PD, AD, HD, ALS and SMA. The studies have shown the effects of these inhibitors to be beneficial in terms of improving memory performance or alleviating disease phenotype (Chuang et al., 2009; Ziemka-Nalecz et al., 2018). However, these HDAC inhibitors are relatively non-specific to any HDAC isoform other than targeting mainly both class I and II HDACs and have had reports of hematological, neurological, metabolic or cardiovascular based toxicity from a variety of Phase I clinical studies of cancer treatment (Bruserud, Stapnes, Ersvaer, Gjertsen, & Ryningen, 2007). This highlights the need to understand the exact nature of the interaction between specific HDACs and their inhibitors in order for the rational design of drugs targeting individual HDACs for treatment of cognitive defects (Peixoto & Abel, 2013).

		Classifications of HDAC Inhibitors			
		Short-chain fatty acid	**Hydroxamic acid**	**Benzamide**	**Cyclic peptides**
Class I	**HDAC1**	Butyric acid, Valproic acid	TSA, Vorinostat, Panobinostat	Entinostat, K560, HDACi 4b, HDACi 106, RGFP136, BML-210, pemlic o-aminobenzamide, RG2833	Romidepsin
	HDAC2			K560, HDACi 4b, HDACi 106, BML-210, pemlic o-aminobenzamide	Romidepsin, Apicidin
	HDAC3			HDACi 4b, HDACi 106, RGFP136, RGFP966, BML-210, pemlic o-	Apicidin

				aminobenzamide, RG2833	
	HDAC8			BML-210, pemlico-aminobenzamide	
Class IIa	**HDAC4**	Butyric acid, Valproic acid	TSA, Vorinostat, Panobinostat	BML-210	
	HDAC5			BML-210	
	HDAC7			BML-210	
	HDAC9			Entinostat, BML-210	
Class IIb	**HDAC6**		TSA, Vorinostat, Tubacin	Tubastatin A	
	HDAC10		TSA, Vorinostat		
Class IV	**HDAC11**		Vorinostat, Panobinostat	Entinostat	

Figure 1.6: List of common HDAC inhibitors
Each HDAC inhibitors in this figure have been reported to inhibit its respective HDAC(s). The HDAC inhibitors listed in the boxes have been used in neurodegenerative studies. Adapted from Chuang et al. (2009) & Ziemka-Nalecz et al. (2018)

Currently, there have been several studies conducted on the role of Class I HDACs in memory, either through genetic manipulation of individual HDACs or by use of HDAC-specific inhibitors. A study by Bahari-Javan et al. (2012) utilised, MS-275, an entinostat HDAC inhibitor specific to HDAC1, 9 and 11, to show that HDAC1 is required for the extinction of contextual fear memories in mice. This is a gradual process in which the animal learns to dissociate a response from a noxious stimulus, resulting in a diminished fear response over time, with MS-275 administration impairing this memory extinction process. Although HDAC1 plays a role in promoting memory extinction, it does not affect memory formation as demonstrated in a study by Guan and colleagues in which mice overexpressing HDAC1 in the hippocampus displayed a comparable level of freezing (a fear conditioned behaviour response to cues associated with electric shock) to the control mice, which suggests normal hippocampal-dependent memory formation. Rather, the formation of memory appears to be specifically repressed by HDAC2, as mice overexpressing HDAC2 in the hippocampus exhibited decreased fear associated response, suggesting an impairment in the formation of fear memory (Guan et al., 2009). This suggests that the role of HDAC1 involves regulation of genes required for memory extinction while HDAC2 promotes repression of genes required for memory formation

(Bahari-Javan et al., 2012). In fact, among the Class I HDACs, HDAC2 was identified as the most suitable drug target for treatment of impaired memory associated with AD (Gräff et al., 2012). This study did not however investigate the role of the third Class I HDAC, HDAC3, which has also been found to regulate memory formation. Both hippocampal deletion of *HDAC3* in mice as well as the use of HDAC3 specific inhibitor, RGFP136, resulted in the enhancement of LTM in a memory test for location-dependent object recognition (McQuown et al., 2011). In addition, HDAC3 has also been associated with cocaine context memory formation. It is highly expressed in the nucleus accumbens of mice, a region of the brain associated with cocaine-induced histone acetylation and conditioned place preference, and knockout of *HDAC3* in the nucleus accumbens resulted in the enhancement of cocaine-induced memory (Rogge, Singh, Dang, & Wood, 2013). HDAC3 has also been implicated in neuroinflammation associated with AD and HD. Elevated levels of HDAC3 led to an increase in activated microglia in the hippocampus and striatum respectively (Jia et al., 2016; Zhu et al., 2017). Conversely, knock down (KD) of *HDAC3* in AD mice reduced the amount of activated microglia, while treatment with the HDAC3 inhibitor RGFP966 also resulted in a decrease in activated astrocyte in HD mice (Jia et al., 2016; Zhu et al., 2017).

Research into the role of Class II HDACs in neurological function has not been as extensive as the Class I members, with most studies focused on their roles in the development and function of skeletal muscle (Cohen et al., 2009; Cohen et al., 2007; Lu, McKinsey, Zhang, & Olson, 2000; Tang et al., 2009). However in recent years it has become clear that the Class IIa HDACs, HDAC4 and 5, are involved in the pathogenesis of several neurological conditions including AD, HD, and depression (Agis-Balboa, Pavelka, Kerimoglu, & Fischer, 2013; Burli et al., 2013; Hobara et al., 2010; Iga et al., 2007; Sung et al., 2013), which will be discussed in detail in the next section. With regard to the Class IIb HDACs, only HDAC6 has been reported to have a role in neuronal function in which it acetylates α-tubulin to regulate cytoskeletal stability and intracellular transport/trafficking. Inhibition of HDAC6 was shown to compensate for an intracellular transport defect in striatal cell cultures derived from HD mice through the increased acetylation of α-tubulin (Dompierre et al., 2007). In an AD mouse model, knockout of *HDAC6* also led to an increase in acetylation of α-tubulin, resulting in the protection of hippocampal neurons from β-amyloid toxicity caused by impaired mitochondrial trafficking (Govindarajan et al., 2013).

Finally, little is known about the role of the sole Class IV HDAC, HDAC11, in the brain. Its expression in oligodendrocytes, large glial cells responsible for the production of myelin sheath insulation of neurons, suggest that its role might be better understood through the study of demyelination. Interestingly, demyelination is a hallmark feature of multiple sclerosis, which results from immune cells infiltrating myelin and leads to its degeneration (Broide et al., 2007). Indeed, a recent study showed that knockout of *HDAC11* in a mouse model of multiple sclerosis is associated with reduced demyelination and phenotypic recovery (Sun et al., 2018).

Taken together, these studies indicate that HDACs play differing roles in the CNS, further highlighting the importance of investigating the specific mechanisms through which individual HDACs regulate neuronal processes.

1.6.2 Class IIa HDACs and neurological function

Among the four vertebrate Class IIa HDACs, HDAC4 and HDAC5 are reported to be highly expressed in several brain regions, in particular, the hippocampus (Broide et al., 2007; Kim et al., 2012; Uhlén et al., 2015). As mentioned briefly in Section 1.6, HDAC4 and 5 localise to both the nucleus and cytoplasm and their subcellular distribution is regulated through activity-dependant nucleocytoplasmic shuttling (Chawla et al., 2003; Morrison et al., 2007; Thul et al., 2017). The ability for subcellular compartmentalisation of these HDACs suggest that they may have activities in both the nucleus and cytoplasm, however, there has been little investigation of the role of Class IIa HDACs outside of the nucleus. Immunostaining of HDAC4 in the mouse brain has revealed that the distribution of HDAC4 between the nucleus and cytoplasm varies differently in different parts of the brain. Furthermore, in the majority of brain regions, HDAC4 is largely detected outside the nucleus in the axons, dendrites and synapses. These data further suggest a potential interaction of HDAC4 with non-histone proteins in the cytoplasm and the study of the activities of HDAC4 in these subcellular regions warrants further investigation (Darcy et al., 2010).

HDAC4 has been implicated in the pathogenesis of several neurological conditions including AD, HD, PD, ALS, Ataxia-telangiectasia, 2q37 deletion syndrome (previously known as brachydactyl-mental retardation syndrome), post-traumatic stress disorder and

stroke; and HDAC5 has also been associated with AD and HD (Federspiel, Greco, Lum, & Cristea, 2019; Hoshino et al., 2003; Kong et al., 2018; Li, Chen, et al., 2012; Maddox et al., 2018; Pigna et al., 2019; Shen, Chen, Li, Kofler, & Herrup, 2016; Williams et al., 2010; Wu, Yang, Zhang, Zhang, & Feng, 2017). In contrast to the memory-enhancing phenotypes resulting from inhibition of Class I HDACs, the loss of HDAC5 has been associated with memory impairment in a mouse model of AD, suggesting that development of drugs inhibiting HDAC5 should be avoided for future treatment towards AD (Agis-Balboa et al., 2013). The possibility exists that the difference in neurological response compared to the other HDACs involved in memory formation could be due to an unknown cytoplasmic role of HDAC5 that positively regulates processes of memory formation. In a study of HDACs activity in neuronal cultures, it was discovered that the expression of huntingtin protein containing an expanded polyglutamine tract (a hallmark mutation of HD that leads to pathogenesis) led to an increase nuclear translocation of HDAC5 (Hoshino et al., 2003). The change from cytoplasmic to nuclear localisation may suggest that HDAC5 plays a role in the pathogenesis of HD. However, the lack of research into cytoplasmic HDAC5 means its exact function in the cytoplasm is still unknown.

A role for HDAC4 in the cytoplasm has also been suggested by research in mouse model of Ataxia-telangiectasia. In this model, a loss of function mutation of the *ATM* gene, which encodes a protein kinase that phosphorylates proteins involved in DNA repair and damage recognition, promoted nuclear accumulation of HDAC4. This correlated with neurodegeneration and impaired motor function which was improved when HDAC4 activity was inhibited through TSA administration (Li, Chen, et al., 2012). The result, by itself, would suggest that it is the nuclear activities of HDAC4 that are driving the disease progression. However, the researchers further demonstrated that expression of a cytoplasm-restricted HDAC4 transgene in the cerebellum of $ATM^{-/-}$ mice resulted in similar improvements to the disease phenotype, suggesting it is neuroprotective (Li, Chen, et al., 2012). These results therefore indicate that nuclear and cytoplasmic HDAC4 have different roles which promote neurodegeneration and neuroprotection, respectively. Further supporting evidence that nuclear HDAC4 promotes neurodegeneration comes from a recent investigation into the role of HDAC4 in PD. A mouse model was employed in which α-synuclein is expressed in the dopaminergic neurons (a hallmark of PD). It was observed that HDAC4 accumulated in the nucleus when exposed to the PD-inducing neurotoxin MPTP. This resulted in alterations in gene expression that promoted cell death

through repression of CREB and MEF2, however when HDAC4 was phosphorylated by PKC, it retained its predominantly cytoplasmic distribution which alleviated the phenotype (Wu et al., 2017). Although, these studies did not directly demonstrate a cytoplasmic role but rather the negative impact HDAC4 has when abundantly localised to the nucleus, it suggests that redirecting its distribution away from the nucleus to cytoplasm may be sufficient to improve phenotypic symptoms.

The nuclear accumulation of HDAC4 has also been associated with AD. Sen and colleagues (2015) reported that expression of apolipoprotein E4, which is known to increase β-amyloid deposition, promotes HDAC4 nuclear accumulation. This accumulation leads to the reduction in BDNF expression which is crucial for LTM formation. Additionally, nuclear accumulation of HDAC4 caused by the loss of ATM also correlates with the manifestation of AD, further supporting a pathogenic role of nuclear HDAC4 in AD (Shen et al., 2016). This association of HDAC4 with AD is strongly suggestive of an involvement in memory formation, and moreover, it was also reported to repress CREB which is one of the key transcription factors required for LTM (Li, Chen, et al., 2012). However, the role in which cytoplasmic HDAC4 plays in this neuronal process remains unknown. In summary, the increasing evidence that associates HDAC4 with several neurological disorders, its potential of having multiple binding partners due to its extended N-terminal region and its seemingly dual functions depending on its subcellular distribution support the investment of research efforts into further elucidating its functions in neurons.

1.6.3 *HDAC4* and memory formation

The association of *HDAC4* with AD highlights a link between *HDAC4* and memory impairment, the most common phenotype of the disease. Therefore, investigating the link between *HDAC4* and memory may aid in understanding the underlying molecular basis of AD. (Sen et al., 2015; Shen et al., 2016).

Brain-specific knockout of *HDAC4* in the mouse resulted in memory impairment when tested in the Morris water maze, an assay which provides a measure of spatial memory (Kim et al., 2012). The requirement of HDAC4 in learning and memory was also demonstrated in a *Drosophila melanogaster* model through a courtship memory assay. It

was shown that RNAi-mediated KD of *HDAC4* in the mushroom body (a region in the insect brain involved in learning and memory) led to memory impairment which indicated that *HDAC4* is required for normal memory formation (Fitzsimons, Schwartz, Given, & Scott, 2013).

In humans, deletion of the chromosomal region 2q37 that includes *HDAC4* results in brachydactyly-mental retardation syndrome (BDMR) which presents as developmental delay, autism spectrum disorder, and intellectual disability (Morris et al., 2012; Williams et al., 2010). Among the genes that were affected by 2q37 deletion, *HDAC4* was identified via the overlapping phenotypes of patients with BDMR and Smith-Magenis syndrome (a developmental disorder that has similar phenotypes to BDMR), which narrowed the genetic loci in common to a region that overlapped in both 2q37 deletions. Sequencing of the overlaps revealed *de novo* mutations in the *HDAC4* gene (Williams et al., 2010). While intellectual disability is often multigenic in origin (Androschuk, Al-Jabri, & Bolduc, 2015; Bolduc & Tully, 2009), *HDAC4* is considered to be the primary genetic contributor to 2q37 deletion syndrome following an analysis of 103 cases (Le, Williams, Alaimo, & Elsea, 2019). Since then, HDAC4 has been implicated in other neurodevelopmental disorders, such as the cyclin-dependent kinase-like 5 (CDKL5) disorder, which presents as severe intellectual disability. HDAC4 is a target for CDKL5 phosphorylation and *CDKL5* knockout mice exhibit reduced HDAC4 phosphorylation and increased nuclear retention, which impedes neuronal survival and maturation (Trazzi et al., 2016). *HDAC4* is also required for normal retinal development in mouse (Chen & Cepko, 2009). Additionally, brain samples from individuals with autism have elevated level of HDAC4 and a genetic association between HDAC4 and autism was identified in a genome-wide association study of over 16,000 afflicted individuals (Anney et al., 2017; Nardone et al., 2014). Therefore, the neurodevelopmental requirement of HDAC4 is another aspect of research to focus on that may help better understand the role of HDAC4 in neurological function that could relate to memory formation.

Increased abundance of HDAC4 also impairs cognitive function; transgenic mutant mice expressing a truncated *HDAC4* gene lacking the deacetylase domain displayed deficiencies in formation of memory while navigating through the Barnes maze, another spatial learning and memory test (Sando et al., 2012). As the catalytic domain of wild-type (WT) mammalian HDAC4 is inactive due to a single amino acid mutation at Y976H (Bottomley et al., 2008), the results suggest that the memory impairment is not caused by

the loss of deacetylase activity. Additionally, the truncated *HDAC4* gene was also lacking a nuclear export signal and it was demonstrated that expression of this mutant HDAC4, which is nuclear-restricted, in cultured neurons repressed the expression of genes important for LTP induction. (Sando et al., 2012). Therefore, this evidence suggests that increased abundance of nuclear-restricted HDAC4 impairs memory formation. Indeed, a novel mutation within the 14-3-3ζ binding site of HDAC4 which is also predicted to result in nuclear accumulation was discovered in BDMR individuals with intellectual disability which could then potentially affect memory performance (Wakeling et al., 2021). Together, these data indicate that HDAC4 is required for normal memory function but that it also impairs memory when it accumulates in the nucleus. It should also be noted that the nuclear accumulation is accompanied by cytoplasmic depletion, however it is not clear whether it is one or both that contribute to the memory impairments.

A role for cytoplasmic HDAC4 has also been reported by Wang, Cheng, et al. (2011) in *C. elegans*. By using a thermotaxis behavioural assay to assess the memory performance of the worms, they discovered that WT worms overexpressing cytoplasmic-restricted *HDAC4* showed a significant increase in memory performance but did not show any difference when expressed in an *HDA4* (*C.elegans* homolog of *HDAC4*) mutant background. This study could suggest a pro-memory role for cytoplasmic HDAC4 but the lack of performance difference when expressed in an *HDA4* null background and also that *HDA4* knockout alone was able to enhance LTM formation highlights that having just cytoplasmic HDAC4 is insufficient and perhaps a regulated level of distribution of both subcellular compartments is required for memory formation (Wang, Cheng, et al., 2011).

More recently, WT mice subjected to contextual fear conditioning were shown to transiently accumulate HDAC4 six hours after training in the nuclei of neurons in the somatosensory cortex, CA1 and CA3 regions of the hippocampus as well as the dentate gyrus, which are all areas important for memory formation. A further assessment of HDAC4 localisation in hippocampal neurons expressing the substrate, Fos, a protein required in the early phase of memory formation, showed that in most of the Fos positive neurons, HDAC4 was restricted to the cytoplasm (Zhu et al., 2019). The nuclear-restricted HDAC4 along with HDAC5 was also shown to redundantly block the expression of a reporter gene driven by a promoter that contain DNA-binding sites of transcription factors involved in memory such as CREB, MEF2 and SRF (Barbosa et al., 2008; Etkin et al.,

2006; Ortega-Martínez, 2015; Zhu et al., 2019). This indicates the role of HDAC4 as a transcription factor repressor when in the nucleus and suggests that HDAC4 briefly enters the nucleus during learning but proceeds to translocate back out to the cytoplasm to derepress gene transcription required for memory storage (Zhu et al., 2019).

In *Drosophila*, the overexpression or KD of *HDAC4* in the mushroom body resulted in impairment of 24-hour courtship memory, suggesting that overabundance of HDAC4 represses memory formation but is still required at a basal level for normal memory performance (Fitzsimons et al., 2013). In summary, both vertebrate and *Drosophila melanogaster* HDAC4 (DmHDAC4) appear to have multiple roles in memory, however, it is uncertain how increased HDAC4 impairs memory, and whether its essential role in normal memory requires nuclear or cytoplasmic HDAC4, or both. The use of *Drosophila* as a model organism may allow further understanding of the dual-functional role of HDAC4 due to the efficient gene manipulation techniques that have been developed.

1.7 The *Drosophila melanogaster* model in neuroscience research

The fruit fly brain consists of about 250,000 neurons which is significantly lower than the 100 billion neurons in the human brain. This indicates a simpler neuronal architecture in comparison to vertebrates which makes the fruit fly an ideal model to study complex processes such as learning and memory (Spindler & Hartenstein, 2010). Additionally, the close homology of *Drosophila* genes with human genes associated with neurodegenerative diseases has also allowed the modelling of these diseases in a less complex way (Sang & Jackson, 2005). Lastly, the short generation time (approximately 10 days from egg to adult) and inexpensive cost of maintenance provides the means to quickly generate large samples of progeny for analysis.

1.7.1 The basic neuronal circuitry of *Drosophila* olfactory learning and memory

To understand the model for learning and memory in fruit flies, it is necessary to be familiar with the basic neuronal circuitry of olfactory learning and memory (McGuire,

Deshazer, & Davis, 2005). This circuit allows the discrimination of odours that are detected by odorant receptors present on the dendrites of olfactory receptor neurons that are found in the flies' antenna and maxillary pulp (Stocker, 1994). The axons of these olfactory receptor neurons project towards the antennal lobes which are made up of 43 glomeruli on each lobe. These glomeruli are dendritic fields of the projection neurons which then directs their axons toward the mushroom body (MB) dendrites which are clustered in a region known as the calyx (**Figure 1.7A**).

The MB is a bilaterally symmetrical structure found in the brains of insects and arthropods (**Figure 1.7B**). It plays an essential role in learning and memory and decision making by processing stimuli from extrinsic input neurons and projecting to extrinsic output neurons that drive the behavioural response to the stimulus (Campbell & Turner, 2010). In *Drosophila*, the MB consists of approximately 2000 intrinsic neurons per hemisphere named Kenyon cells (KCs), that comprise of three subtypes (α/β, α'/β' and γ). The KCs project their dendrites to form the calyx and project axon bundles to the anteroventral part of the brain to form the peduncle. At the anterior region of the brain, the axon bundles organise into five different lobe structures which are formed through branching and segregation. These lobes comprise of the dorsal α and α' lobes and the medial β, β' and γ lobes which form connections with different extrinsic output neurons made up of glutamatergic, GABAergic and cholinergic neurons. These neurons are then projected towards different regions of the brain where responses are elicited accordingly (Aso et al., 2014; Lee, Lee, & Luo, 1999) (**Figure 1.7**). There are also other extrinsic neurons that innervate the MB such as the dopaminergic neurons that modulate the output from KCs at localised regions of the MB structures (Li et al., 2020).

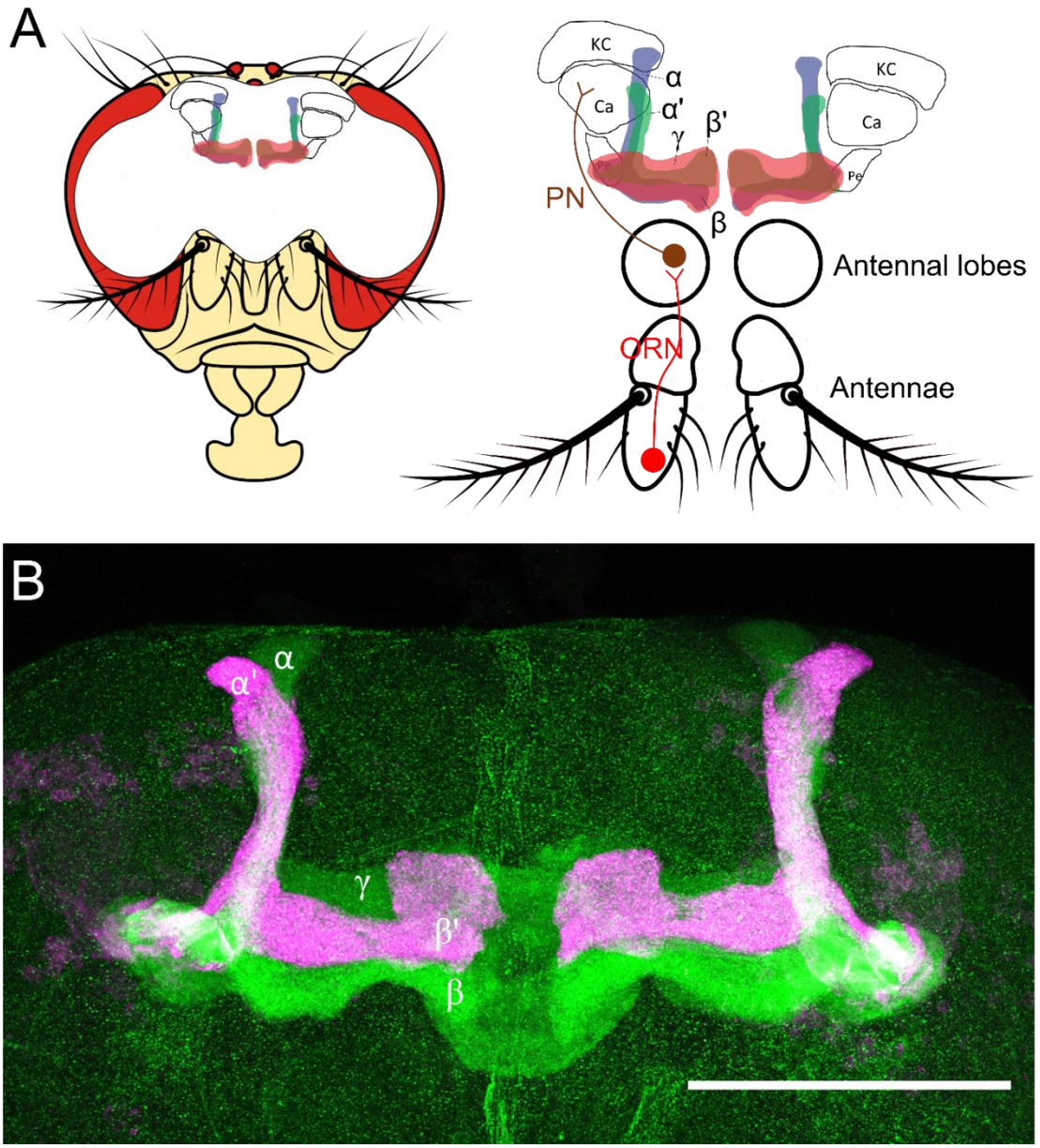

Figure 1.7: Diagrammatic representation of *Drosophila* mushroom bodies
(A) The position of the MB in the *Drosophila* head and brain (white area). Red represents the γ lobes; blue, α and β lobes; green, α' and β' lobes. (KCs) Kenyon cells, (Ca) calyx, (Pe) Peduncle. (B) Confocal image of mushroom bodies staining using antibodies that target proteins that expressed in specific subtype of KCs, thus allowing structural differentiation between the subtypes. Scale bar=100μm.

1.7.1.1 *Drosophila* MB development and its use as an assay for neurodevelopment

In *Drosophila* neurodevelopmental research, one of the most commonly assessed neuronal phenotypes is the development of the MB, therefore, it is crucial to understand the basic development of the MB structures. The formation of the five MB lobes occurs at different developmental stages in *Drosophila*. After hatching from eggs, the γ neurons

start developing during the 1st instar larval stage, projecting axons both dorsally and medially to form the initial γ lobes. This is followed by the formation of the dorsal α' and medial β' lobes during the 3rd instar stage and dorsal α and medial β lobes at the pupa stage. During the beginning of puparium formation, the dorsal and medial γ lobes undergo a developmental pruning process which prunes the neurons to the point before it bifurcates. This process is then followed by the formation of only the medial γ lobe throughout the remaining time in the pupa stage (Lee et al., 1999) (**Figure 1.8**).

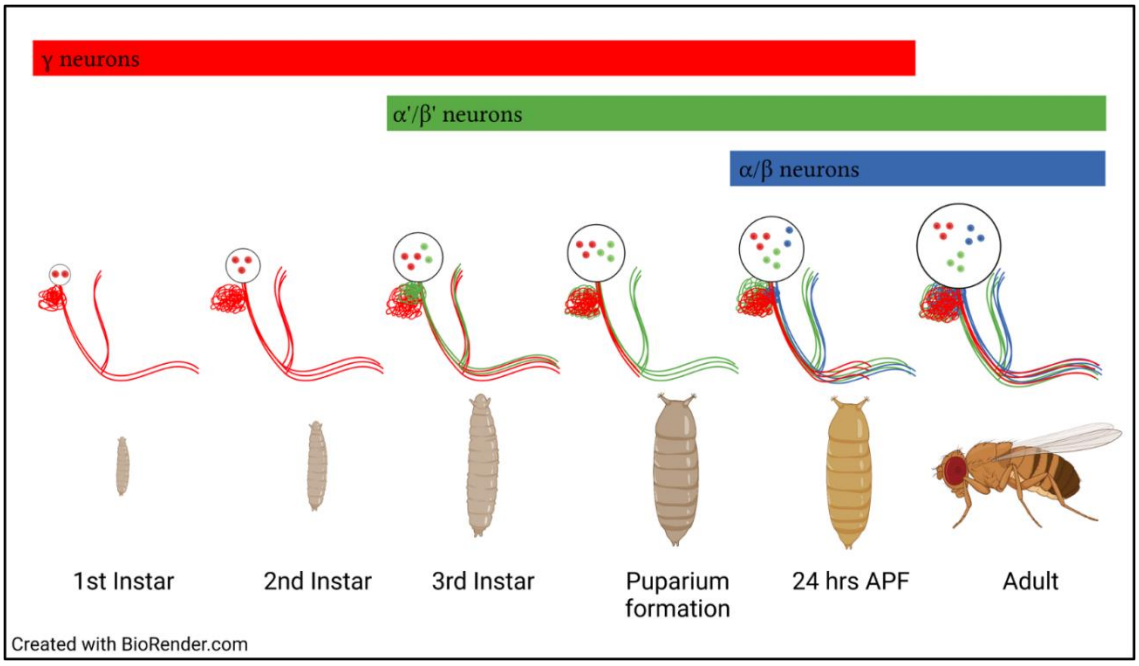

Figure 1.8: The development of mushroom bodies
The MB lobes arise at different timepoints commencing with the γ neurons development during the 1st and 2nd instar stages follow by the α' and β' neurons during the 3rd instar stage. Shortly after puparium formation γ neurons undergoes developmental pruning and 24 hours after puparium formation (APF) medial γ neurons start to emerge as well as the α and β neurons. The developed mushroom bodies then comprise of the dorsal α and α' lobes and medial β, β' and γ lobes

By using tools available for genetic manipulation in *Drosophila*, questions about the role of specific MB neurons and the genes they express during development and memory formation can be answered quickly using overexpression or KD techniques in specific subregions of the brain (Akalal et al., 2006; Fitzsimons et al., 2013; Schwartz, Truglio, Scott, & Fitzsimons, 2016).

The analysis of MB phenotypes is useful for assessing genetic factors involved in the tightly regulated developmental processes and many studies investigating the role of a

specific gene in neurodevelopment have used axon morphogenesis in the MB as a model (Hattori et al., 2007; Kim, Kim, Park, Park, & Lee, 2021; King et al., 2011; Michel, Kraft, & Restifo, 2004). For example, Hattori and colleagues (2007) discovered a collapsed α lobe phenotype resulting from mutation of gene of interest, *Down syndrome cell adhesion molecule* (*DSCAM*). Based on the known functions of the gene and further experimentation, they were able to predict a model in which DSCAM is required for branching of the KC axons through homophilic binding and self-repulsion between branches of the same neuron that result in the distinct MB lobe formation.

1.7.1.2 The basis of learning and memory in *Drosophila* courtship behaviour

Several paradigms for quantitative assessment of learning and memory have been developed, including olfactory, visual and courtship conditioning (Androschuk et al., 2015). In olfactory learning and memory, the flies are presented with a choice of two odours in a T-maze. The flies make choices based on their previous learned experience in which one of the odours was associated with either sugar or an electric shock stimulus (reward or punishment), and when subsequently exposed to both odours in the absence of the stimulus, they move towards the rewarding odour or away from the shock-associated odour. The visual learning and memory model also involves making choices except that the cue is visual based. Reward or punishment are presented on a walking surface lit by two different coloured LED which allows the flies to learn and memorise which surface colour to move towards for the reward or away from the punishment (Kottler & van Swinderen, 2014).

The *Drosophila* courtship suppression assay is another model in which the flies exhibit learning and memory behaviour and as the name implies, this assay utilises the courtship interaction between the male and female *Drosophila* and assesses the ability of the male to remember its previous courtship experience.

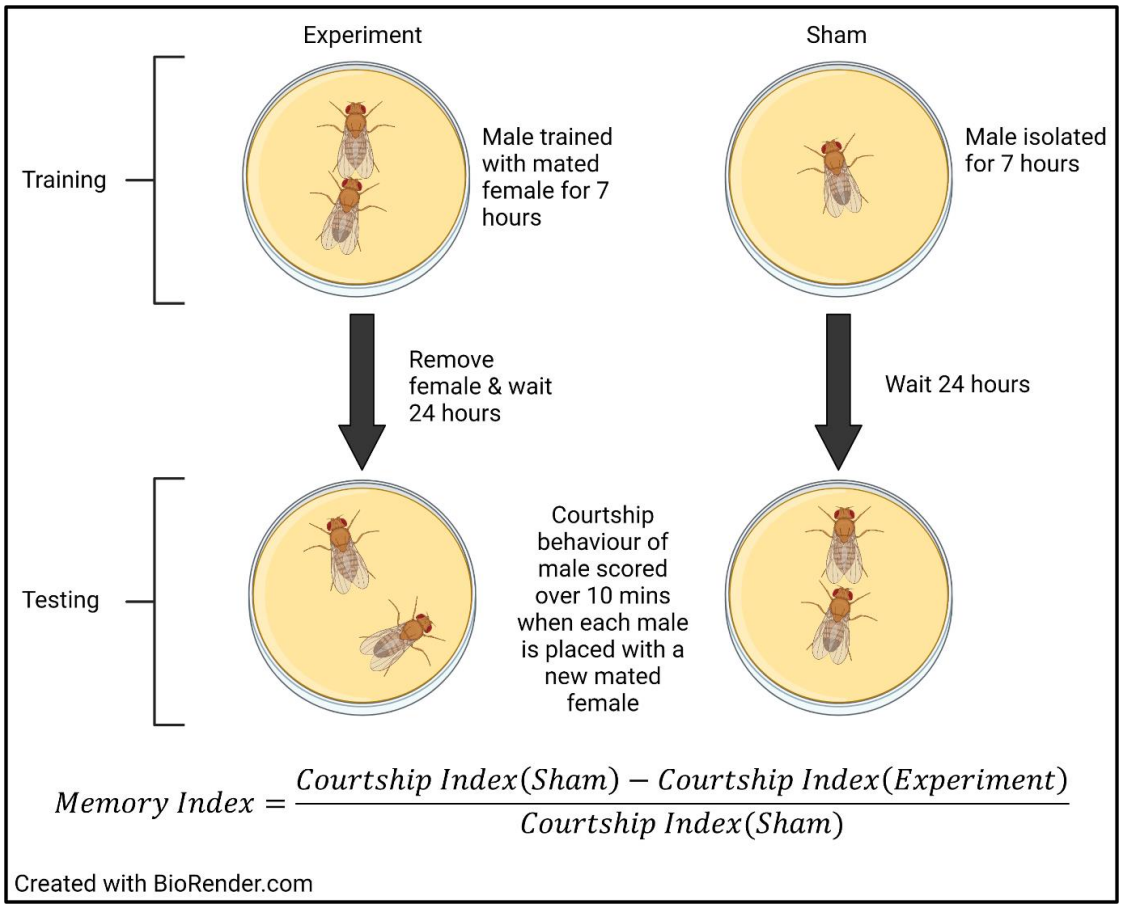

Figure 1.9: *Drosophila* courtship suppression assay
Prior to training, the males will first be isolated individually for 5 days after which a freshly mated female fly will be introduced to the experimental male fly for training for 7 hours while the sham male fly will continue to remain in isolation. After training, the female fly will be removed, and the male will be isolated for another 24 hours. Finally, another freshly mated female will be introduced to both experimental and sham male flies and the proportion of time the males spend courting the female over 10 minutes will be scored to determine the courtship index. A memory index can then be calculated. Typically, at least 20 flies will be tested per genotype.

Generally, both adult male and female flies reach sexual maturity several hours after eclosion. When a male fly initiates mating with a female, it typically starts by orientating itself towards the targeted female and executing a series of behaviours associated with mating attempts. These behaviours include the male tapping the female, "singing" to the female through the rhythmic vibration of a single wing and licking of the genitalia, all of which are observable characteristics. After the female senses the behavioural cues, she then chooses whether to mate with the male (Sokolowski, 2001). If mating occurs, the male pheromone, 11-cis-vaccenyl acetate (cVA), is transferred to the female. When a male has previously experienced rejection behaviours, he will reduce courtship towards other mated females in an enhanced response to cVA. Male flies with memory

impairment will not become sensitised to cVA and will typically attempt copulation again shortly after rejection. Therefore, a typical basic courtship suppression experiment will first involve housing an experimental and sham male fly separately in a chamber alone for 4 to 5 days after which the experimental male will be trained with a mated female for 7 hours to induce courtship suppression memory while the sham male continues to be isolated. After training, the female flies will be removed and after 24 hours, a newly mated female will be introduced to the male fly and the courtship behaviour of the male will be scored over 10 minutes (**Figure 1.9**). The memory index of the fly is calculated by determining proportion of time the experimental and sham males spend courting over 10 minutes (courtship index) and applying it to the formula shown in Figure 1.9. Male flies with impaired memory formation will court at the same level as sham males and thus have a memory index close to 0, whereas the memory index of a male with intact memory will be closer to 1 (Raun, Jones, & Kramer, 2021; Sokolowski, 2001). An intact MB is required for the formation of short-term and long-term courtship memory; control males displayed courtship suppression following training, whereas trained males with an ablated MB did not, indicating impairment of courtship memory (McBride et al., 1999). It was subsequently demonstrated that courtship memory is mediated through a specific class of dopaminergic neurons that innervate the γ lobe, and output from the γ lobe to specific classes of output neurons is required for courtship memory (Zhao, Lenek, Dag, Dickson, & Keleman, 2018).

1.7.1.3 The *Drosophila* compound eye for neurodevelopmental research

The *Drosophila* compound eye is a large organ that is rich in photoreceptor neurons that are organised in a hexagonal formation. Each hexagon is an eye made up of an ommatidia comprising of 8 R cell photoreceptor neurons (R1-8) and 4 non-neuronal cone cells arranged in a stereotypical manner which are surrounded by red pigment glial cells and interommatidial bristle organs. The pigment glial cells form compartmental lattice structures throughout the compound eyes with each compartment housing an ommatidia, thus forming the discrete hexagon units (**Figure 1.10A**). The compound eye differentiates from the eye imaginal disc that develops between the 3rd instar larva and early pupa stages and contains approximately 750 ommatidia units (Baker, Li, Quiquand, Ruggiero, & Wang, 2014; Edwards & Meinertzhagen, 2010). The photoreceptors in the ommatidium

project their axons towards the *Drosophila* optic lobes where visual signals received by the photoreceptors are processed for features such as shape, motion and colour and this information is further transmitted to the neurons in the central complex (Nériec & Desplan, 2016). While the eyes are important for the animal to identify visual cues, impairment to the organ, whether during or post-development, does not affect the viability of the fly. Adult eye phenotypes can be easily visualised using a stereomicroscope or scanning electron microscope (SEM) to observe for changes to the eye colour and/or the ommatidial arrangement which results in "rough eye" phenotypes (**Figure 1.10B, C & D**). These phenotypes which can be scored easily which will indicate the degree of neurodevelopmental perturbation or neurodegeneration based on the number of phenotypes observed. Additionally, the ommatidial arrangement has a very precise formation which makes it easy to identify even the most subtle phenotypes (Baker et al., 2014).

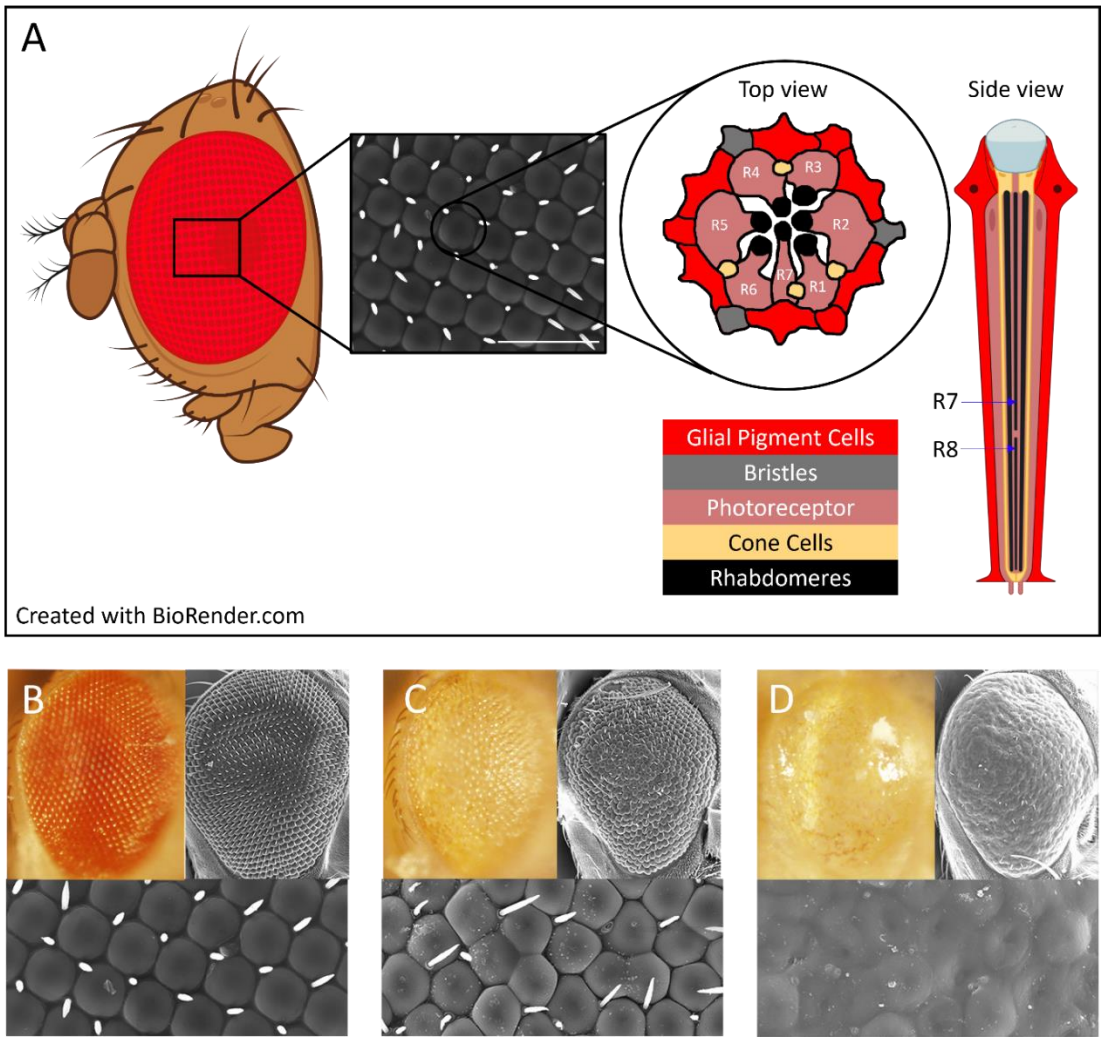

Figure 1.10: Schematic of *Drosophila* compound eyes and an ommatidia unit
(A) *Drosophila* compound eyes comprised of approximately 750 ommatidia. (Top view) Each ommatidia is made up of 8 R cell photoreceptors (R1-8, R8 position is obscured from top view) and cone cells in a hexagonal shaped stereotypical arrangement. Red pigment glial cells surround the ommatidia, thus giving the fly its defining red compound eyes feature. (Side view) R8 is situated below the other R cells with its rhabdomere directly below R7's rhabdomere. (B) represents a normal eye. Some examples of abnormal eye phenotype includes but not limited to (C) partial loss of pigmentation, disorganisation of ommatidia, partial loss of bristles or (D) complete of pigmentation, fused ommatidia and complete loss of bristles. Scale bar=40μm.

1.7.2 The genetic tools of *Drosophila melanogaster*

For over a century since Thomas H. Morgan developed the *Drosophila melanogaster* as a model organism for his study on heredity, the fruit fly model system has been widely used for different biological research particularly in genetic studies (Beckingham, Armstrong, Texada, Munjaal, & Baker, 2005). Since then, there have been many genetic tools and techniques developed by researchers all over the world to help elucidate the molecular mechanism of cellular processes (Beckingham et al., 2005; Spindler & Hartenstein, 2010).

1.7.2.1 The GAL4/UAS system

In the *Drosophila melanogaster* model system, the GAL4/UAS system is one of the most powerful and widely used techniques for functional genetic analysis (Busson & Pret, 2007). This system is based on a transcriptional activation system found in yeast which is the binding of the transcription factor GAL4 to an upstream activating sequence (UAS) of a target gene (Brand & Perrimon, 1993). By adopting this system into the fruit fly model, a binary system can be developed by engineering flies with a GAL4 inserted into the downstream sequence of a tissue-specific promoter or a transgene with a UAS inserted into the upstream sequence (**Figure 1.11**). Through genetic crossing between flies with GAL4 and UAS, the F1 hybrids will possess both the GAL4 and UAS in their genome, thus enabling tissue-specific expression of the transgene. This system has many applications such as the visualisation of cells by fusing reporter genes downstream of the UAS or via expression of effectors or gene KD. KD relies on generating or obtaining specific lines containing siRNA or shRNA (downstream of the UAS) that target a specific gene of interest. The wide usage of this system has led to the accumulation of many GAL4

drivers in libraries of fly lines over many years of *Drosophila* research which allows for expression of a transgene in almost any tissue or cell type by crossing the UAS-transgene line to the appropriate GAL4 driver line. Additionally, there are also libraries of UAS RNAi lines and protein-trap lines available from international stock centres. The availability and ease of obtaining these fly stocks allows for overexpression, KD or tissue visualisation quickly by simply crossing the flies, bypassing the need to generate the transgenic flies (most of the time) which can be time consuming.

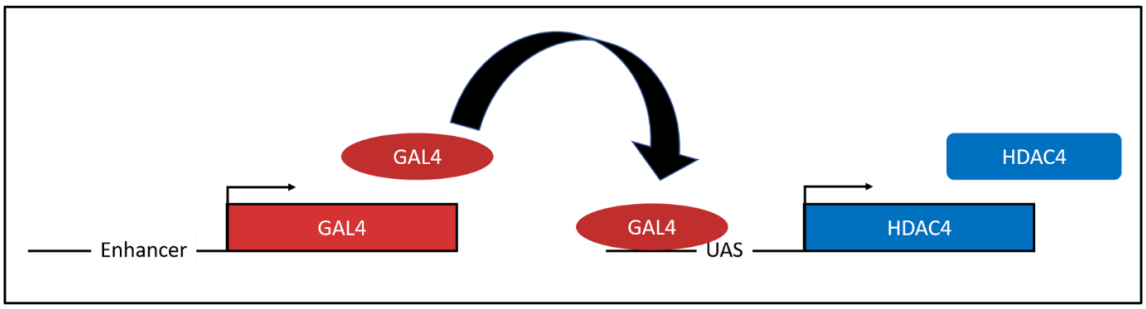

Figure 1.11: Diagrammatic representation of the GAL4/UAS system
A tissue specific enhancer driving the expression of GAL4. GAL4 protein then binds to the UAS to activate transcription of the downstream gene.

1.7.2.2 The TARGET system

There are many genetic tools in the *Drosophila* model that build upon the GAL4/UAS system and one of these tools allows temporal and regional gene expression targeting (TARGET). This relies on the presence of the yeast transcription repressor GAL80 which binds to and represses GAL4. A temperature-sensitive version of GAL80 ($GAL80^{ts}$) is used in this system which allows the temperature to toggle between inactivation (30°C) and activation (18°C) of the repressor (**Figure 1.12A**). Therefore, flies possessing the GAL4/UAS system and a copy of $GAL80^{ts}$ can be manipulated to temporally express the transgene downstream of the UAS in specific tissues at any given time point by increasing or decreasing the temperature (McGuire, Le, Osborn, Matsumoto, & Davis, 2003; McGuire, Mao, & Davis, 2004).

Although the $GAL80^{ts}$ seems to present a dichotomous switch for turning on or off the activity of GAL4, Schwartz et al. (2016) demonstrated that expression of luciferase driven by a MB-specific GAL4 driver in the presence of ubiquitously expressed $GAL80^{ts}$ showed a linear increase in expression as the temperature was linearly increased, indicating that the system is dose-responsive and the level of expression can be fine tuned

by modulating the temperature (**Figure 1.12B)**. This characteristic is potentially useful for moderating the amount of gene expression driven by GAL4.

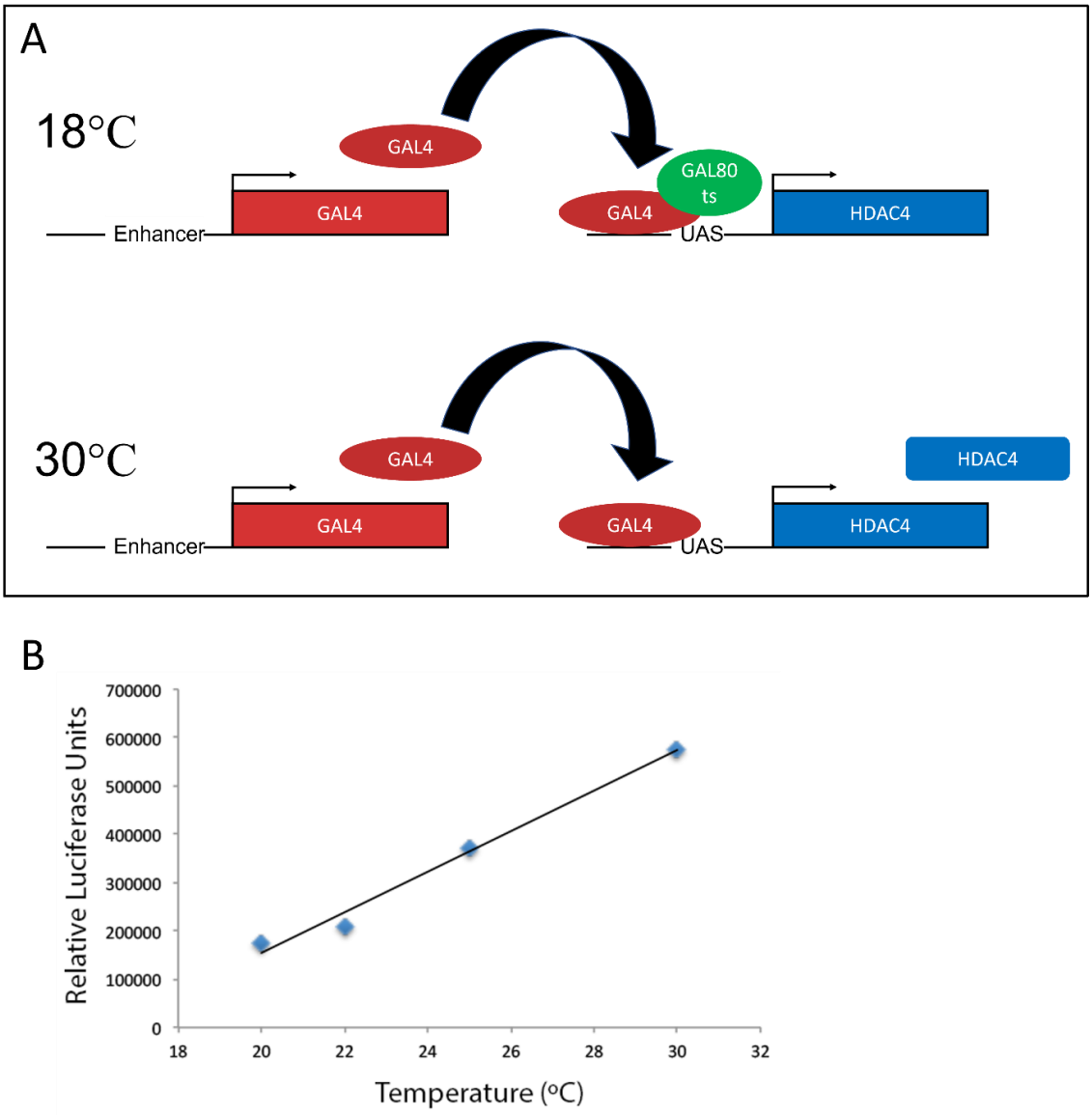

Figure 1.12: Diagrammatic representation of the TARGET system
(A) Ubiquitiously expressed GAL80^{ts} are able to suppress GAL4 transcription activation when exposed to a low temperature (18°C) environment. When the temperature is raised to 30°C, GAL80^{ts} is suppressed, therefore the GAL4/UAS activity is restored. (B) Flies with MB GAL4 driver, tubulin driven GAL80^{ts} and UAS luciferase were incubated at 20, 22, 25 and 30°C for 48 hours and head lysate was used for luciferase assay. Graph from Schwartz (2016) reproduced with permission from Oxford University Press.

1.7.2.3 deGradFP

As mentioned briefly, UAS transgenic lines allow expression of any transgene inserted downstream of the UAS which, depending on the nature of the transgene, is then able to

introduce exogenous functions such as KD or overexpression of a particular gene in a specific cell type. A unique method of KD known as deGradFP was developed recently to target fluorescently-tagged proteins. It relies on a UAS-driven modified F-box containing a fluorescence protein antibody fragment to target fluorescence tagged proteins and facilitate their degradation through complex formation with E3 ligase and ubiquitin-conjugating E2 enzymes (**Figure 1.13**). This method can be used to reduce expression of any gene endogenously tagged with GFP, which then allows simultaneous expression of mutants of the same gene and potentially minimises cross interaction between exogenous and endogenous functions (Caussinus, Kanca, & Affolter, 2011).

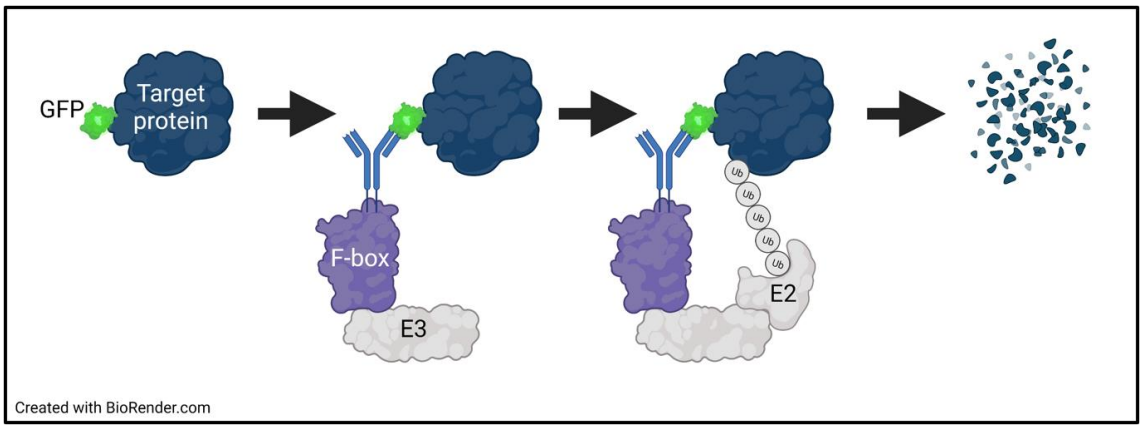

Figure 1.13: Mechanism of deGradFP
The modified *Drosophila* F-box protein with fluorescence protein antibody combines with protein complex, E3 ligase to target GFP tagged protein. The E3 complex than mediates the ubiquitination of the protein E2 which then targets the protein of interest for degradation by proteasome.

1.7.3 *Drosophila melanogaster HDAC4*

The fruit fly genome consists of six HDACs: *Rpd3*, *HDAC3*, *HDAC4*, *HDAC6-S*, *HDAC6-L* and *Sir2*. Similarly, to mammalian HDACs, *Drosophila* HDACs share sequence homology to yeast original enzymes, with *Rpd3* and *HDAC3* belonging to Class I; *HDAC4*, Class IIa; *HDAC6-S* and *HDAC6-L*, Class IIb; and *Sir2*, Class III. Each of the *Drosophila* HDACs has been shown to be unique in its temporal expression patterns and transcriptional targets (Cho, Griswold, Campbell, & Min, 2005). Therefore, the study of *DmHDAC4*, the sole Class IIa HDAC in *Drosophila* allows avoidance of the redundancy effect that could occur between the vertebrate Class IIa isoforms. For example, in a rodent study that showed memory impairment through inactivation of CREB as a result of isoflurane (an anaesthetic) inducing increased nuclear HDAC4, a redundancy effect with

other Class IIa isoform cannot be excluded as other HDACs have been known to interact with CREB (Sen & Sen, 2016).

DmHDAC4 possesses an overall 35% amino acid identity and 59% similarity to human HDAC4 (hHDAC4). Like vertebrate HDAC4, it has a conserved NLS and serine residues that when phosphorylated, bind the chaperone protein, 14-3-3ζ, allowing nuclear localisation and cytoplasmic translocation, respectively (Fitzsimons et al., 2013) (**Figure 1.14**). DmHDAC4 localises predominantly in the cytoplasm of MB neurons, with nuclear HDAC4 detectable in only a subset of MB nuclei. This largely cytoplasmic pattern of distribution is similar to that seen in the mouse hippocampus (Darcy et al., 2010; Fitzsimons et al., 2013). Taken together, the conserved characteristics of DmHDAC4 makes it suitable for modelling HDAC4 function.

Although the deacetylase domains of DmHDAC4 and hHDAC4 are highly conserved (57% amino acid identity and 84% similarity) (Fitzsimons et al., 2013), unlike hHDAC4, DmHDAC4 possesses an active deacetylase domain (Lahm et al., 2007). However, expression of a DmHDAC4 mutant with no deacetylase activity also resulted in impairment of courtship memory in *Drosophila* similar to that induced by DmHDAC4^{WT} (Fitzsimons et al., 2013), highlighting the conserved non-deacetylase dependent role between the two species of HDAC4.

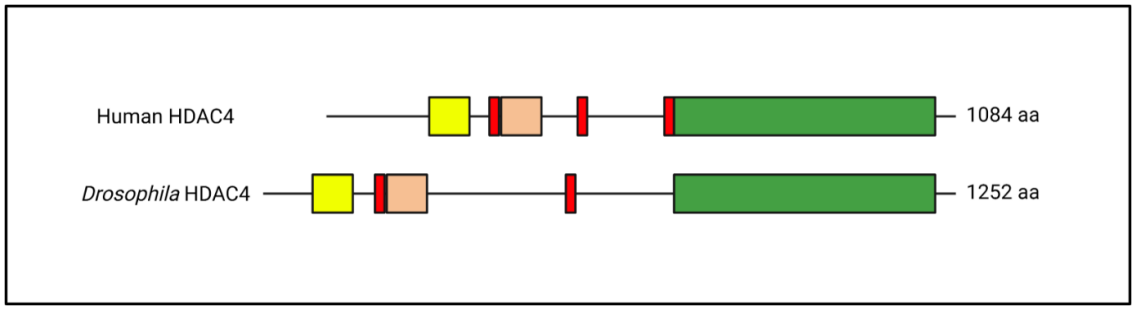

Figure 1.14: Comparison between *DmHDAC4* and *hHDAC4* sequence
(A) Schematics of DmHDAC4 (Isoform D, GenBank accession NP_572868, 1252 amino acids) and human HDAC4 (GenBank accession NP_006028, 1084 amino acids). Yellow boxes represent myocyte enhancer factor 2 (MEF2) binding domains, red boxes represent serine residues that when phosphorylated, are bound by 14-3-3ζ for nuclear export, brown boxes represent NLS sequences and green represents the deacetylase domain.

1.7.4 DmHDAC4 and neuronal function

To date, there have only been two reported studies investigating the role of DmHDAC4 in *Drosophila* neurological function. As briefly introduced in Section 1.6.3, both KD and overexpression of *DmHDAC4* in the MB impaired 24-hour LTM in the courtship memory suppression assay. The impairment resulting from KD of *DmHDAC4* indicates that it is required for normal memory formation, however its overexpression also leads to impairment of memory formation (Fitzsimons et al., 2013; Schwartz et al., 2016). Additionally, overexpression of *DmHDAC4* specifically in the γ neurons of the MB has been shown to impair memory formation, whereas no impairment was observed when *DmHDAC4* was overexpressed in the α/β and α'/β' neurons, indicating the importance of γ neurons in memory formation and differential role between KC subtypes (Fitzsimons et al., 2013). This also emphasizes the importance of targeted expression in subregions of the brain in order to investigate the requirement of HDAC4 in specific neuronal subtypes.

Overexpression of *DmHDAC4* has also been shown to disrupt neuronal development. In a *Drosophila* rough eye phenotype analysis, overexpression of DmHDAC4 disrupts eye development in a dose-dependent manner. Expression of one copy of $DmHDAC4^{WT}$ transgene elicited only a minor rough eye phenotype, while two copies of the transgene severely impacted development, resulting in complete loss of both red pigmentation and disruption of ommatidial arrangement. When overexpressed in the whole brain during neurodevelopment, severe deficits in axon growth and guidance of MB neurons were observed (Schwartz, 2016).

Transcriptome analysis via RNA-Seq on *Drosophila* brains in which HDAC4 was pan-neuronally overexpressed revealed only minimal transcriptional changes. Therefore, a reverse genetic screen relying on the *Drosophila* rough eye phenotype assay was also conducted to identify genetic modifiers of *DmHDAC4*. In addition to identifying genes that have already been known to interact with vertebrate *HDAC4*, novel genes that play a role in transcriptional regulation, SUMOylation and cytoskeletal regulation were also identified (Schwartz et al., 2016). These genetic interactions provide insights into the potential neuronal mechanism of HDAC4 to the roles mentioned and are discussed below in Section 1.8.

Although Schwartz and colleagues (2016) reported minimal transcriptional changes in flies overexpressing *DmHDAC4*, given that HDAC4 is able to shuttle between the nucleus and cytoplasm, it was still unknown during the time when this PhD project was conceived, whether transcriptional changes would be uncovered if DmHDAC4 was restricted to the nucleus.

Taken together, the findings from these studies highlight the need to further investigate the subcellular roles of DmHDAC4 in both normal memory and brain development as well as the molecular mechanisms that underpin the DmHDAC4 overexpression-induced impairments in memory and brain development.

1.8 Potential mechanisms through which HDAC4 regulates neuronal development and memory formation

Over the past decade, there has been a rising interest in the role of HDAC4 in brain research. The association of HDAC4 with neurological disorders affecting cognition such as AD, Ataxia-telangiectasia, HD, PD, BDMR and autism highlight the need to better understand the mechanistic role of HDAC4 (Anderson et al., 2015; Cao et al., 2008; Li, Chen, et al., 2012; Mielcarek et al., 2013; Sen et al., 2015; Shen et al., 2016; Villavicencio-Lorini et al., 2013; Williams et al., 2010; Wu et al., 2017; Wu et al., 2016). Some studies relating to these roles of HDAC4 were briefly described in the earlier section on its involvement in learning and memory or neurodevelopment as well as activities outside the traditional HDAC enzymatic role (Fitzsimons et al., 2013; Li, Chen, et al., 2012; Sando et al., 2012; Wang, Cheng, et al., 2011). Further description and evidence for additional potential mechanisms through which HDAC4 may influence neuronal development and memory are described in the following sections.

1.8.1 Complex formation of HDAC4 with HDAC3

In vertebrates, the deacetylase domain of HDAC4 is reported to be inactive (Bottomley et al., 2008). However, it has been shown to facilitate deacetylation indirectly through complex formation with the nuclear receptor corepressor 1 (NCoR), the silencing

mediator for retinoid and thyroid hormone receptors (SMRT) and HDAC3. When the complex formation was blocked, deacetylase activities were shown to be inhibited. Therefore, deacetylation is facilitated through the catalytic domain of HDAC3 when the SMRT/NCoR·HDAC3 complex is formed and HDAC4 could serve as a bridge for transcription regulation by the complex to target transcription factors such as MEF2 (Fischle et al., 2002) (**Figure 1.15**). The formation of this complex has also been associated with learning and memory in mice where deletion of *HDAC3* was shown to enhance LTM formation alongside a reduction in *HDAC4* expression (McQuown et al., 2011).

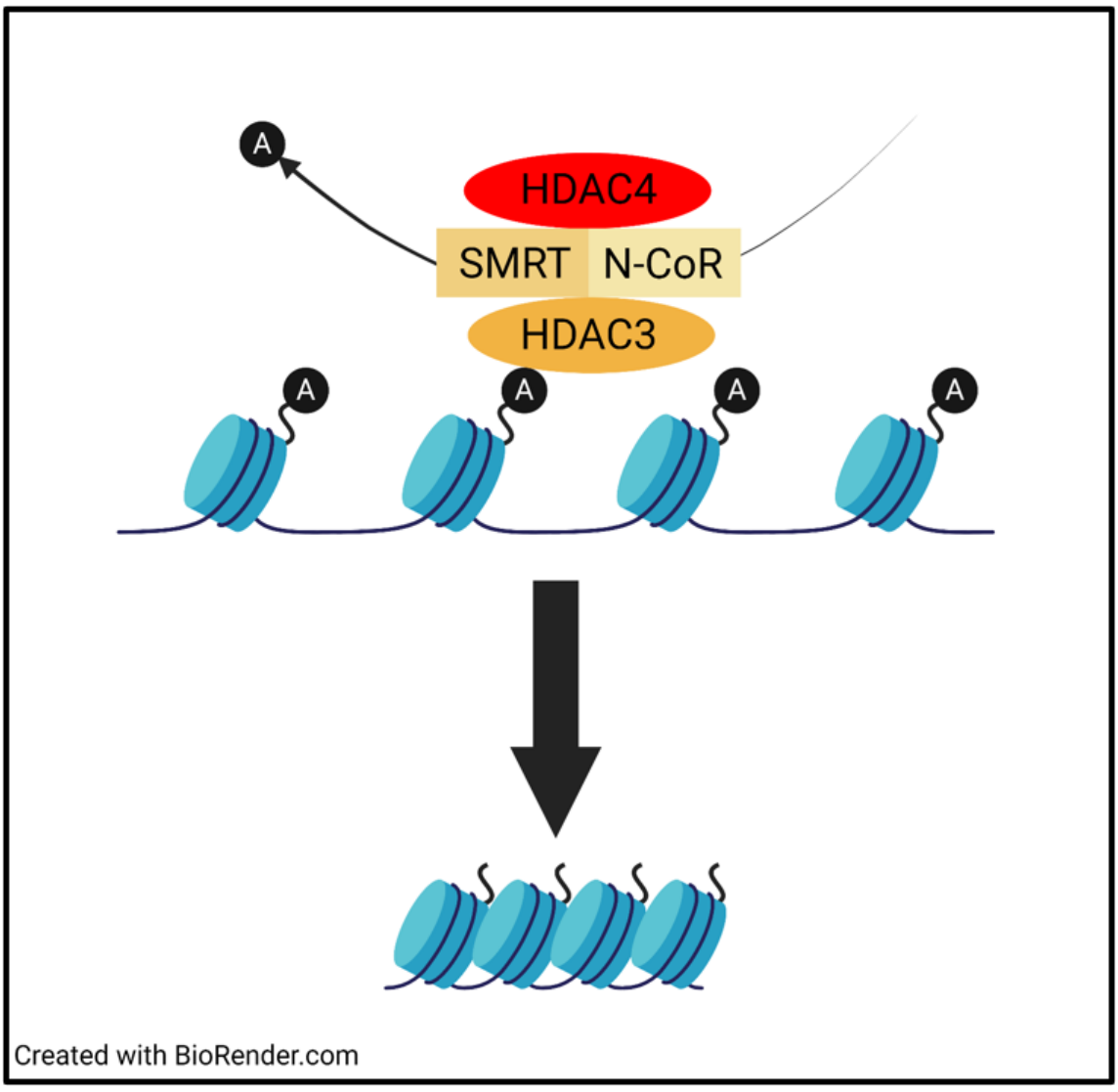

Figure 1.15: HDAC4 mediates HDAC3 deacetylation of histones
HDAC4 forms a complex with SMRT/NCoR·HDAC3 in the nucleus to deacetylate histones via HDAC3 catalytic domain.

1.8.2 Interaction of HDAC4 with MEF2

The most commonly reported interactors of HDAC4 are transcription factors, and as mentioned in Section 1.6.3, several of these transcription factors including CREB, MEF2 and SRF have been implicated in the processes of memory formation. Among these, MEF2 and SRF have been the least studied in the context of learning and memory. MEF2 is traditionally known for its role in transcription activation in myocytes but has also been implicated in neuronal development, synaptic function and memory (Barbosa et al., 2008; McKinsey, Zhang, & Olson, 2002; Shalizi et al., 2006). Elucidating the role of MEF2 in learning and memory has been an emerging topic of research and unlike most transcription factors, it has been suggested to be a repressor of memory formation (Rashid, Cole, & Josselyn, 2014). The interaction between HDAC4 and MEF2 is a direct physical binding between the MEF2-binding domain located near the N-terminus of the HDAC4 protein (**Figure 1.16**), and early studies identified that HDAC4 represses the activity of MEF2 in the nucleus (Miska et al., 1999). Further investigation of this interaction may assist in understanding whether the impairments to memory formation following KD of *HDAC4* are due to the de-repression of MEF2, which would result in increased transcription of MEF2 target genes (Fitzsimons et al., 2013).

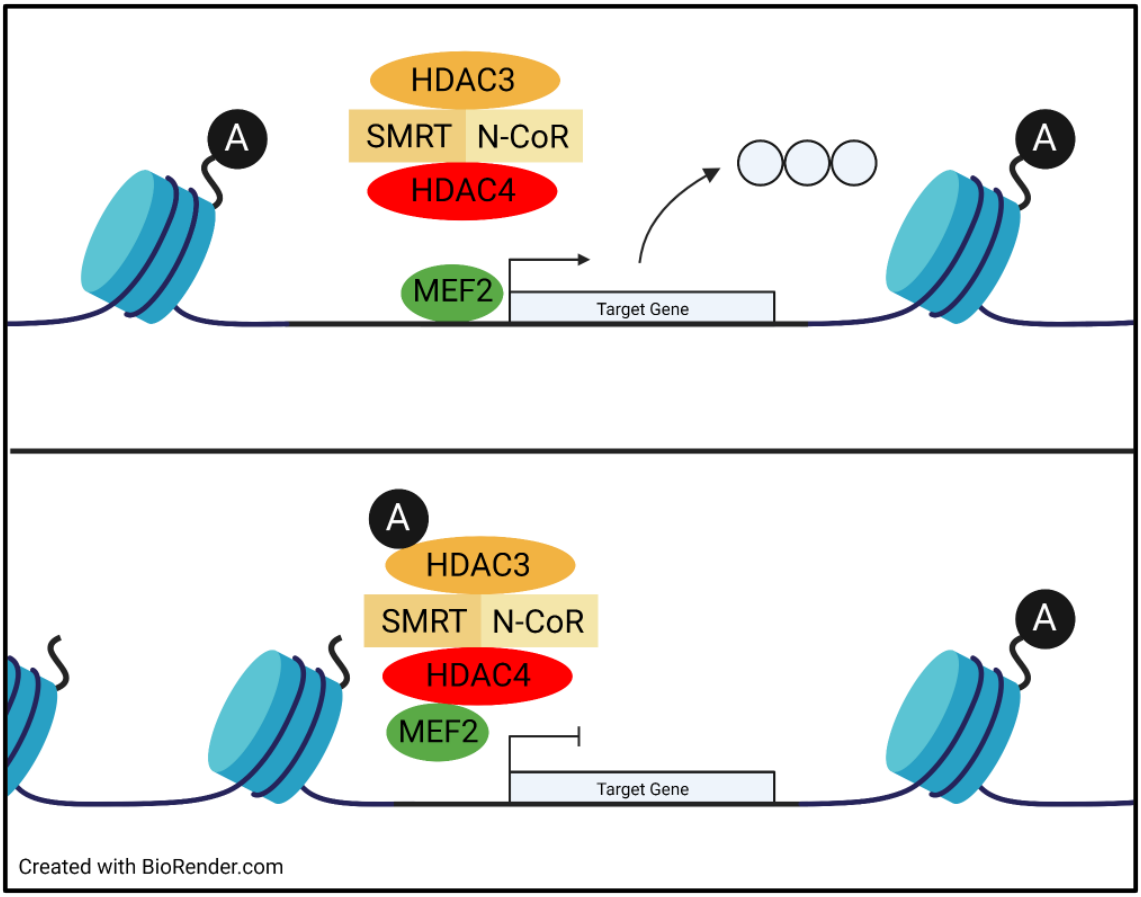

Figure 1.16: HDAC4 represses transcriptional activity by MEF2
HDAC4 can directly bind to MEF2 in the nucleus and might have served as a bridge for SMRT/NCoR·HDAC3 complex to deacetylate histone, leading to chromatin condensation which results in suppression of transcription activity.

As mentioned in the previous section, HDAC4 may serve as a bridge to guide the SMRT/NCoR·HDAC3 complex by binding MEF2 to inhibit its transcriptional targets (**Figure 1.16**). However, a point mutation in HDAC4 which results in defective MEF2-binding domain has been shown to restrict HDAC4 localisation to the cytoplasm in 3T3 fibroblast cells (Wang & Yang, 2001). The nucleocytoplasmic shuttling of HDAC4 is regulated through the phosphorylation of three serine resides, S246, S467 and S632 and when it is constitutively phosphorylated, it binds to the chaperone 14-3-3ζ which escorts it to the cytoplasm where it remains while phosphorylated (**Figure 1.17**) (McKinsey, Zhang, & Olson, 2000).

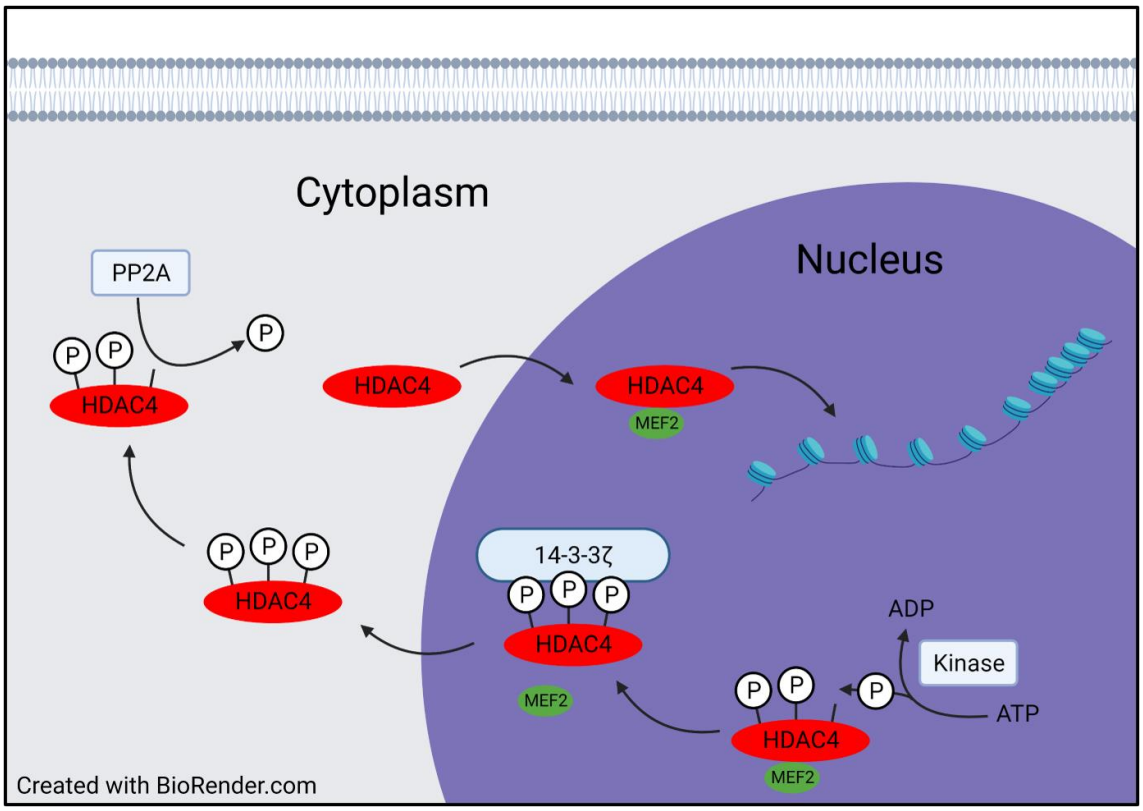

Figure 1.17: HDAC4 nucleocytoplasmic shuttling
Phosphorylated HDAC4 recruits chaperone protein, 14-3-3ζ, for translocation to the cytoplasm. Dephosphorylation of HDAC4 by PP2A leads to nuclear import where it is able to bind the transcription factor, MEF2, and repress its activity.

However, inhibition of myogenesis by HDAC4 repression of MEF2 can be rescued through CaMK signalling. This appears to be paradoxical in that phosphorylation by CaMK results in cytoplasmic retention of HDAC4, but MEF2-binding to HDAC4 is sufficient for nuclear retention (Wang & Yang, 2001). Therefore, the authors suggest that HDAC4 may undergo a change in phosphorylation status when it binds to MEF2 in the nucleus which could result in an eventual gain of sensitivity to CaMK signalling and phosphorylation, thus allowing the binding of 14-3-3ζ in order for it to be transported out into the cytoplasm (McKinsey et al., 2000; McKinsey, Zhang, & Olson, 2001). More recently, *de novo* mutations in the HDAC4 14-3-3ζ binding site were discovered in patients who presented features of developmental delay and/or intellectual disability (Wakeling et al., 2021). The association of the defective binding site with a neurodevelopmental disorder of unknown cause further highlights the importance of investigating the neurological roles of the subcellular pools of HDAC4.

The role of MEF2 in learning and memory was first observed through the promotion of dendritic spine growth following KD of MEF2 (Flavell et al., 2006; Rashid et al., 2014; Shalizi et al., 2006). Moreover, enhanced MEF2 activity resulted in a reduced number of excitatory synapses and dendritic spines in cultured hippocampal neurons (Flavell et al., 2006). MEF2 has also been shown to inhibit excitatory input (dendritic claw) formations in cultured cerebellar granule cells (Shalizi et al., 2006). These data may, therefore, indicate a reduction of the synaptic strength that is important for memory formation. Indeed, there have been several studies that observed downregulation of MEF2 expression and activity during learning and memory (Rashid et al., 2014). The formation of spatial and fear memories in mice has been associated with a reduction in MEF2-mediated transcription (Cohen & Greenberg, 2008; Greer & Greenberg, 2008). It could therefore be logical to hypothesise that nuclear HDAC4 represses MEF2 to promote LTP formation. However, on the contrary, a nuclear-restricted HDAC4 variant also represses memory formation. This may be due to complex formation of HDAC4 with SMRT/NCoR·HDAC3 resulting in suppression of plasticity-related genes (Sando et al., 2012; Shu et al., 2018). Therefore, the interaction between HDAC4 and MEF2 is complex and highlights the need for further research to tease apart the nuclear and cytoplasmic roles of HDAC4.

1.8.3 Interactors of cytoplasmic HDAC4 and SUMOylation

Although HDAC4 dynamically shuttles between the nucleus and cytoplasm, in cultured neurons it is predominantly localised to the cytoplasm (Chawla et al., 2003). The studies by Wang, Cheng, et al. (2011) and Li, Chen, et al. (2012), respectively, showed an enhancement in memory performance in *C. elegans* and improvement in motor performance in $Atm^{-/-}$ mice when a cytoplasm-restricted HDAC4 variant was introduced. These could suggest a pro-memory effect or neuroprotective role of cytoplasmic HDAC4 (Fitzsimons, 2015). Despite the lack of focus on the potential functions of HDAC4 in the cytoplasm, there has been some efforts focused on identifying its cytoplasmic interactors through mass spectrometry analysis. Paroni et al. (2008) found that HDAC4 interacts physically with motor proteins involved in subcellular trafficking as well as cytoskeletal components such as tubulin and alpha-spectrin (**Figure 1.18**). These interactors could play a significant role in protein transportation since HDAC4 has also been shown to

localise at the post-synaptic density, a composition of proteins at the post-synaptic membrane required for synaptic functions (Darcy et al., 2010).

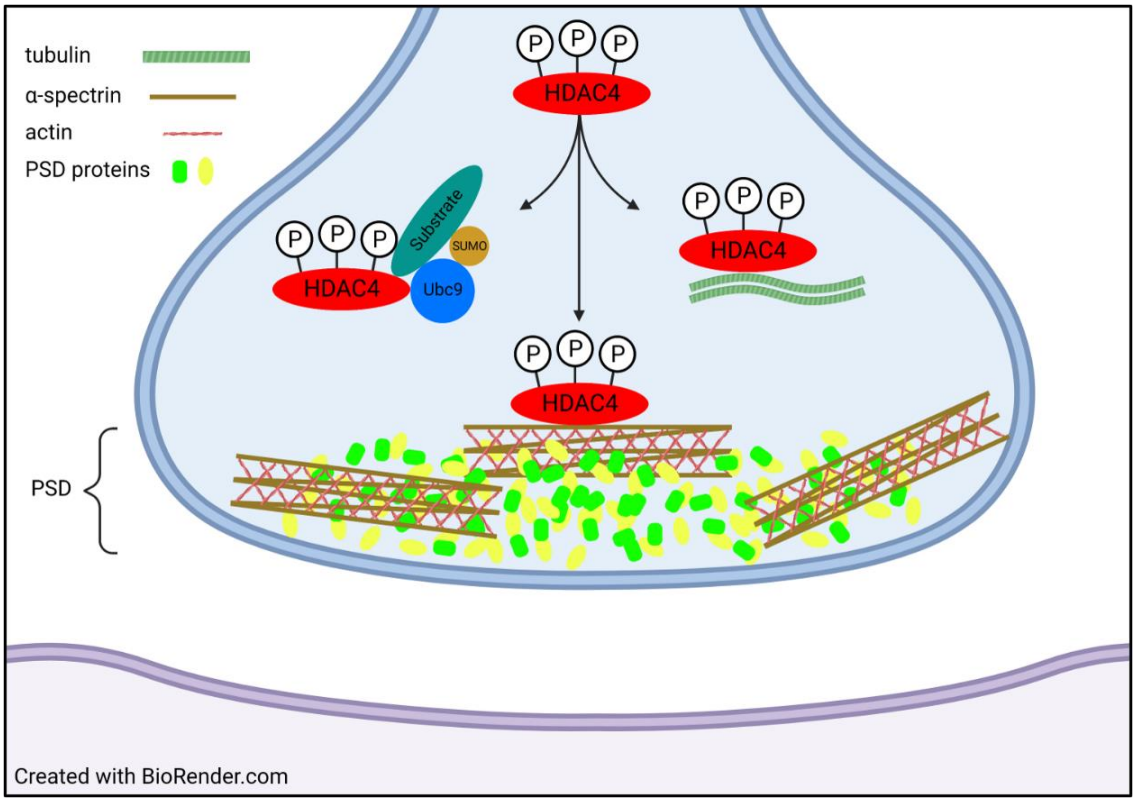

Figure 1.18: Potential role of cytoplasmic HDAC4
In the cytoplasm, HDAC4 has been shown to interact with tubulin and alpha-spectrin. HDAC4 is also able to interact with SUMO-conjugating enzymes to mediate SUMOylation of substrates.

In a *Drosophila* screen for genes that interact genetically with HDAC4, several genes that encode enzymes in the SUMOylation machinery were identified. SUMOylation is an enzymatic post-translational modification process where protein substrates are conjugated to small ubiquitin-like modifier (SUMO) proteins through covalent bonding to be targeted for functional modification and subcellular redistribution. This process is similar to ubiquitination with the difference being that proteins are tagged for degradation in the latter process (Fitzsimons, 2015). The conjugation of SUMO to target proteins is facilitated by SUMO E3 ligase enzymes, and a study by Gregoire and Yang (2005) indicated that HDAC4 enhances SUMOylation of MEF2 in nuclei of cultured myoblast, suggesting it may act as a SUMO E3 ligase. This may have some relevance to HDAC4 role in learning and memory as the importance of SUMOylation in neurons has been highlighted in several studies (Craig & Henley, 2012; Martin, Wilkinson, Nishimune, &

Henley, 2007; Scheschonka, Tang, & Betz, 2007). Interestingly, the SUMOylation enzymes are localised to the synaptic terminals of rat hippocampal neurons and SUMOylation of synaptic proteins is modulated by neuronal activity, with depolarisation of the neurons resulting in a transient increase in activity of the SUMO-conjugating enzymes, Aos1 and Ubc9, at the presynaptic terminal (Loriol, Khayachi, Poupon, Gwizdek, & Martin, 2013). *DmHDAC4* has been shown to genetically interact with *Ubc9*, where simultaneous overexpression of *DmHDAC4* and KD of *Ubc9* in the MB resulted in a synergistic increase in memory impairment in the courtship assay (Schwartz et al., 2016). Taken together, these data indicate that further investigation into the role of HDAC4 with the SUMOylation machinery may reveal more insights into the role of *HDAC4* in memory formation (**Figure 1.18**).

1.8.4 Interaction of *HDAC4* and *Ankyrin 2*

A *Drosophila*-based genetic screen conducted by Schwartz et al. (2016) discovered a genetic interaction between *DmHDAC4* and the *Drosophila Ankyrin* genes, *Ankyrin 1* (*Ank1*) and *Ankyrin 2* (*Ank2*). The ankyrins are a family of ubiquitously expressed adaptor proteins that are involved in linking membrane-associated proteins with the spectrin cytoskeleton (Bennett & Baines, 2001). Examples of these membrane proteins include anion exchangers, voltage-gated ion channels and L1 cell adhesion molecules (L1CAM) (Mohler, Gramolini, & Bennett, 2002), all of which are required for normal synaptic plasticity (Maness & Schachner, 2007; Voglis & Tavernarakis, 2006). The interactions between *DmHDAC4* and the two *Ankyrin* genes were first identified in a *Drosophila* rough eye enhancer-suppressor screen in which KD of both *Ank1* and *Ank2* caused an enhancement of the rough eye phenotype resulting from overexpression of *HDAC4*, suggesting that they act in the same molecular pathway to influence photoreceptor development (Schwartz et al., 2016). Further investigation revealed that simultaneous overexpression of *HDAC4* and KD of *Ank2* specifically in the mushroom bodies resulted in significantly increased impairment in long-term courtship memory, however unlike *Ank2*, *Ank1* was found to be dispensable in MB development (Schwartz, 2016). The genetic interaction with *Ank2* is perhaps not surprising considering HDAC4 harbours an ankyrin repeat-binding domain which has been known to attract proteins containing ankyrin repeats such as ankyrin repeat family A protein 2 (ANKRA2) and regulatory

factor X associated ankyrin-containing protein (RFXANK) (McKinsey, Kuwahara, Bezprozvannaya, & Olson, 2006; Wang et al., 2005). In fact, preliminary GST pull-down assay by Schwartz (2016) did suggest binding between HDAC4 and Ank2. However, it was uncertain whether the interaction between the two proteins was a result of direct or indirect binding (Schwartz, 2016) and was unable to be verified by coimmunoprecipitation (Schwartz, Wilson, Hale, & Fitzsimons, 2021).

In humans, two separate studies on autism have associated both *Ankyrin 3* (*Ank3*) (human homologue of *Drosophila Ank2*) and *HDAC4* with this neurodevelopmental disorder (Bi et al., 2012; Nardone et al., 2014). Whole-genome sequencing of individuals with autism revealed mutations in the *Ank3* gene (Bi et al., 2012) and moreover, analysis of DNA methylation showed HDAC4 to be highly expressed in individuals with autism (Nardone et al., 2014). Taken together, these data suggest an important interacting role between *HDAC4* and ankyrins in both memory formation and neurodevelopment which warrants further investigation.

2. AIMS & OBJECTIVES

To date, the studies on the role of *HDAC4* in the brain have yielded promising results that recognise its importance in memory formation as well as differential roles in the nucleus and cytoplasm (Kim et al., 2012; Sando et al., 2012). By assessing memory performance in animal models in which mutant variants of *HDAC4* were expressed in neurons, nuclear-restricted *HDAC4* mutant has been shown to impair memory and a cytoplasm-restricted *HDAC4* mutant appears to have a neuroprotective or pro-memory role (Sando et al., 2012; Wang, Cheng, et al., 2011).

In *Drosophila*, HDAC4 is also involved in learning and memory, however, memory impairment was observed when *DmHDAC4* was both knocked down or overexpressed, which suggests it is required for normal memory formation but also represses memory when increased in abundance (Fitzsimons et al., 2013). However, it still is unclear how the nuclear and cytoplasmic activities of DmHDAC4 impact neuronal function in *Drosophila*, i.e., whether the essential role of HDAC4 in normal memory formation is due to pro-memory activities in the nucleus, or cytoplasm, or both. It is also unclear what mechanisms are involved in the neurodevelopmental or memory formation processes and whether they are mediated through deacetylase activity, MEF2-binding and/or ankyrin-binding. Moreover, Schwartz (2016) conducted RNA-Seq experiments on brains expressing $DmHDAC4^{WT}$ to identify potential target genes that may be involved in mechanistic pathways of neuronal processes, however minimal transcriptional changes were observed. It is unclear whether this indicates that HDAC4 acts largely through non-transcriptional mechanisms in the brain or whether the predominant cytoplasmic localisation is masking transcriptional changes that may be elicited by nuclear HDAC4. These data emphasise the importance of assessing the impact of both nuclear and cytoplasmic-restricted mutants which may reveal processes that are not revealed through analysis of the phenotypic and transcriptional changes resulting from $DmHDAC4^{WT}$ overexpression.

This project will focus on the following objectives to attempt to address some of these gaps in knowledge:

1) **To determine the role of DmHDAC4 in neuronal function through the use of subcellular and domain specific mutant variants.**

Prior to the commencement of this project, transgenic fly lines that expresses UAS driven *DmHDAC4*^{WT} as well as other mutant variants have already been generated. Therefore, the first objective will start with characterising the expression of subcellular distribution of the DmHDAC4^{WT} and the mutant variants in KC neurons. This will be followed by assessment of the impact these lines have on the development of the KCs axons that form the MB lobes, and the eye.

The original objectives that were included in this aim also includes performing courtship suppression assay on flies expressing the variants to evaluate memory. However, due to time constraints, this analysis was eventually excluded to focus on the developmental aspect of neuronal function (refer to **Appendix 9.6: Explanation of COVID-19 Impacts DRC Form**).

The hypotheses for this aim are as follow:

-Overexpression of DmHDAC4^{WT} impairs neurodevelopment.

-Overexpression of nuclear-restricted DmHDAC4 will increase impairment of neurodevelopment.

-Overexpression of cytoplasmic-restricted DmHDAC4 will alleviate impairment of neurodevelopment.

-Overexpression of DmHDAC4 domain mutants will increase impairment of neurodevelopment.

2) To examine the transcriptional changes in whole fly head as a result of *DmHDAC4* variants overexpression.

RNA from fly heads pan-neuronally expressing DmHDAC4 or the mutant variants will be extracted and processed for RNA-Seq. The resulting transcriptional profiles will be analysed to determine gene targets of pathways regulated by the variants.

3) **Identify downstream targets of DmHDAC4 and pathways that can be implicated based on analysis of transcriptional changes.**

The results from the RNA-Seq analysis will allow identification of differentially expressed genes and determine potential genetic pathways that are affected when DmHDAC4 or its variants are overexpressed. Gene candidates can then be selected and assessed to determine whether KD of each gene results in similar phenotypes as HDAC4 overexpression, and subsequent genetic interaction studies will also be performed to determine whether the genes interact with HDAC4 (refer to **Appendix 9.6: Explanation of COVID-19 Impacts DRC Form**).

3. MATERIALS AND METHODS

3.1 Fly stocks and maintenance

The fly lines used in this study are listed in the appendix (**Supplementary Table 9.17**). Flies were raised on standard fly food media (10 g/L agar, 130 g/L sugar, 40 g/L yeast, 110 g/L ground cornmeal, 23.7 g/L molasses, 3.3 g/L methyl 4-hydrobenzoate (Moldex) and 3.5% ethanol). Flies were kept under a 12-hour light/dark cycle and raised in a controlled 25°C environment unless otherwise indicated. Fly food media was replaced approximately every 21 days for each fly lines to ensure continual healthy generation of progeny.

The *white* mutant Canton-Special fly line (*w(CS10)*) (**Supplementary Table 9.17 #1**) was used in control crosses. *ElavGAL4;tubGAL80^{ts}* and *OK107GAL4;tubGAL80^{ts}* were used as pan-neuronal and MB TARGET drivers respectively (**Supplementary Table 9.17 #23 & 24**). *GMR-GAL4* was used as an eye-specific driver (**Supplementary Table 9.17 #5**). The UAS driven DmHDAC4^{WT} and mutant variants were original fly lines designed in this laboratory with the plasmid synthesis and site-directed mutagenesis carried out by Genscript (New Jersey, USA) and the transgenic flies generated by GenetiVision (Houston, TX) (refer to Section 3.2) (**Supplementary Table 9.17 #11-16, #29-31**). The mutation of *UAS-DmMEF2-T148A-HA* was designed with reference to the study by Crittenden, Skoulakis, Goldstein, and Davis (2018) and the construct was also generated by Genscript and transgenic line generated by GenetiVision (refer to Section 3.2) (**Supplementary Table 9.17 #32**)

The KD lines *UAS-HDAC4 RNAi(shRNA), UAS-HDAC4 RNAi(dsRNA), UAS Pepck RNAi #1, UAS Pepck RNAi #2, UAS tobi RNAi #1, UAS tobi RNAi #2* and *UAS Teq RNAi* were obtained from Vienna *Drosophila* Resource Center (VDRC) and *UAS-Nslmb-vhhGFP4(2), UAS-Nslmb-vhhGFP4(3), UAS nebula RNAi and Rh-Marf RNAi* were obtained from the Bloomington *Drosophila* Stock Center (BDSC) (**Supplementary Table 9.17 #7-10, #33-39**). Fly lines with multiple transgenes on the same chromosome were generated in-house through meiotic recombination within fly crosses (**Supplementary Table 9.17 #17-22**). The Split GAL4 lines which includes *γ lobes Split GAL4, α/β lobes Split GAL4* and *α'/β' lobes Split GAL4* were obtained from BDSC (**Supplementary Table 9.17 #25-27**).

3.2 Generation of transgenic lines

The open reading frame of *DmHDAC4*^{WT} (nucleotides 461 – 4216 of NCBI reference sequence NM_132640) was synthesised with a C-terminal 6x*Myc* tag and subcloned into the pUASTattB plasmid (Groth, Fish, Nusse, & Calos, 2004) by Genscript to create pUASTattB-DmHDAC4. This plasmid contains a 5x*UAS* sequences and an attB site for homologous recombination into the *Drosophila* genome, and the mini-*white* gene (*mw*$^{+}$) for selection of transformants. HDAC4 variants were generated by site directed mutagenesis by Genscript (see **Appendix 9.1**).

pUASTattB-DmMEF2-HA (nucleotides 1057 – 2601 of NCBI reference sequence NM_057670.5 with a C-terminal 3x HA tag) and pUAST-DmMEF2 T184A were generated via site directed mutagenesis of nucleotides 1498-1500, ACG to GCC (see **Appendix 9.2**).

Transgenic flies were generated by GenetiVision with the insertion into the attP site on chromosome 3L at 68A4 (P2 strain, *DmHDAC4*^{WT} and variants) and chromosome 2R at 57F5 (VK22 strain, *DmMEF2* T148A). Progeny were outcrossed to *w(CS10)* and transformant F1 progeny flies were selected by their orange eye colour (indicating the presence of *w*$^{+}$) and further outcrossed 5 times into the *w(CS10)* genetic background.

3.3 Fly crossing and sample size selection

Manipulation of gene expression was carried out by selecting appropriate GAL4 lines and crossing them to the desired UAS lines (**Figure 3.1**). A typical cross was set with at least five males and five females in vials or ten males and ten females in bottles. Flies were left in their respective containers of fly food media for three days in 25°C (unless otherwise stated) to ensure mating and sufficient production of fertilised eggs. Parental flies were then discarded after three days to prevent progeny overcrowding.

In experiments that require incorporation of more than two transgene in the same or different chromosome, flies were generated by first crossing to balancer chromosome (see **Supplementary Figure 9.3** for example) via the standard fly crossing method mentioned above.

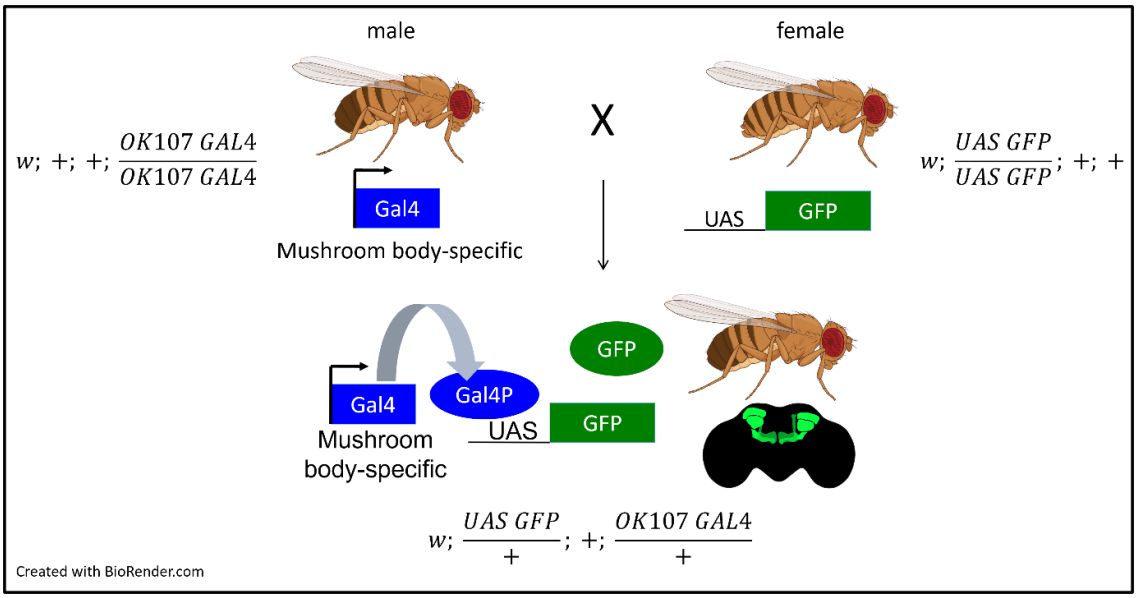

Figure 3.1: Example of a *Drosophila* genetic cross
An example of a genetic cross between a male homozygous for MB driver *OK107-GAL4*, on the fourth chromosome with a female homozygous for *UAS-GFP* on the second chromosome. The F1 will possess one copy of *OK107-GAL4* and *UAS-GFP* transgenes and thus allow the visualisation of the MB via confocal microscopy. Chromosome positions are relative to the position between each semicolon which indicates the separation between chromosome. (;) denotes the separation between chromosome.

The sample size selection from progenies derived from fly crosses varies with the type of experimental analysis. Sample size for rough eye phenotype assay was selected at between 6 to 12 flies as the phenotype for each genotype was observed to be consistent across all samples (further explanation in Section 3.4). However, the samples for assessing MB morphology had high variability, therefore a larger sample size was required. Based on previous experiments conducted in the lab for analysis of MB phenotypes, a sample size of 20 was considered sufficient to see a significant difference between groups.

3.4 Rough eye phenotype assay

The rough eye phenotype assay is one of the most powerful and efficient tools for *Drosophila* genetic studies. It relies on the detection of morphological changes to the eye as a result of gene manipulation to determine if a gene has a role in development. This genetic screen is useful for preliminary studies to identify potential candidates or gene function, usually via overexpression or KD.

This assay relies on the promoter element, *glass multiple reporter* (GMR), to drive the expression of GAL4, which is a commonly used driver for expression of transgenes specifically in developing *Drosophila* retina (Li, Li, Zheng, Zhang, & Xue, 2012). *GMR-GAL4* flies were crossed to UAS lines and F1s were raised at the specified temperature. After eclosion, adult eyes were examined under a light microscope (Olympus SZX12, DP controller imaging software, manual exposure, ISO 200, zoom 108mm, exposure time 1/20sec) and scored for abnormal eye phenotypes. As it was observed that all samples within the same genotype displayed similar phenotypes but there was high variability across different genotypes, a qualitative approach was used to assess the phenotype severity (Schwartz et al., 2016). The core phenotypes observed were changes to bristle arrangement, ommatidia arrangement, loss of pigmentation and the presence of necrotic tissue. These phenotypes can manifest in any combination with varying severity across different genotypes, therefore each of the phenotypes were deemed as a category and assigned an incremental score base on its severity. For example, for the ommatidia phenotype, it was noted that the most severe phenotype is complete fusion of ommatidia, therefore, this phenotype was assigned a severity score of 1.00. Subsequently, any phenotypes within the category of ommatidia that were milder were assigned half the score of the next severity level (e.g. partial ommatidia fusing: 0.50, disorganised ommatidia: 0.25). Since all samples within a genotype exhibited the same phenotype, the phenotypes were tabulated in a table based on the score and the total score of each genotype provided a numerical measure of severity across the different genotypes.

3.5 Scanning electron microscopy (SEM)

F1 progeny of the same flies that were imaged by light microscopy were anesthetised with FlyNap (Carolina) before being transferred to a vial of primary modified Karnovsky's fixative (3% gluteraldehyde, 2% formaldehyde in 0.1 M phosphate buffer, pH 7.2) and Triton X-100 and incubated at room temperature for approximately 24 hours. Following fixation, fly samples were washed in phosphate buffer (0.1 M, pH 7.2) 3 times for 10 minutes each, followed by dehydration in a series of graded ethanol steps (25%, 50%, 75%, 95%, 100%), each lasting 10 to 15 minutes with the final step for 1 hour. After dehydration, samples were critical point dried using liquid CO_2 and 100% ethanol (Polaron E3000 series II critical point drying apparatus). The dehydration and critical

point drying steps were performed by Mr Raoul Solomon at the Manawatu Microscopy and Imaging Centre (MMIC), School of Natural Sciences, Palmerston North. After samples had been dried, fly heads were gently detached from the body by cutting the neck using a surgical blade. The heads were then mounted onto aluminium stubs before being sputter coated in gold (Baltex SCD 050 sputter coater). The mounted head samples were then imaged using the FEI Quanta 200 Environmental Scanning Electron Microscope at an accelerating voltage of 20 kV.

3.5 SDS-PAGE and Western blotting

For the preparation of fly head lysates, approximately 50 male flies were collected for each genotype and stored separately in 15 mL tubes. The tubes were submerged in dry ice/ethanol bath after which they were vortexed to snap the fly heads from the bodies. The heads were quickly separated under a dissecting microscope on a 5 cm by 10 cm piece of transparency sheet placed over dry ice. The whole-cell lysate was extracted from the heads using 50 µL of RIPA buffer (150 mM sodium chloride, 50 mM Tris pH 8.0, 0.1% Triton X-100, 0.5% sodium deoxycholate, 0.1% SDS) with cOmplete^{TM} EDTA-free protease inhibitor (Roche) and homogenised using a motorised pestle for approximately 30 seconds. Homogenates were then centrifuged at 13,000 g for 2 minutes at 4°C and the supernatant was retained as the whole-cell extract. The Pierce BCA Protein Assay Kit (ThermoFisher) was used to quantify for the protein concentration. A set of protein standards provided by the kit was used to produce the standard curve and each standard and lysate sample were measured in triplicates. The 562 nm absorbance read was measured using the BioTek PowerWave XS plate reader and analysed in Excel to determine the protein concentration (µg/µL) based on the standard curve plot. Following protein quantification, 30 µg of each sample was loaded onto a precast 4-20% gradient gel (Mini-PROTEAN TGX Gels) and resolved at 30 V for the first 15 minutes before increasing to 180 V for approximately another hour. Proteins were transferred onto a nitrocellulose membrane and blocked for at least one hour in 5% skim milk in TBST (20 mM Tris, 150 mM sodium chloride, 0.1 % Tween-20, pH 7.6). Each membrane was incubated overnight at 4°C in the appropriate primary antibody (**Table 3.1**) and one hour in the respective secondary HRP-conjugated antibody (**Table 3.2**). Detection of protein

bands was performed using Amersham ECL Prime Western blotting detection reagent (GE Healthcare) on the Azure Biosystems c600 imaging system.

Antibody name	Protein target	Class	Host	Source	Dilution
Ab290 anti-GFP	GFP	Polyclonal	Rabbit	Abcam	WB 1:1000, IHC 1:1000
9E10 c-Myc	Myc-tag	Monoclonal	Mouse	DSHB	WB 1:500, IHC 1:500
Ab9106	Myc-tag	Polyclonal	Rabbit	Abcam	WB 1:500, IHC 1:500
12G10 anti-Tubulin	Tubulin	Monoclonal	Mouse	DSHB	WB 1:2000
1D4 anti-Fasciclin II	Fasciclin II (FasII)	Monoclonal	Mouse	DSHB	IHC 1:20
anti-MEF2	MEF2		Rabbit	Gift from Dr Bruce Paterson, National Cancer Institute, Bethesda	IHC 1:500
9.4A anti-Trio	Trio	Monoclonal	Mouse	DSHB	IHC 1:1000
3F10 anti-HA	HA-tag	Polyclonal	Rat	Sigma Aldrich	IHC 1:500

Table 3.1: List of primary antibodies used in western blotting and immunohistochemistry. DSHB, Developmental Studies Hybridoma Bank

Antibody name	Species target	Origin	Source	Dilution
AlexaFluor® 488 Anti-Rabbit	Rabbit	Goat	Sigma Aldrich	IHC 1:500
AlexaFluor® 488 Anti-Mouse	Mouse	Goat	Sigma Aldrich	IHC 1:500
AlexaFluor® 647 Anti-Mouse	Mouse	Goat	Sigma Aldrich	IHC 1:500
AlexaFluor® 647 Anti-Rat	Rat	Goat	Sigma Aldrich	IHC 1:500
AlexaFluor® 555 Anti-Mouse	Mouse	Goat	Sigma Aldrich	IHC 1:500

ECL™ peroxidase Anti-Rabbit NA934VS	Rabbit	Goat	GE Healthcare Life Sciences	WB 1:40,000
ECL™ peroxidase Anti-Mouse NA931VS	Mouse	Goat	GE Healthcare Life Sciences	WB 1:20,000

Table 3.2: List of secondary antibodies used in western blotting and immunohistochemistry

3.6 Immunohistochemistry

Flies were culled by emersion into 100% ethanol for not more than one minute before transferring them to 1xPBT (1xPBS, 0.5% TritonX-100). The brains for a genotype were dissected for using two pairs of Dumont no. 5 forceps in 1xPBT on a silicon dissecting pad and transferred to a PCR tube with 3% formaldehyde solution to be fixed for 45 minutes in room temperature on a nutator. After fixation, the formaldehyde solution were replaced with immunobuffer (5% normal goat serum in 1xPBT) to be blocked for one hour in room temperature on a nutator after which the immunobuffer was replaced with the appropriate primary antibodies (**Table 3.1**) and incubated overnight at 4°C. After primary incubation, brains were washed with 1xPBT three times for five minutes each and followed by secondary antibodies incubation (**Table 3.2**) overnight at 4°C. After secondary incubation, brains were again washed three times for five minutes with 1xPBT and samples that required nuclear staining were incubated in DAPI stain solution (300 nM) for 5 minutes follow by three times five minutes of 1xPBT wash. The brains were then mounted in antifade (1xPBS, 70% glycerol, 0.2% n-propyl gallate in DMSO) on microscope slides which are covered by a slightly elevated glass coverslip and sealed with nail polish to ensure secure positioning of the sample. For confocal imaging, optical sections were taken with Leica TCS SP5 DM6000B Confocal Microscope. Image stacks were taken at intervals of 0.5 µm (for MB lobes) or 0.25 µm (for KC nuclei) and processed with ImageJ software. Processed images of the MB were divided into the anterior and posterior stacks to minimise signal loss or overlap during image stacking for clearer MB visualisation (**Figure 3.2**).

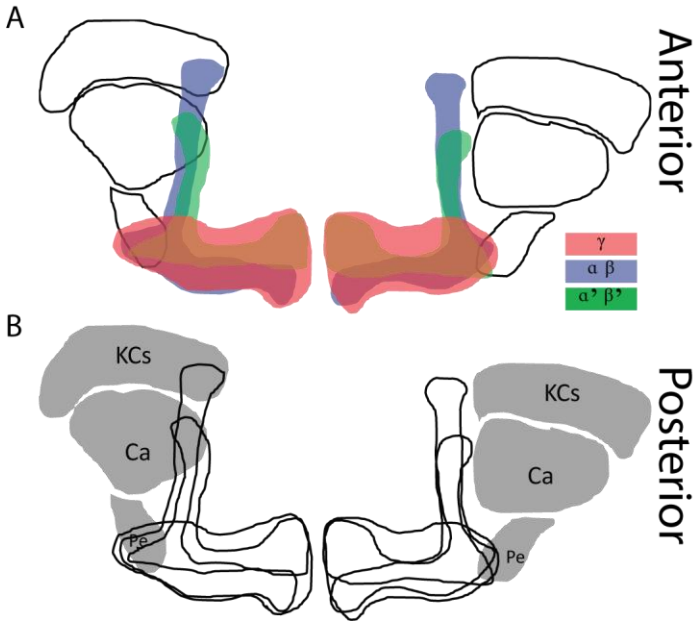

Figure 3.2: Diagrammatic MB visualisation aid for confocal images
A diagrammatic representation of the anterior MB stack (A) and posterior MB stack (B) from confocal slices. The coloured regions represent the visible portion of the mushroom bodies when the slices are stacked. Red represents the γ lobes; blue, the α/β lobes; and green, the α'/β' lobes.

3.7 Assessment of MB morphology

Confocal images of MB were assessed semi-quantitatively. In order to reduce phenotype bias, the confocal images of MB expression pattern or phenotype were scored blindly and recorded for significant characteristics, which are described in the results section. For assessment of MB phenotypes, a one-tailed Fisher's exact test was used to confirm the significance of penetrance exhibited by a genotype against its control and any statistical significance were accepted at $p<0.05$.

3.7 Fly heads isolation for RNA extraction

For collection RNA samples from fly heads, whole flies from the genotype of interest were anaesthetised with CO_2 and collected in 15 mL tubes. Whole flies were collected until approximately the 5 mL mark for each genotype. Flies were snap frozen by submerging the falcon tubes in liquid nitrogen for 30 seconds. After freezing, the tubes

containing the frozen flies were vortex three times for 10 seconds each to snap the head from the thorax. Prior to snap freezing, 1.7 mL microcentrifuge tubes, a glass funnel, a standard number 25 and a number 40 sieves were prechilled in -80°C freezer. After all fly heads had been snap separated, the 1.7 mL tubes, glass funnel and sieves were taken out of the freezer and placed on dry ice. To filter out the fly bodies and legs, the number 25 sieve was stacked on top of number 40 sieve. The vortexed samples were then poured onto the number 25 sieve to filter out the fly body and allow the fly heads and legs to go through while the number 40 sieve caught the fly heads and allowed the unwanted legs to fall through the sieve. The prechilled glass funnel was fitted to the mouth of a 1.7 mL tube and all the fly heads captured on the number 40 sieve were poured into the funnel. Heads in 1.7 mL tubes were placed on dry ice for same day processing or stored at -80°C.

3.8 RNA extraction

RNA extraction was carried out using the QIAGEN RNAeasy Plus kit with a modified protocol. QIAzol Lysis Reagent (200 µL) was first added to each 1.7 mL tube containing heads (Section 3.7) and homogenised using a motorised pestle for about 10 seconds. Another 700 µL of QIAzol Lysis Reagent was added and samples were thoroughly homogenised for 20 seconds. The homogenates were left at room temperature for 5 minutes after which 100 µL of gDNA Eliminator Solution (QIAGEN, RNAeasy Plus) was added. The tubes were capped securely, shaken vigorously for 15 seconds. 180 µL of chloroform was added and mixed thoroughly by vigorous shaking for another 15 seconds. The samples were left at room temperature for 3 minutes. The homogenates were centrifuged at 12,000 x g for 15 minutes at 4°C. After centrifugation, the upper aqueous phase (~600 µL) was transferred to a new 1.7 mL tube. One volume of 70% ethanol (~600 µL) was added and mixed thoroughly by pipetting up and down. After mixing, 700 µL of the sample solution was transferred to an RNAeasy Mini spin column (QIAGEN, RNAeasy Plus) placed in a 2 mL collection tube and centrifuged for 1 minute at 8000 rpm at room temperature (collection of flow through to be discarded after every centrifugation step). The remaining sample solution was added to the spin column and again centrifuged at 8000 rpm at room temperature. To wash the membrane on the spin column, 700 µL of Buffer RWT (QIAGEN, RNAeasy Plus) was added to the spin column and centrifuged for 1 minute at 8000 rpm. 500 µL of Buffer RPE (QIAGEN, RNAeasy

Plus) was added to the spin column and centrifuged for 1 minute at 8000 rpm and was repeated again but with two minutes centrifugation. After the washes, the RNA was eluted by placing the spin column onto a new 1.7 mL tube and adding 50 μL of RNAse-free water (QIAGEN, RNAeasey Plus) to the spin column followed by centrifugation for 1 minute at 8000 rpm. The elution step was repeated using the eluate collected to maximise the yield. Eluted RNA samples were stored in -80°C until ready for quantification and sequencing. It should be noted that due to the large number of samples (eight genotypes in quadruplicates = 32 samples), this protocol was carried out in batches of eight with four samples per batch to ensure the duration for each steps could be closely followed for each sample.

3.9 Transcriptome analysis

RNA samples were sent to Novogene for library construction and 2x150bp paired end sequencing of each sample. Following the sequencing of each sample library, the raw data was sent to Massey Genome Services for pre-analysis which was performed by bioinformatician, Mr Mauro Truglio. The pre-analysis process will be detailed in Section 6.2 but in brief, the raw data were processed using Salmon, an alignment-free tool and quantified for expression of transcripts using the *Drosophila* genome from Berkeley *Drosophila* Genome Project (BDGP) 6.28 (Ensembl release 102). The read counts of mapped reads were then compared between treatment group which can then be used to generate the $\log_2$ fold change of transcriptional changes. Transcriptional changes that were significant were further analysed with Database for Analysis, Visualisation, and Integrated Discovery (DAVID) to identify processes that have been enriched.

3.10 Reactive oxygen species (ROS) detection using dihydroethidium

Flies were briefly anaesthetised with CO_2 and dissected using two pairs of Dumont no. 5 forceps in Schneider's medium (Invitrogen) on a silicone dissecting pad and transferred to a PCR tube with 200 μL of fresh Schneider's medium. The limit on the number of flies

to be dissected for each experiment was set at nine due to the risk of premature ROS production as a result of long processing time. Therefore, each experiment consisted of three genotypes and three fly brains for each genotype, which could be quickly dissected in a short amount of time. After dissection, the Schneider's medium in the PCR tube was replaced with 20 μM of dihydroethidium (Invitrogen) and the brains were incubated for 10 minutes in a dark chamber at room temperature on a nutator. Subsequently, the brains were washed with Schneider's medium three times for five minutes with the same conditions as the incubation. Brains were mounted in 1xPBS between coverslips and imaged on the same day. All brain samples were mounted on the same slide under the same coverslip to minimise variation in signal intensity and imaged immediately. Signals throughout the brain slices were captured at a 0.5 μm interval using Leica TCS SP5 DM6000B Confocal Microscope with an excitation/emission wavelength of 518 nm/606 nm (Invitrogen specification).

3.11 Lipid droplet detection using Nile Red staining

Whole fly heads were first detached from fly bodies using a pair of Dumont no. 5 forcep and fixed in a PCR tube with 200 μL of 3% formaldehyde for one hour on a nutator. Subsequently, the fly retinas were dissected in cold 1xPBS and again fixed for 30 minutes in a PCR tube with 200 μL formaldehyde. After fixing, retinas were washed three times for five minutes in 1xPBS. The PBS was then replaced with a 1:1000 dilution of 1 mg/mL Nile Red (Sigma Aldrich) in 1xPBS and incubated for 15 minutes at room temperature on a nutator. Subsequently, retina samples were washed with 1xPBS for three times for five minutes and mounted in antifade (1xPBS, 70% glycerol, 0.2% n-propyl gallate in DMSO) between coverslips. Retinas were imaged on the same day using Leica TCS SP5 DM6000B Confocal Microscope with an excitation/emission 554 nm/638 nm (Sigma Aldrich specification).

4. CHARACTERISING THE SUBCELLULAR DISTRIBUTION AND DEVELOPMENTAL IMPACT OF HDAC4 VARIANTS

To investigate the importance of the subcellular distribution and the functional domains in HDAC4 overexpression-induced neurodevelopmental phenotypes, five mutants were generated that either altered the subcellular distribution of HDAC4 or disrupted functional domains/motifs thought to be critical to the neuronal function of HDAC4. The specific mutants (hereafter termed *DmHDAC4* variants) are described as follows and specific details of the amino acid substitutions were described and shown in Section 3.2 and Appendix 9.1:

UAS-DmHDAC4-dNLS-myc – mutation of seven conserved residues in the NLS restricts HDAC4 to the cytoplasm (Wang & Yang, 2001) (**Figure 4.1B**).

UAS-DmHDAC4-3A-myc – mutation of three conserved serine residues prevents phosphorylation, which in turn prevents 14-3-3ζ mediated nuclear export and thus restricts HDAC4 to the nucleus (Wang & Yang, 2001) (**Figure 4.1C**).

UAS-DmHDAC4-Y1142H-myc – Mutation of Tyr-1142 to His, which is required for catalytic activity of the deacetylase domain (Lahm et al., 2007) (**Figure 4.1D**).

UAS-DmHDAC4-dMEF2-myc – mutation of three conserved residues in the MEF2-binding site restricts protein to the cytoplasm (Jayathilaka et al., 2012; Wang & Yang, 2001) (**Figure 4.1E**).

UAS-DmHDAC4-dANK-myc – mutation of four conserved residues in the putative ankyrin-binding site is predicted to prevent binding of ankyrin repeat-containing proteins (Xu et al., 2012) (**Figure 4.1F**).

Each of the *DmHDAC4* variants as well as *DmHDAC4*^{WT} (**Figure 4.1A**) were synthesised with a 6xMYC epitope-tag at the C-terminus (designed by Dr Helen Fitzsimons and generated by GenScript) and subcloned into the pUASTattB plasmid downstream of 5XUAS to allow for regulation of expression with the GAL4/UAS system (Section

1.7.2.1) (Groth et al., 2004). Transgenic flies were generated by GenetiVision via site-specific ϕC31 mediated homologous recombination into attP at position 68A4 in the left arm of the third chromosome (**Figure 4.1G**) (fly genotypes described in **Supplementary Table 9.17**). The choice of chromosomal insertion location was based on previous experience in which insertion of the transgene cassette at this locus induces high expression with minimal leakiness (Fitzsimons et al., 2013).

To verify the expression of the *DmHDAC4* variants, each *UAS-DmHDAC4* variant line was crossed to a pan-neuronal TARGET driver line (*elavGAL4;tubGAL80^{ts}*) (**Figure 4.1H**), which consists of GAL4 under control of the *embryonic lethal abnormal vision* (*elav*) promoter that drives expression in all post-mitotic neurons, and constitutively expressed GAL80^{ts} for temperature-dependent regulation of temporal expression (Section 1.7.2.2). To avoid the developmental abnormalities in the MB caused by overexpression of *DmHDAC4* throughout neuronal development (Schwartz, 2016), F1 progeny were raised at 18°C until eclosion and then separated into two groups: one undergoing 48-hours of post-developmental incubation at 30°C to induce expression and the other kept in 18°C as an uninduced control. Western blot analysis of fly heads lysates revealed appropriate induction of expression of an approximately 134kDa protein, which corresponds to the expected molecular weight of DmHDAC4-myc and variants, confirming that expression was efficiently controlled by the TARGET system (**Figure 4.1I**).

Although very low levels of protein were detectable in some of the uninduced (18°C) lane, this was minimal and considered to be at an acceptable level, based on previous studies using this system (Schwartz et al., 2016), as well as the lack of MB phenotype in the uninduced DmHDAC4 brains (see Section 1.7.4). There was no statistically significant difference in the level of expression between the variants following normalisation to tubulin, indicating that none of the mutations significantly altered the stability of any of the proteins (**Figure 4.1J**).

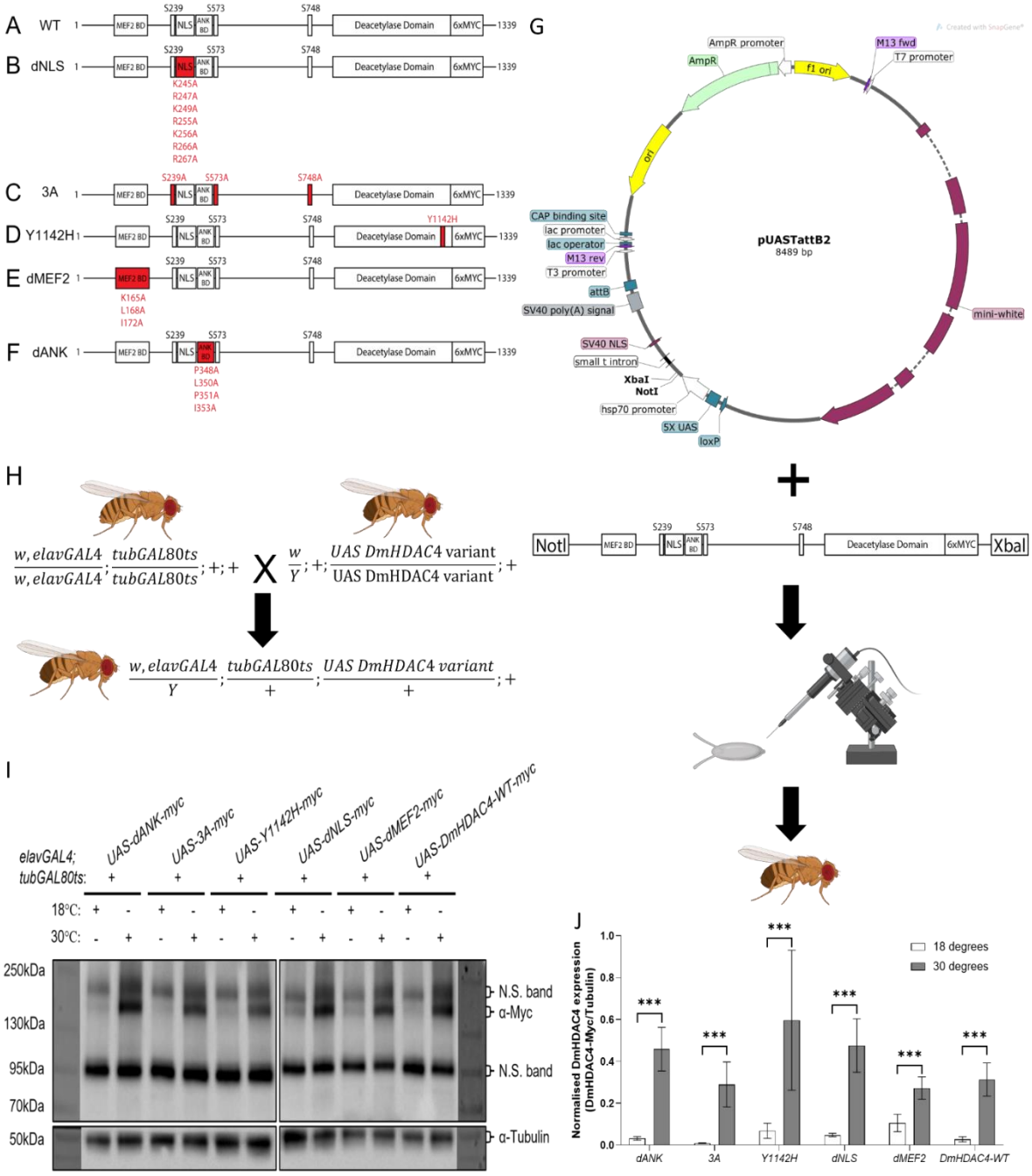

Figure 4.1: Schematic diagrams of *DmHDAC4* variant constructs and methodology for generation of transgenic flies

(A-F) All DmHDAC4 variants sequence consist of a 6xMYC tagged at the C-terminus. Red box denotes a domain or point that has been mutated. Red text represents the change in amino acid within the mutated domain. The *DmHDAC4* variants consist of WT (A), cytoplasmic-restricted (B), nuclear-restricted (C), catalytically inactive (D), MEF2-binding mutant (E) and ankyrin-binding mutant (F). (G) Each of this variant sequence is flanked by NotI and XbaI restriction enzyme sequence and subcloned into the pUASTattB plasmid which contained a 5xUAS and attB. The plasmid construct is then introduced into the embryo of a line carrying attP on the third chromosome (68A4) which then allow the plasmid to be incorporated into the genome via ϕC31 mediated homologous recombination. (H) Female flies with pan-neuronal TARGET driver were crossed to male flies with UAS-DmHDAC4 variant lines. F1s were raised at 18°C until the adults eclosed after which the male F1s were collected and separated into two groups for 18°C and 30°C incubation over two days. (I) Western blot analysis was carried out on the lysates (n=50) from each genotype. (N.S.)

denotes non-specific band. (J) Two-way ANOVA analysis of western blot triplicate (*** $p<0.001$ 30°C vs 18°C). Each bar represents the mean ± SEM of normalised DmHDAC4 expression.

4.1 Characterisation of the expression and subcellular distribution of DmHDAC4 variants overexpression in the MB

Next, the expression and the subcellular distribution of each variant was examined in whole brains to confirm the expected subcellular distribution of the predicted nuclear and cytoplasmic-restricted mutants and to determine whether the expression pattern is altered in any of the mutant variants as compared to *DmHDAC4*^{WT}. Since HDAC4 is required in the MB for both memory and neuronal development, expression was analysed in Kenyon cells (KCs, the intrinsic neurons of the MB, see Section 1.7.1). *DmHDAC4* variants were expressed specifically in adult KCs by crossing each UAS variant line to a MB-specific TARGET driver line (*OK107GAL4; tubGAL80*^{ts}). F1 progeny were raised at 18°C, then adult male flies were raised at 18°C or 30°C for 48 hours. Brains were then dissected and processed for anti-Myc immunohistochemistry and counterstained with the nuclear marker DAPI to visualise the DmHDAC4 localisation pattern within KCs (**Figure 4.2**). All brains were imaged by confocal microscopy with identical settings to allow for direct comparison of expression levels between the genotypes.

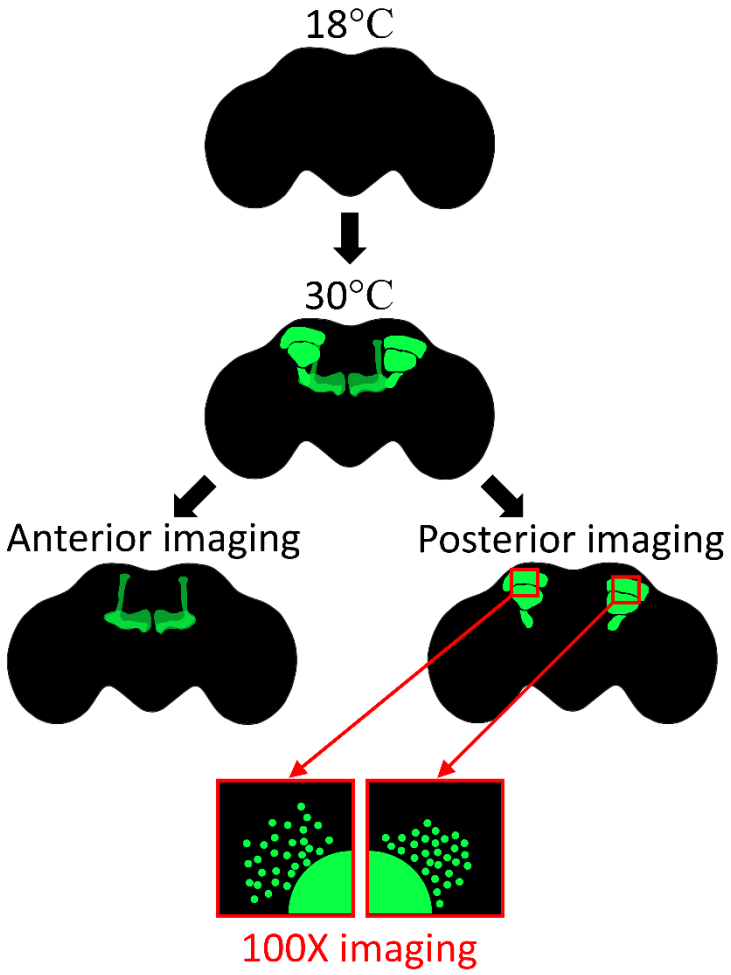

Figure 4.2: Workflow for characterising subcellular distribution of temperature-induced expression
Drosophila adults were incubated at 30°C for 48 hours to induce expression of *DmHDAC4* and variants. Immunohistochemistry was performed on dissected brains and imaged anteriorly for visualisation of the KC lobes and posteriorly for visualisation of KC nuclei and calyces. Nuclei and calyces were further imaged at 100X magnification.

4.1.1 Wild-type DmHDAC4

DmHDAC4^{WT} was distributed through the entire MB, with protein detected in the nucleus, calyx (dendritic field), peduncle and the KC lobes (axon bundles). HDAC4 protein distributed predominantly to the lobes of the α/β KCs, weakly to the γ KCs and was not detected in the lobes of the α'/β' KCs (**Figure 4.3B & D**) (Refer to section 1.7.1.1 of introduction for MB structure). The overall expression pattern is consistent with that observed previously in FLAG- and GFP-tagged DmHDAC4 (Fitzsimons et al., 2013; Main, Tan, Wheeler, & Fitzsimons, 2021). However, the lack of detection in the α'/β' KCs was due to low confocal gain in order to reduce the background to prevent image

oversaturation of the expression pattern at the nuclei of the KCs, additionally the brain samples were positioned with the posterior side faced up which reduces the efficacy for imaging deeper sections with weaker expression. The differences in expression between MB neuronal subtypes also suggest that the subcellular distribution of DmHDAC4 is differentially regulated in different KC subtypes. This could also be due to OK107 promoter activity varying across KC subtypes, leading to weak γ and α'/β' expression during the adult stage, however this is less likely the case as OK107 drives strong expression of GFP in all lobes (Aso et al., 2009). DmHDAC4 also localises to a subset of nuclei with some exhibiting puncta, suggesting aggregation of DmHDAC4 when abundant (**Figure 4.3G & H**). However, it cannot be determined from these images as to whether these puncta are specific to a KC subtype as the nuclei of all three MB neuronal subtype are clustered together and morphologically indistinguishable. In a result which will be presented later in this chapter (Section 4.3.1), the differential regulation between subtypes was observed using a Split GAL4 driver; expression of Dm HDAC4 in γ KCs displayed weaker expression in the γ lobes but appeared to have a higher concentration of nuclear expression when compared to other lobe subtypes, which could suggest weaker lobe expression could be due to the protein being more restricted to the nucleus.

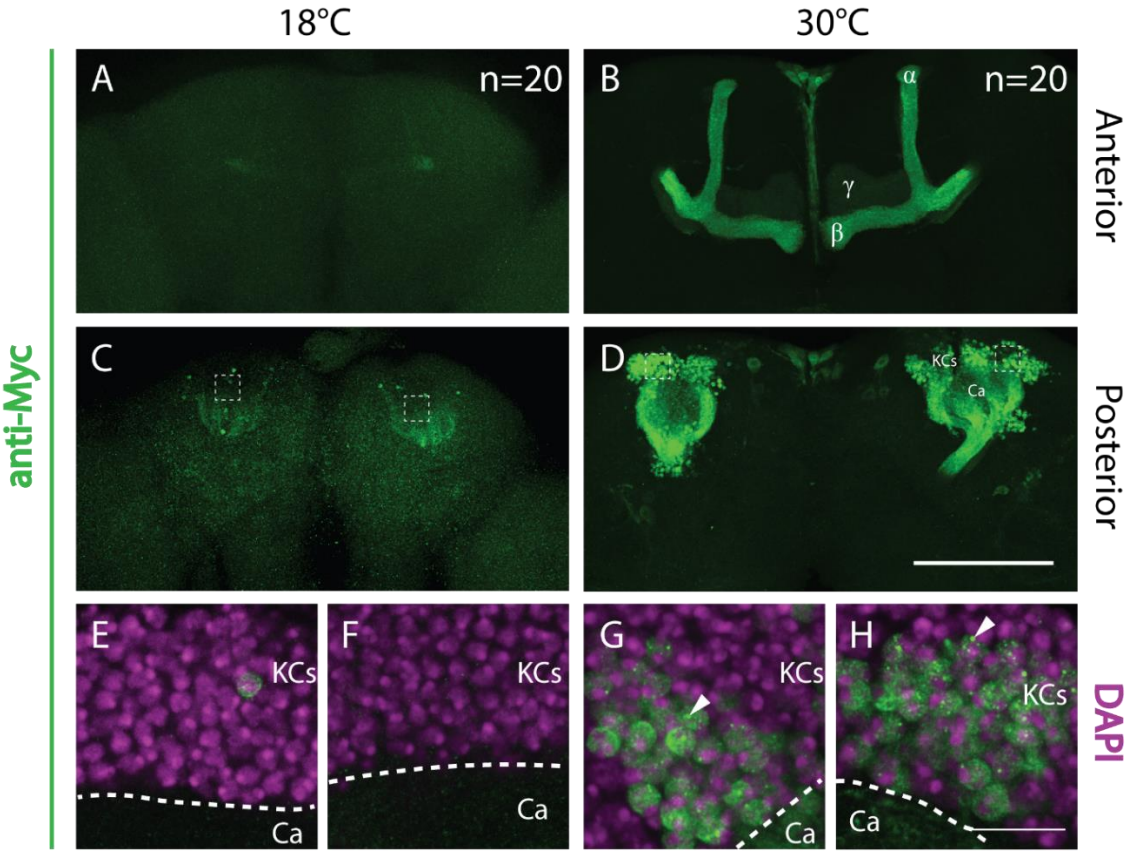

Figure 4.3: Expression of *DmHDAC4^{WT}* in MB neurons using the TARGET system
Representative images from analysis of 20 brains/genotype of the anterior regions of the MB containing the lobes (A & B) and posterior region of the MB containing the KC bodies and calyx (C & D) at either 18°C (uninduced) (A, C, E & F) or 30°C (induced) (B, D, G & H). White dashed boxes in the posterior images (C & D) represent the corresponding magnified images shown directly below on the left (E & F) and right (G & H) KCs. White dashed lines outline the boundary between the KCs and the calyx (Ca). Images A to D consist of maximum Z-stack projections through the anterior (A & B) and the posterior (C & D) regions of the MB whereas images E to H are single optical sections. Top scale bar = 100μm, bottom scale bar = 10μm.

The MB-specific TARGET driver was effective in its temperature-dependent regulation of expression as DmHDAC4 was minimal in the control (18°C) (**Figure 4.3A, C, E & F**), which is consistent with the western blot analysis (**Figure 4.1I**). Although the leaky expression of DmHDAC4 was extremely low, its expression during development could nevertheless have influenced maturation of KCs. Developmental expression of DmHDAC4 leads to abnormalities including fused β-lobes and loss of α/β lobes due to impaired elongation (Main et al., 2021; Schwartz, 2016). Examination of the brains in which *DmHDAC4* expression was not induced until adulthood (i.e. raised at 18°C and incubated at 30°C after eclosion) did not reveal any detectable phenotypic difference when compared to a WT MB, (i.e. the γ and α/β lobes showing normal axon guidance, branching and growth termination) (**Figure 1.7**). Hence, the minor leaky expression through MB development appeared to be phenotypically inconsequential.

4.1.2 3A variant (nuclear-restricted)

3A was not detected in the MB lobes, peduncle or calyx (**Figure 4.4B & D**) and only detected in the nuclei of KCs, with intense puncta present (**Figure 4.4D, G & H**), confirming that the 3A mutations lead to nuclear retention of DmHDAC4.

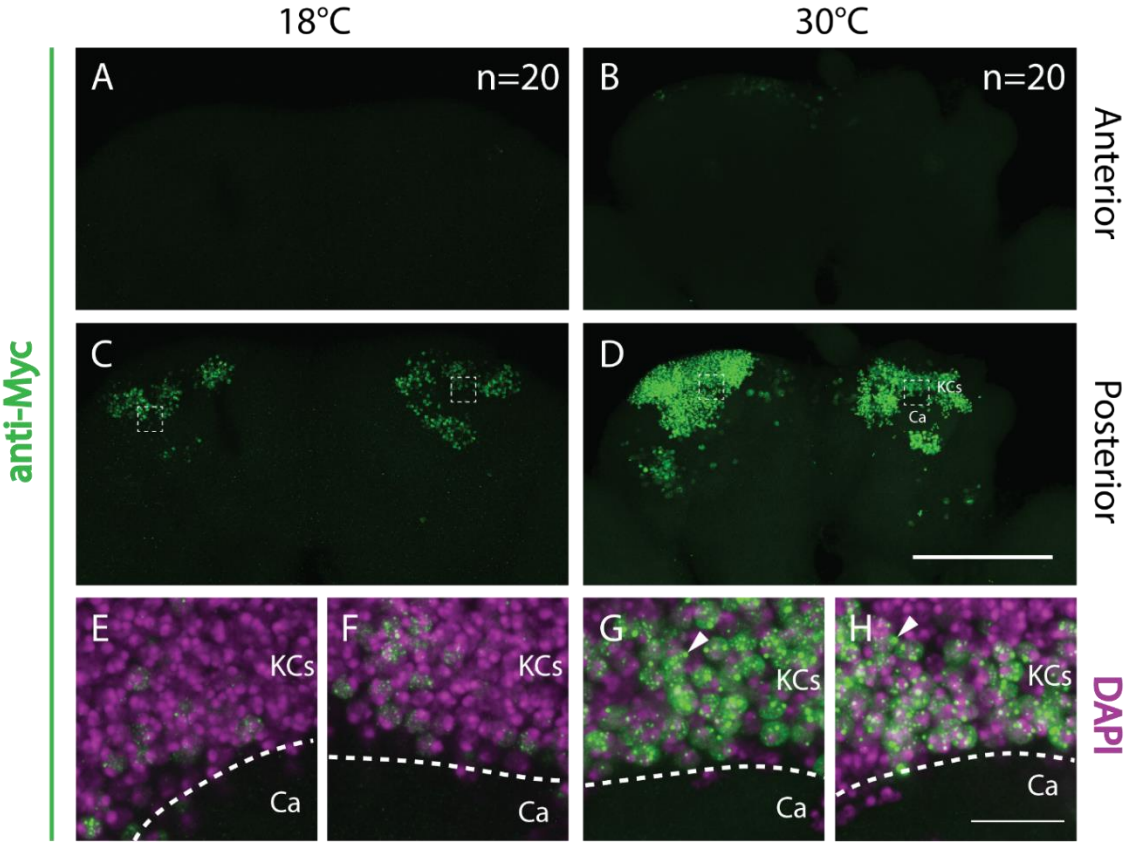

Figure 4.4: Expression of nuclear-restricted *DmHDAC4* in MB neurons using the TARGET system
Representative images from analysis of 20 brains/genotype of the anterior regions of the MB containing the lobes (A & B) and posterior region of the MB containing the KC bodies and calyx (C & D) at either 18°C (uninduced) (A, C, E & F) or 30°C (induced) (B, D, G & H). White dashed boxes in the posterior images (C & D) represent the corresponding magnified images shown directly below on the left (E & F) and right (G & H) KCs. White dashed lines outline the boundary between the KCs and the calyx (Ca). Images A to D consist of maximum Z-stack projections through the anterior (A & B) and the posterior (C & D) regions of the MB whereas images E to H are single optical sections. Top scale bar = 100μm, bottom scale bar = 10μm.

4.1.3 dNLS variant (cytoplasmic-restricted)

DmHDAC4 dNLS was almost completely restricted to the cytoplasm when expressed in KCs (**Figure 4.5B & D**). Although low level HDAC4 protein could still be detected in the nuclei, the majority of the protein was restricted to the cytoplasm and observed as cytoplasmic haloes surrounding the nuclei of the KCs, indicating that these nuclei were devoid of DmHDAC4 (**Figure 4.5G & H**).

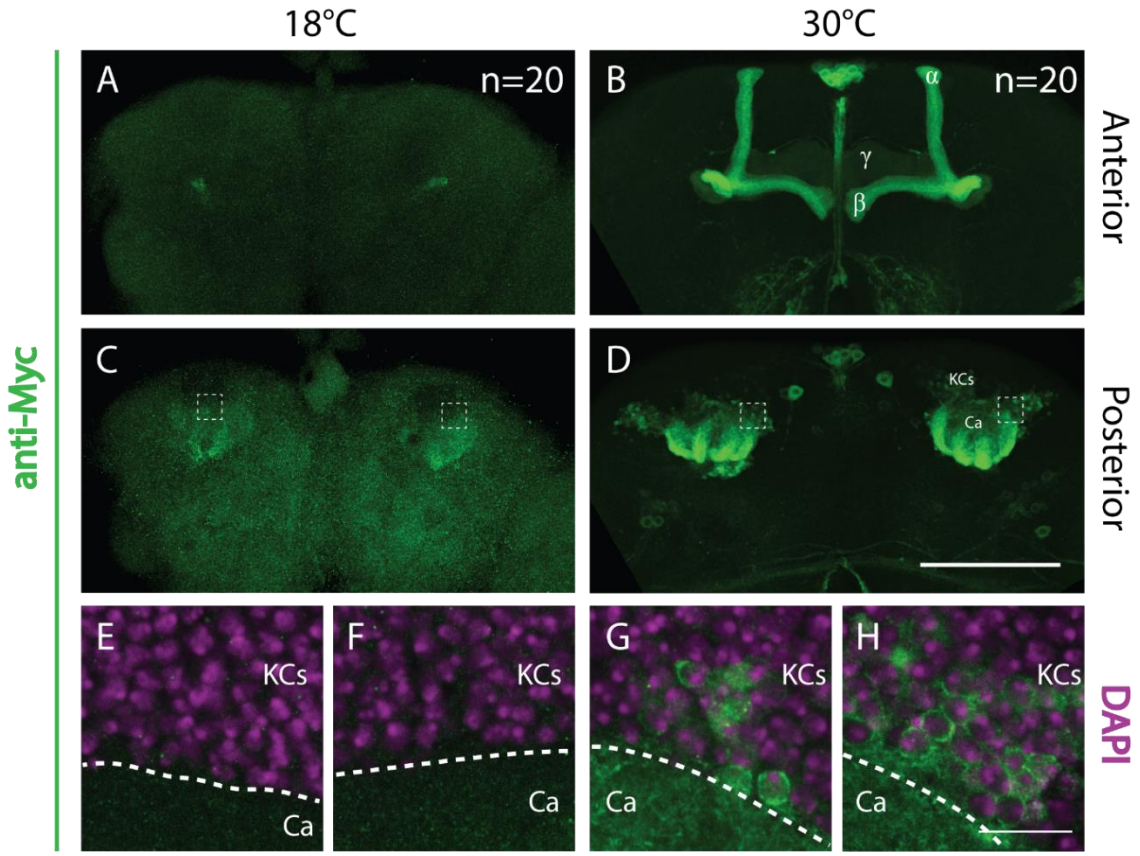

Figure 4.5: Expression of cytoplasmic-restricted *DmHDAC4* in MB neurons using the TARGET system
Representative images from analysis of 20 brains/genotype of the anterior regions of the MB containing the lobes (A & B) and posterior region of the MB containing the KC bodies and calyx (C & D) at either 18°C (uninduced) (A, C, E & F) or 30°C (induced) (B, D, G & H). White dashed boxes in the posterior images (C & D) represent the corresponding magnified images shown directly below on the left (E & F) and right (G & H) KCs. White dashed lines outline the boundary between the KCs and the calyx (Ca). Images A to D consist of maximum Z-stack projections through the anterior (A & B) and the posterior (C & D) regions of the MB whereas images E to H are single optical sections. Top scale bar = 100μm, bottom scale bar = 10μm.

4.1.4 Y1142H variant (catalytically inactive mutant)

Y1142H displayed very similar subcellular distribution to DmHDAC4^{WT} with protein detected in the axons, dendritic field and in some KC nuclei, with nuclear puncta present (**Figure 4.6B, D, G & H**). This indicates that, as expected, loss of deacetylase activity does not impact nucleocytoplasmic shuttling.

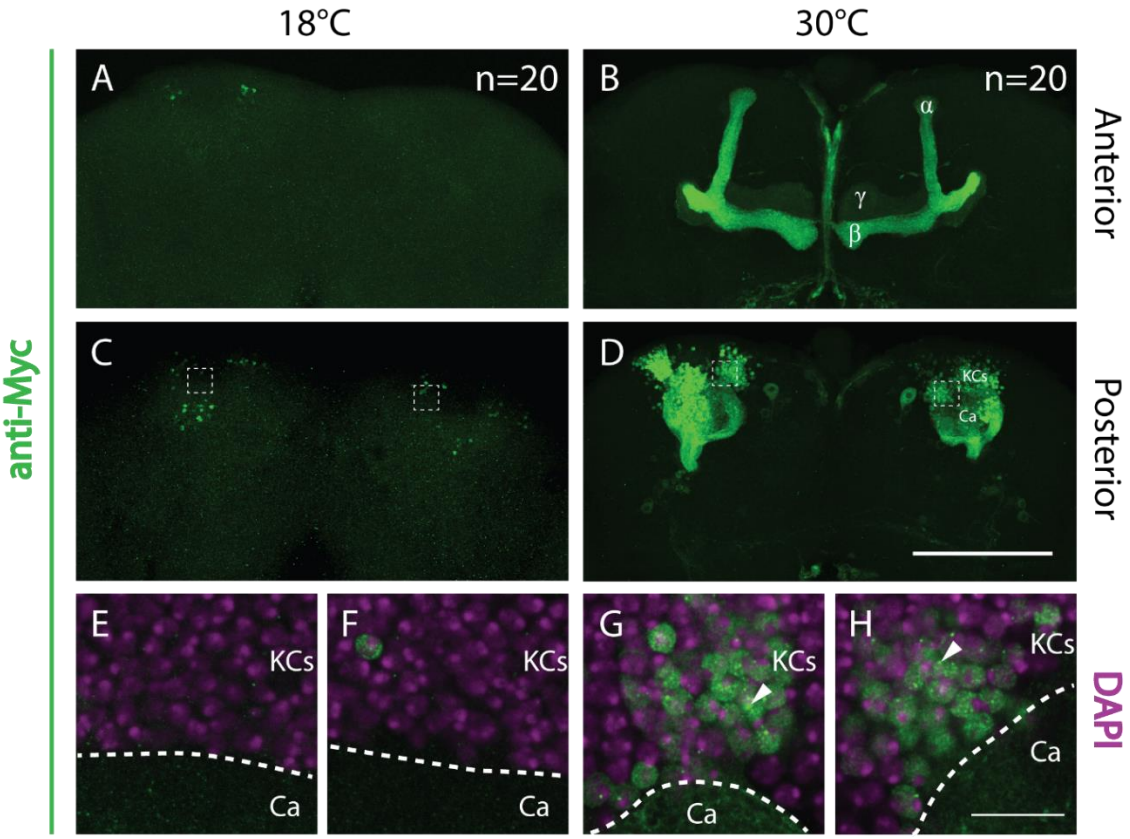

Figure 4.6: Expression of catalytically-inactive *DmHDAC4* in MB neurons using the TARGET system
Representative images from analysis of 20 brains/genotype of the anterior regions of the MB containing the lobes (A & B) and posterior region of the MB containing the KC bodies and calyx (C & D) at either 18°C (uninduced) (A, C, E & F) or 30°C (induced) (B, D, G & H). White dashed boxes in the posterior images (C & D) represent the corresponding magnified images shown directly below on the left (E & F) and right (G & H) KCs. White dashed lines outline the boundary between the KCs and the calyx (Ca). Images A to D consist of maximum Z-stack projections through the anterior (A & B) and the posterior (C & D) regions of the MB whereas images E to H are single optical sections. Top scale bar = 100μm, bottom scale bar = 10μm.

4.1.5 dMEF2 variant (mutated MEF2-binding domain)

Expression of dMEF2 also resulted in a cytoplasmic-restricted phenotype with a strong distribution to the lobes (**Figure 4.7B, D, G & H**) and cytoplasmic haloes observed around the nuclei. As a minor amount of HDAC4 protein can still be detected in some nuclei of the *dNLS* variant (**Figure 4.5G**), this suggests that MEF2-binding of DmHDAC4 is required for nuclear translocation and is consistent with studies in mammalian cells showing the requirement of MEF2-binding for HDAC4 nuclear import (Wang & Yang, 2001).

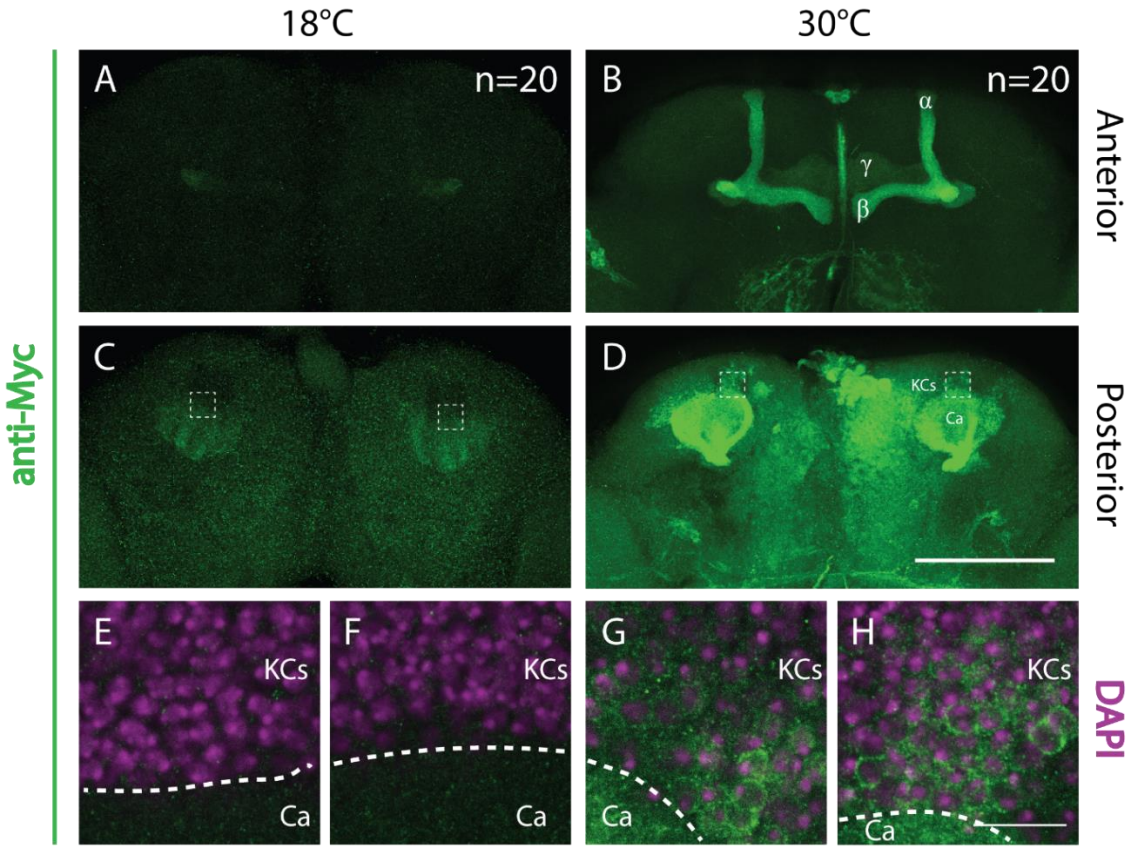

Figure 4.7: Expression of *DmHDAC4* with mutated MEF2-binding site in MB neurons using the TARGET system
Representative images from analysis of 20 brains/genotype of the anterior regions of the MB containing the lobes (A & B) and posterior region of the MB containing the KC bodies and calyx (C & D) at either 18°C (uninduced) (A, C, E & F) or 30°C (induced) (B, D, G & H). White dashed boxes in the posterior images (C & D) represent the corresponding magnified images shown directly below on the left (E & F) and right (G & H) KCs. White dashed lines outline the boundary between the KCs and the calyx (Ca). Images A to D consist of maximum Z-stack projections through the anterior (A & B) and the posterior (C & D) regions of the MB whereas images E to H are single optical sections. Top scale bar = 100μm, bottom scale bar = 10μm.

4.1.6 dANK variant (mutated ankyrin-binding domain)

dANK was also distributed throughout the KCs in a pattern indistinguishable from DmHDAC4^{WT} (**Figure 4.8B, D, G & H**).

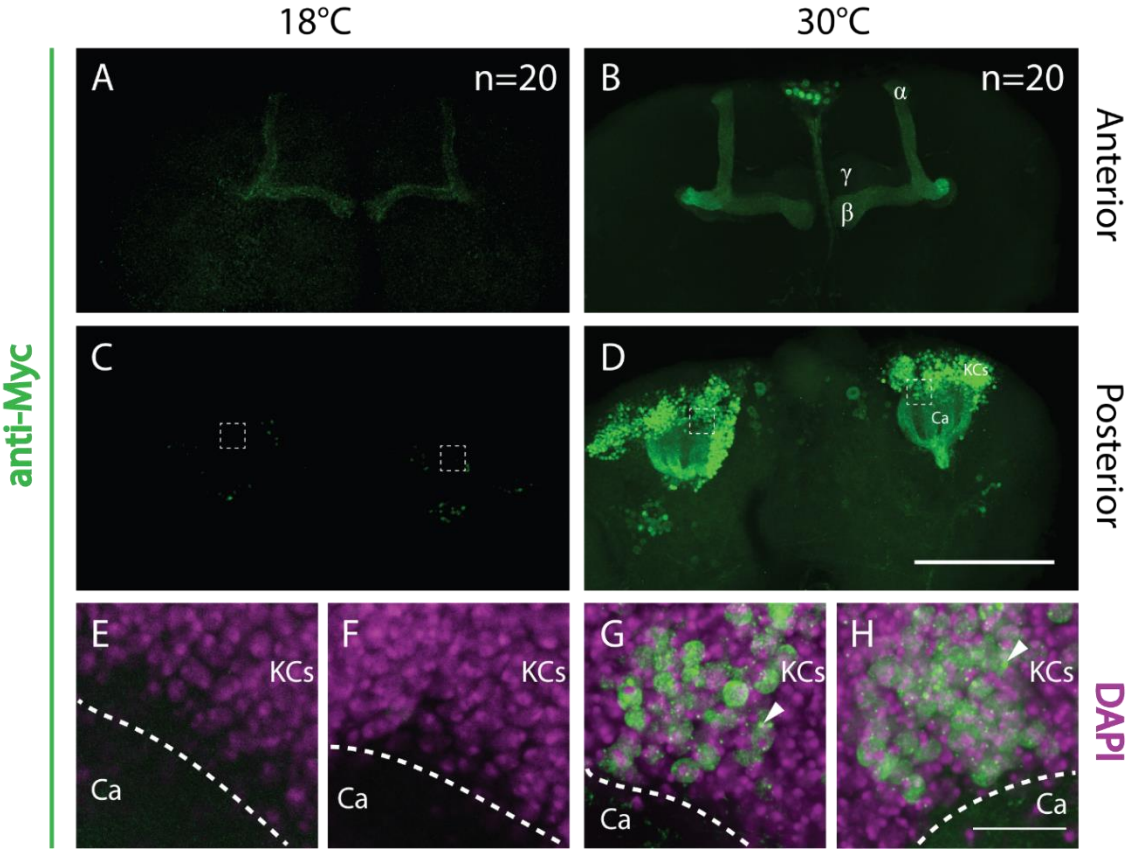

Figure 4.8: Expression of *DmHDAC4* with mutated ankyrin-binding domain in MB neurons using the TARGET system
Representative images from analysis of 20 brains/genotype of the anterior regions of the MB containing the lobes (A & B) and posterior region of the MB containing the KC bodies and calyx (C & D) at either 18°C (uninduced) (A, C, E & F) or 30°C (induced) (B, D, G & H). White dashed boxes in the posterior images (C & D) represent the corresponding magnified images shown directly below on the left (E & F) and right (G & H) KCs. White dashed lines outline the boundary between the KCs and the calyx (Ca). Images A to D consist of maximum Z-stack projections through the anterior (A & B) and the posterior (C & D) regions of the MB whereas images E to H are single optical sections. Top scale bar = 100µm, bottom scale bar = 10µm.

Together these data confirm that DmHDAC4^{WT} and all five variants were expressed in the MB and displayed the predicted distribution patterns.

4.2 Characterisation of the impact of expression of *DmHDAC4* variants on development

Overexpression of *DmHDAC4* has been previously shown to impair memory formation and MB development (Fitzsimons et al., 2013; Schwartz, 2016). Indeed, increased abundance of HDAC4 in mammals has been implicated in various neurological disorders

such as AD (Shen et al., 2016), in mouse models of AD (Anderson et al., 2015; Sen et al., 2015), PD (Takahashi-Fujigasaki & Fujigasaki, 2006) and ataxia-telangiectasia (Li, Chen, et al., 2012). Additionally, 2q37 chromosomal deletion syndrome, the clinical features of which include developmental delay and intellectual disability, is associated with deletion of a region containing the HDAC4 locus (Villavicencio-Lorini et al., 2013; Williams et al., 2010) and haploinsufficiency of HDAC4 is considered to be the primary contributor to the disease phenotype (Le et al., 2019). In addition, individuals with developmental delay and intellectual disability have been shown to possess mutations to the 14-3-3ζ binding site of HDAC4 which then suggest the defect in HDAC4's nuclear export capability and subsequent nuclear abundance to be a detrimental cause (Wakeling et al., 2021). However, the mechanism through which the dysregulation of HDAC4 causes disease are not well understood, therefore, characterisation of the phenotypes resulting from expression of the mutant variants could help to understand the contribution of subcellular distribution as well as the importance of specific domains within DmHDAC4 to normal and impaired neurodevelopment. Since the developmental phenotypes resulting from increased abundance of HDAC4 in the *Drosophila* eye and MB have been carefully characterised (Main et al., 2021; Schwartz et al., 2016), and are both easily scored in terms of severity of the phenotype, it was decided that these would be ideal and appropriate models to assess the impact of the HDAC4 mutations on neuronal development. To that end, the rough eye phenotype assay and an analysis of MB development were conducted to characterise and compare the developmental defects resulting from expression of *DmHDAC4* variants.

4.2.1 Characterisation of the impact of DmHDAC4 variant expression on retina development

Analysis of the impact of increased DmHDAC4 on eye development was assessed by crossing the *HDAC4* variant lines to the *GMR-GAL4* driver which drives expression in post-mitotic photoreceptors (Freeman, 1996). It was previously shown that *GMR-GAL4* driven expression of *DmHDAC4* results in a mild rough eye phenotype with misaligned ommatidia, missing bristles and a reduction in pigmentation. Expression of two copies of the *DmHDAC4* transgene resulted in a dose dependent increase in phenotypic severity with ommatidial fusion, an almost complete loss of bristles and loss of pigmentation

(Schwartz et al., 2016). It was decided that expression of two copies of each variant would be an ideal system to adopt, as both increased or reduced phenotypic severity compared to DmHDAC4^{WT} could be easy to assess visually. Accordingly, transgenic fly lines were generated in which one copy of the *GMR-GAL4* driver and two copies of an *HDAC4* variant were present (**Supplementary Figure 9.3**). Six male and six female eyes were assessed per genotype and the phenotypes within a genotype did not vary between samples with respect to the scoring criteria, however the phenotype characteristic over all genotypes encompass a large range of morphological categories, making it a challenge for quantification. Therefore, each phenotype characteristic was arbitrarily assigned a severity score based on the phenotype classification and the severity (**Figure 4.9**) (see Section 3.4 for method). As GAL4 activity is temperature dependent with higher temperature associated with stronger expression (Duffy, 2002), flies were initially raised at 22°C at which the temperature induced *DmHDAC4^{WT}* eye phenotype is moderate (**Figure 4.9B**), with subtle disorganisation of the ommatidia arrangement, reduction of pigmentation and loss of bristles in comparison (**Score 1.25**) to control eyes (**Score 0.00**) (**Figure 4.9A**) of both male and female flies. The nuclear-restricted *DmHDAC4* variant *3A* exhibited a severe phenotype which presented as fusion of ommatidia, and complete loss of bristles and red pigmentation (**Score: 2.50**) (**Figure 4.9C**), while the cytoplasm-restricted variants *dNLS* and *dMEF2* displayed similar phenotypic patterns to *DmHDAC4^{WT}* (**Score: 1.25**) (**Figure 4.9D & I**). Although a previous study indicated that deacetylase activity is dispensable for the *HDAC4* overexpression-induced deficits in memory formation (Fitzsimons et al., 2013), expression of *Y1142H* led to a less severe phenotype than WT *HDAC4* (**Score 1.00**) (**Figure 4.9J**), suggesting that the manifestation of the DmHDAC4-induced deficits in eye development are dependent on its deacetylase activity.

Also of interest, the eye phenotype exhibited by *dANK* was more severe than *DmHDAC4^{WT}* (**Score: 1.75**) (**Figure 4.9K**), with increased ommatidial disorganisation and fusion. This suggests a role for the ankyrin-binding site in restraining the developmental deficits caused by *DmHDAC4* overexpression. This could then imply that the ankyrin-binding site is crucial for normal eye development, however this does not necessarily involve an interaction with Ank2 as there are also other ankyrin-binding proteins expressed in the fly brain such as kidney ankyrin repeat-containing proteins (KANK) and RFXANK (Gee et al., 2015; Larkin et al., 2020; McKinsey et al., 2006).

To further exacerbate the phenotypes to see if a difference could be uncovered between the phenotypes that were similar, the flies were also raised at 27°C. At this temperature, *DmHDAC4*^{WT} expression resulted in completely fused ommatidia and an absence of bristles (**Score: 2.00**) (**Figure 4.9F**). Expression of *3A* at 27°C also resulted in complete ommatidial fusion and loss of pigmentation but was more severe than *DmHDAC4*^{WT} with retina indentations and necrotic patches, which were present as brown patches across the retina (**Score: 3.50**) (**Figure 4.9G**). Surprisingly, when raised at 27°C, *dNLS* also induced an extremely severe phenotype similar to *3A* (**Score: 3.50**) (**Figure 4.9H**), however the other cytoplasmic-restricted mutant dMEF2 was less severe, with an appearance akin to that of *DmHDAC4*^{WT} (**Score: 2.00**) (**Figure 4.9L**). As the *dNLS* mutant retains the MEF2-binding site, these data may suggest a role for DmHDAC4 MEF2-binding activity in impairment of eye development, and therefore that the *dNLS* mutant could potentially be conducting its activity through MEF2-binding, an observation that warrants further investigation.

At 27°C, *Y1142H* again induced only minor phenotypes including mildly disorganised ommatidia and loss of bristles (**Score: 1.25**) (**Figure 4.9M**). The *dANK* phenotype was again more severe than *DmHDAC4*^{WT} at 27°C, at which it induced complete loss of pigmentation while *DmHDAC4*^{WT} still exhibited some degree of red pigmentation (**Score: 2.50**) (**Figure 4.9N**).

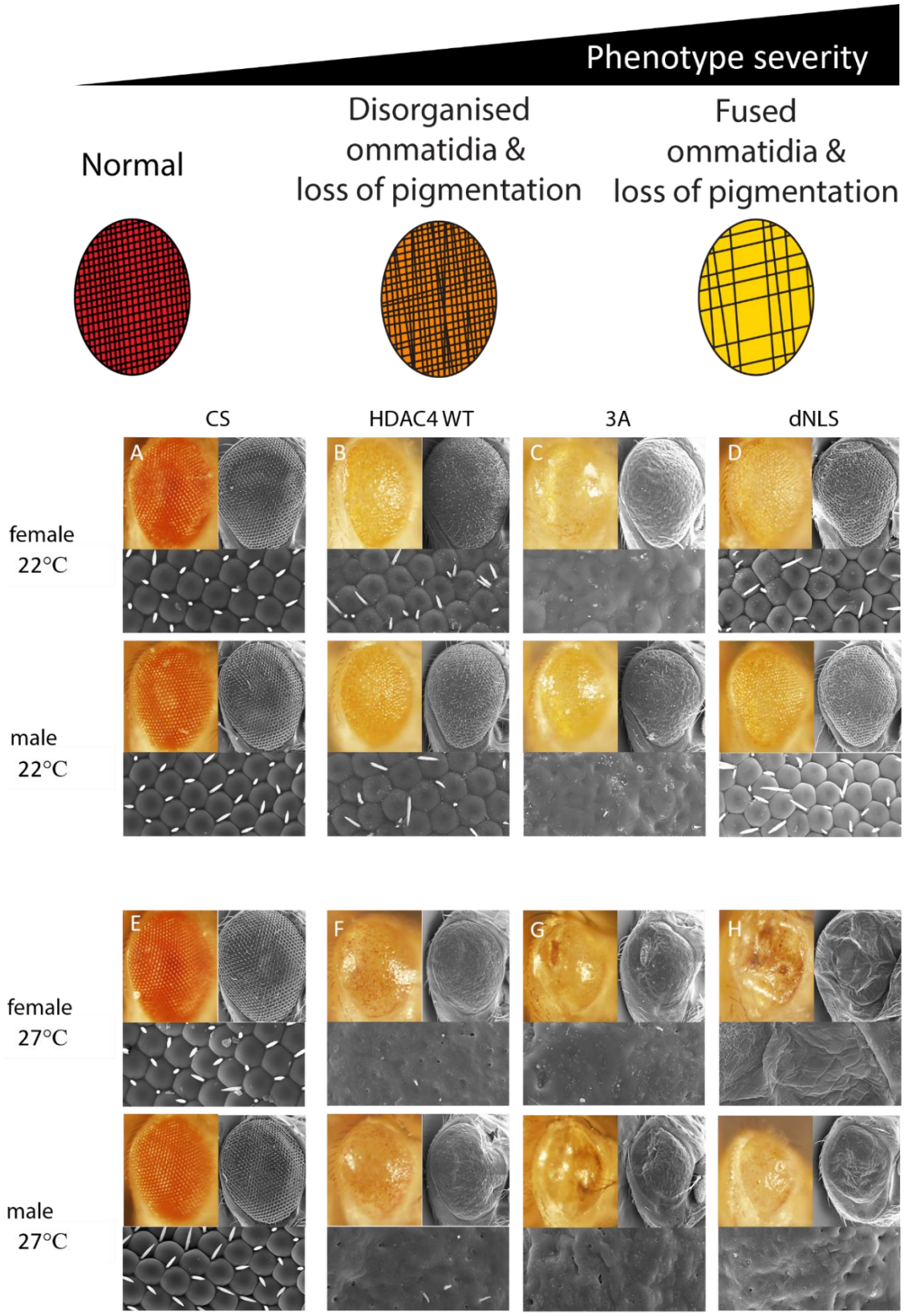

Continue next page ->

74

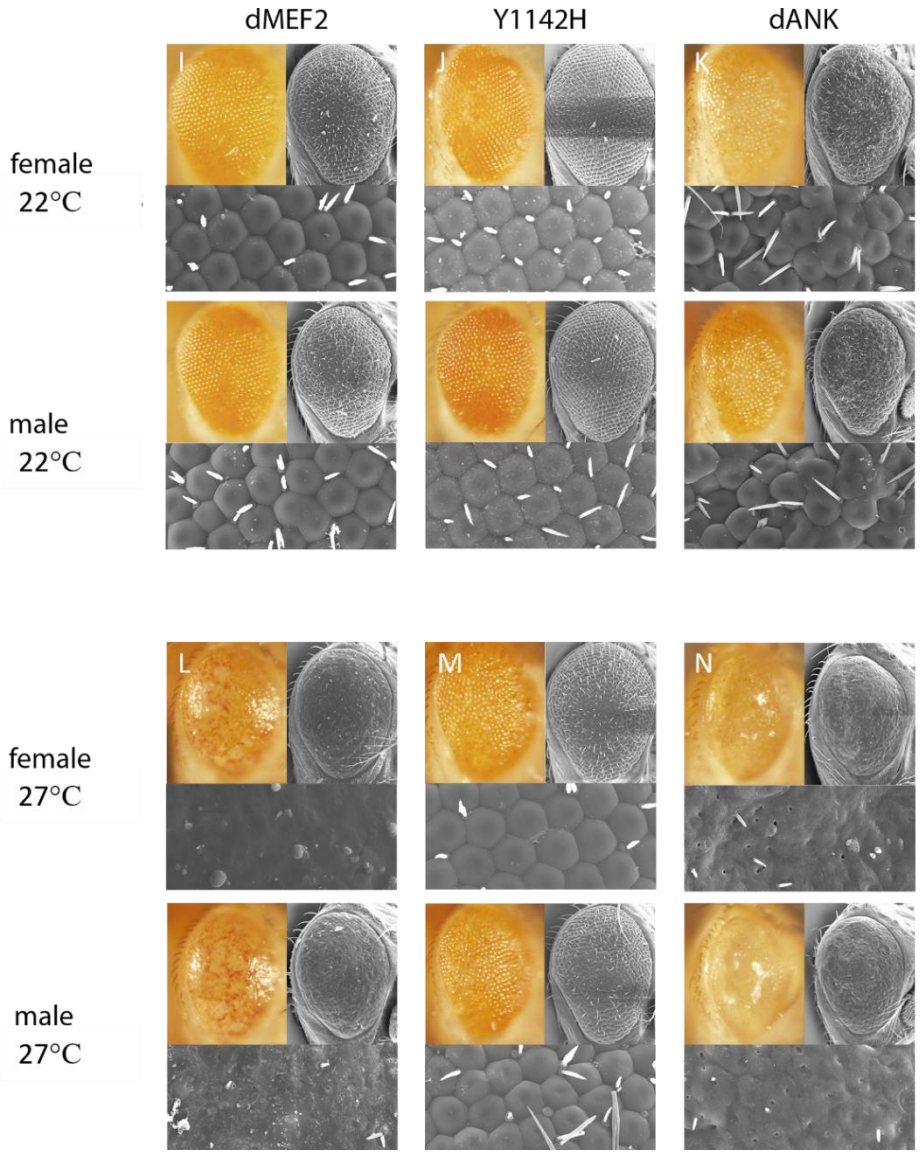

Raised at 22°C								
Phenotypes	**Severity Score**	**CS**	**DmHDAC4 WT**	**3A**	**dNLS**	**dMEF2**	**Y1142H**	**dANK**
Disorganised/missing bristles	0.50		√	√	√	√	√	√
Disorganised ommatidia	0.25		√		√	√		√
Partial ommatidia fusing	0.50							√
Complete ommatidia fusing	1.00			√				
Partial loss of pigmentation	0.50		√		√	√	√	√
Complete loss of pigmentation	1.00			√				
Patches of necrotic tissue	1.00							
Total Score		0.00	1.25	2.50	1.25	1.25	1.00	1.75

Raised at 27°C								
Phenotypes	**Severity Score**	**CS**	**DmHDAC4 WT**	**3A**	**dNLS**	**dMEF2**	**Y1142H**	**dANK**
Disorganised/missing bristles	0.50		√	√	√	√	√	√
Disorganised ommatidia	0.25						√	
Partial ommatidia fusing	0.50							
Complete ommatidia fusing	1.00		√	√	√	√		√
Partial loss of pigmentation	0.50		√			√	√	
Complete loss of pigmentation	1.00			√	√			√
Patches of necrotic tissue	1.00			√	√			
Total Score		0.00	2.00	3.50	3.50	2.00	1.25	2.50

Figure 4.9: Stereomicroscopy and SEM images of eye phenotypes from overexpression of *DmHDAC4* variants in the retina

Representative images of *Drosophila* female or male retina morphology of a control (CS, progeny of *GMR-GAL4* crossed to WT *w(CS10)* strain) and each *DmHDAC4* variant driven

by GMR-GAL4 driver raised at 22°C and 27°C. Top SEM image within each genotype was imaged at 250x magnification and bottom SEM image was imaged at 1500x magnification. Each genotype is n=12 which includes both males (n=6) and females (n=6). Tables summarise the phenotypes that were observed from each genotype. Severity score is an arbitrary value assigned to each phenotype based on its classification (E.g., ommatidia, pigments) and severity. Total score is an approximate measure of the overall phenotype. The higher the total score, the more severe the phenotype.

In order to confirm that the phenotypes observed in the eyes were due to the expression of each mutant rather than a non-specific effect, each variant was co-expressed with a *UAS-HDAC4* inverted repeat RNAi that targets the *HDAC4* mRNA for degradation (Dietzl et al., 2007). Knock down of *HDAC4* in a WT background does not impair eye development (**Supplementary Figure 9.7H**), therefore, expression of the RNAi was expected to reduce the eye deficits resulting from *DmHDAC4* variant expression. It was observed that these were reversed on co-expression of each variant with the RNAi, which confirms that the phenotypes were a specific result of expression of the variants (**Supplementary Figure 9.7I-N**).

In summary, increased *DmHDAC4* expression interferes with normal eye development, and this is dependent on the presence of an active deacetylase domain. Overexpression of nuclear-restricted *DmHDAC4* was shown to exhibit a more severe eye phenotype compared to $DmHDAC4^{WT}$, suggesting that nuclear HDAC4 is responsible for the majority of the phenotype. However, *dNLS* severely impacted development when expressed at a higher level, indicating a likely contribution from cytoplasmic DmHDAC4. Interestingly, the second cytoplasmic-restricted mutant, *dMEF2*, displayed a reduced phenotype compared to *dNLS*, therefore the mechanism through which *dNLS* impacts eye development may be mediated through an interaction with the MEF2-binding site. Lastly, the increased severity of the phenotype displayed by *dANK* suggests that the ankyrin-binding domain of DmHDAC4 may play a role in restraining the DmHDAC4 induced phenotype.

Although the rough eye phenotype assay provides an insight into the mechanisms through which increased DmHDAC4 impacts neurodevelopment, it should be noted that this analysis does not necessarily reflect the role of DmHDAC4 in other regions of the brain, thus it is desirable to also assess the variants in other neuronal populations, such as the KCs.

4.2.2 Characterisation of the impact of DmHDAC4 variant expression on MB development

The impact of expression of *DmHDAC4* variants on MB development was investigated by using the pan-neuronal GAL4 driver, *elavGAL4*, to selectively overexpress the variants during the developmental stages of MB formation. *elavGAL4* flies were crossed to each *DmHDAC4* variant as well as the *w(CS10)* (WT strain) control, and raised at 25°C over the course of development. Adult brains were dissected and processed for immunohistochemistry against FasII, a cell adhesion molecule that is highly expressed in the γ and α/β neuron and is a commonly used method for visualisation of the MB and assessment of MB developmental phenotypes. Each sample was blindly scored for its developmental defects in the γ, α and β lobes. Examples of the range of phenotypes observed are shown in **Figure 4.10**.

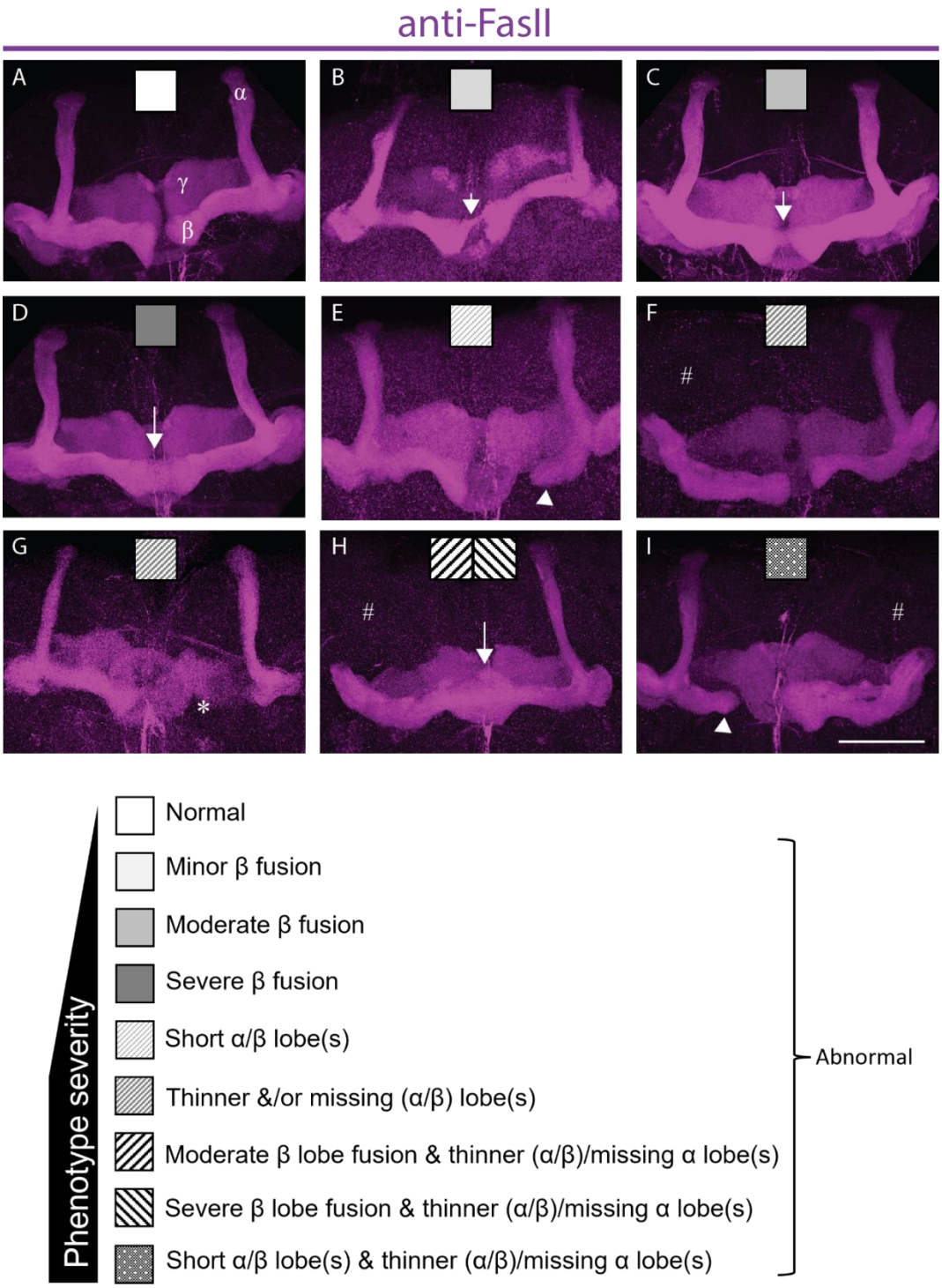

Figure 4.10: Representative images of MB phenotypes
Each image represents a distinct MB morphology identified from the phenotype assessment. Some of the more severe phenotypes were categorised together with a possibility of having multiple combination of characteristics. The phenotypic descriptions of each phenotype are listed in the order of least to the most severe with accompanying symbols that are used to depict the phenotypes in the subsequent bar graph figures. Arrowhead with short, medium, and long tails points to a minor, moderate and severe β fusion respectively. Arrowhead with no tail points to a shortened lobe. (#) represents missing α lobe while (*) represents missing β lobe. The image stacks are comprised of only the anterior MB image slices. Scale bar = 75µm.

The normal lobe phenotype is shown in **Figure 4.10A**. Abnormal phenotypes resulting from increased *DmHDAC4* expression include: β lobe fusion, which can be categorised as minor (**Figure 4.10B**), moderate (**Figure 4.10C**) or severe fusion (**Figure 4.10D**); a short (**Figure 4.10E**) or a missing α or β lobe (**Figure 4.10F & G**), both of which result from premature axon elongation; or multi-defect phenotypes such as having both β lobe fusion along with missing α lobe (**Figure 4.10H**); and shortened β lobe with missing or collapsed α lobe (**Figure 4.10I**).

The phenotypes described above are common developmental defects observed in other studies of MB development (Freymuth & Fitzsimons, 2017; Michel et al., 2004). A short or missing lobe indicates either an impairment in axon elongation leading to premature termination or guidance defect whereby the lobe elongates in an abnormal direction. The fusion of β lobes is also an elongation defect which results in axonal overgrowth and erroneous crossing of the brain's midline boundary (Kelly, Elchert, & Kahl, 2017; Michel et al., 2004). These phenotypes could indicate a defect in motility and navigation which then suggests a guidance mechanism has been impacted such as an alteration in expression or localisation of cell adhesion molecules which could in turn alter the dynamics of the actin cytoskeleton (Gomez & Letourneau, 2014). The brains were scored for the total percentage of abnormal samples for each genotype and broken down into percentages of sample exhibiting a particular morphological phenotype as shown above. Apart from the normal phenotype, all the phenotypes regardless of the number or severity were classified under the abnormal category for statistical testing of penetrance (**Figure 4.10**).

The *DmHDAC4* mutants were expressed in the *Drosophila* brain throughout development using the pan-neuronal driver line, *elavGAL4*, and the MB morphologies observed for each genotype were recorded. In an initial analysis to provide an indication of the phenotypic penetrance, the total percentage of abnormal brains observed for each variant was compared to the control (**Figure 4.11**). Pan-neuronal expression of $DmHDAC4^{WT}$, *3A*, *dANK* and *Y1142H* led to 100% phenotypic penetrance (i.e. all MBs displayed abnormal phenotypes). The *dNLS* mutant also exhibited increase in level of penetrance (~79%) compared to control but also had a significantly lower penetrance when compared to overexpression of $DmHDAC4^{WT}$. Interestingly, ~95% of *dMEF2* brains appeared normal with the remaining ~5% displaying only minor β lobe fusion, indicating that the MEF2-binding site plays an important role in contributing to the MB defects. It is also

worth noting that since *dNLS* and *dMEF2* are cytoplasmic-restricted mutants and *dMEF2* appeared to have a significantly lower penetrance compared to *dNLS*, this may suggest a role for DmHDAC4 in the cytoplasm that requires the MEF2-binding site.

Since a high percentage of brains with abnormal MBs does not necessarily indicate severity as the MB phenotypes encompasses a range of morphological characteristics, each genotype was qualitatively assessed based on its overall morphology to better understand each variant's function (**Figure 4.11)**. Approximately 21% (n=33) of *DmHDAC4*^{WT} brains exhibited multiple phenotypes with severe β lobe fusion and abnormal α lobes, ~12% displayed an α lobe phenotype and the remaining ~67% displayed only severe β lobe fusion. However, approximately ~45% (n=20) of the *3A* brains displayed the multiple phenotype pattern. The higher proportion of multiple phenotypes suggests that increased expression of nuclear-restricted *DmHDAC4* has strong influence on MB development. *dNLS* brains also exhibited some of the more severe phenotypes, with ~37% displaying multiple phenotypes and ~26% with severe β lobe fusion. The remaining morphologies were normal or less severe phenotypes such as moderate and minor β lobes fusion (~10% and ~5% respectively). Therefore, cytoplasmic-restricted *DmHDAC4* appears to have lesser impact on MB development than *3A*. Expression of *dANK* resulted in a high proportion of brains with multiple morphological defects than *DmHDAC4*^{WT} (n=18, ~61% with severe β lobes fusion and thinner (α/β)/missing α lobe(s)). Conversely, *Y1142H* had lesser impact on MB development with no brains displaying multiple defects. In this experiment, the *DmHDAC4* variants were expressed throughout the entire brain, therefore to provide further support to these finding and to investigate whether HDAC4 acts in a cell autonomous manner to induce MB deficits, expression of the variants was restricted to the MB.

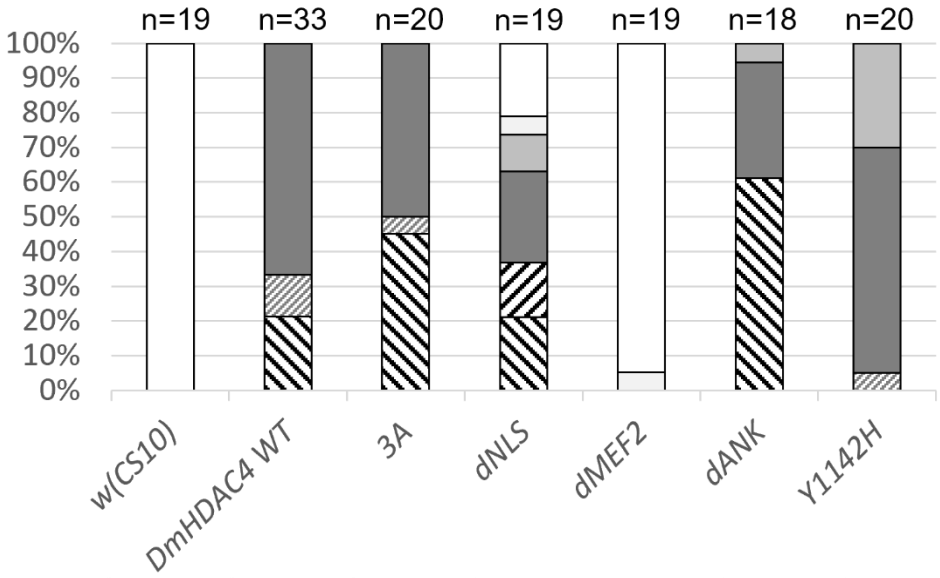

Genotype:	*w(CS10)*	*DmHDAC4 WT*	*3A*	*dNLS*	*dMEF2*	*dANK*	*Y1142H*
Normal	19	0	0	4	18	0	0
Abnormal	0	33	20	15	1	18	20

One-tailed Fisher's exact test:

w(CS10) vs *DmHDAC4 WT* – ***p<0.001
w(CS10) vs *3A* – ***p<0.001
w(CS10) vs *dNLS* – ***p<0.001
w(CS10) vs *dANK* – ***p<0.001
w(CS10) vs *Y1142H* – ***p<0.001
DmHDAC4 WT vs *dNLS* – **p<0.01
dNLS vs *dMEF2* – ***p<0.001

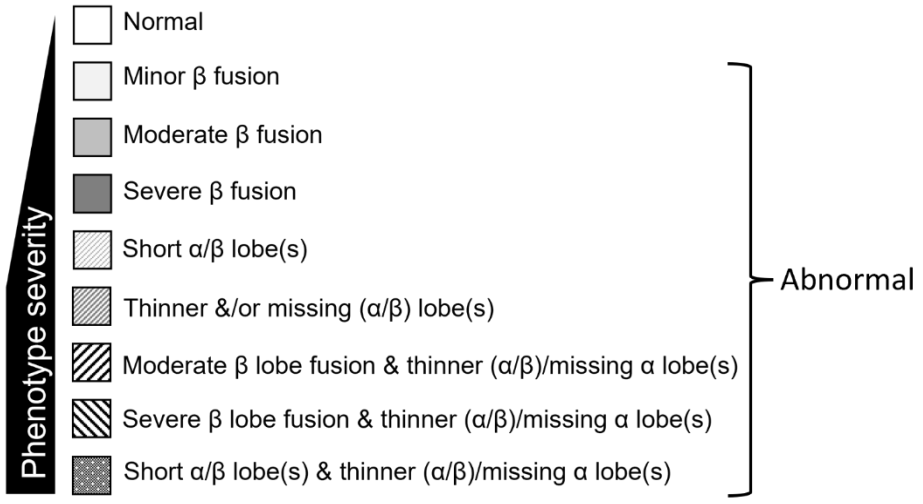

Figure 4.11: Phenotypes resulting from elavGAL4 driven expression of *DmHDAC4* variants in the MB

Each bar is comprised of the percentage of brains displaying each phenotype. The x-axis represents genotype of the control or UAS variant lines with the pan-neuronal (elavGAL4) driver raised at 25°C. The sample size for each genotype is indicated above each bar. Table displays the number of samples with normal or abnormal (combination of all phenotypes

within treatment). One-tailed Fisher's exact test was used for significance testing between comparison of interest.

The pan-MB TARGET driver *OK107GAL4;tubGAL80^{ts}* was used to drive expression in the MB, and the F1 progeny were raised at 30°C throughout development to induce expression (**Figure 4.12A**). A second set of crosses was raised at 18°C, at which expression remained uninduced and only a small number of minor defects were observed (**Figure 4.12B**). At 30°C, the overall phenotypic penetrance observed was very similar to that resulting from pan-neuronal expression, with the exception that the reduced penetrance of *dNLS* was not statistically significant when compared to *DmHDAC4^{WT}*, therefore, it is likely that *DmHDAC4* acts in a cell autonomous manner to impair MB development. However, the phenotypes were reduced in severity which was observed across all genotypes when expressed with *OK107GAL4;tubGAL80^{ts}*. This likely reflects a lower level of expression, although does not rule out non-autonomous effects.

A

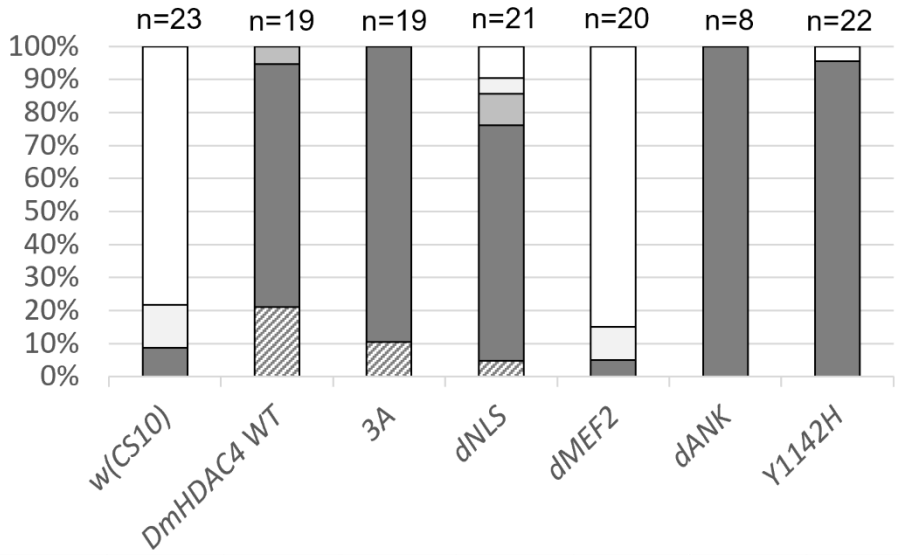

Genotype:	*w(CS10)*	*DmHDAC4 WT*	*3A*	*dNLS*	*dMEF2*	*dANK*	*Y1142H*
Normal	18	0	0	2	17	0	1
Abnormal	5	19	19	19	3	8	21

One-tailed Fisher's exact test:

w(CS10) vs *DmHDAC4 WT* – ***p<0.001
w(CS10) vs *3A* – ***p<0.001
w(CS10) vs *dNLS* – ***p<0.001
w(CS10) vs *dANK* – ***p<0.001
w(CS10) vs *Y1142H* – ***p<0.001
dNLS vs *dMEF2* – ***p<0.001

B

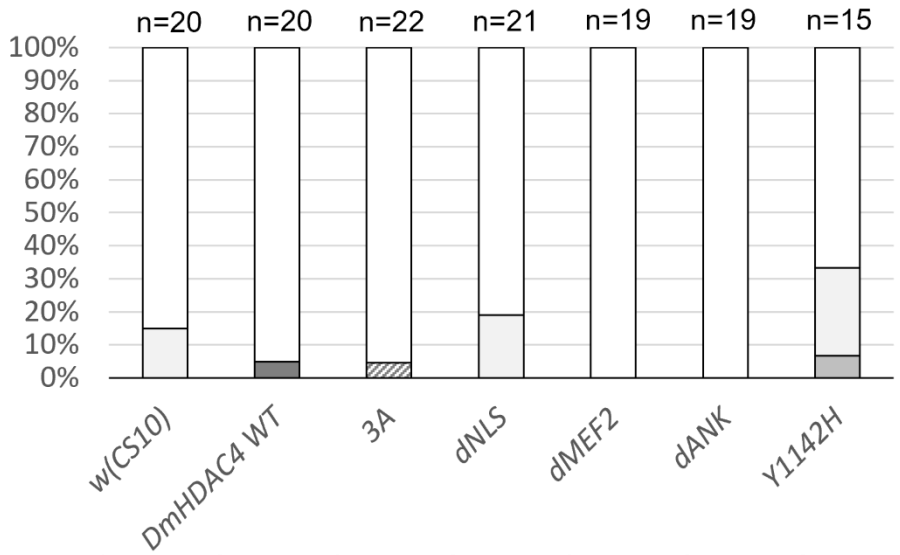

Genotype:	*w(CS10)*	*DmHDAC4 WT*	*3A*	*dNLS*	*dMEF2*	*dANK*	*Y1142H*
Normal	17	19	21	17	19	19	10
Abnormal	3	1	1	4	0	0	5

Figure 4.12: Phenotypes resulting from *OK017GAL4* TARGET driven expression of *DmHDAC4* variants in the MB
Each bar is comprised of the percentage of brains displaying each phenotype. The x-axis represents genotype of the control or UAS variant lines with the pan-MB (OK107GAL4; tubGAL80^{ts}) driver raised at (A) 30°C and (B) 18°C The sample size for each genotype is indicated above each bar. Tables display the number of samples with normal or abnormal (combination of all phenotypes within treatment). One-tailed Fisher's exact test was used for significance testing between comparison of interest.

Overall, the results of the MB phenotype penetrance indicate expression of *DmHDAC4^{WT}* impairs MB development in all brains when driven by pan-neuronal or MB-specific drivers. The phenotypes appear to be more severe with *3A* and *dANK*. The reduction in penetrance by *dNLS* was only significant when pan-neuronally expressed, however, the reduction in phenotype resulting from expression of *dMEF2* was highly significant for both drivers, indicating that MEF2-binding in the cytoplasm may be important in manifestation of the deficits. Deacetylase activity does not appear to be required in eliciting the phenotype.

4.2.3 Evaluating the efficacy of endogenous DmHDAC4 KD using the genetic tool: deGradFP

Initial analyses of the impact of expression of the variants on MB development uncovered differences that require further investigation, in particular the importance of the MEF2-binding site and the dispensability of the intact deacetylase domain. However, due to the 100% phenotypic penetrance, it is difficult to tease apart differences between *DmHDAC4^{WT}* and *3A*, *dANK* and *Y1142H*. In addition, since these initial analyses are a result of increased ectopic expression of WT or variant *HDAC4* in an endogenous *HDAC4* background, it would be ideal to partially replace endogenous *HDAC4* with each variant as a closer approximation to that which occurs in humans with heterozygous mutations or in disease models that cause dysregulation of the subcellular distribution of endogenous HDAC4.

The strategy chosen to address this was to incorporate the deGradFP genetic tool (see Section 1.7.2.3) into flies carrying protein-trapped HDAC4 (endogenous DmHDAC4 fused to a fluorescent protein such as GFP) (**Figure 4.13A**). When deGradFP is expressed, it binds the HDAC4::GFP protein and targets it for degradation. A *UAS-HDAC4* variant can also be co-expressed such that when the flies are subjected to 30°C

heat shock during development, endogenous DmHDAC4 will be degraded and the DmHDAC4 variant will be simultaneously expressed to replace endogenous HDAC4 (**Figure 4.13B**). Therefore, the next step was to first test the efficacy of deGradFP KD and its impact on MB development.

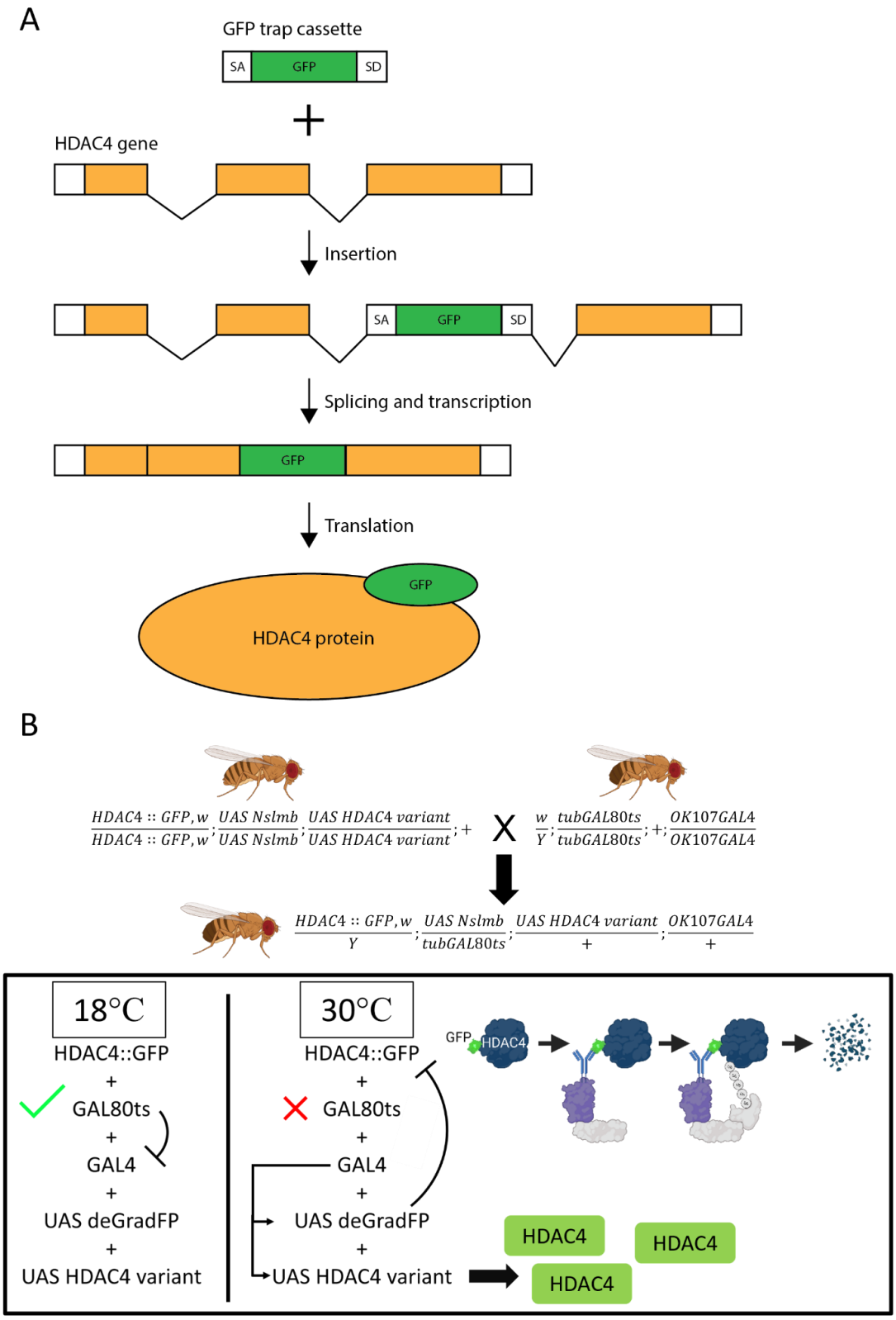

Figure 4.13: Strategy for expressing *DmHDAC4* variant in a reduced endogenous DmHDAC4 background using deGradFP
(A) Simplified illustration of a GFP trap cassette being introduced into *HDAC4*. (B)The diagram illustrates the generation of a fly line that will carry five transgene required for simultaneous KD of endogenous GFP trapped DmHDAC4 and expression of variant DmHDAC4 via temperature-regulated expression with $GAL80^{ts}$.

The UAS-deGradFP line (*UAS-Nslmb-vhhGFP4*) was crossed to a line carrying the pan-neuronal driver, *elavGAL4*, in a genetic background harbouring the HDAC4::YFP protein trap (*elavGAL4*, *HDAC4::YFP*), in which endogenous DmHDAC4 carries an insertion of YFP flanked by splicing sites in the second intron resulting in an internal fusion of YFP within the translated protein. Western blot analysis was first performed following KD with two individual deGradFP lines expressing the UAS transgene on the second (*UAS-Nslmb-vhhGFP4(2)*) or third chromosome (*UAS-Nslmb-vhhGFP4(3)*). These were compared to two different *UAS-HDAC4 RNAi* lines consisting of short hairpin and inverted repeat double-stranded RNA. Both deGradFP lines were effective at knocking down HDAC4::YFP as protein bands were not detected in either of the lines when compared to control (**Figure 4.14A**). As for the RNAi KD, only the dsRNA appeared to be effective in knocking down the protein level to an observable difference. In addition, when immunohistochemistry was conducted on brain samples derived from the same line of flies and assessed for MB phenotype using the anti-FasII antibody, both deGradFP KD resulted in a significant increase in MB defects (~36%), suggesting that DmHDAC4 is required in the fly brain for MB development (**Figure 4.14B**). These observations of the KD phenotype along with the assessment of the phenotype caused by the overexpression of $DmHDAC4^{WT}$ imply that tightly regulated expression of *DmHDAC4* is crucial during development to allow proper MB formation.

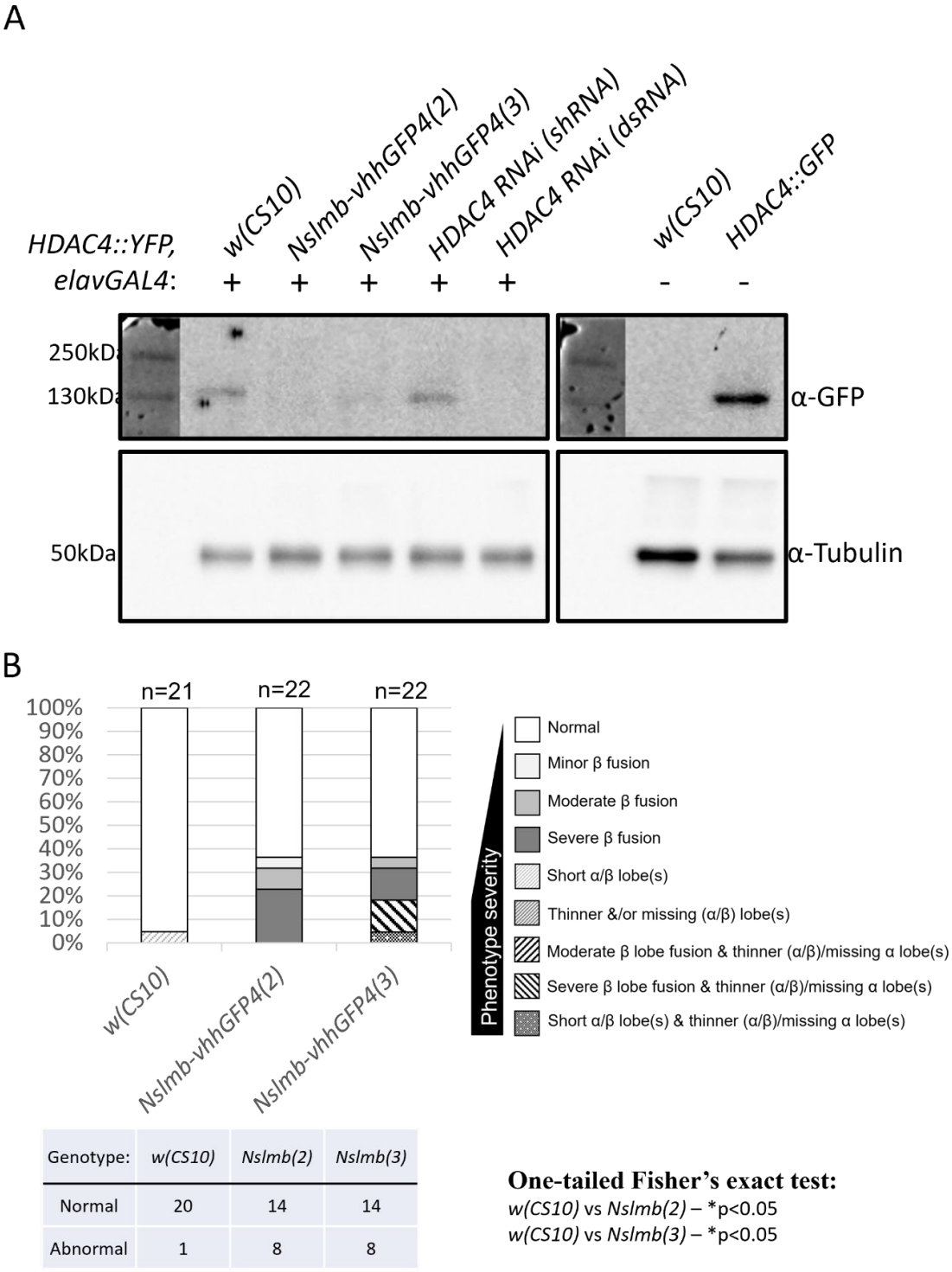

Genotype:	*w(CS10)*	*Nslmb(2)*	*Nslmb(3)*
Normal	20	14	14
Abnormal	1	8	8

One-tailed Fisher's exact test:
w(CS10) vs *Nslmb(2)* – *p<0.05
w(CS10) vs *Nslmb(3)* – *p<0.05

Figure 4.14: Expression levels of knocked down YFP tagged HDAC4
(A) Left panel: Western blot analysis of lysates (n=50 heads) of flies in which *elavGAL4* drives pan-neuronal expression of *deGradFP* (*Nslmb*) or *HDAC4* RNAi for KD of *HDAC4::YFP*. Right panel: Western blot analysis detection of GFP in lysates (n=50) of *HDAC4::GFP* or control *w(CS10)* heads. (B) Phenotypic analysis of MB defects resulting from deGradFP KD of HDAC4::YFP. Table displays the number of samples with normal or abnormal (combination of all phenotypes within treatment). One-tailed Fisher's exact test was used for significance testing between comparison of interest.

While these analyses confirm that the deGradFP construct is functional and effective at knocking down HDAC4::YFP, the detection of HDAC4::YFP was relatively weak, thus an alternate line with GFP-tagged endogenous HDAC4 (*HDAC4::GFP*) was obtained to determine if this protein trap line allows better detection. The presence of HDAC4::GFP was confirmed by western blot and resulted in a higher level of expression than HDAC4::YFP (**Figure 4.14A**), therefore further analyses were performed with HDAC4::GFP.

4.2.3.1 Generation of deGradFP transgenic crosses

With the transgenic tools verified, a strategy was required to combine the five transgenic constructs (*HDAC4::GFP*, *UAS-Nslmb-vhhGFP(2)*, *UAS-DmHDAC4 variant*, *OK107GAL4* and *tubGAL80^{ts}*) into the same fly line, which requires several generations of crosses. The crosses must be performed in an order that maximises the animal viability between crosses (combining multiple transgenes in one fly often results in reduced viability) and at the same time allows the tracking of each transgene through all generations of crosses. For this task, flies with balancer chromosomes were used to achieve the desired genotypes. Balancer chromosomes are genetically engineered chromosomes that contain mutations made up of inverted repeats throughout the chromosome which suppresses recombination. The balancer chromosomes are also homozygous lethal which then makes them suitable for maintaining recessive lethal lines. Additionally, the inverted repeat mutations exhibit dominant phenotype which can be easily visually observed (e.g. curly wings or additional thoracic bristles), thus these body markers serve to keep track of allele transmission between crosses (Beckingham et al., 2005).

In order to keep the genetic background of each transgenic flies consistent so as to minimise background effects, *HDAC4::GFP* and *UAS-Nslmb-vhhGFP4(2)* lines were initially placed into the same background as the UAS variant lines by backcrossing to the *w(CS10)* control line six times. After backcrossing, *HDAC4::GFP* was crossed into a double balancer line (balancers on the second and third chromosomes to aid in tracking *UAS-Nslmb-vhhGFP4(2)* and *UAS-DmHDAC4 variant* transgene) (**Supplementary Figure 9.4**). Next, the double balanced *HDAC4::GFP* line was crossed to the six UAS variant lines (**Supplementary Figure 9.5A)** and *UAS-Nslmb-vhhGFP4(2)*

(**Supplementary Figure 9.5B)** after which each of the balanced *HDAC4::GFP*;*UAS-DmHDAC4* lines was crossed to the balanced *HDAC4::GFP*;*UAS-Nslmb-vhhGFP4(2)* line and made homozygous. This combined all the necessary *UAS-DmHDAC4* transgenes with *UAS-Nslmb-vhhGFP4(2)* in an *HDAC4::GFP* background in a single fly line (**Supplementary Figure 9.6A)**. Finally, the female flies of the *HDAC4::GFP;UAS-Nslmb-vhhGFP4(2);UAS-DmHDAC4 variant* lines were crossed to *OK107GAL4;tubGAL80^{ts}* males, and F1 males were selected for analysis (all transgene are present only in male progeny as *HDAC4::GFP* is on the X chromosome and since it is not present in the *OK107GAL4;tubGAL80^{ts}* line, when females of the *HDAC4::GFP*;*UAS-Nslmb-vhhGFP4(2)*;*UAS-DmHDAC4* line are used, male progeny will carry one X chromosome from the *HDAC4::GFP*;*UAS-Nslmb-vhhGFP4(2)*;*UAS-DmHDAC4* line and the Y from the *OK107GAL4;tubGAL80^{ts}* line, whereas female progeny will only carry *HDAC4::GFP* on one of their two X chromosomes) (**Supplementary Figure 9.6B**).

After the crosses were generated, western blotting was performed on the *HDAC4::GFP* deGradFP lines expressing *3A* and *dNLS* to initially confirm the presence of *HDAC4::GFP* (**Supplementary Figure 9.8A**). Immunohistochemistry of the same genotypes was also performed with a Myc antibody to detect the presence of 3A and dNLS in the KCs, which also confirms that the flies possess the variant transgene (**Supplementary Figure 9.8B**). These verifications were also subsequently carried out on the other variants (data not shown). Although HDAC4::GFP was detected in all samples, the KD efficacy cannot be evaluated via western blot as the MB neurons in which *OK107* driver is active (i.e. driving expression of deGradFP) constitutes a small percentage of the total cells in a fly brain whereas HDAC4::GFP is expressed throughout the brain, therefore, the KD cannot be detected at a whole brain level. It was also noticed that the immunohistochemistry staining of HDAC4::GFP in the KCs lobes appears to be weaker in expression compared to the expression of *OK107GAL4* driven *UAS-DmHDAC4^{WT}* (**Supplementary Figure 9.8C**). While it is not appropriate to compare the expression pattern of these two genotypes as they were derived from two different antibodies (anti-GFP and anti-Myc) and Myc has been shown to also have non-specific binding from earlier western blot (**Figure 4.1I**), it raises the possibility that there could be a stronger expression of the UAS variant by *OK107* driver than that of endogenous HDAC4.

Having confirmed that the transgenes are in the *HDAC4::GFP* background, *3A* and *dNLS* were selected for a preliminary MB phenotype assessment to further determine the efficacy of the deGradFP system. These mutants (*HDAC4::GFP*;*Nslmb-vhhGFP4(2)*;*3A* and *HDAC4::GFP*;*Nslmb-vhhGFP4(2)*;*dNLS*) along with their respective controls (*HDAC4::GFP*;*3A* and *HDAC4::GFP*;*dNLS* in which the *deGradFP* transgene is not present and thus *HDAC4::GFP* will not be knocked down) were crossed to the *OK107GAL4;tubGAL80^{ts}* driver line. Two sets of each cross were set up and raised at 18°C and 30°C. Brains of male F1 progeny were dissected and assessed for MB defects. KD of *HDAC4::GFP* with *deGradFP* resulted in mild developmental defects when compared to the *HDAC4::GFP* control, indicating that DmHDAC4 is autonomously required in the MB (**Figure 4.15A**) for proper development, confirming the results as observed with *HDAC4::YFP* (**Figure 4.14B**). However, there was no significant difference in phenotypes between the variants expressed with or without deGradFP (i.e. *HDAC4::GFP;Nslmb-vhhGFP4(2)*;*3A* vs *HDAC4::GFP;3A*) (**Figure 4.15A**). The observed phenotypes were extremely similar to the range and severity of the defects that results from expression of the variants in the MB in the absence of KD (compare **Figure 4.15A** and **Figure 4.12A**). This suggests that the *DmHDAC4* variants were expressed at such a level that KD of endogenous DmHDAC4 was insufficient to reduce the overall expression of *DmHDAC4* to a level close to WT (and thus reduce the deficits). This is consistent with literature demonstrating that *OK107* driver promotes a high level of expression in all MB neurons (Aso et al., 2009), and the robust expression observed here for *DmHDAC4^{WT}* (**Supplementary Figure 9.8C**). In the 18°C crosses, some leaky penetrance, although insignificant, was detected in lines without deGradFP but not the ones with deGradFP. This suggests that the level of deGradFP is sufficient to suppress the leaky expression (**Figure 4.15B**). Since this system was engineered to include GAL80^{ts} for temperature-dependent control of GAL4 expression, the next step was to determine whether the expression of *DmHDAC4^{WT}* could be dialled down while still knocking down endogenous *DmHDAC4*. In Section 1.7.2.2, it was mentioned that GAL80^{ts} activity decreases linearly with respect to an increasing temperature between 20°C to 30°C (Schwartz et al., 2016) (**Figure 1.12B**), therefore, the objective was to use the assessment of MB phenotypes to identify the temperature that will allow GAL80^{ts} activity to moderate the expression of *DmHDAC4^{WT}* while also allowing sufficient KD of endogenous *DmHDAC4* to restore the overall level of DmHDAC4 close to WT levels. A

balance between the KD and transgene expression should theoretically display minimal or reduced phenotypic penetrance.

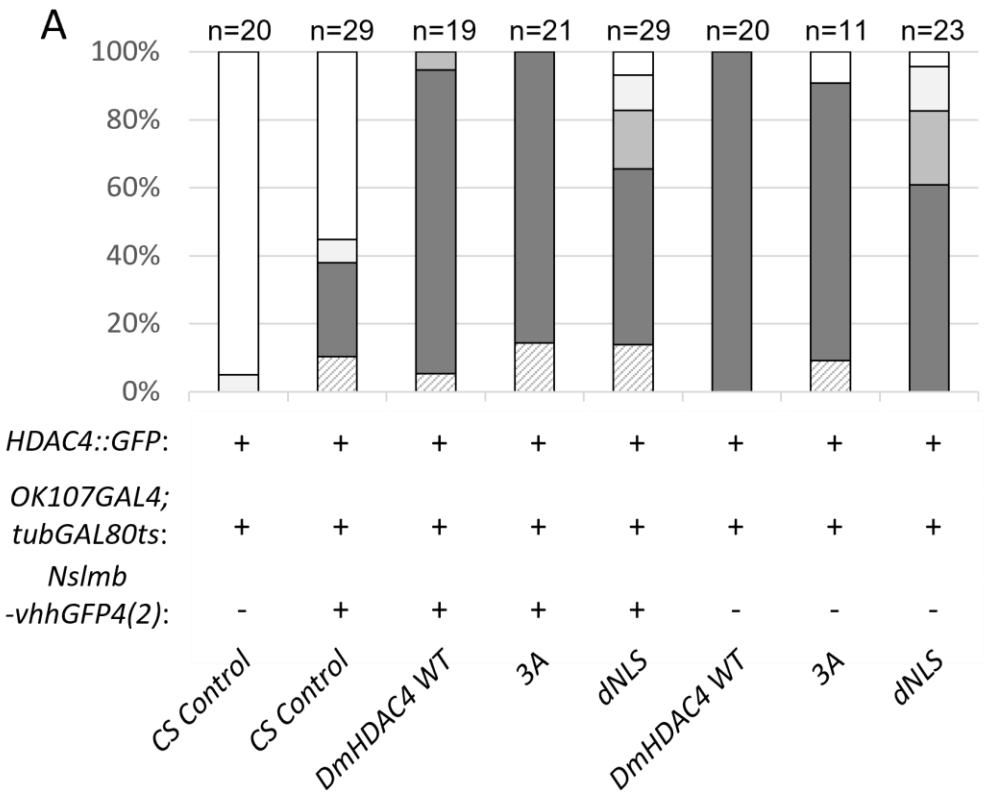

Genotype:	*CS*	*CS* w/ *deGradFP*	*DmHDAC4 WT* w/ *deGradFP*	*3A* w/ *deGradFP*	*dNLS* w/ *deGradFP*	*DmHDAC4 WT*	*3A*	*dNLS*
Normal	19	16	0	0	2	0	1	1
Abnormal	1	13	19	21	27	20	10	22

One-tailed Fisher's exact test:
CS vs *CS* w/ *deGradFP* – *p<0.05

Continue next page ->

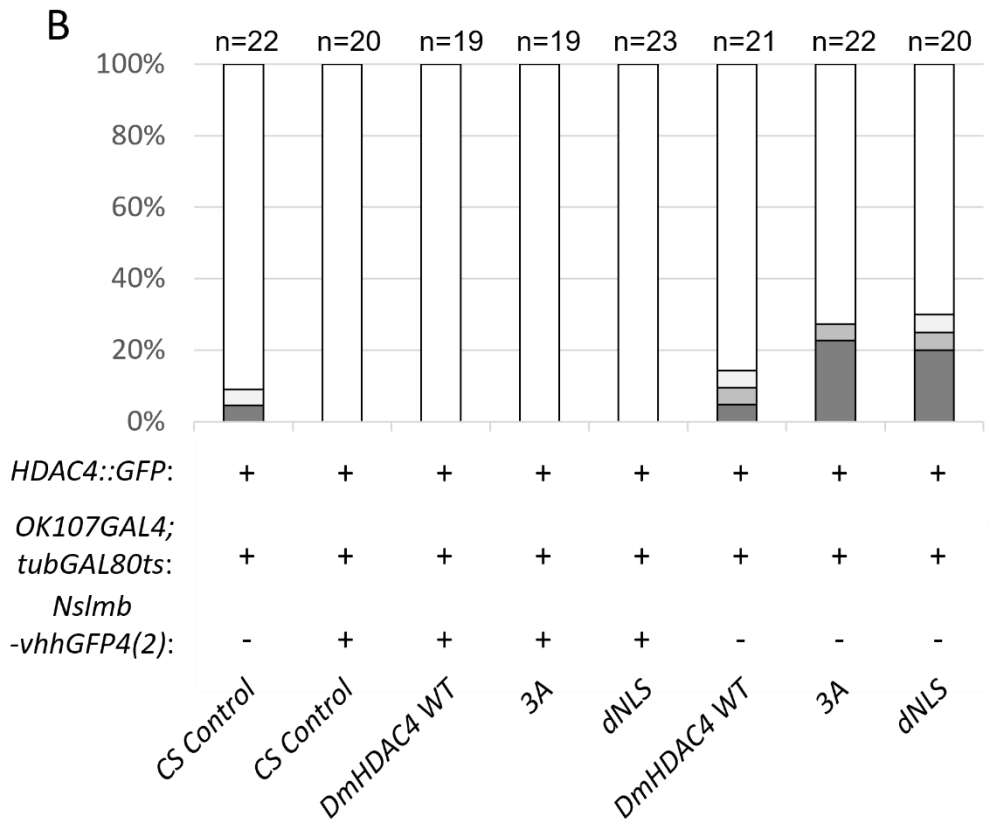

Genotype:	*CS*	*CS* w/ *deGradFP*	*DmHDAC4 WT* w/ *deGradFP*	*3A* w/ *deGradFP*	*dNLS* w/ *deGradFP*	*DmHDAC4 WT*	*3A*	*dNLS*
Normal	20	20	19	19	23	18	16	14
Abnormal	2	0	0	0	0	3	6	6

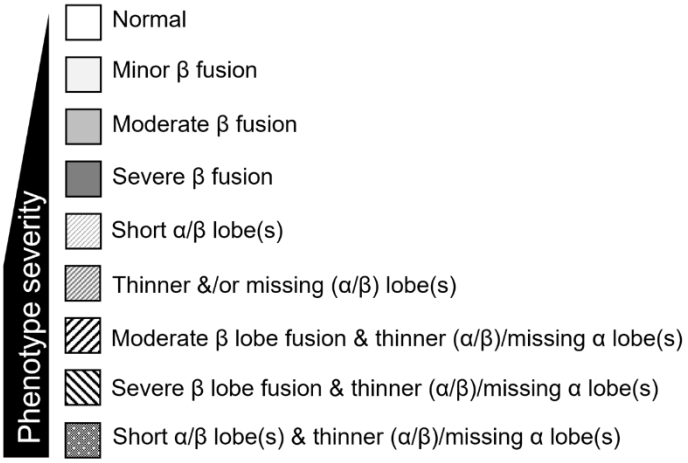

Figure 4.15: MB phenotypic penetrance of *DmHDAC4* variant expression in a deGradFP system background

Each bar represents the percentage of phenotypic distribution of a genotype. The x-axis represents genotype of the control or UAS variant lines with the transgenes required in a deGradFP system raised at (A) 30°C and (B) 18°C The sample size for each genotype is indicated above each bar. Tables display the number of samples with normal or abnormal (combination of all phenotypes within treatment). One-tailed Fisher's exact test was used for significance testing between comparison of interest.

A range of intermediate temperatures of 22°C, 25°C and 27°C were selected to raise the progeny of crosses between *OK107GAL4;tubGAL80^{ts}* and *HDAC4::GFP;Nslmb-vhhGFP4(2)* or *HDAC4::GFP;Nslmb-vhhGFP4(2);DmHDAC4* to determine if any of these temperatures would be suitable to establish a baseline MB phenotype penetrance resulting from *DmHDAC4^{WT}* expression in the presence of endogenous *DmHDAC4* KD (**Figure 4.16**). Another set of crosses using only *OK107GAL4* was also carried out to compare the MB defects resulting from *tubGAL80^{ts}*-regulated expression with those resulting from constitutively expressed *DmHDAC4* at each temperature (**Figure 4.16B & D**). The results suggest that at 22°C, the level of *tubGAL80^{ts}* expression is sufficient to dial down *DmHDAC4* transgene expression such that the defects are completely suppressed, however the endogenous *DmHDAC4* KD did not exhibit a phenotype, suggesting that the expression of deGradFP was also insufficient (**Figure 4.16A)**. A similar pattern of penetrance was also observed when the F1 progeny were raised at 25°C (**Figure 4.16C**). Finally at 27°C, approximately 35% of brains displayed defects in the presence of deGradFP, suggesting an efficient KD, and the defects observed when *DmHDAC4* was co-expressed were much lower than those without *tubGAL80^{ts}* (comparison not in figure), with the majority of the defects observed as minor β lobe fusion (**Figure 4.16E**). Therefore, this suggests that the *DmHDAC4^{WT}* expression has been dialled down to a level at which the overall amount of HDAC4 is not much higher than total endogenous HDAC4, and 27°C was deemed to be the suitable temperature to carry out the deGradFP experiment.

A

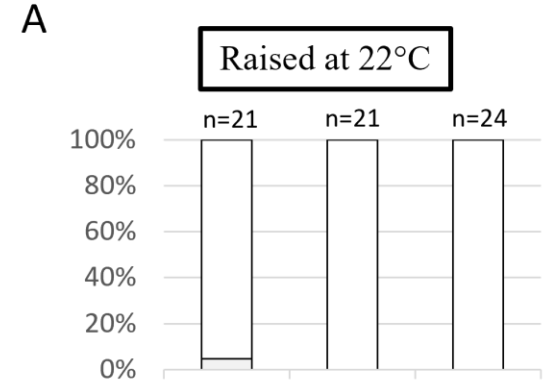

HDAC4::GFP:	+	+	+
Nslmb -vhhGFP4(2):	-	+	+
DmHDAC4 WT:	-	-	+

OK107GAL4; tubGAL80ts

Genotype: *HDAC4::GFP*	*HDAC4::GFP w/ deGradFP*	*HDAC4::GFP w/ deGradFP +DmHDAC4 WT*
Normal	20	21	24
Abnormal	1	0	0

B

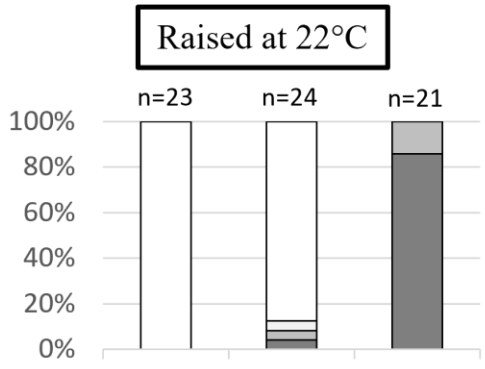

HDAC4::GFP:	+	+	+
Nslmb -vhhGFP4(2):	-	+	+
DmHDAC4 WT:	-	-	+

OK107GAL4

Genotype: *HDAC4::GFP*	*HDAC4::GFP w/ deGradFP*	*HDAC4::GFP w/ deGradFP +DmHDAC4 WT*
Normal	23	21	0
Abnormal	0	3	21

C

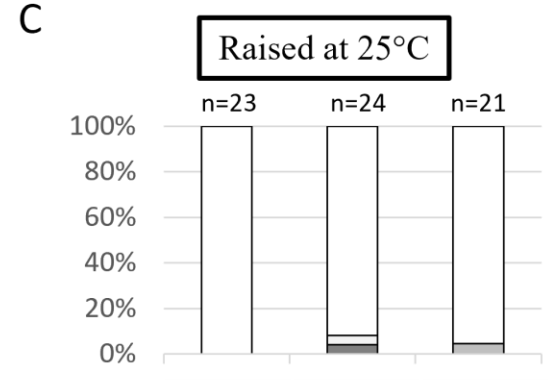

HDAC4::GFP:	+	+	+
Nslmb -vhhGFP4(2):	-	+	+
DmHDAC4 WT:	-	-	+

OK107GAL4; tubGAL80ts

Genotype: *HDAC4::GFP*	*HDAC4::GFP w/ deGradFP*	*HDAC4::GFP w/ deGradFP +DmHDAC4 WT*
Normal	23	22	20
Abnormal	0	2	1

D

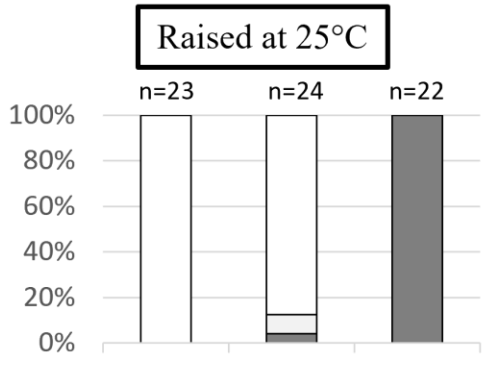

HDAC4::GFP:	+	+	+
Nslmb -vhhGFP4(2):	-	+	+
DmHDAC4 WT:	-	-	+

OK107GAL4

Genotype: *HDAC4::GFP*	*HDAC4::GFP w/ deGradFP*	*HDAC4::GFP w/ deGradFP +DmHDAC4 WT*
Normal	23	21	0
Abnormal	0	3	22

Continue next page ->

94

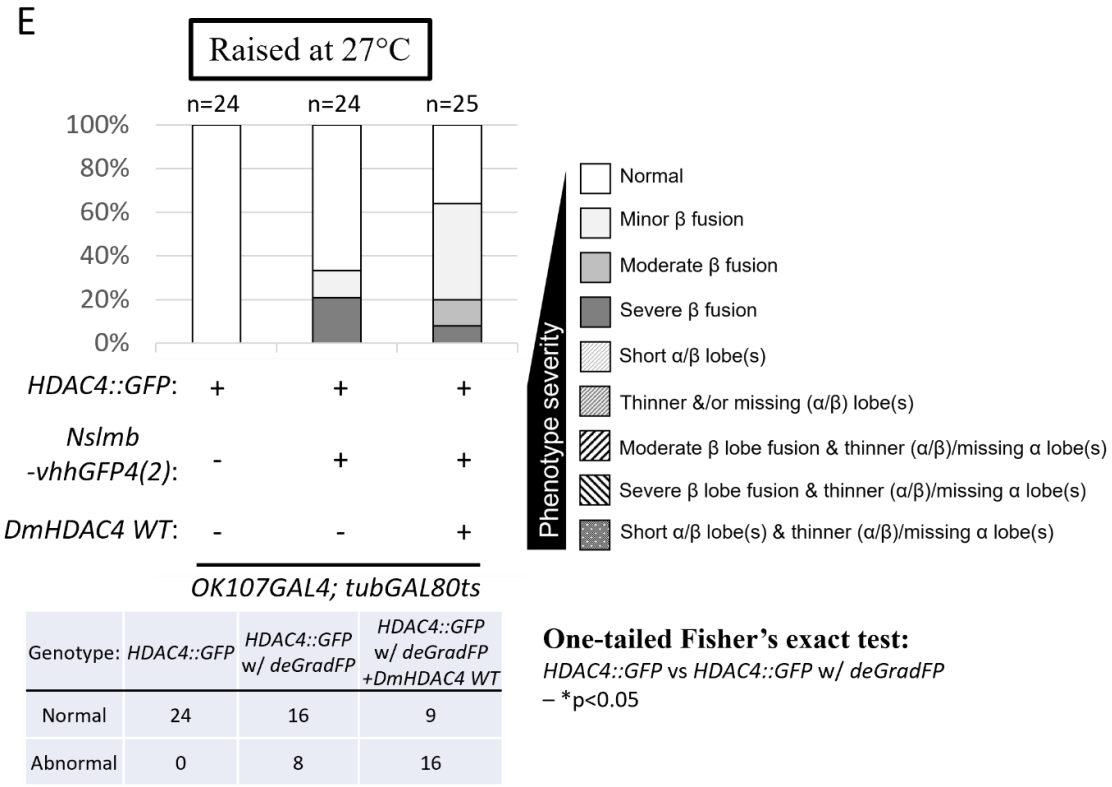

Genotype:	*HDAC4::GFP*	*HDAC4::GFP* w/ *deGradFP*	*HDAC4::GFP* w/ *deGradFP* +*DmHDAC4 WT*
Normal	24	16	9
Abnormal	0	8	16

One-tailed Fisher's exact test:
HDAC4::GFP vs *HDAC4::GFP* w/ *deGradFP*
– *p<0.05

Figure 4.16: Efficacy of MB specific TARGET line in driving Nslmb and UAS DmHDAC4 WT expression under different temperatures
Each bar represents the percentage of phenotypic distribution of a genotype. The x-axis represents the genotypes crossed to OK107GAL4; tubGAL80^{ts} driver raised at (A) 22°C, (C) 25°C and (E) 27°C. In (B) and (D), genotypes were crossed to only OK107GAL4 for 22°C and 25°C respectively. The sample size for each genotype is indicated above each bar. Tables display the number of samples with normal or abnormal (combination of all phenotypes within treatment). One-tailed Fisher's exact test was used for significance testing between comparison of interest.

4.2.4 The effects of DmHDAC4 variants on MB development when endogenous HDAC4 is reduced

Having determine the optimal temperature to carry out the experiment, all variant lines carrying *HDAC4::GFP* and *deGradFP* were crossed to *OK107GAL4;tubGAL80^{ts}*, and F1 progeny were raised at 27°C along with the respective controls. As seen in the pilot experiment (**Figure 4.16E**), expression of *DmHDAC4^{WT}* resulted in reduced penetrance with approximately 35% of brains displaying defects (**Figure 4.17**).

Interestingly, in the presence of endogenous *HDAC4* KD, only *3A* and *dANK* exhibited a significant increase in MB defects compared to *DmHDAC4^{WT}* (**Figure 4.17**). Therefore, the lack of significant difference between *DmHDAC4^{WT}* and *dNLS*, *dMEF2* or *Y1142H* suggest that these mutations do not affect MB phenotype when expressed at level close

to endogenous HDAC4. The expression of 3A, which is expressed at the same level as *DmHDAC4*^{WT} but accumulates in the nucleus, results in a significantly more severe phenotype, indicating that nuclear HDAC4 is detrimental to development. *dANK* also has a significantly higher penetrance compared to *DmHDAC4*^{WT} which highlights the importance of the putative ankyrin-binding site for proper MB development. It should also be noted that between the two cytoplasmic mutants, *dNLS* with *deGradFP* and *dMEF2* with *deGradFP*, while the difference was not statistically significant unlike *dNLS* versus *dMEF2*, it could also potentially imply a role for MEF2-binding site being required by cytoplasmic HDAC4.

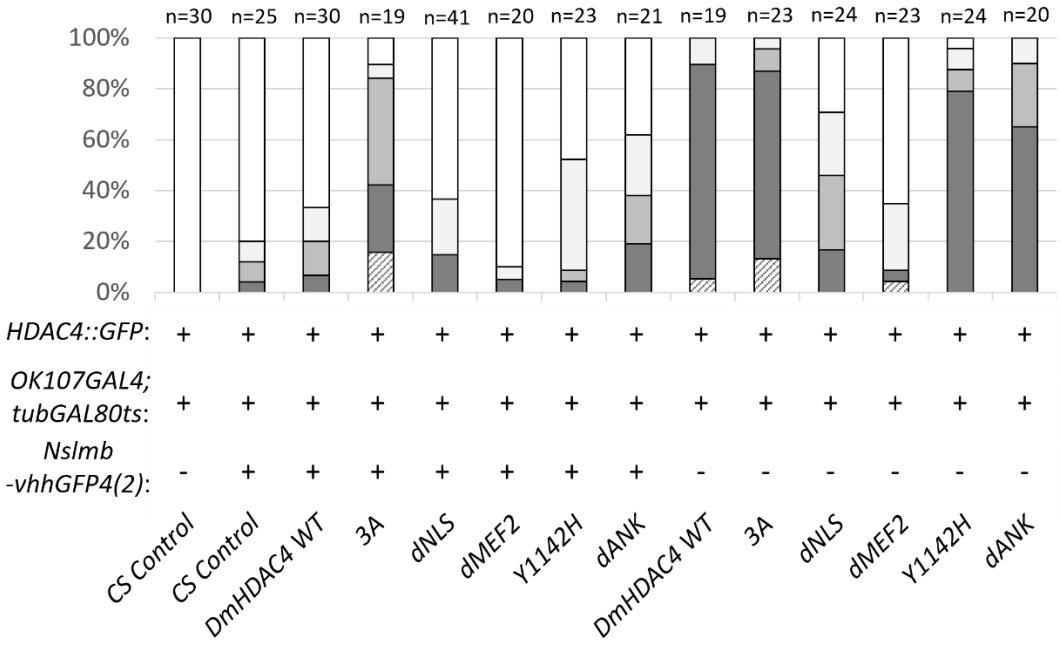

Genotype:	*CS*	*CS* w/ *deGradFP*	*DmHDAC4 WT* w/ *deGradFP*	*3A* w/ *deGradFP*	*dNLS* w/ *deGradFP*	*dMEF2* w/ *deGradFP*	*Y1142H* w/ *deGradFP*	*dANK* w/ *deGradFP*	*DmHDAC4 WT*	*3A*	*dNLS*	*dMEF2*	*Y1142H*	*dANK*
Normal	30	20	20	2	26	18	11	8	0	0	7	15	1	0
Abnormal	0	5	10	17	15	2	12	13	19	23	17	8	23	20

One-tailed Fisher's exact test:

CS vs *CS* w/ *deGradFP* – *p<0.05

DmHDAC4 WT w/ *deGradFP* vs *3A* w/ *deGradFP* – ***p<0.001

DmHDAC4 WT w/ *deGradFP* vs *dANK* w/ *deGradFP* – *p<0.05

dNLS vs *dMEF2* – *p<0.05

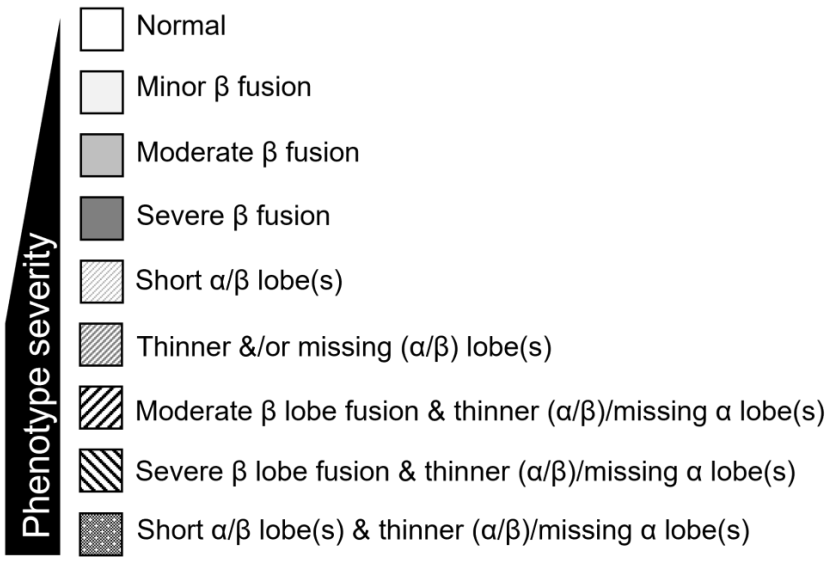

Figure 4.17: MB phenotypic penetrance of *DmHDAC4* variant expression with or without deGradFP raised at 27°C
Each bar represents the percentage of phenotypic distribution of a genotype. The x-axis represents genotype of the control or UAS variant lines with the transgenes required in a deGradFP system raised at 27°C. The sample size for each genotype is indicated above each bar. Table displays the number of samples with normal or abnormal (combination of all phenotypes within treatment). One-tailed Fisher's exact test was used for significance testing between comparison of interest.

4.3 The feasibility of Split GAL4 for MB subtype expression

The pan-MB GAL4 driver, *OK107*, enables robust transgene expression in all three MB intrinsic neurons (KCs), however, it does not allow for KC subtype-specific targeting. It is well established that the MB subtypes are functionally distinct from each other in terms of their roles in learning and memory (Fitzsimons et al., 2013; Freymuth & Fitzsimons, 2017) and therefore, it is important to be able to differentiate the subtypes. For example, expression of *DmHDAC4* or KD of the cytoskeletal regulator *Moesin* in the γ neurons impairs long-term courtship memory whereas expression in the α/β and α'/β' does not (Fitzsimons et al., 2013; Freymuth & Fitzsimons, 2017). Therefore, it is unclear whether MB defects resulting from expression of the *DmHDAC4* variants was a result of expression in all MB neurons or just a subset, and whether the defects in a particular KC subtype (e.g. elongation defects in the α lobe) occur in a cell autonomous manner, i.e. are a result of increased HDAC4 expression in that particular subtype. This is of interest as elongation of axons of the α lobe involves interaction with the neighbouring α' lobe axons (Siegenthaler, Enneking, Moreno, & Pielage, 2015). Additionally, most of the current KC subtype specific drivers have also been shown to drive expression in other brain regions

outside of the MB (Aso et al., 2009). This non-specificity could potentially have a confounding effect when overexpression or KD by these drivers are carried out. Therefore, the use of the Split GAL4 driver was proposed for manipulating gene expression in specific KC subtypes.

4.3.1 The Split GAL4 system

In the traditional GAL4/UAS system, specific promoters driving GAL4 enable tissue-specific expression of the UAS transgene in only the tissues in which the promoter is active. However, it is often the case that the promoters expressed in a region of interest are also expressed in other unwanted regions. This could pose a problem in a functional study which requires the expression to be specific to a certain region and having non-specific expression could introduce potential confounding effects. Therefore, the Split GAL4 system was designed to improve this problem (Luan, Peabody, Vinson, & White, 2006).

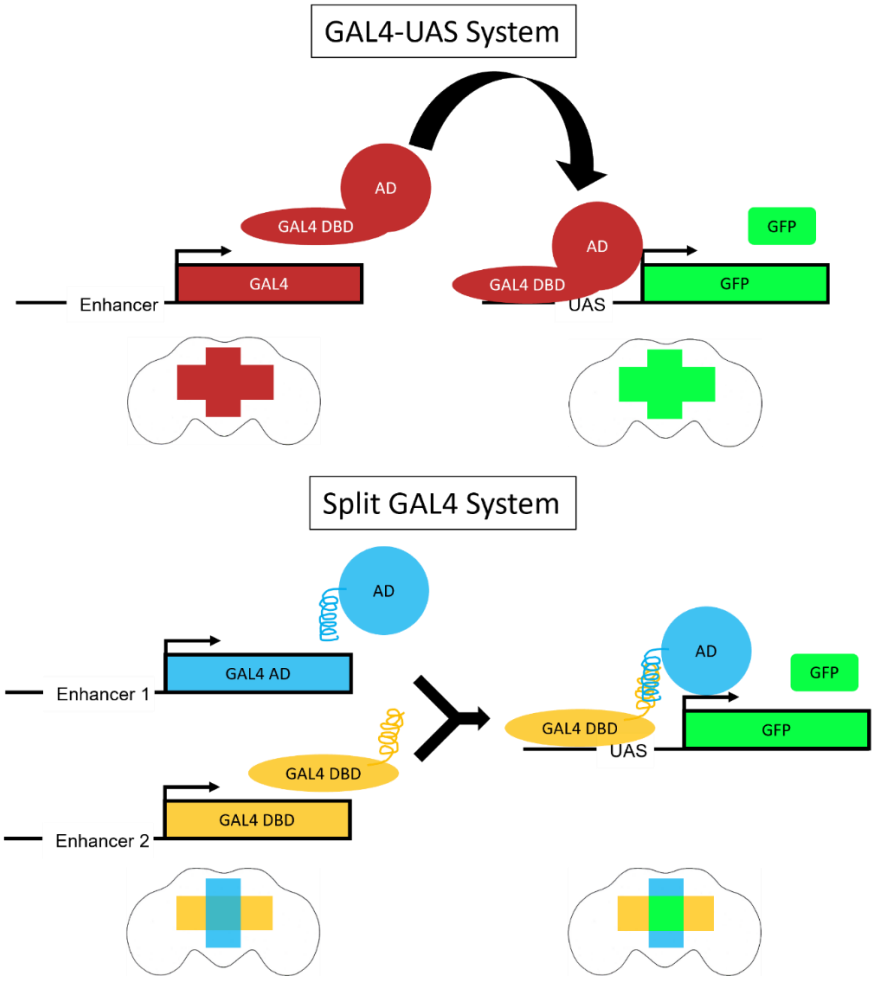

Figure 4.18: Comparison between the GAL4/UAS system and the Split GAL4 system
The traditional GAL4/UAS system (top) relies on a enhancer/promoter to drive the functional GAL4 which is then able to immediately bind to the UAS to drive the expression of the transgene (GFP) in all cells that express the promoter. In the Split GAL4 system, an enhancer (Enhancer1) is responsible for driving the transcription activating domain (AD) of the GAL4 and another enhancer (Enhancer 2) is driving the DNA-binding domain (DBD). The GAL4 will only be functional when the AD and DBD come together and join via the leucine zipper, therefore only cells that express both Enhancer 1 and Enhancer 2 can drive UAS expression. Modified from Luan *et al*. 2006

The Split GAL4 relies on the separation of expression of the GAL4 DNA binding domain (DBD) and the transcriptional activation domain (AD) by two different promoters or enhancers. At regions where the expression overlaps, the DBD and AD will come together to form a functional GAL4 which will then be able to activate expression of the UAS transgene only in these overlapping regions (**Figure 4.18**). This enables expression to be limited to a very small subset of cells, which minimises unwanted expression and can also provide better visualisation of a particular cellular subset in a dense neuronal population (Luan et al., 2006).

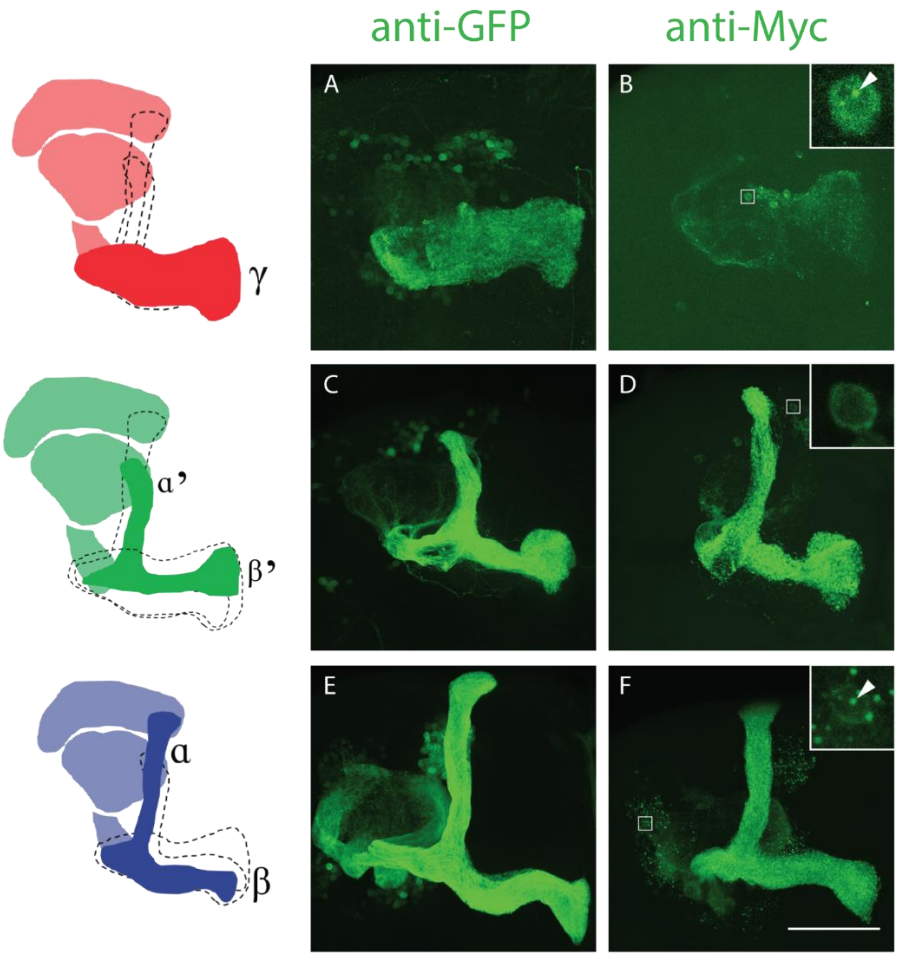

Figure 4.19: Representative images of GFP and DmHDAC4^{WT} expression pattern with KC subtype-specific Split GAL4 drivers
Split GAL4 driving GFP expression in the γ, α'/β' and α/β neurons of the MB are shown in (A), (C) and (E) respectively. Split GAL4 driving DmHDAC4^{WT} expression in the γ, α'/β' and α/β neurons of the MB are shown in (B), (D) and (F) respectively. White squares represent the single Kenyon cell bodies shown in the insets. Arrowhead points to an HDAC4 punctum. Each image of Split GAL4 expression pattern is a representative image of n=10 brains. The image stacks comprised of both the anterior and posterior MB image slices. Scale bar = 50μm.

To assess the specificity of the MB Split GAL4 drivers that are available to drive expression in the three KC subtypes (α/β, α'/β' and γ KCs), the expression of GFP was first characterised by crossing each Split GAL4 driver to a *UAS-GFP* line. Each lobe-specific Split GAL4 driver was shown to be robustly expressed and specific to its respective lobes (**Figure 4.19A, C & E**). Non-specific GFP expression in other brain regions was also not detected (not shown). This indicated high specificity which then allows the analysis of the overexpression pattern of *DmHDAC4^{WT}* in each of these drivers. However, the *γ lobe Spilt GAL4* driver was shown to drive very weak expression of *DmHDAC4* with minimal detection in the lobes (**Figure 4.19B**) and most of the brains had no detectable expression. This could be due to reduced promoter activity in the adult brain and protein turnover resulted in the degradation of the Myc-tagged DmHDAC4 prior to sample analysis. Despite the lack of DmHDAC4 detection with the γ lobe Split GAL4 driver, expression driven by the α'/β' and α/β Split GAL4 drivers led to strong detection in their respective lobes (**Figure 4.19D & F**). The difference in expression strength between γ lobe Split GAL4 and the other two Split GAL4s could suggest that the latter drivers remained active during the adult stage.

The level of DmHDAC4 in KC nuclei was also examined and punctate DmHDAC4 expression was observed in the γ and α/β neuronal nuclei with the nuclei of γ subset appearing to have higher expression compared to α/β (**Figure 4.19B inset & F inset**). This could perhaps also explain why the lobe expression of HDAC4 is weaker in the γ lobe which could have been due to a predominantly higher expression in the nucleus compared to cytoplasm.. Additionally, α'/β' Split GAL4 expression of DmHDAC4^{WT} exhibited strong lobe expression and a cytoplasmic halo phenotype around the nuclei, further suggesting that subcellular distribution of DmHDAC4 may be differentially regulated between the different KCs subtypes. Therefore, there could be a difference in protein environment between neuronal subtypes that may change the way HDAC4 behaves in nucleocytoplasmic shuttling. Interestingly, the level of lobe-specific

expression between α'/β' and α/β was similar despite the nuclear expression being markedly different.

4.3.2 Split GAL4 overexpression of *DmHDAC4*^{WT} on MB development

While assessing the expression pattern of DmHDAC4^{WT} in each of the Split GAL4 lines, it was noticed that developmental phenotypes that were observed on pan-neuronal or pan-MB *DmHDAC4*^{WT} overexpression were absent when expression was restricted to an individual lobe (KC subtype). This lack of phenotype could be due to a non-autonomous process by *DmHDAC4* expression in neighbouring KC cell-types exerting its effect on the lobe of interest (**Figure 4.20**). Therefore, the lobes of all KC subtypes were assessed for developmental defects resulting from *DmHDAC4* expression driven by each of the three Split GAL4 drivers via the anti-FasII antibody to label the α/β and γ lobes and the anti-Trio antibody which labels the α'/β' lobes.

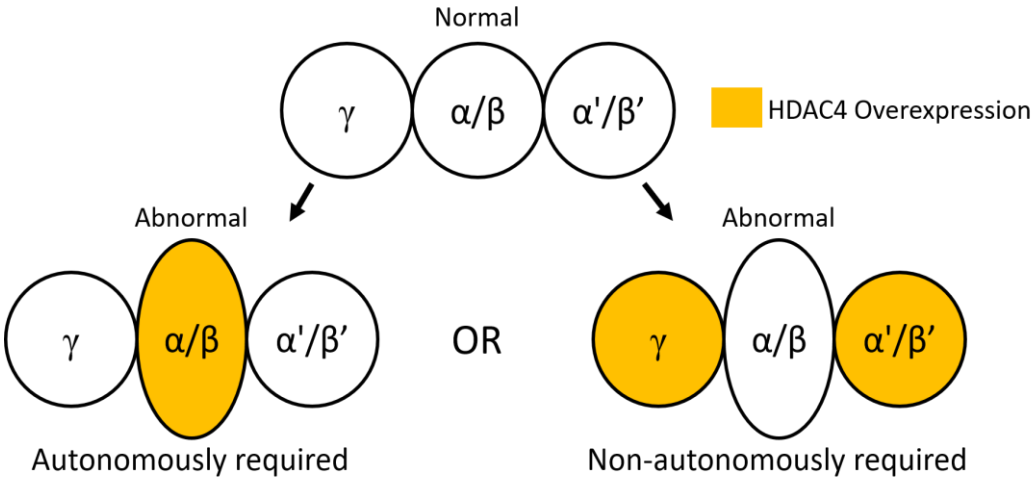

Figure 4.20: Diagrammatic representation of cell autonomy
The different types of MB neurons are represented by the circles which indicate normal development while ovals denote abnormal development. Abnormal development of cells caused by specific overexpression of HDAC4 to the cell type will suggest that HDAC4 is autonomously required in the development while abnormal development caused by non-specific overexpression of HDAC4 in other cell types will suggest that HDAC4 is non-autonomously required.

Surprisingly, it was discovered that all subtype-specific expression of *DmHDAC4*^{WT} did not exhibit any kind of MB structural defect (**Figure 4.21A-C**). Although expression of *DmHDAC4*^{WT} was not detected in the lobes when driven by the γ lobe Split GAL4 driver

in this analysis (**Figure 4.21A**), it was assumed that expression did occur at an earlier stage based on previous samples that exhibited weak DmHDAC4 expression (**Figure 4.19B**). Therefore, it was rationalised that the absence of developmental phenotype could be due to the nature of how the Split GAL4 operates. The system is only functional when the two hemi-drivers are activated (**Figure 4.18**). This additional step in requiring two different enhancers to drive expression for the formation of functional GAL4 could potentially cause a delay in expression due to differences in temporal activities by each enhancer (i.e. functional GAL4 will only be formed when both drivers are active). Therefore, this will affect the function during development when the formation of the functional GAL4 misses the window of crucial development stage, making this driver unsuitable for developmental study. However, the presence of DmHDAC4 expression in α'/β' and α/β neurons in the developed brains suggest that α'/β' and α/β lobe Spilt GAL4 drivers could be useful for post-developmental functional studies.

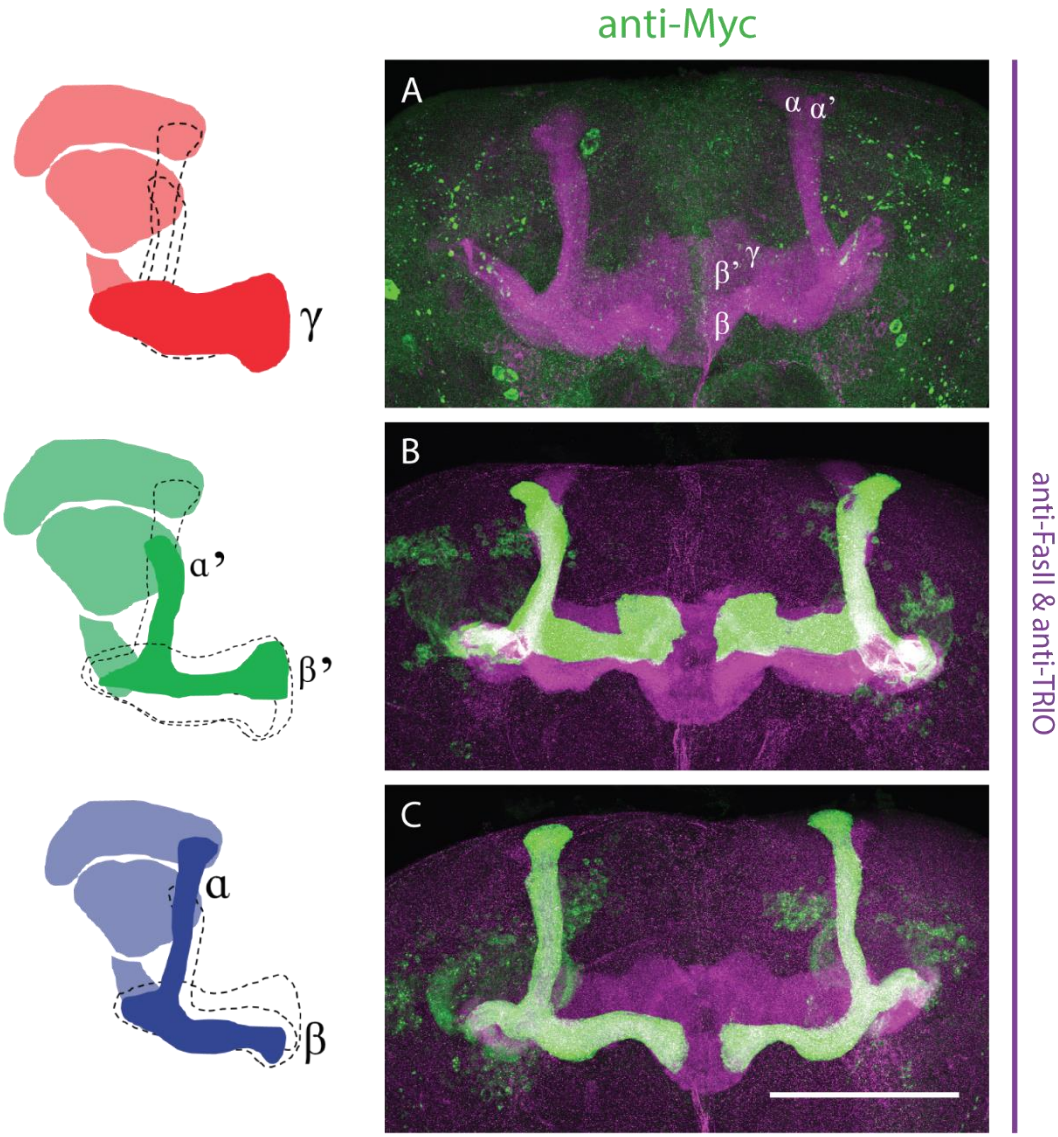

Figure 4.21: Representative images of MB structures with OE of DmHDAC4^{WT} by MB Split GAL4
(A, B & C) Each image shows the MB morphology through the counterstaining of FasII and TRIO antibody and the expression pattern of WT HDAC4 by its respective Split GAL4 drivers. Each image is representative of n=20 brains. The image stacks comprised of both the anterior and posterior MB image slices. Scale bar = 100µm

4.4 Discussion

Elucidating the role of HDAC4 in regulation of neuronal function has been a topic of interest in the neuroscience research community over this recent decade. As briefly introduced in the background section, knockout of *HDAC4* in the mouse brain leads to memory impairment (Kim et al., 2012), while in humans, deletion of the HDAC4 locus is the major genetic contributor to 2q37 deletion syndrome which impacts neuronal

development and results in intellectual disability (Le et al., 2019; Villavicencio-Lorini et al., 2013; Williams et al., 2010). Another neurodevelopmental disorder, CDKL5 disorder, is associated with reduced HDAC4 phosphorylation and a concomitant increase in nuclear retention (Trazzi et al., 2016). Increased abundance of nuclear HDAC4 has also been associated with memory impairment in mice (Sando et al., 2012). A role for cytoplasmic HDAC4 was also reported in *C. elegans* where overexpression was shown to increase memory performance (Wang, Cheng, et al., 2011). This suggests that HDAC4 has differing roles that are dependent on its subcellular distribution. While traditional roles of HDAC4 such as its ability to undergo nucleocytoplasmic shuttling and its role in regulating MEF2 activity have been studied over the past decades (Chawla et al., 2003; Haberland et al., 2009; Miska et al., 1999), the mechanism through which it affects neuronal function is still not well understood. In *Drosophila*, the overexpression or KD of *HDAC4* in the MB results in impairment of 24-hour courtship memory (Fitzsimons et al., 2013), therefore using *Drosophila* as a model for the neuronal studies of HDAC4 could provide further insights into the underlying mechanism. Here, a system was developed to evaluate the importance of subcellular distribution and specific domains motifs within HDAC4 in development of the CNS *in vivo*.

4.4.1 Characterisation and confirmation of the appropriate expression and distribution of HDAC4 mutant in neurons

The expression patterns of transgenic flies that expressed different variants of Myc tagged DmHDAC4 were characterised in the MB. Expression of DmHDAC4^{WT} showed that it localised to both the nucleus and lobes (axons) of KCs, although only a subset of nuclei contained DmHDAC4, which is a similar distribution pattern to that observed in the mouse brain in which HDAC4 is predominantly cytoplasmic but localises to nuclei in some regions of the brain (Darcy et al., 2010). The presence of DmHDAC4 in subset of KCs nuclei suggests nucleocytoplasmic shuttling of the protein and this could point to a conserved role with the mammalian system where localisation of HDAC4 in cultured hippocampal neurons (neurons important for learning and memory) was dynamically regulated in response to environmental stimuli such as synaptic activation (Chawla et al., 2003). In a recent study conducted by Main and colleagues (2021) where GFP-tagged *DmHDAC4* and *hHDAC4* were expressed in KCs, it was revealed that, similarly to this

study, DmHDAC4 protein was observed in some nuclei despite being predominantly cytoplasmic. However, when *hHDAC4* was expression, KC nuclei were completely devoid of hHDAC4 protein, suggesting a fundamental difference in regulation of subcellular distribution between vertebrate and invertebrate HDAC4. This is unlikely to be a result of an overexpression effect resulting in nuclear accumulation as *hHDAC4* was expressed at the same driver as *DmHDAC4*. While the reason for this difference is unclear, a possibility could be due to the efficacy of the 14-3-3ζ in exporting HDAC4 out of the nucleus through the binding to the phosphorylated serine residues. As 14-3-3ζ binds to HDAC4 in a phosphorylation-dependent manner, which then leads to its dissociation from transcription factors such as MEF2 (McKinsey et al., 2001; Miska et al., 2001), it is speculated that although hHDAC4 is able to translocate to the cytoplasm in *Drosophila* KC neurons, because it is not native to *Drosophila*, it could perhaps be lacking in its ability to bind transcription factors in *Drosophila* neurons. This could potentially lead to more unbound phosphorylated hHDAC4 which could then be easily transported out of the nucleus by 14-3-3ζ with minimal hindrance, thus resulting in a complete cytoplasmic distribution pattern that was observed by Main et al. (2021). However, this would require verification such as doing co-immunoprecipitation on hHDAC4 expressing flies to determine the efficacy of binding to *Drosophila* MEF2.

The nuclear-restricted mutant 3A localised only to the nuclei of the KCs where it accumulated into puncta. Main et al. (2021) also showed hHDAC4 with *3A* mutations to have a similar phenotype. Additionally, hHDAC4 in cell culture was shown to localise to the nuclei when the corresponding serine residues were mutated to alanines (Paroni et al., 2004). Nuclear puncta were also observed with $DmHDAC4^{WT}$ overexpression, however, the puncta were much smaller and much of the protein was still distributed evenly across the nuclei, thus increased abundance of DmHDAC4 in the nucleus is associated with increased puncta formation. These HDAC4 aggregates are proposed to be formed through HDAC4 tetramerization via its N-terminal glutamine-rich domain which is arranged into an α-helix formation. When increased in abundance, the tetramers have been shown to oligomerise in vitro (Guo, Han, Bates, Cao, & Chen, 2007). This formation of protein aggregates resembles the hallmark of diseases such as AD where the accumulation of β-amyloid proteins results in plaque formation in the brain (Murphy & LeVine, 2010). Indeed, it was observed in post-mortem AD brain that HDAC4 accumulation in the nuclei of hippocampal neurons increase in relation to the disease severity (Shen et al., 2016). In

brainstems from PD individuals, HDAC4 was shown to colocalise with α-synuclein, which is the main component of the protein aggregates that form the Lewy bodies, which impede neuronal function (Takahashi-Fujigasaki & Fujigasaki, 2006). Spinocerebellar ataxia type-1, a neurodegenerative disease that is caused by the formation of ataxin-1 aggregates has been shown to involve interaction with HDAC4. An *ataxin-1* mutant that impairs HDAC4 binding displays reduced neurotoxicity in neuronal cell culture (Bolger, Zhao, Cohen, Tsai, & Yao, 2007). Therefore, it will be interesting to further understand the formation of DmHDAC4 puncta aggregates and their role in contributing to neurotoxicity. In fact, this topic is currently a PhD project that is undertaken by another student in this laboratory.

The cytoplasmic-restricted mutants *dNLS* and *dMEF2* were both highly localised to the lobes of the KCs but not within the nuclei, confirming that mutation of the NLS prevents HDAC4 from entering the nucleus and that the MEF2-binding site is also important for targeting HDAC4 to the nucleus, as has previously been shown for vertebrate HDAC4 (Wang & Yang, 2001). A similar mutation in the MEF2-binding site of hHDAC4 was generated by Main and colleagues (2021) and this mutant was also restricted to the cytoplasm, thus suggesting the conserved role of the regulation of nuclear entry by MEF2 across vertebrates and invertebrates. The dANK and Y1142H mutants displayed subcellular distribution pattern that was similar to DmHDAC4^{WT}, which indicates that these mutants are not involved in the process of nucleocytoplasmic shuttling.

4.4.2 Disruption of HDAC4 subcellular distribution, enzyme activity and ankyrin-binding alters developmental phenotypes in photoreceptors

Expression of the variants in developing photoreceptor neurons revealed a range of developmental phenotypes among the different variants. Expression of *DmHDAC4^{WT}* disrupted normal eye development, and the phenotype was more severe when restricted to the nucleus, with increased fusion of ommatidia and the presence of necrotic tissue. This could be through the increased formation of puncta, as described above, and/or alterations to transcription, which will be investigated and discussed in Chapter 6. While it is unclear how the increased in puncta formation leads to a more severe phenotype, a possibility is that an increase nuclear presence could lead to more repression of developmental related genes. However, aggregation of HDAC4 puncta may potentially

impair its normal function. Perhaps, aggregation of HDAC4 could impede normal nuclear processes by sequestering transcription factors or proteins required for normal function. This could potentially lead a to loss or gain of function depending on the protein it binds to and the process that was impacted. Therefore, a study is currently underway in this laboratory to identify the proteins that can bind to these nuclear-restricted HDAC4 using a co-immunoprecipitation and mass spectrometry approach. This could potentially provide insights into the pathways that might be affected when HDAC4 aggregates into nuclear puncta.

dNLS expression also resulted in a similar phenotype to *3A* when flies were raised at 27°C. Since, *dNLS* exhibited a less severe phenotype compared to *3A* at 22°C, it highlights a fundamental difference in eye development that is due to DmHDAC4 subcellular localisation and could potentially implicate HDAC4 in an unknown cytoplasmic role that results in impairments to eye development when highly expressed. Interestingly, the loss of the MEF2-binding site resulted in reduced phenotype severity which suggests that the MEF2-binding site is required for the full range of defects resulting from expression of cytoplasm-restricted DmHDAC4, however it should be noted that the *dMEF2* phenotype was still significant. Since MEF2 is a transcription factor found only in the nucleus, it is therefore puzzling to discover that MEF2-binding site is required in the cytoplasm to elicit eye defect shown in *dNLS* which has a functional MEF2 binding site. This leads to the question of what other proteins could be interacting with the MEF2-binding site when HDAC4 is in the cytoplasm that may have caused the impairment to eye development. It should also be noted that the expression of *dMEF2* mutant which has similar eye developmental phenotype severity to *DmHDAC4*^{WT}, could also suggest its activity in the cytoplasm to influence eye development process can also potentially be independent of MEF2-binding. Therefore, the role of MEF2 binding in HDAC4 function will be further examined in Chapter 5.

The *Y1142H* mutant had minimal impact on eye development, which indicates that the deacetylase activity of HDAC4 is critical to the developmental impairments. This also highlights a difference in requirement for the different functional domains of HDAC4 for specific neuronal function. For example, expression of a different catalytically inactive *DmHDAC4* mutant (*H968A*) in the adult fly brain was shown to impair courtship memory similar to *DmHDAC4*^{WT}, suggesting that HDAC4 memory impairment is not deacetylase dependent (Fitzsimons et al., 2013). Although vertebrate HDAC4 has been deemed to be

catalytically inactive in nature, Sando et al. (2012) also further confirm a non-dependency of its deacetylase domain via expression of mutant HDAC4 with a truncated deacetylase domain and missing NES. This mutant was able to maintain activity as a transcription repressor when restricted to the nucleus, thus confirming that the deacetylase activity is dispensable. However, it will be crucial to confirm whether there is a difference in deacetylase activity between *DmHDAC4*^{WT} and *Y1142H*, which could be determined by assaying for the difference of deacetylase activity presence using an HDAC activity assay kit or by assessing the acetylation of histone H3 with a histone H3 acetylation assay kit in lysates of developing imaginal discs or adult retina. There is also the possibility that DmHDAC4 deacetylates non-histone targets as vertebrate HDACs have been previously shown to deacetylate transcription factors and other proteins such as α-tubulin, however HDAC4 was not reported to be among these HDACs most probably due to its inactive catalytic domain in vertebrate (Glozak et al., 2005), therefore, the active catalytic domain in DmHDAC4 could indicate that it might possess non-histone targets.

Lastly, the slight increase in phenotype severity of *dANK* in comparison to *DmHDAC4*^{WT} suggests a role for the putative ankyrin-binding site which will be discussed further below.

The range of phenotypes displayed on expression of the different variants highlights important roles of subcellular distribution and deacetylase activity on eye development. As each ommatidium is comprised of eight stereotypically arranged R cell photoreceptors, disorganisation of ommatidia is most likely an indication of R cells miswiring. The loss of red pigment likely indicates the loss of the pigment glial cells which ensheath the photoreceptor neurons (Baker et al., 2014; Edwards & Meinertzhagen, 2010). Glial cells are required for the proper development of neurons as well as their survival (Edwards & Meinertzhagen, 2010), therefore the loss of pigment glial cells may be the underlying cause of the ommatidial disorganisation. Additionally, the necrotic patches which likely suggests neurodegeneration were mostly observed in retina completely devoid of pigment glial, suggesting that the glial dysfunction might be the cause and warrants further investigation.

4.4.3 Disruption of HDAC4 subcellular distribution, MEF2-binding and ankyrin-binding alters developmental phenotypes in the MB

The impact of increased expression of DmHDAC4 and the mutant variants on neurodevelopment was also investigated in KC neurons, which form part of the circuitry through which memory is formed in *Drosophila*. A comparison of the subcellular distribution mutants revealed that *dNLS* had a slightly reduced penetrance compared to *DmHDAC4*^{WT}, therefore restricting DmHDAC4 to the cytoplasm somewhat ameliorates the phenotype, whereas nuclear-restriction resulted in a higher proportion of brains with a severe phenotype. Expression of *dMEF2* had minimal impact on development, therefore the MEF2-binding site is crucial for the DmHDAC4-induced impairment of MB development. Interestingly, *Y1142H* exhibited a similar penetrance of MB phenotype to *DmHDAC4*^{WT}, indicating that the deacetylase activity is dispensable in MB development unlike eye development. This could also suggest a cell type-specific role of DmHDAC4 deacetylase activity during development which will need to be explored further.

Since most of the mutants exhibited 100% phenotypic penetrance that comprised of a range of phenotypes, it is difficult to determine whether there were significant differences in the impact of 3A, dNLS, dANK and Y1142H. Therefore, the mutant variants were expressed at lower, more physiologically relevant levels in a background in which endogenous DmHDAC4 was reduced using the deGradFP. This method ideally attempts to replace the loss of endogenous DmHDAC4 with the mutant variants, thus reducing the overexpression effect. It was then revealed that only *3A* and *dANK* mutants had a significant impact on MB development when expressed in a reduced DmHDAC4 background. Therefore, in combination with the overexpression data, the results establish that the serine phosphorylation sites and putative ankyrin-binding site are important for proper development of the MB. While mutations to NLS partially rescues the phenotype caused by DmHDAC4 overexpression, it does not contribute to exacerbated defects when the proteins are at a reduced level, and this is also true for the MEF2-binding site.

Although the theory of using deGradFP to achieve endogenous KD of DmHDAC4 and simultaneously reintroducing DmHDAC4 variants to replace the endogenous DmHDAC4 is a reasonable approach to determine the role of the mutants. In reality, there were limitations to this approach which was demonstrated in the results as both increased and reduced HDAC4 led to manifestation of MB phenotypes under the same GAL4 driver

and the difference in penetrance level between the two makes it difficult to determine a WT baseline of HDAC4. Other genetic tools can be considered in the future such as the recently developed clustered regularly interspaced short palindromic repeats (CRISPR)-mediated integration cassette (CRIMIC) that is a cassette flanked by homologous target intron sequence containing a splice acceptor, T2A-GAL4 and a polyA tail sequence (**Figure 4.22**). This cassette can be inserted into an intronic region of interest such as *DmHDAC4*, mediated by Cas9 which cuts the gene of interest at the intron site directed by a single guide RNA (sgRNA). The insertion of the cassette into the intron will result in a mutated DmHDAC4 due to protein truncation caused by the cassette but the T2A-GAL4 expressed together with the truncated protein can be used to drive a UAS variant which then provides the ability to replace the non-functional protein (Lee et al., 2018). However, there is also the need to make the mutation tissue-specific and this could probably be done in combination with CRISPR-mediated tissue-restricted mutagenesis (CRISPR-TRiM) which use enhancer driven Cas9 to target specific tissue for Cas9 expression in a background with ubiquitous sgRNA expression (Poe et al., 2019) (**Figure 4.22**). The combination of these two techniques has not been reported in any studies and would likely require intensive optimisation which was one of the reason the deGradFP system was chosen as it does not require design of new construct such as sgRNA to target *HDAC4* introns. Additionally, libraries of fly lines required for the deGradFP system were already available. Therefore, the establishment of the deGradFP system in the lab was deemed as the more feasible approach in working within the required timeline for this project.

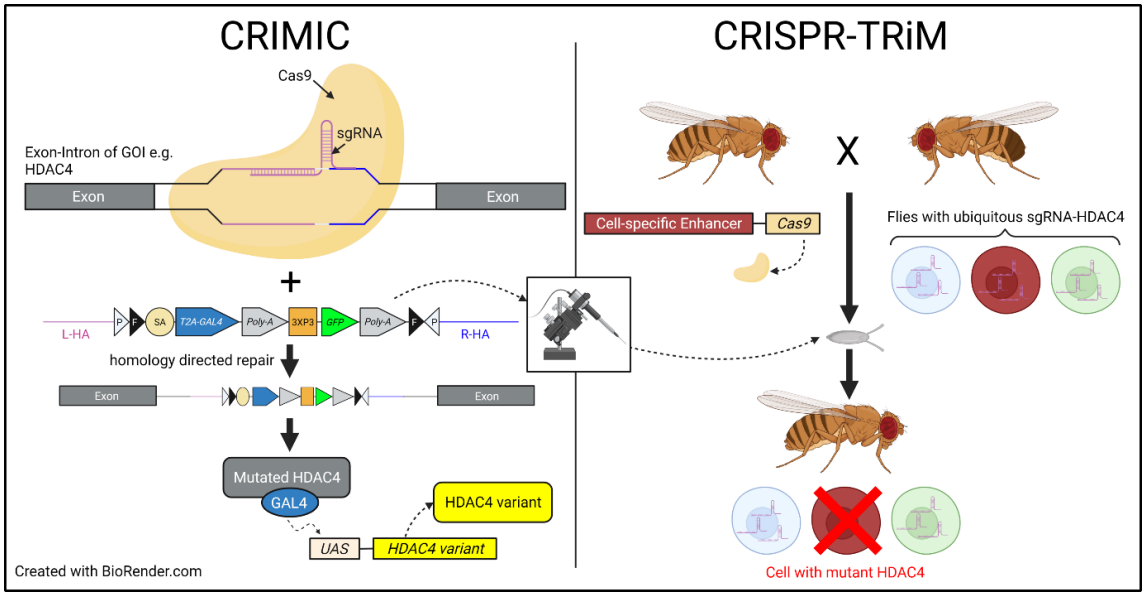

Figure 4.22: Schematics of CRIMIC and CRISPR-TRiM methods
Left panel shows the simplified diagram of CRIMIC. (GOI) Gene of interest, (L-HA) left homologous arm, (R-HA) right homologous arm, (P) attP site, (F) FRT site, (3XP3) 3XP3 promoter. Cutting of target intron region mediated by Cas9 which was directed by sgRNA. This allows incorporation of CRIMIC cassette into the intron via the recognition of the left and right homologous arms of the cassette which led to homology directed repair. Integration of cassette into the gene will lead to a truncated mutant but also lead to the formation of GAL4 which can be used to drive other UAS transgene. Right panel shows the simplified diagram of CRISPR-TRiM using flies expressing Cas9 driven by cell-specific (red cell) enhancer and crossing them to flies that is ubiquitously expressing sgRNA. The F1 progeny will result in only the cells where the enhancer is active to have the gene mutation. These two methods could theoretically be possible to combine by injecting donor vector comprising of the CRIMIC cassette into the F1 embryo of a CRISPR-TRiM cross, resulting in cell-specific truncated mutants with the ability to also express other UAS driven gene. This figure is an original artwork created with referenced to Lee et al. (2018) and Poe et al. (2019).

In the study by Main and colleagues (2021), expression of *hHDAC4*^{WT} and *hHDAC4 3A* was also shown to impact MB development with *3A* being more severe, which further suggests the conservation of function between DmHDAC4 and hHDAC4. In addition, in the courtship suppression assay, only *hHDAC4 3A* expression resulted in significant memory impairment (the cytoplasmic-restricted mutant had no effect). Although, the investigation of the impact of *DmHDAC4* variants on memory formation has not yet been carried out in this study, it will be interesting to determine whether the *dANK* mutant can impair memory formation. Additionally, the memory performance between *dMEF2* and *dNLS* could also be investigated to determine whether increased cytoplasmic HDAC4 impacts memory and whether this is dependent on the MEF-binding site.

4.4.4 HDAC4 influences eye and MB development through different mechanisms

In both the eye and the MB, increased nuclear-restricted DmHDAC4 was detrimental to its development. The deGradFP system further confirmed that *3A* impacted MB development when endogenous DmHDAC4 was reduced, indicating that nuclear HDAC4 impairs MB development. However, an intact deacetylase domain was critical for the eye impairments but dispensable for the MB and conversely, mutation of the MEF2-binding site prevented impairments in the MB but had little impact in the eye. The differing developmental impact of mutants and between neuronal cell types imply the existence of a broad range of roles that DmHDAC4 can play with its different functional domains which are dependent on the cellular environment. It is therefore reasonable to speculate that based on its requirement of serine phosphorylation sites and MEF2-binding site,

DmHDAC4 might act through MEF2 (i.e. via inhibition of MEF2 or other transcription factors) in the nucleus to regulate MB development whereas in the eyes, it could be deacetylating histones or non-histone targets to regulate gene expression and other processes. The potential impact on transcriptional-related processes will be investigated and further discussed in Chapter 6. Another potential mechanism DmHDAC4 has on development is its cytoplasmic role via the MEF2-binding site which could then suggest the site may have other roles beyond MEF2-binding such as interaction with other protein partners in the cytoplasm. The role of MEF2-binding will be investigated further in Chapter 5.

Like *3A*, expression of *DmHDAC4* with a mutated ankyrin-binding domain, dANK, was also shown to be detrimental to both eye and MB development. The identification of a genetic interaction between *HDAC4* and *Ank2* during eye development (Schwartz et al., 2016), suggests that Ank2 may be the ankyrin repeat-containing protein that binds HDAC4 to influence MB and eye development, however no physical interaction between HDAC4 and Ank2 in the *Drosophila* brain was detected by co-immunoprecipitation (Wilson, 2021). However, there are other proteins expressed in the fly brain that contain ankyrin repeats such as KANK and CG5846 (*Drosophila* orthologue of RFXANK) and studies of interaction between DmHDAC4 and CG5846 is currently being conducted by another PhD student, Sarah Wilson, with preliminary data (unpublished) showing RNAi KD of *CG5846* to be required in the eye and MB development. This leads to the question of whether KD of *CG5846* could lead to reduce binding with DmHDAC4 which would also require co-immunoprecipitation to test for binding interaction. If CG5846 does bind to DmHDAC4, does it bind to the ankyrin-binding domain and will this interaction lead to a reduced neuronal developmental impairment? Also, another project by PhD student, Hannah Hawley, aims to determine other protein binding partners of DmHDAC4 through co-immunoprecipitation of *Drosophila* brain samples of DmHDAC4^{WT} and variants including dANK followed by mass spectrometry to identify protein candidates that may interact with the ankyrin-binding domain of DmHDAC4.

4.4.5 Utility of the Split GAL4 system for investigating functional differences between KC subtypes

As the KCs comprise of three different subtypes of neurons that have been shown to play different functional roles in learning and memory (Akalal et al., 2006), it is therefore important to be able to individually examine the role of HDAC4 to each of these neuronal subtypes. Additionally, certain KCs subtypes such as the γ neurons have been associated with an impairment in courtship memory when HDAC4 is specifically overexpressed in the subtype (Fitzsimons et al., 2013). Hence, Split GAL4 drivers was used to investigate whether overexpression of *DmHDAC4*^{WT} specifically in the α/β, α'/β' or γ neurons could directly or indirectly affect the development of certain MB lobes. The preliminary testing of the Split GAL4 system using UAS GFP indicated that expression pattern of all the subtype specific Split GAL4 drivers were highly restricted to only the neurons of interest with no non-specific expression. However, expression of DmHDAC4 with the γ Split GAL4 drivers resulted in weak or no expression. Additionally, expression of DmHDAC4 did not result in a visible phenotype with any of the Split GAL4 drivers, which suggests a lack of GAL4 expression during the developmental phase. However, this will need to be verified by examining for expression in the developing MB in larvae or pupae to determine the stage in which the expression turns on. Although this genetic tool will be useful for post-developmental studies, the majority of this project comprises of developmental analysis, therefore, the Split GAL4 was excluded from the remainder of this project and will only be utilised in future post-developmental analyses such as evaluation of memory with the courtship suppression assay.

5. INVESTIGATING THE IMPORTANCE OF THE DmHDAC4 MEF2-BINDING SITE IN HDAC4 FUNCTION

In the previous chapter, it was determined that mutation of the MEF2-binding site (*dMEF2*) prevented the severe MB defects resulting from increased expression of *DmHDAC4*^{WT} in the MB to the extent that the phenotype was no different to the uninduced control (**Figure 4.11 & 4.12A**). Immunohistochemistry confirmed that the dMEF2 (**Figure 4.7G & H)** and dNLS (**Figure 4.5G & H**) mutants were largely restricted to the cytoplasm, however the phenotypes resulting from expression of these mutants differed in both the eye and the MB (**Figure 4.9, 4.11 & 4.12A**). The significantly reduced severity of phenotypes resulting from dMEF2 compared to dNLS in both the eye and MB suggest that the presence of the MEF2-binding site may be important to DmHDAC4 function in the cytoplasm. Therefore, the next step was to further investigate the importance of the MEF2-binding site to the manifestation of the dNLS-induced eye and MB deficits. Furthermore, it was also investigated as to whether the MEF2-binding site is also required for the activity of HDAC4 in the nucleus. Hence, the mutations to the dMEF2 binding site were introduced into the 3A and dNLS variants to generate the double mutant flies, *UAS 3A_dMEF2* and *UAS dNLS_dMEF2*. In addition, since expression of the dANK mutant also resulted in defects in MB and eye development, a *UAS dANK_dMEF2* double mutant was also generated. These double mutants were designed and generated using the same strategy as the single mutants (see Section 3.2 & Appendix 9.1) .

5.1 Characterisation of the expression and subcellular distribution of *DmHDAC4* double mutant in the MB

The expression pattern of each of the double mutants was initially confirmed and characterised with respect to subcellular distribution via detection of the Myc-tag. The MB-specific TARGET driver was used to facilitate expression of *3A_dMEF2* and *dNLS_dMEF2*, which were restricted to the nucleus and cytoplasm respectively.

3A_dMEF2 was present at high levels in the nuclei where it aggregated into puncta (**Figure 5.1B**), as previously observed for 3A. It exhibited weak Myc staining in the MB lobes (**Figure 5.1A**), whereas dNLS_dMEF2 appeared absent in nuclei (**Figure 5.1D**) and was largely restricted to the lobes (**Figure 5.1C**). While the cytoplasmic-restriction of dNLS_dMEF2 was expected, 3A_dMEF2 remained predominantly nuclear-specific with HDAC4 puncta present (**Figure 5.1B**). This indicates that the three serine phosphorylation sites are required for dMEF2 restriction to the cytoplasm. The loss of MEF2-binding site prevents HDAC4 from localising to the nucleus efficiently which then favours nuclear export, however nuclear export requires 14-3-3ζ binding to the phosphorylated serines which have been mutated to prevent phosphorylation, thus leading to nuclear accumulation similarly to the 3A single mutant.

dANK_dMEF2 was also restricted to the cytoplasm (**Figure 5.1E & F**). Since the subcellular distribution of dANK was the same as DmHDAC4^{WT}, it is not surprising that the mutation of the MEF2-binding site in dANK would restrict it to the cytoplasm in similar way to the single mutant dMEF2 (compare **Figure 4.7B, D, G & H** with **Figure 5.1E & F**).

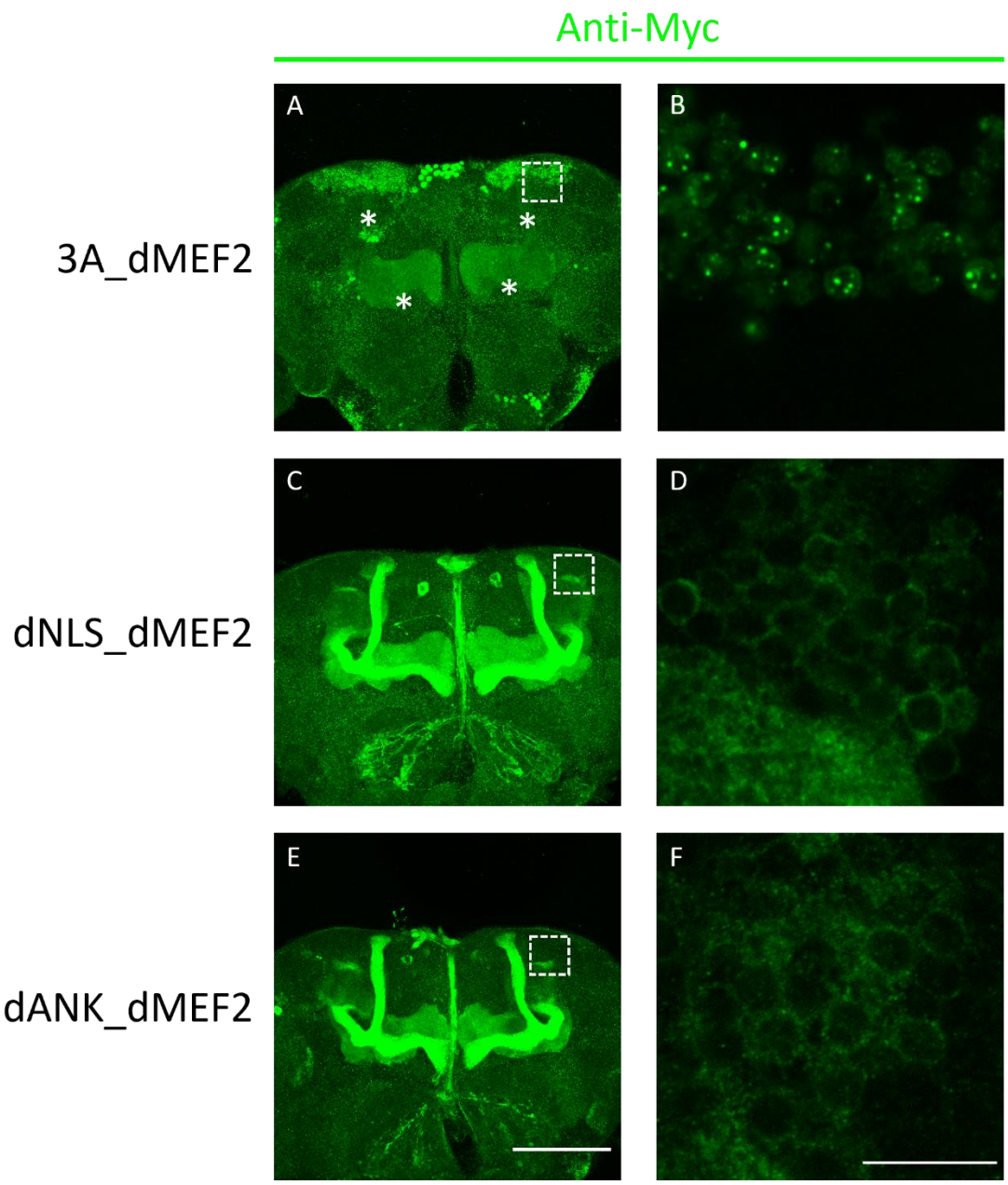

Figure 5.1: Expression of DmHDAC4 variant double mutants, 3A_dMEF2, dNLS_dMEF2 and dANK_dMEF2 in MB neurons using the TARGET system
Representative images of the anterior to posterior projection of the MB at 40x magnification (A, C & E). White dashed boxes represent the 100x magnified region of the KCs (B, D & F). Image A, C, and E consist of stacked slices of confocal images whereas image B, D and F are single slice images. (*) indicates missing lobes expression. Left scale bar = 100μm, right scale bar = 10μm.

5.2 Characterisation of the impact of expression of the double mutants on eye development

Next, the impact of expression of the double mutants on eye development was assessed via expression with *GMR-GAL4* raised at 27°C. When compared to the phenotypes resulting from expression of the respective single mutants, only *dNLS_dMEF2* displayed a reduction in phenotype severity (**Figure 5.2B & E, dNLS Score: 3.50 vs dNLS_dMEF2 Score: 2.00**), exhibiting some degree of red pigmentation and along with the absence of necrotic patches. This indicates a requirement of the MEF2-binding site for full manifestation of the *dNLS* phenotype, however the *dNLS_dMEF2* phenotype was still relatively severe, with complete fusion of ommatidia and loss of bristles, which was an identical phenotype to that of the single mutant *dMEF2* and $DmHDAC4^{WT}$ shown in the previous chapter (**Figure 4.9F & L, Score: 2.00**).

The phenotype resulting from expression of *3A_dMEF2* (**Figure 5.2D, Score: 3.50**) was no different compared to that of 3A (**Figure 5.2A, Score: 3.50**), therefore nuclear DmHDAC4 does not require its MEF2-binding site to affect eye development. The *dANK_dMEF2* mutant (**Figure 5.2F, Score: 2.50**) also did not show any difference in phenotype when compared to *dANK* (**Figure 5.2C, Score: 2.50**), despite the shift from distribution in the nucleus and cytoplasm to predominantly cytoplasmic (compare **Figure 4.8B, D, G & H** with **Figure 5.1E & F**).

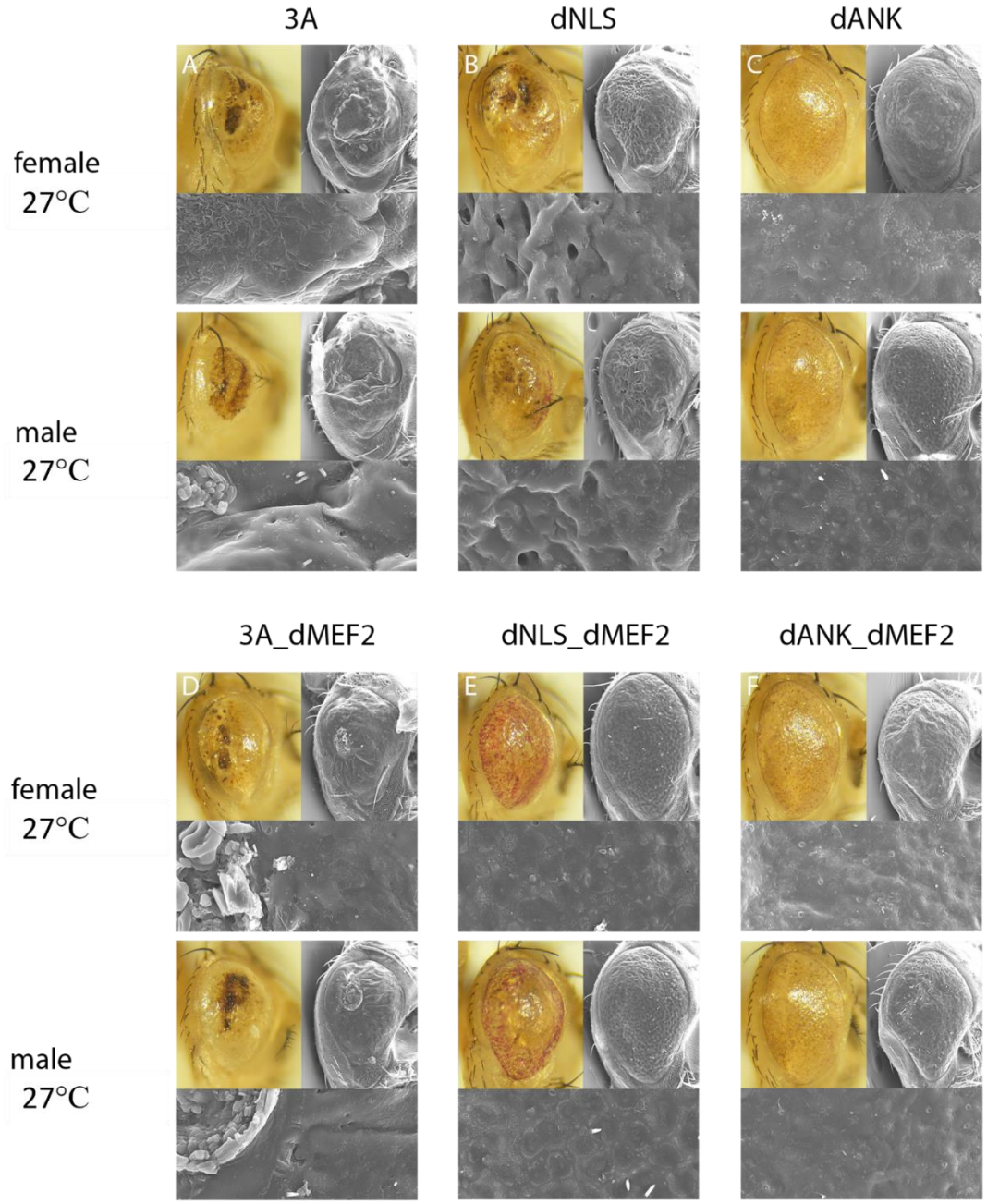

Raised at 27°C							
Phenotypes	**Severity Score**	**3A**	**3A_dMEF2**	**dNLS**	**dNLS_dMEF2**	**dANK**	**dANK_dMEF2**
Disorganised/missing bristles	0.50	√	√	√	√	√	√
Disorganised ommatidia	0.25						
Partial ommatidia fusing	0.50						
Complete ommatidia fusing	1.00	√	√	√	√	√	√
Partial loss of pigmentation	0.50				√		
Complete loss of pigmentation	1.00	√	√	√		√	√
Patches of necrotic tissue	1.00	√	√	√			
Total Score		3.50	3.50	3.50	2.00	2.50	2.50

Figure 5.2: Stereomicroscopy and SEM images of eye phenotypes
Representative images of *Drosophila* female or male retina morphology expressing each of the indicated mutants driven by *GMR-GAL4* at 27°C. Top SEM image within each genotype was imaged at 250x magnification and bottom SEM image was imaged at 1500x magnification. Each genotype is n=6 which includes both males (n=3) and females (n=3).

Table summarises the phenotypes that were observed from each genotype. Severity score is an arbitrary value assigned to each phenotype based on its classification (e.g., ommatidia, pigments) and severity. Total score is an approximate measure of the overall phenotype. The higher the total score, the more severe the phenotype.

5.3 Characterisation of the impact of expression of the double mutants on MB development

Pan-neuronal expression of each of the double mutants resulted in significantly reduced MB deficits when compared to the single mutants, with only minor or moderate defects observed (**Figure 5.3A**). These was further verified by expressing the mutants with the MB TARGET driver, *OK107GAL4; tubGAL80^{ts}* (**Figure 5.3B**), which also resulted in a significantly lower phenotypic penetrance.

Together these data indicate that for DmHDAC4 to elicit defects in the MB when accumulated in the nucleus (3A) or cytoplasm (dNLS), it requires an intact MEF2-binding site, as does the dANK mutant.

This is in contrast to the mechanism through which increased DmHDAC4 resulted in disruption of eye development, in which the mutation of the MEF2-binding site had no impact on 3A or dANK-induced defects and only reduced the dNLS phenotype slightly (**Figure 5.2**). As hypothesised in the previous chapter, this suggests that HDAC4 acts through different mechanisms in these different organs, whereby the developmental defects in the MB are dependent on MEF2, whereas they are independent of MEF2 in the eye.

A

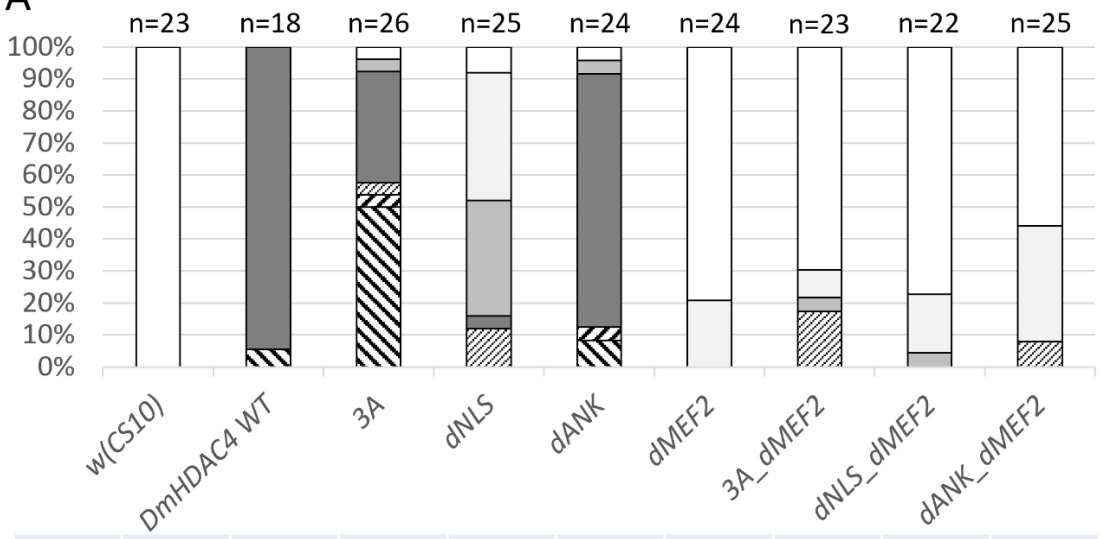

Genotype:	w(CS10)	DmHDAC4 WT	3A	dNLS	dANK	dMEF2	3A_dMEF2	dNLS_dMEF2	dANK_dMEF2
Normal	23	0	1	2	1	19	16	17	14
Abnormal	0	18	25	23	23	5	7	5	11

One-tailed Fisher's exact test:

3A vs *3A_dMEF2* – ***p<0.001
dNLS vs *dNLS_dMEF2* – ***p<0.001
dANK vs *dANK_dMEF2* – ***p<0.001

B

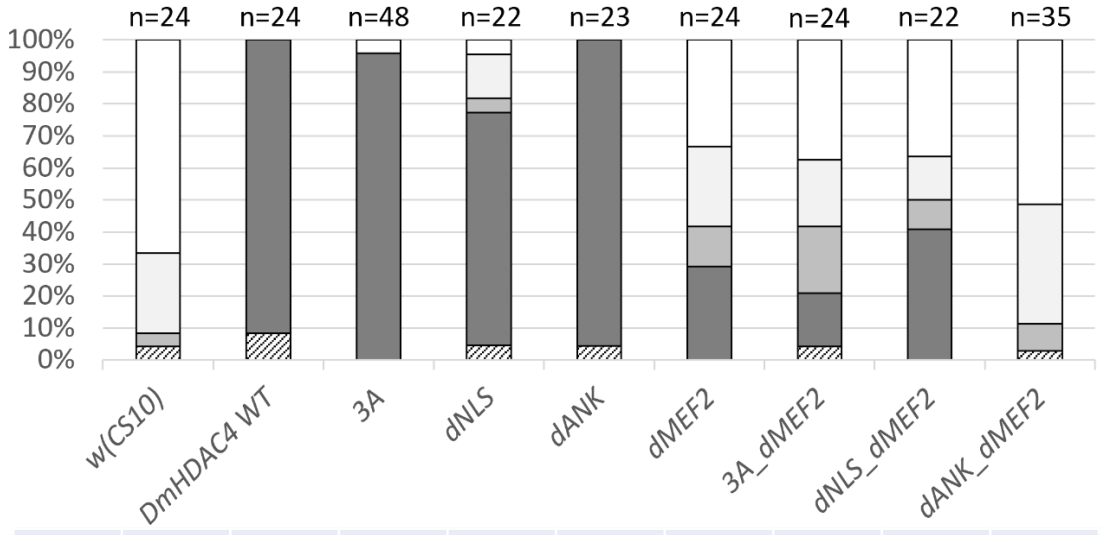

Genotype:	w(CS10)	DmHDAC4 WT	3A	dNLS	dANK	dMEF2	3A_dMEF2	dNLS_dMEF2	dANK_dMEF2
Normal	16	0	2	1	0	8	9	8	18
Abnormal	8	24	46	21	23	16	15	14	17

One-tailed Fisher's exact test:

3A vs *3A_dMEF2* – ***p<0.001
dNLS vs *dNLS_dMEF2* – ***p<0.001
dANK vs *dANK_dMEF2* – ***p<0.001

Continue next page ->

120

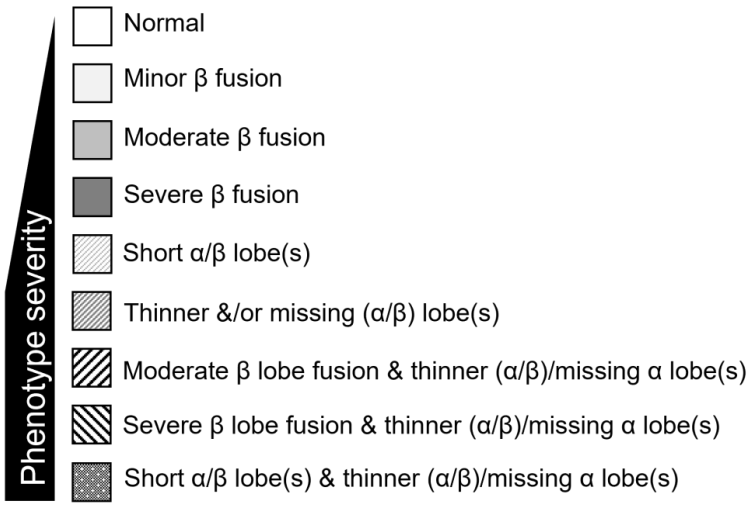

Figure 5.3: Developmental defects in the MB resulting from expression of *DmHDAC4* double mutants
Each bar represents the percentage of phenotypic distribution of a genotype. The x-axis represents genotype of the control or UAS variant lines with the pan-neuronal (*elavGAL4*) driver raised at (A) 25°C and pan-MB (*OK107GAL4; tubGAL80^{ts}*) driver raised at (B) 30°C. The sample size for each genotype is indicated above each bar. Tables display the number of samples with normal or abnormal (combination of all phenotypes within treatment) from variant expression driven by (A) *elavGAL4* or (B) *OK107GAL4; tubGAL80^{ts}*. One-tailed Fisher's exact test was used for significance testing between comparison of interest.

5.4 Mutations to MEF2-binding site reduce the binding of DmHDAC4 to DmMEF2

The cytoplasmic distribution of the dMEF2 mutant indicates that the MEF2-binding site was no longer able to bind *Drosophila* MEF2 (DmMEF2) and therefore prevent MEF2-dependent nuclear entry of DmHDAC4, however, the lack of interaction between DmHDAC4 and DmMEF2 has not been directly confirmed. Since the 3A_dMEF2 mutant is restricted to the nucleus and accumulates in nuclear puncta similarly to 3A, the co-localisation of DmMEF2 to the puncta can be compared between 3A_dMEF2 and 3A to determine whether binding to 3A_dMEF2 is reduced. To that end, *OK107GAL4; tubGAL80^{ts}* flies were crossed to *UAS-DmHDAC4-3A-myc* and *UAS-DmHDAC4-3A_dMEF2-myc* and raised at 18°C until adult eclosion after which adult flies were then transferred to 30°C for 72 hours to induce expression. Immunohistochemistry was carried out on dissected whole brain using Myc and MEF2 antibodies and KC nuclei were imaged (**Figure 5.4A-F**). Quantification of puncta revealed that expression of 3A_dMEF2 resulted in a significantly reduced number of DmHDAC4 puncta that were positive for

MEF2-positive puncta (**Figure 5.4G**), confirming that the mutation of the MEF2-binding site does significantly inhibit the binding of DmMEF2.

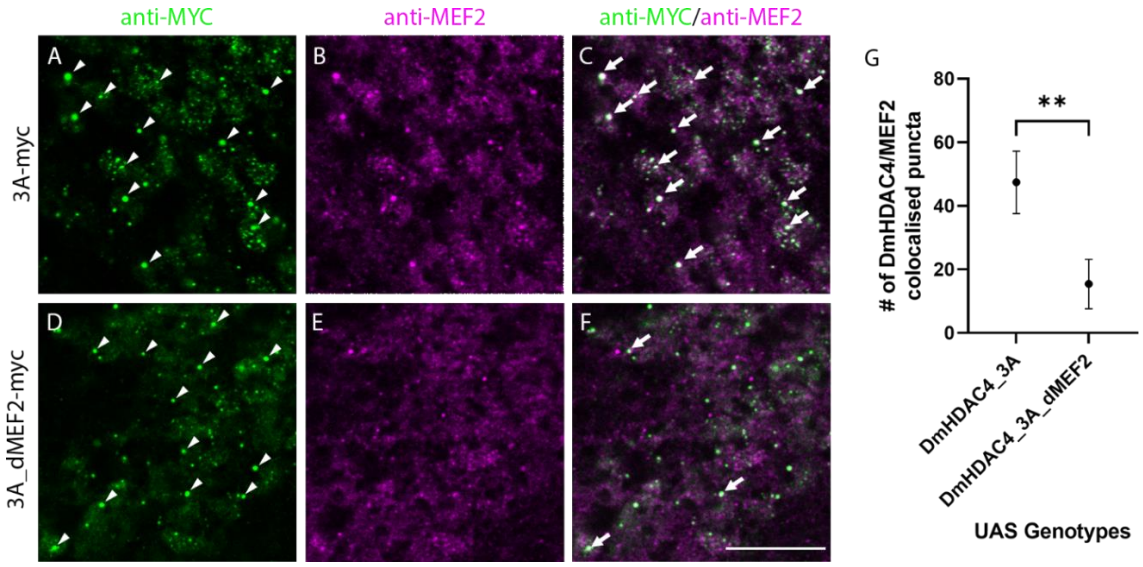

Figure 5.4: Co-localisation comparison of DmHDAC4 and MEF2 between 3A variant and double mutant 3A_dMEF2
Flies of the indicated genotypes were crossed to *OK107GAL4; tubGAL80^{ts}* raised at 18°C then incubated at 30°C for 72 hours after eclosion followed by immunohistochemistry on whole brains with anti-Myc (green) and anti-DmMEF2 (magenta). Images are representative single optical section images expression of nuclear-restricted DmHDAC4 puncta (arrowhead) (A & D) and DmMEF2 (B & E) in the nuclei imaged at 100x magnification. Image overlaps of the two channels reveal the co-localisation of the nuclear-restricted DmHDAC4 and DmMEF2 that appeared as white puncta (arrow) (C & F). A Z-stack of the KCs of ~40 optical sections were obtained at 0.25µm intervals. The number of white puncta for each optical section were counted using ImageJ. (G) The amount of DmHDAC4/DmMEF2 co-localisation was significantly reduced for 3A_dMEF2 (n=7 brains) in comparison to 3A (n=5 brains). *t*-test $t_{(10)} = 4.587$, ** $p < 0.001$. Statistical analysis was carried out using PRISM. This figure is an original data intended for this thesis but was also used as a supplementary data in the publication by Main et al. (2021). Images and graph used under CC BY 4.0 (http://creativecommons.org/licenses/by/4.0). Scale bar = 10 µm.

5.4.1 Further investigation into the relationship between cytoplasmic DmHDAC4 and MEF2

The developmental deficits in the MB induced by the expression of the cytoplasmic-restricted mutant dNLS was rescued when mutations to MEF2-binding site were introduced, which is a curious finding given that MEF2 is a nuclear transcription factor. This could either suggest that MEF2 interacts with DmHDAC4 in the cytoplasm or that DmHDAC4 could be interacting with another protein in the region of the MEF2-binding site, and the interaction is disrupted on mutation of the MEF-binding site. Therefore, to investigate whether an interaction between cytoplasmic DmHDAC4 and DmMEF2 could

be detected, the expression of dNLS and endogenous DmMEF2 was visualised to determine whether the binding of dNLS to DmMEF2 leads to the latter be sequestered out of the nucleus as a result of increased cytoplasmic abundance. Brains expressing dNLS were co-stained with Myc and MEF2 antibodies which revealed a clear separation between cytoplasmic-restricted DmHDAC4 (expression in calyx and cytoplasmic halo) and the endogenous DmMEF2 (expression only in the nucleus) with the cytoplasmic halo of DmHDAC4 surrounding the nuclear-specific DmMEF2 expression (**Figure 5.5A-C**), thus DmMEF2 appeared exclusively cytoplasmic. However, it should also be noted that some co-localisation of DmHDAC4 and DmMEF2 in nuclear puncta can be detected (**Figure 5.5C**). It is likely that this low level of dNLS in nuclei is a result of incomplete cytoplasmic sequestration as previously observed in previous chapter (**Figure 4.5G**).

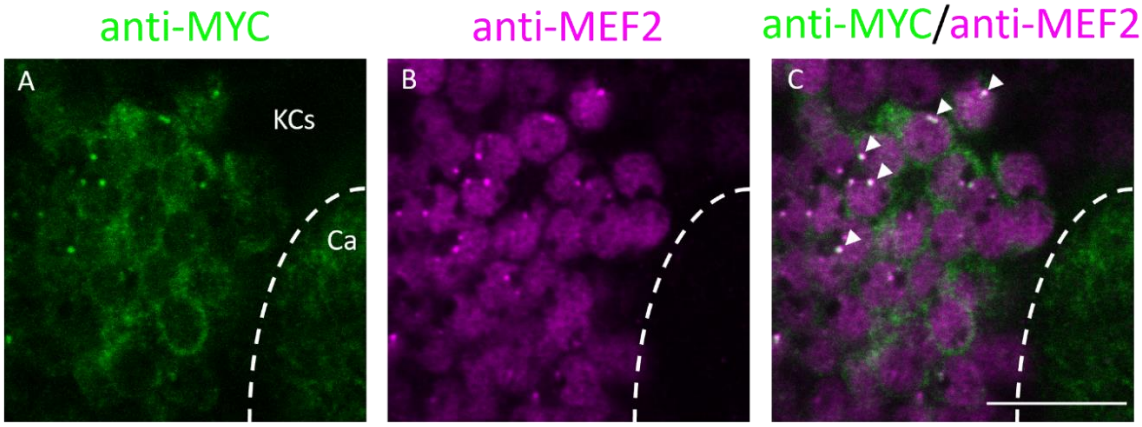

Figure 5.5: Expression of Myc tagged DmHDAC4 and endogenous MEF2 within MB TARGET driven UAS DmHDAC4-dNLS-Myc variant
Representative single slice image showings cytoplasmic-restricted DmHDAC4 expression in the Ca and around the KCs' nucleus (A) along with MEF2 expression within KCs nucleus (B) were imaged at a 100x magnification. Image overlaps of the two expressions reveal differences in subcellular distribution expression between the two proteins with some co-localisation puncta in an unknown subcellular region (white arrowhead). Scale bar = 10 μm.

These data suggest that expression of dNLS does not alter the nuclear localisation of DmMEF2. To further investigate this, it was hypothesised that if DmHDAC4 is acting through DmMEF2 in the cytoplasm, albeit at a level not detected by immunostaining, then increasing cytoplasmic DmMEF2 would exacerbate the dNLS phenotype, i.e. if DmMEF2 binds dNLS in the cytoplasm, and this binding somehow facilitates the deleterious impact of dNLS on MB development, then increasing the amount of DmMEF2 in the cytoplasm will allow more binding to dNLS. In addition, it was also of interest to determine whether increasing the abundance of DmMEF2 in the cytoplasm

would enable nuclear DmHDAC4 to be transported out into the cytoplasm and whether such a scenario will alleviate the MB phenotype. A cytoplasmic-restricted MEF2 mutant, T148A has previously been reported (Crittenden et al., 2018). A construct containing T148A with a C-terminal HA tag under the control of UAS expression was synthesised and transgenic flies generated (see Section 3.2 and Appendix 9.2). However, the subcellular distribution of T148A was shown to still be nuclear-restricted, similarly to that of endogenous DmMEF2 (**Figure 5.6A-C**). Due to time constraints, further investigation was put on hold in favour of other aims.

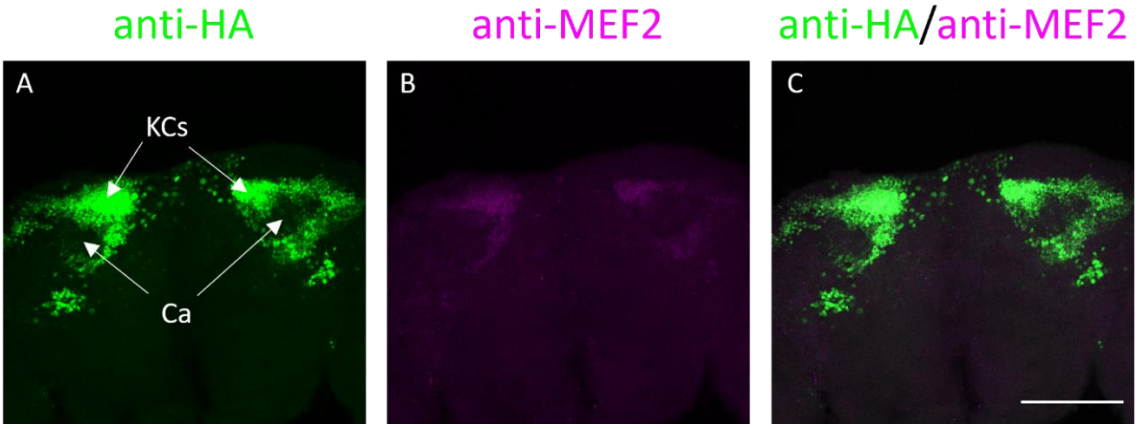

Figure 5.6: Expression of HA tagged MEF2 and endogenous MEF2 within MB TARGET driven UAS MEF2-T148A-HA variant
Representative image showing expression of HA tagged MEF2 (A) and endogenous MEF2 (B) in nuclei of KCs but absent from calyx and MB lobes. Image overlaps show both expression specific to the nucleus with robust HA tagged MEF2 expression. Images consist of stacked slices of confocal images which were imaged at a 40x magnification. Scale bar = 10 μm.

5.5 Investigating the relationship between expression of DmHDAC4 variants and dysregulated FasII expression in the MB

As described in Section 4.2.2, the visualisation of the MB lobes is facilitated by immunostaining with an antibody that detects FasII, as it localises strongly to the α, β and γ lobes of the MB, with little expression elsewhere, thus highlighting the structure of the MB lobes and allowing easy detection and assessment of developmental defects. While assessing the MB phenotypes of the DmHDAC4 variants, it was noticed that there was often a reduction in FasII staining in the MB lobes (**Figure 5.7A & B**). This was of

interest and warranted further investigation, since FasII is a cell adhesion molecule that is required by the KCs to form axon fascicles which result in the distinct MB lobes. In the *Drosophila* ventral nerve cord, *FasII* mutants lack normal axon fasciculation while overexpression of *FasII* led to fusing between axons that are normally separated (Lin, Fetter, Kopczynski, Grenningloh, & Goodman, 1994). In the MB, the impact of FasII mutant on the MB development has been conflicting with Kurusu et al. (2002) reporting defects such as thin dorsal lobes and fused medial lobes while Cheng et al. (2001) reported no defect. *OK107GAL4* driven overexpression has also been shown to exhibit lobe branching defects (Fushima & Tsujimura, 2007; Kurusu et al., 2002). These results together highlight the important role of FasII in proper axon guidance.

The level of expression of FasII was quantified following pan-neuronal expression of the DmHDAC4 variants. To monitor the level of variability in immunostaining between brains, the intensity of FasII staining in the ellipsoid body (EB) was also assessed. The EB is a central complex structure posterior to the medial MB lobes comprising of neuronal axon bundles arranged in an ellipsoid shaped ring (**Figure 5.7C & D**). The intensity of FasII displayed by the EB was consistent across the samples, confirming that there was no significant variability in antibody binding efficacy across the samples. Additionally, the robust MB expression of Myc-tagged DmHDAC4 in such samples also shows that the MB was intact and that the reduction in FasII was not a result of axonal defects or reduction (**Figure 5.7B'**). Therefore, the FasII intensity of the MB normalised to the intensity of the EB was measured in all genotype samples and was discovered to be significantly lower in brains expressing DmHDAC4^{WT}, 3A and dANK (**Figure 5.7E**). As these mutants induced developmental defects in the MB, this suggests one of the mechanisms through which increased expression of HDAC4 impairs MB development may be through downregulation of FasII. It is notable that the cytoplasmic-restricted mutants did not exhibit reduced FasII expression. When expression was restricted just to the MB via the KC specific *OK107GAL4;tubGAL80^{ts}* TARGET driver, only 3A and dANK FasII reduction was significant (**Figure 5.7F**). It is surprising that FasII reduction by DmHDAC4^{WT} was only observable with pan-neuronal expression. If the FasII reduction is a non-autonomous effect, then the MB-specific expression of 3A and dANK would not have exhibited FasII reduction. Therefore, these results could suggest both an autonomous and non-autonomous role of HDAC4 in FasII down regulation, with the serine phosphorylation sites and ankyrin-binding domain of HDAC4 being autonomously

required in maintaining normal FasII expression during neurodevelopment while the deacetylase domain and NLS could be responsible for any non-autonomous effect. However, further validation will be necessary to determine any potential non-autonomous role of Y1142H and dNLS in FasII regulation.

Although the FasII intensity of EB was mostly consistent in the samples which makes it seem an ideal target for normalisation, its intensity variability has also been occasionally measured to be slightly lower than MB. This results in some genotypes appearing to have a normalised intensity of >1.0 but this does not indicate that the FasII in MB is expressed higher compared to other samples (**Supplementary Figure 9.9A & D**).

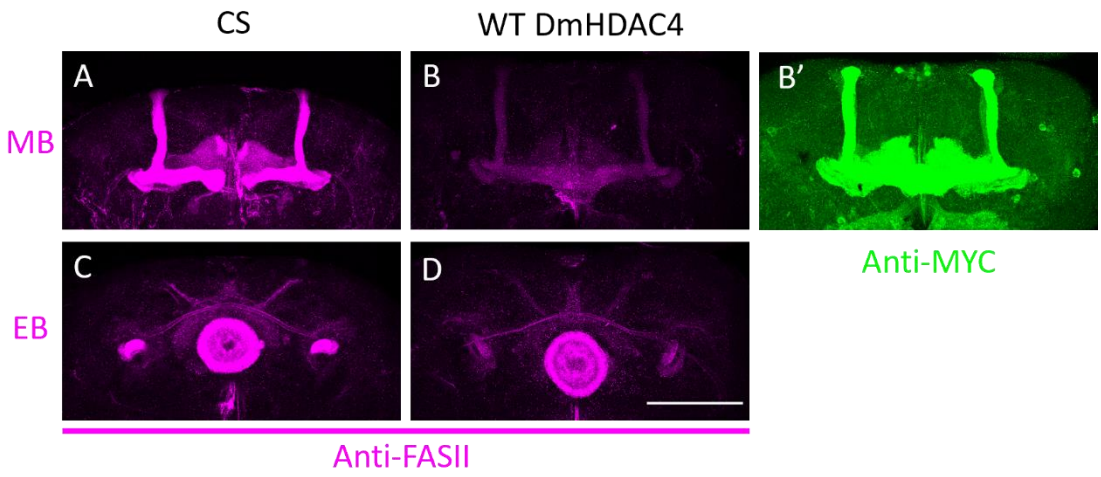
CS
WT DmHDAC4
A
B
B'
MB
C
D
EB
Anti-MYC
Anti-FASII

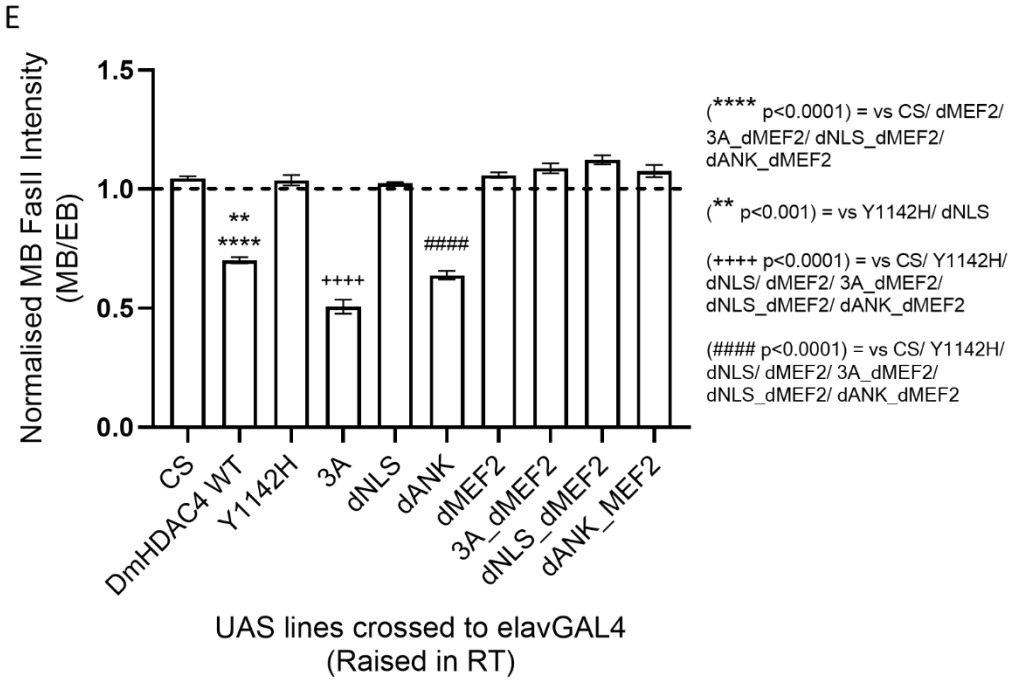
E
Normalised MB FasII Intensity (MB/EB)
1.5
1.0
0.5
0.0
**
****
++++
####
CS
DmHDAC4 WT
Y1142H
3A
dNLS
dANK
dMEF2
3A_dMEF2
dNLS_dMEF2
dANK_MEF2
UAS lines crossed to elavGAL4
(Raised in RT)
(**** p<0.0001) = vs CS/ dMEF2/ 3A_dMEF2/ dNLS_dMEF2/ dANK_dMEF2
(** p<0.001) = vs Y1142H/ dNLS
(++++ p<0.0001) = vs CS/ Y1142H/ dNLS/ dMEF2/ 3A_dMEF2/ dNLS_dMEF2/ dANK_dMEF2
(#### p<0.0001) = vs CS/ Y1142H/ dNLS/ dMEF2/ 3A_dMEF2/ dNLS_dMEF2/ dANK_dMEF2

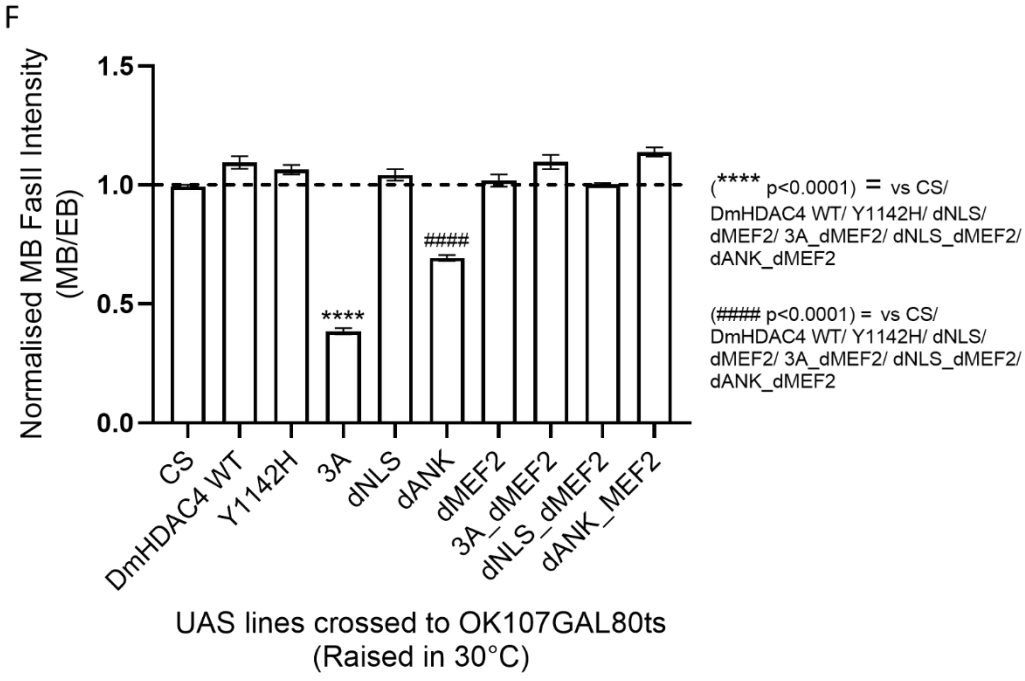
F
Normalised MB FasII Intensity (MB/EB)
1.5
1.0
0.5
0.0
****
####
CS
DmHDAC4 WT
Y1142H
3A
dNLS
dANK
dMEF2
3A_dMEF2
dNLS_dMEF2
dANK_MEF2
UAS lines crossed to OK107GAL80ts
(Raised in 30°C)
(**** p<0.0001) = vs CS/ DmHDAC4 WT/ Y1142H/ dNLS/ dMEF2/ 3A_dMEF2/ dNLS_dMEF2/ dANK_dMEF2
(#### p<0.0001) = vs CS/ DmHDAC4 WT/ Y1142H/ dNLS/ dMEF2/ 3A_dMEF2/ dNLS_dMEF2/ dANK_dMEF2

Figure 5.7: Quantification of FasII in brains with developmental expression of DmHDAC4 variants

Representative images showing FasII intensity differences between CS control (A & C) and DmHDAC4^{WT} (B & D), driven pan-neuronally by *elavGAL4*. Expression of DmHDAC4^{WT} resulted in reduced FasII intensity (B) compared to the driver only control (CS) (A). Expression of Myc-tagged DmHDAC4 indicates the MB lobes are intact (B'). FasII intensity in the EB was similar between control and DmHDAC4 expressing brains (C & D). Images consist of Z-stack projections of optical sections imaged at 40x magnification. Graphs displayed the comparison of FasII intensity between each genotype driven by either *elavGAL4* (E) or *OK107GAL4/tubGAL80^{ts}* (F). FasII intensity of the MB and EB for each sample was recorded from the 3 different regions of the structure on stacked images of MB and EB using ImageJ and calculated for the average intensity per sample. Each bar represents the mean ±SEM. FasII average intensity in the MB was normalised to FasII average intensity in the EB. Dashed line demarcates the level in which the FasII average intensity between MB and EB are the same. Statistical analysis was carried out in PRISM using Kruskal Wallis test (non-parametric one-way ANOVA) on (E) [$H(9)=169.6$, $p<0.0001$] and (F) [$H(9)=252.9$, $p<0.0001$] followed by Dunn's multiple comparisons post hoc test to determine significance between genotypes. Scale bar = 100 μm.

Interestingly, FasII expression was unaltered (≃1.0 or >1.0) on expression of the double mutants, 3A_dMEF2 and dANK_dMEF2, for both pan-neuronal and MB specific TARGET driver (**Figure 5.7E & F**). This suggests that the pathway that downregulates developmental FasII expression caused by overexpression of 3A or dANK is mediated through the MEF2-binding site.

5.5.1 FasII dysregulation is specific to only the developing MB

To determine whether the downregulation of FasII by 3A and dANK is restricted to only the developing brain, variants crossed to *OK107GAL4;tubGAL80^{ts}* were raised at 18°C and underwent 72 hours of post-developmental 30°C incubation following eclosion. FasII expression was unchanged (**Figure 5.8**), indicating that the downregulation of FasII by 3A and dANK is a developmental effect and does not occur in the mature adult brain.

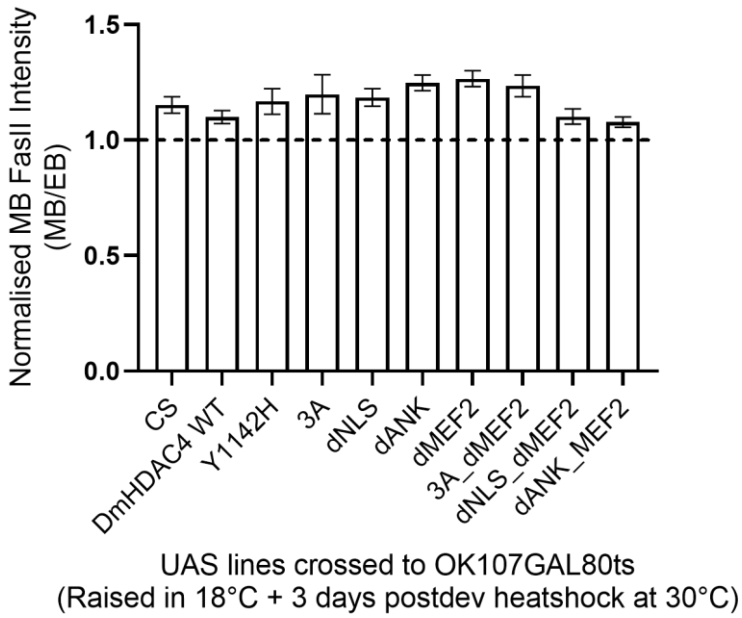

Figure 5.8: Quantification of FasII in brains with post-developmental expression of DmHDAC4 variants
Graphs displayed the comparison of FasII intensity in brains in which expression of the HDAC4 variants was induced post-developmentally in the MB with *OK107GAL4/tubGAL80^{ts}*. FasII intensity of the MB and EB for each sample was recorded from the 3 different regions of the structure on stacked images of MB and EB using ImageJ and calculated for the average intensity per sample. Each bar represents the mean ±SEM. FasII average intensity in the MB was normalised to FasII average intensity in the EB. Dashed line demarcates the level in which the FasII average intensity between MB and EB are the same. Statistical analysis was carried out in PRISM using Kruskal Wallis test followed by Dunn's multiple comparisons post hoc test to determine significance between genotypes.

FasII intensity was also quantified in brains in which endogenous HDAC4 was depleted with deGradFP and replaced with *3A* and *dANK* as described in Section 4.2.4. No reduction of FasII was observed (**Figure 5.9**). When raised at 27°C, the total level of HDAC4 expression is close to WT, suggesting that downregulations of FasII requires a higher level of transgene expression that is significantly above WT levels. This lack of a reduction in FasII also suggests that the MB phenotype might not have been completely caused by a loss of FasII and that 3A and dANK might be acting in other parallel pathway to exert its developmental influence on the MB. Nevertheless, it will be interesting to determine whether co-expression of a WT FasII transgene in the 3A and dANK brains can rescue the MB phenotypes, as FasII has been reported to be required in the α'/β' neurons to properly form α'/β' and α/β lobes (Fushima & Tsujimura, 2007).

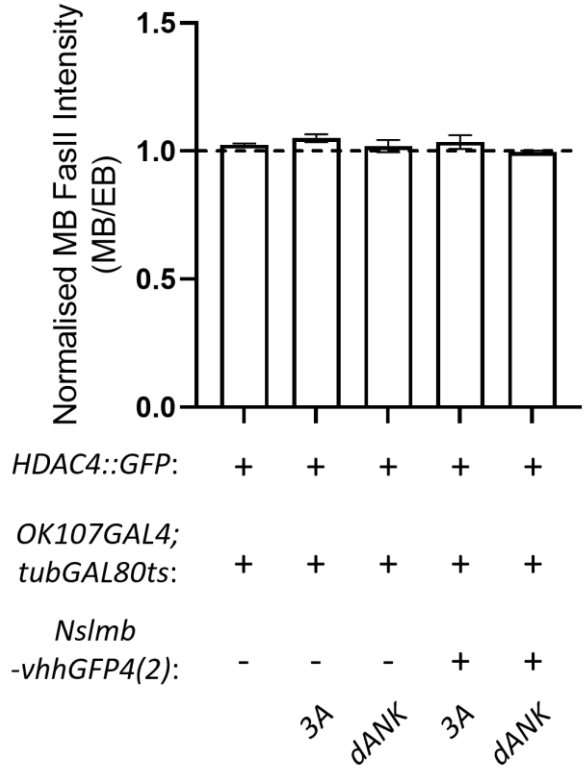

Figure 5.9: Quantification of FasII in brains in which endogenous HDAC4 has been knocked down and replaced with 3A or dANK
Graphs displayed the comparison of FasII intensity between each genotype. X-axis indicates the presence of absence of the deGradFP system and the DmHDAC4 variants. Flies were raised at 27°C. FasII intensity of the MB and EB for each sample was recorded from the 3 different regions of the structure on stacked images of MB and EB using ImageJ and calculated for the average intensity per sample. Each bar represents the mean ±SEM. FasII average intensity in the MB was normalised to FasII average intensity in the EB. Dashed line demarcates the level in which the FasII average intensity between MB and EB are the same. Statistical analysis was carried out in PRISM using Kruskal Wallis test followed by Dunn's multiple comparisons post hoc test to determine significance between genotypes.

5.6 Discussion

The less severe eye and MB phenotype resulting from expression of the dMEF2 variant in comparison to DmHDAC4^{WT} indicated that DmHDAC4 may act through MEF2 to impair axon morphogenesis in the MB. Despite that, many studies have also made cytoplasmic mutants by mutating the MEF2-binding site (L175A) (Main et al., 2021) or deleting the N-terminal region which also spans the binding site (Wang & Yang, 2001), thus the ability for dMEF2 to affect cytoplasmic dependent changes may also be confounded by the mutant's altered ability to interact with MEF2 or other transcription factor which could potentially influence other processes that might also affect protein

export. Therefore, to further understand the role of MEF2, the dMEF2 mutation was introduced into the dNLS, dANK and 3A mutants, and their expression patterns and impact on eye and MB development was assessed.

5.6.1 dMEF2 with mutations to serine phosphorylation sites are restricted to the nucleus

The ability for nuclear entry of HDAC4 has been shown to be dependent on its intact MEF2-binding site (Wang & Yang, 2001), which is consistent with the data from this study (**Figure 4.7G & H**). The expression pattern of dNLS_dMEF2 in the KCs was shown to be specific to the cytoplasm, as expected. The dANK_dMEF2 mutant was also cytoplasmically-restricted. It should also be noted that in myoblast cultures, co-transfection of HDAC4 with a human MEF2 mutant lacking its NLS led to a significant number of cells displaying a cytoplasmically restricted HDAC4 (Borghi et al., 2001). This highlights the importance of MEF2 in mediating HDAC4 subcellular distribution through its binding. Despite this, the 3A_dMEF2 was still largely restricted to the nucleus, perhaps this could suggest that the intact NLS is still able to facilitate nuclear entry albeit at a lower level, however the mutation of the serine residues which prevents nuclear exit could lead to the gradual accumulation of DmHDAC4 in the nucleus, thus preventing the cytoplasmic-restriction phenotype of dMEF2 from manifesting. It should also be noted that the characterisation of the subcellular distribution of the variants was carried out only in KCs, it is therefore not yet known if the subcellular distribution is the same in photoreceptors. Therefore, it will be crucial to investigate this by looking at the distribution pattern of DmHDAC4 and its variants in the developing eye imaginal discs of larva or adult photoreceptor using *GMR-GAL4* to drive the variants to determine if the pattern is consistent with the KCs.

5.6.2 MEF2-binding is required for the DmHDAC4-induced phenotype in the MB but not the eye

3A_dMEF2 accumulates in the nucleus and aggregates into puncta, additionally, its ability to bind DmMEF2 was severely compromised, indicating the mutations to the

MEF2-binding site does impact interaction with DmMEF2. It has been shown in mammalian *in vitro* experiments that HDAC4 is crucial for muscle differentiation and could be regulating this process by inhibiting MEF2-targeted gene transcription required for myogenesis (Miska et al., 2001). This could potentially suggest that the severe MB phenotype resulting from nuclear accumulation of the single mutant 3A could be due to excessive repression of MEF2-regulated developmental genes and that mutating the MEF2-binding site prevents interaction with MEF2. However, only expression of *3A_dMEF2* in the MB showed a reduced phenotype when compared to the *3A* mutant, whereas the eye phenotype did not show any difference. This suggests a difference in cell-specific function in which the MEF2-binding site is required for MB but not eye development. Conversely *dNLS_dMEF2* displayed an alleviated eye phenotype similar to *dMEF2* in both the MB and the eye when compared to *dNLS* alone. Although this could point to the potential possibility of cytoplasmic-restricted DmHDAC4 requiring the MEF2-binding site to impact the development of both the MB and the eye, because dNLS_dMEF2 and dMEF2 have similar phenotype patterns in both the MB and the eye and both mutants were shown to restrict to the cytoplasm completely as opposed to dNLS alone which still display a small number of nuclear puncta, the reduction in phenotype could also be due to dNLS_dMEF2 and dMEF2 being completely cytoplasmic-restricted. Therefore, the further removal of MEF2-binding site in dNLS could then reduce the phenotype further that is similar to dMEF2 alone.

It should also be noted that phenotypes displayed by the MB is very different to the eye in the sense that they are of two different tissue types. While MB analysis allows us to look directly at neuronal morphologies, the eye is only a visual assessment of visible exterior tissues. As there is no literature examining MEF2 expression in the eye, it will be important to focus on photoreceptor analysis at the cellular level in the future. An analysis of the larval eye imaginal disc (from which the adult eye develops), was conducted by another PhD student in this laboratory, and has revealed that MEF2 is not expressed which is consistent with the lack of impact of mutation of the MEF2-binding site in the *3A* and *dANK* mutants (Hannah Hawley, unpublished data). Perhaps this lack of interaction could then result in more HDAC4 being translocated out of the nucleus during development. MEF2 expression will also need to be assessed in the developing MB for future experiments.

For dANK_dMEF2, which was also cytoplasmically-restricted, the phenotypes resulting from expression in the eye did not show any morphological difference when compared to dANK alone, indicating dANK is acting in the cytoplasm. This suggests a role for HDAC4 in the cytoplasm that could not be determine between *dNLS* versus *dNLS_dMEF2*. In the MB, activities at the MEF2-binding site and the putative ankyrin-binding site could be acting in parallel pathways to impact MB development. Further analyses will be required to determine if dMEF2 is rescuing the phenotype caused by dANK (by sequestering in the cytoplasm) or the overexpression effect of DmHDAC4 itself. To do that, proteins that can bind to ankyrin-binding site will first need to be identified though co-immunoprecipitation followed by mass spectrometry. Gene candidates that are identified can then be knocked down while simultaneously expressing DmHDAC4^{WT} to determine if a more severe phenotypes can arise after which dMEF2 will be introduced with the gene KD to see if the severe phenotype can be rescued. Rescue could then indicate that the effects caused by the lack of candidate protein interaction (a result of KD) with HDAC4 through its ankyrin-binding site can be mediated by MEF2-binding site (**Figure 5.10**). The role of ankyrin-binding domain will be further discussed in the next section.

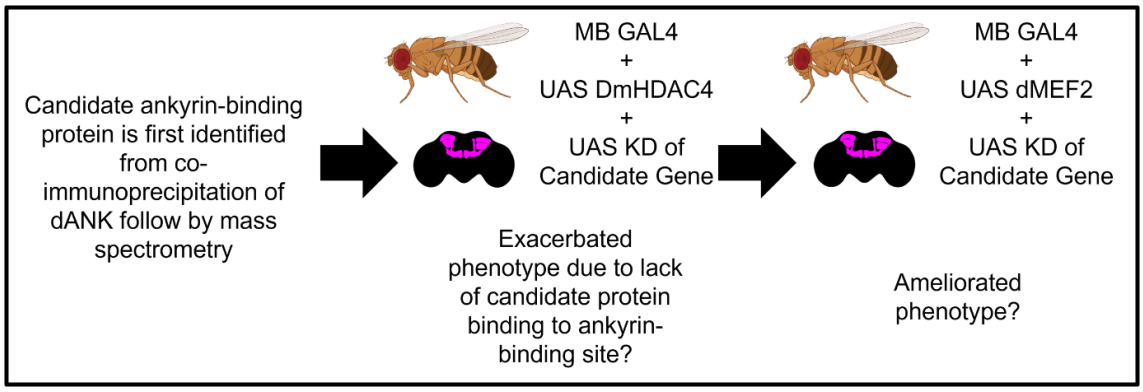

Figure 5.10: Future direction workflow to study the impact of DmHDAC4 MEF2-binding site on potential ankyrin-binding protein candidate

As mentioned above, since 3A was shown to co-localise with DmMEF2 puncta and the co-localisation of 3A_dMEF2 was reduced, this led to the question of whether cytoplasmic accumulation of DmHDAC4 (i.e. the dNLS mutant) could alter distribution of DmMEF2 via binding and sequestering it to the cytoplasm. However, visualisation of endogenous DmMEF2 revealed that the expression was still highly restricted to nucleus even when DmHDAC4 was restricted to the cytoplasm through mutation of the NLS. A

transgenic line for expression of a reportedly cytoplasmic-restricted MEF2 (T148A) was generated to better understand the relationship between DmHDAC4 and DmMEF2 and whether if DmMEF2 that is restricted to the cytoplasm can sequester DmHDAC4 to the cytoplasm. This could potentially indicate whether DmHDAC4 in the cytoplasm is still able to bind DmMEF2 which could also highlight a role for DmMEF2 in the cytoplasm. However, the T148A mutant was still nuclear and thus did not fulfil its intended function which leaves the question of whether DmHDAC4 can interact with DmMEF2 in the cytoplasm unanswered. As DmMEF2 does not possess the bipartite NLS which is present in vertebrate MEF2 (Borghi et al., 2001; Yu, 1996), the deletion or mutation of an NLS is not feasible. A different approach will have to be considered in the future such as adding an NES to DmMEF2 to see if it is able to translocate to the cytoplasm and by performing western blots on nuclear and cytoplasmic fraction to detect for DmHDAC4 protein changes among the subcellular compartments. Alternatively, western blots on nuclear and cytoplasmic fraction from heads of flies expressing dNLS can be performed to confirm that DmMEF2 has not been sequestered to the cytoplasm, as suggested by immunostaining. Additionally, co-immunoprecipitation with mass spectrometry can also be utilised to explore the difference in protein interaction between dMEF2 and dNLS to determine process that can be involved in the cytoplasm. This could potentially reveal other transcription factors or protein binding partners that interact at or near the MEF2-binding site. In fact, the binding domain of the transcription factor, RUNX2, has been identified in mice to also include MEF2-binding domain (Vega et al., 2004) which is also adjacent to a SRF-binding domain (Davis et al., 2003).

Recently, there has been a rising interest on MEF2 impact on brain development in which many MEF2 regulated genes have been associated to risk of autism (Assali, Harrington, & Cowan, 2019; Harrington et al., 2016). In fact, in *Drosophila*, Crittenden et al. (2018) has shown that DmMEF2 is required for the proper development of MB, furthering its importance in neurodevelopment. Perhaps, $DmHDAC4^{WT}$ could be made to express in the MB of flies that are mutant for *DmMEF2* to determine whether phenotypes can be ameliorated. As DmHDAC4 dMEF2 mutant was shown to have reduced phenotypes which suggest that its lack of ability to bind DmMEF2 was what led to the reduction, phenotype amelioration would suggest the interaction between DmHDAC4 and DmMEF2 is important to induce phenotype. Additionally, RNA-Seq can also be performed on developing brains derived from larvae or pupae that express DmHDAC4

or its variants to identify gene candidate that may have been the target of MEF2 regulation. A gene that is known to be regulated by DmMEF2 is the cell adhesion molecule gene, *FasII*, which will be discussed further in the next section (Sivachenko, Li, Abruzzi, & Rosbash, 2013).

In the recent study conducted by Main and colleagues (2021), the interaction between HDAC4 and MEF2 was investigated in adult flies harbouring a MEF2-response element that is fused to luciferase for detection of MEF2-binding activity, however there was no significant luciferase activity detected from overexpression of HDAC4 and the lack of activity from endogenous or transgene-expressed MEF2 suggest that HDAC4 interaction with MEF2 may not be via repression of the transcription factor. This suggests that impaired memory performance exhibited from the courtship suppression assay is not dependent on repression by MEF2 on transcription (Main et al., 2021). However, this analysis was performed on adult flies (i.e. post development). In addition, whole heads were used, so any effect restricted to specific cell types or brain regions could potentially be diluted. Therefore, it will be interesting to perform the same luciferase assay from lysates dissected from developing larval brains.

5.6.3 DmHDAC4 downregulates the cell adhesion molecule FasII

While assessing the MB for developmental phenotypes using the FasII antibody to visualise the gross structure of the MB lobes, it was noticed that pan-neuronal expression of *DmHDAC4*^{WT}, *3A* and *dANK* exhibited significantly reduced amount of FasII. When expression was limited to the KCs, a reduction in FasII was still observed but only for *3A* and *dANK*. Given that FasII is a cell adhesion molecule that is known to play a role in axon guidance and fasciculation (Fushima & Tsujimura, 2007), it was then speculated that *DmHDAC4* overexpression could lead to reduced expression of FasII which in turn could impair MB development. The reduction of FasII by *DmHDAC4*^{WT} overexpression is only observed on pan-neuronal expression which could imply a non-autonomous developmental effect, however, reduction of FasII in *3A* and *dANK* expression by pan-MB driver could then suggest an autonomous role by the serine phosphorylation site and putative ankyrin-binding site. While it is possible that both non-autonomous and autonomous role could exist depending on the mutation, the difference in FasII expression from *DmHDAC4*^{WT} between *elavGAL4* and *OK107GAL4/tubGAL80*^{ts} could also likely be

due to different expression levels and this could be repeated with a stronger MB GAL4 drivers or simply with *OK107GAL4* raised at a higher temperature which should drive higher expression than the maximal induction of *OK107GAL4/tubGAL80^{ts}*.

It is not yet clear how expression of *3A* or *dANK* results in downregulation of FasII and whether this is a transcriptional or post-transcriptional effect. However, this reduction was not present on expression of *dMEF2*, *3A_dMEF2* and *dANK_dMEF2* which suggests that 3A and dANK are acting through the MEF2-binding site to downregulate FasII. In a study that looks into the role of MEF2 on *Drosophila* circadian rhythm, it was shown through chromatin immunoprecipitation with DNA microarray that MEF2 binds to the genomic region of *FasII* which likely indicates that *FasII* is its transcription target (Sivachenko et al., 2013). Therefore, it will be interesting to verify with immunostaining on whether the overexpression or KD of DmMEF2 in the MB can lead to altered levels of FasII.

In this study, it is unclear whether the reduced FasII observed in *3A* and *dANK* expression causes the MB phenotype. However, as mentioned briefly in Section 5.5, the impact of mutations of *FasII* on MB development has been conflicting between Kurusu et al. (2002) and Cheng et al. (2001) in which the former detected abnormal lobe formation while the latter reported no defects. Kurusu et al. (2002) suggested this was due to differences in genetic background which could then perhaps be a hint that *FasII* has a redundant partner. For example, a reported redundant partner of *FasII* is the L1 cell adhesion molecule, *Neuroglian* (*Nrg*), in which the reduction of FasII expression was shown to exacerbate the phenotype of photoreceptor pioneer axon displayed by the *Nrg* mutant (Kristiansen et al., 2005). Since, HDAC4 genetically interacts with *Ank2* (Schwartz et al., 2016) and Ank2 was also demonstrated to be able to bind Nrg (Enneking et al., 2013), it is therefore worth examining in future studies whether if increased HDAC4 also alters Nrg levels.

While the normal FasII expression of 3A_dMEF2 suggests that nuclear abundance from the expression of *3A* alone could lead to more repression of MEF2 which in turn reduces the amount of FasII, it does not fully support the reduction of FasII caused by *dANK* as DmHDAC4 is present in both nuclear and cytoplasm for this variant. Although there is still significant nuclear DmHDAC4 in the dANK mutant which could still suggest repression of MEF2, the potential loss of binding to ankyrin repeat-containing proteins could also contribute to the reduction of FasII. Therefore, it is hoped that the previously

mentioned co-immunoprecipitation with mass spectrometry experiment can identify for such ankyrin repeat-containing proteins to provide more insights into the role DmHDAC4. The idea of an influence by ankyrin repeat-containing proteins was further reinforced by the genetic interaction study from Schwartz et al. (2016) where it was discovered that *HDAC4* interacts with *Ank2*. In another *Drosophila* study, an *Ank2* mutant which was shown to exhibit impairment to neuromuscular junction (NMJ) development also displayed a reduction in FasII in the presynaptic neurons, therefore it was concluded that Ank2 is required to organise and stabilise synaptic FasII expression (Pielage et al., 2008). Although it has been shown through co-immunoprecipitation that there was no physical interaction between HDAC4 and Ank2 (Wilson, 2021), it is still possible that the mutation of the putative ankyrin-binding site of dANK might prevent binding of other uncharacterised ankyrin repeat-containing proteins (such as CG5846), and this interaction could potentially be required for stabilisation of FasII. Since dANK is present in both nucleus and cytoplasm, the potential of impacting the stabilisation and organisation of FasII in the cytoplasm together with MEF2 being repressed in the nucleus could be the cause of FasII reduction in the MB and the mutation of MEF2-binding site is enough to rescue the expression phenotype.

The downregulation of FasII by *3A* and *dANK* occurred only when they were expressed during the developmental stages. Interestingly, expression of *3A* and *dANK* in the control of the deGradFP system did not show reduction in FasII expression which could suggest that although the serine phosphorylation and ankyrin-binding sites may be required, the extent of the downregulation is dependent on the amount of the mutated DmHDAC4 being expressed, meaning the more the variants are overexpressed, the more obvious the reduction of FasII becomes. Therefore, although *3A* and *dANK* FasII reduction seems to coincide with *3A* and *dANK* impact on MB development, the fact that MB phenotypes are still observable in deGradFP *3A* and *dANK* suggests that FasII reduction might not be the root cause of the MB defect. However, there is also the possibility that FasII reduction could be another parallel pathway to MB development since FasII expression was reported to be required in the α'/β' neurons to properly form α'/β' and α/β lobes (Fushima & Tsujimura, 2007), hence at the time when this thesis was written, an experiment is underway is to determine whether if UAS overexpression of FasII in flies expressing *3A* or *dANK* could lead to some degree of phenotype amelioration.

6. INVESTIGATING THE TRANSCRIPTIONAL EFFECTS OF HDAC4 VARIANTS

In the previous chapters, it was shown that increased nuclear DmHDAC4 disrupted MB development. This was prevented in the double mutant 3A_dMEF2, thus implying that the MEF2-binding site in DmHDAC4 is required for manifestation of the MB phenotype. Given that MEF2 is a transcription factor, this suggests that DmHDAC4 may be repressing transcription of genes required for MB axon morphogenesis through repression of MEF2.

A previous RNA-Seq of RNA samples generated from fly heads overexpressing $DmHDAC4^{WT}$ showed only 28 genes were differentially regulated compared to the control (Schwartz, 2016). It was suggested that this minimal transcriptional effect could be due to HDAC4 being predominantly cytoplasmic, therefore if significant transcriptional changes were occurring in a small number of neurons, they would be diluted out. It was hypothesised that restricting DmHDAC4 to the nucleus would increase transcriptional changes and reveal differentially regulated genes that might help to explain the mechanism through which 3A disrupts MB development and memory (Main et al., 2021).

6.1 RNA sample preparation, sequencing, and quality checking

RNA-Seq was conducted on heads of adult *Drosophila* with pan-neuronal expression of the DmHDAC4 variants. Although majority of this project has been focusing on the function of DmHDAC4 on neuronal development, to allow direct comparison to previous RNA-Seq on *Drosophila* (Schwartz et al., 2016) and human HDAC4 (Main et al., 2021), RNA-Seq was conducted only on brain samples expressing the variants post-developmentally. As *DmHDAC4* has also been shown to be required for *Drosophila* courtship memory (Fitzsimons et al., 2013), RNA-Seq analysis was also performed on samples with pan-neuronal *DmHDAC4* KD using an RNAi to determine the transcriptional targets of endogenous DmHDAC4. RNA was extracted in quadruplicate

from whole fly heads in which the pan-neuronal TARGET driver (*elavGAL4;tubGAL80^{ts}*) drove expression of the *UAS DmHDAC4* variants, *UAS DmHDAC4* inverted repeat RNAi and the *w(CS10)* (named "*CS*") control. Flies were raised at 18°C and expression was induced post-eclosion at 30°C for 72 hours (**Figure 6.1A**). After RNA extraction, the quality of RNA samples was initially assessed via spectrophotometer to ensure that the samples are "pure" with minimal contaminants (**Table 6.1**). Further quality testing was carried out by Massey Genome Service via LabChip®, a microfluidic-based electrophoresis to determine the presence of early-stage RNA degradation. The quality of the RNA samples was determined through the integrity of the most abundant RNA, the ribosomal RNA (rRNA). Typically, ribosomes consist of the small ribosomal subunit derived from the 18S rRNA and the large ribosomal subunit derived from the 28S and 5S rRNA. In insects, an additional cleavage of 28S rRNA into two fragments that are slightly similar in size to 18S rRNA occurs (**Figure 6.1B**). Therefore, the detection of the *Drosophila* rRNA bands from microfluidic electrophoresis yields four bands consisting of a small amount of the uncleaved 28S, 18S, cleaved 28S and 5S (**Figure 6.1C**). The electropherogram of these bands are reflected in peaks in which the heights and distances between peaks were used to compute the RNA integrity number (RIN), 10.0 being the highest integrity value with minimal degradation (**Figure 6.1D & Table 6.1**). The cleavage of 28S rRNA results in a reduced RIN value for insect RNA, however, the absence of "smearing" in the electrophoresis and the clear distinction between each peak in the electropherogram indicates that the samples were not degraded. Therefore, the RIN value of a good quality *Drosophila* RNA samples were accepted at ≳5.0.

A

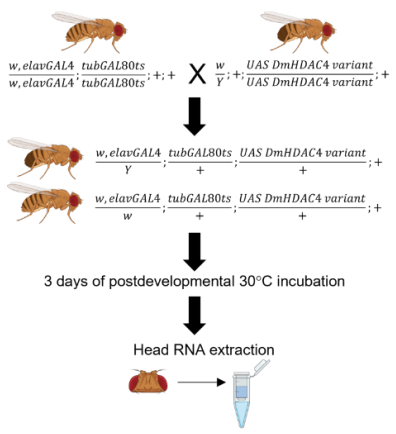

B

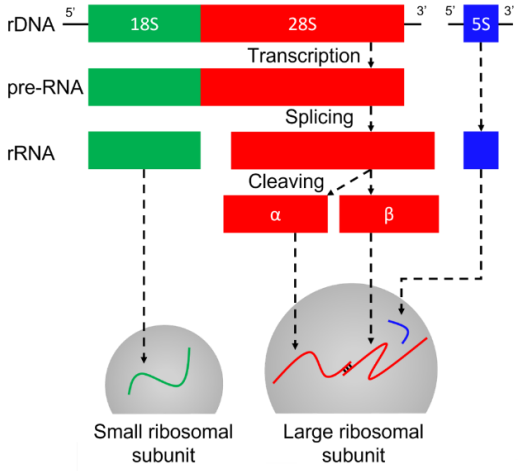

#	Sample	Concentration (ng/ul)	A260	260/230	260/280	RIN
1	CS - 1	218.547	5.4637	2.059	2.058	6.5
2	CS - 2	1110.173	27.7543	2.148	2.087	5.4
3	CS - 3	326.245	8.1561	2.076	2.081	6.3
4	CS - 4	464.850	11.6213	2.061	2.124	6.5
5	HDAC4_WT - 1	200.367	5.0092	1.853	2.032	6.6
6	HDAC4_WT - 2	1061.174	26.5294	2.240	2.090	5.5
7	HDAC4_WT - 3	1708.994	42.7249	2.220	2.153	5.0
8	HDAC4_WT - 4	866.092	21.6523	2.175	2.227	6.3
9	3A - 1	485.559	12.1390	2.087	2.155	6.4
10	3A - 2	308.835	7.7209	1.992	2.063	6.5
11	3A - 3	728.816	18.2204	2.183	2.172	6.2
12	3A - 4	577.338	14.4334	2.160	2.198	6.6
13	dNLS - 1	542.421	13.5605	2.073	2.168	6.5
14	dNLS - 2	1039.002	25.9751	2.186	2.226	5.4
15	dNLS - 3	1948.700	48.7175	2.257	2.178	4.8
16	dNLS - 4	456.852	11.4213	2.300	2.176	6.7
17	Y1142H - 1	349.897	8.7474	2.070	2.100	6.5
18	Y1142H - 2	428.182	10.7046	2.161	2.143	6.3
19	Y1142H - 3	1081.997	27.0499	2.058	2.162	5.4
20	Y1142H - 4	506.708	12.6677	2.121	2.207	6.6
21	dMEF2 - 1	477.344	11.9336	2.142	2.164	5.7
22	dMEF2 - 2	465.228	11.6307	1.985	2.140	6.3
23	dMEF2 - 3	2407.987	60.1997	2.308	2.152	5.0
24	dMEF2 - 4	376.003	9.4001	2.163	2.126	6.5
25	dANK - 1	724.041	18.1010	2.071	2.220	5.5
26	dANK - 2	444.600	11.1150	2.081	2.137	6.2
27	dANK - 3	6044.068	151.1017	2.531	2.349	5.3
28	dANK - 4	502.709	12.5677	2.334	2.200	6.6
29	HDAC4_KD - 1	316.752	7.9188	2.032	2.090	5.6
30	HDAC4_KD - 2	212.176	5.3044	1.966	2.029	6.5
31	HDAC4_KD - 3	1077.798	26.9450	2.067	2.136	5.3
32	HDAC4_KD - 4	436.780	10.9195	2.324	2.163	6.6

C

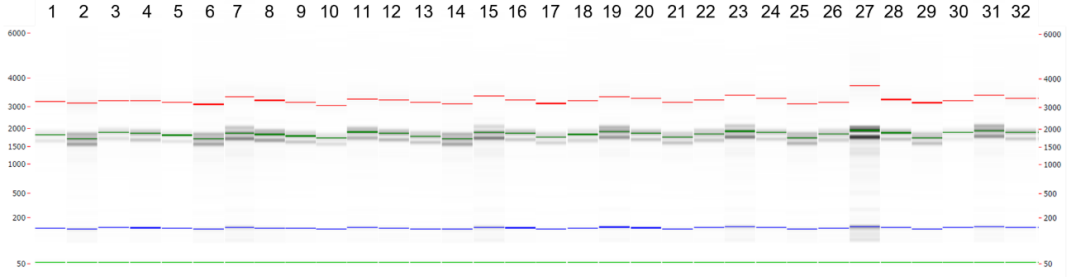

D

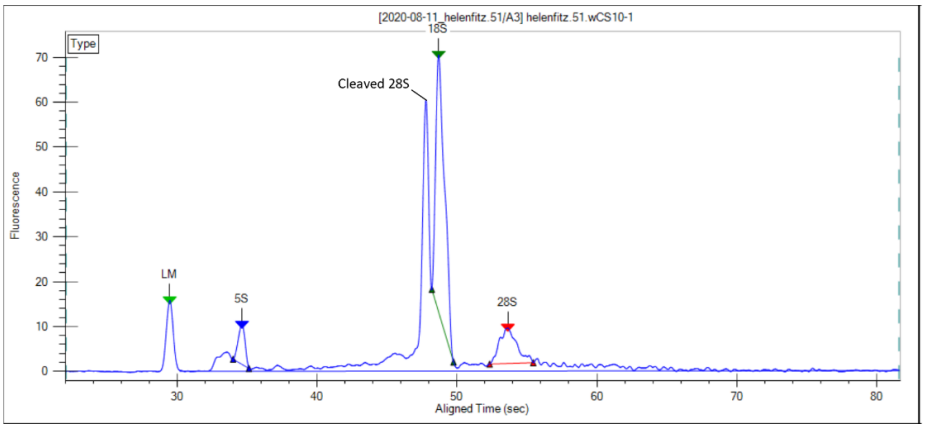

Figure 6.1: Generating the genotypes of RNA samples and Labchip® analysis of RNA quality

(A) Crossing scheme of the fly genotypes required to obtain the heads of F1 flies for RNA extraction. (B) Schematic representation of the formation of insects' small and large ribosomal subunits. Ribosomal DNA undergoes RNA transcription follow by splicing into the 18S and 28S fragment. The 28S undergoes further cleavage resulting in two RNA fragments of 28S that are slightly smaller in size compared to 18S. (C) The analysis of RNA integrity is carried out by assessing the RNA of 28S and 18S for degradation using LabChip®, a microfluidic-based electrophoresis platform. Differences in migration distance between samples were due to the sample concentration. Red, dark green, blue, and light green lines highlight the detection of 28S (uncleaved), 18S, 5S and lower marker [LM (standard)] bands by system. The extra band below 18S belonged to the cleaved 28S fragments. Clear bands with minimal "smearing" generally indicate a high-quality RNA with little to no degradation. The number above each lane corresponds to sample number in the table (**Table 6.1**). (D) Hence, a typical electropherogram of the microfluidic electrophoresis of a high-quality insect RNA should reflect only a 28S peak, a doublet peak with the left and right belonging to the 28S fragment and 18S respectively and a 5S peak. The RNA integrity number (RIN) were derived by the system based on the height of the peaks and distances between peaks.

Table 6.1: Spectrophotometric measurements of concentration and absorbance ratio of RNA samples

The concentration and absorbance ratio of all 8 quadruplicate genotypes. Both 260/230 and 260/280 ratios assess the purity of the RNA samples. RNA absorbance wavelength is 260nm and contaminants such as phenol, protein and carbohydrate have absorbance wavelength of 230nm or 280nm. An RNA sample with ratio of ~2.0 is deemed to be "pure". RNA integrity values are displayed in RIN column with 10.0 being of the highest integrity (Note: Insect RNA generally have a lower RIN value due to the cleavage of 28S).

After quality testing of RNA, the samples underwent further RNA quality testing at Novogene prior to library construction and 2x150bp paired end sequencing of each sample library. The data obtained from the library of each sample were assessed for sequencing quality and error rate. The Phred quality score is a measure of the accuracy of base calling during a sequencing reaction, the higher the Phred score (maximum=40) (**Figure 6.2A**), the higher the chances of correctly detecting the nucleotide at that base position. Generally, a good quality sequencing data will have a Phred score between 30 to 40 over each base position which then indicate a high accuracy of nucleotide calling (99.9% to 99.99% accuracy). A low percentage of error rate is also a good indication of a highly accurate data, the probability of calling an incorrect base at a position was shown to occur only at a rate, range between 0.02%-0.04% (**Figure 6.2B**). The distribution of per base sequence content also show a constant proportion of AT and GC percentage over the read length with almost no undetermined base, indicating good sequence read (**Figure 6.2C**). Finally, apart from the reads of interest, the raw sequence data usually includes adapter base sequence, low quality bases (result of inaccurate base calling) as well as undetermined bases. Therefore, it is essential to filter out such sequences. As all the samples' raw data was shown to have between ~97% to ~98% clean reads, ~1% to ~2%

adaptor sequence read and ~0% of undetermined or low-quality base read, this indicated that the raw data is of very high quality and hence, it was determined that no trimming was necessary (**Figure 6.2D**).

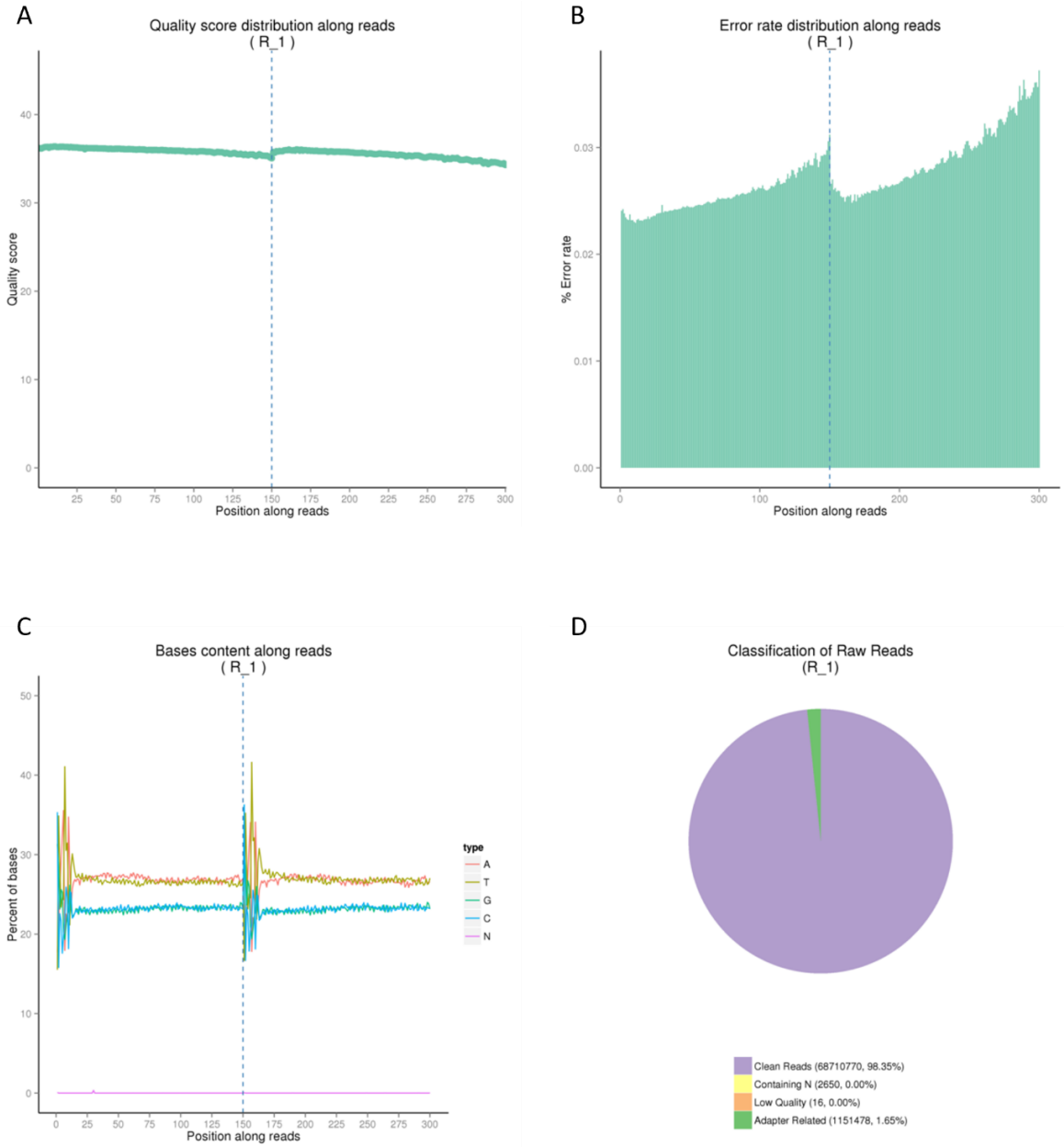

Figure 6.2: Data quality graphs of a sequenced sample which are representative of all 32 samples

The values along the x-axis in all graphs represent the base position along the paired end sequence reads, 0-150 are the base positions of the left read while 150-300 are the base positions of the right read. (A) Per base sequence quality score (Phred score) determines the base calling accuracy at each base position along the reads while (B) error rate distribution along reads determines the probability of an incorrect base call occurring. The respective decrease and increase in quality score and error rate were due to the consumption of sequencing reagent (Jiang et al., 2011). The slightly higher error rate in the first few base positions were resulted from incomplete binding of primers on RNA during cDNA synthesis (Jiang et al., 2011). (C) Per base sequence content assess the percentage distribution of AT

and GC content at each base position along the reads. The non-uniform distribution along the first few base positions were due to primer amplification bias. (D) Percentage proportion of clean reads, adaptor read sequence, undetermined and low-quality reads. All graphs and pie chart were generated by Novogene.

6.2 Analysis of count profiles

The analysis of count profiles and other pre-analysis of data, where indicated, were carried out by a bioinformatician from Massey Genome Service, Mr Mauro Truglio. Sequencing data were processed using Salmon, an alignment-free tool for quantifying expression of transcripts. The *Drosophila* genome from BDGP 6.28 (Ensembl release 102) was used to build an index for quantification and to map reads to genes. The read count profiles were first analysed by plotting the heatmap of all genotypes' transcript count profile together. The overall heatmap analysis reveals distinct cluster separation of the CS control from all treatment genotypes except for HDAC4 KD (**Figure 6.3**). Comparison between control and individual genotype also showed a distinct separation in count profile (**Figure 6.4**), which indicates that the count profiles of the control samples are different from the treatment samples but are closely similar to the HDAC4 KD samples. However, cluster separation was not detected among the treatment groups (**Figure 6.3**). This could suggest that the gene expression changes among the different treatment groups were similar.

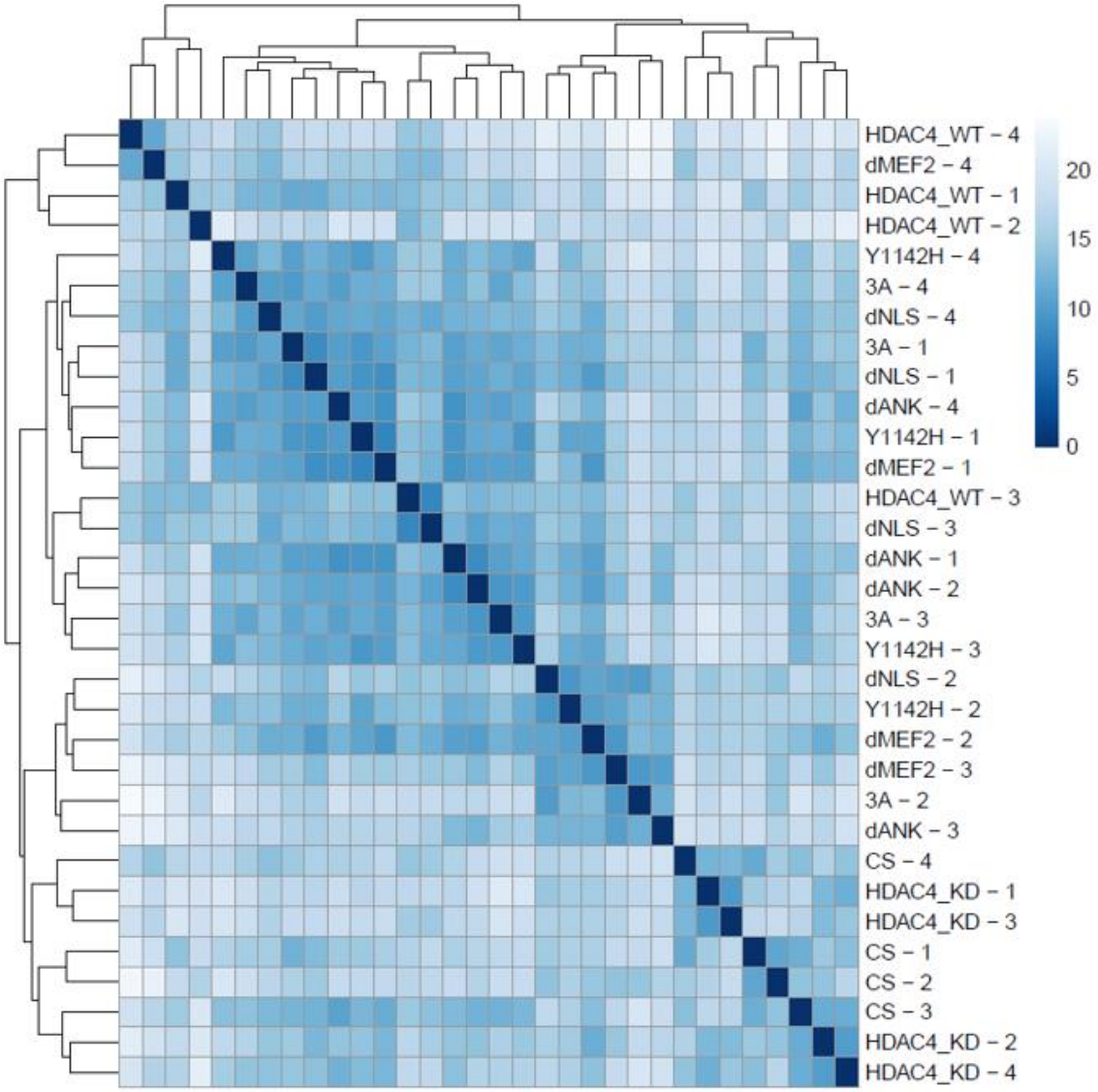

Figure 6.3: Heatmap of all genotype replicates based on transcripts count profiles
Analysis of count profiles of all sequenced samples. Dendrogram on top and left side of the heatmap show hierarchical clustering of the genotypes.

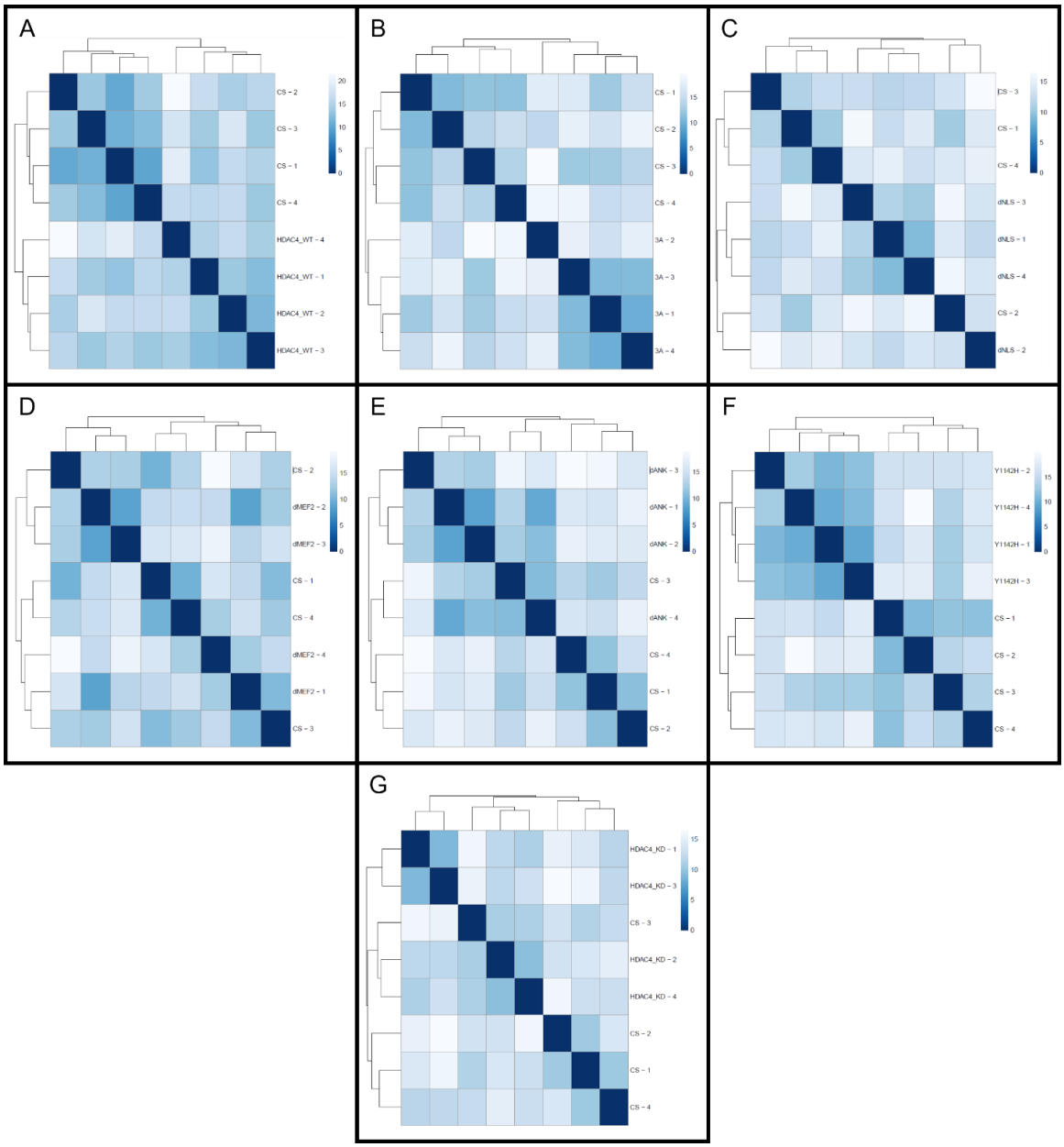

Figure 6.4: Heatmap of individual genotype comparison to control replicates based on transcripts count profiles
Analysis of count profiles of individual sequenced sample compared to CS control. Dendrogram on top and left side of the heatmap show hierarchical clustering of the genotypes.

Therefore, a more targeted analysis of the count profiles using the top 50 most varying genes and comparing the control to individual genotypes was performed. Each genotype comparison to control was analysed using Principal Component Analysis (PCA) which is a standard approach to visualising the variances between multi-dimensional data by limiting the comparison to only the first 2 principal component (dimensions that span the 1st and 2nd largest variation between samples). By reducing the data dimension to only

two directions, a clearer pattern of differences between genotype can be obtained by observing for the cluster separation of data points in the graph.

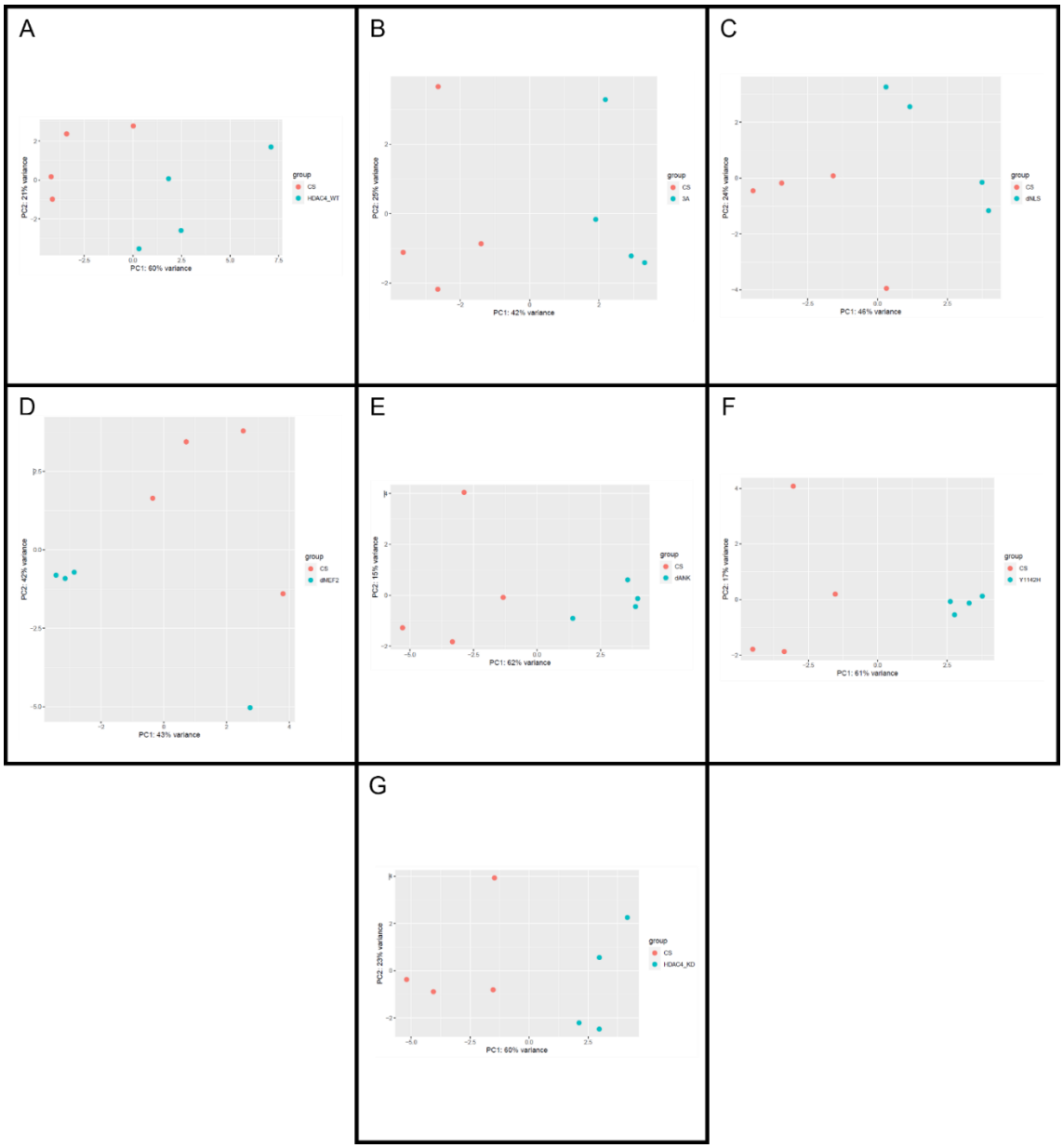

Figure 6.5: PCA analysis plot of the 50 most varying genes between CS control and the individual genotype treatment
Two-dimensional visualisation of samples' variances. The first principal component on the x-axis, PC1, spans the dimension of the largest variation between samples data and the second principal component on the y-axis, PC2, spans the dimension of the second largest variation.

From the analysis of the 50 most differentially expressed genes in each genotype (**Figure 6.5**), a clear cluster separation can be observed between control and all genotypes along PC1 axis with the exception of dMEF2 which has 3 tightly clustered datapoints with another one located in the variance region of the CS control (**Figure 6.5D**). This sample

was therefore deemed to be an outlier. Additionally, an isolated CS control datapoint which was located far away from its cluster group was also considered to be another outlier. Therefore, it was decided that these two samples would be removed from subsequent analysis. Removal of the outliers resulted in an improved separation between control and the individual genotypes along PC1. The variance across PC2 was also further reduced in most of the genotypes, an indication of a more compact variance cluster for the genotype (**Figure 6.6**).

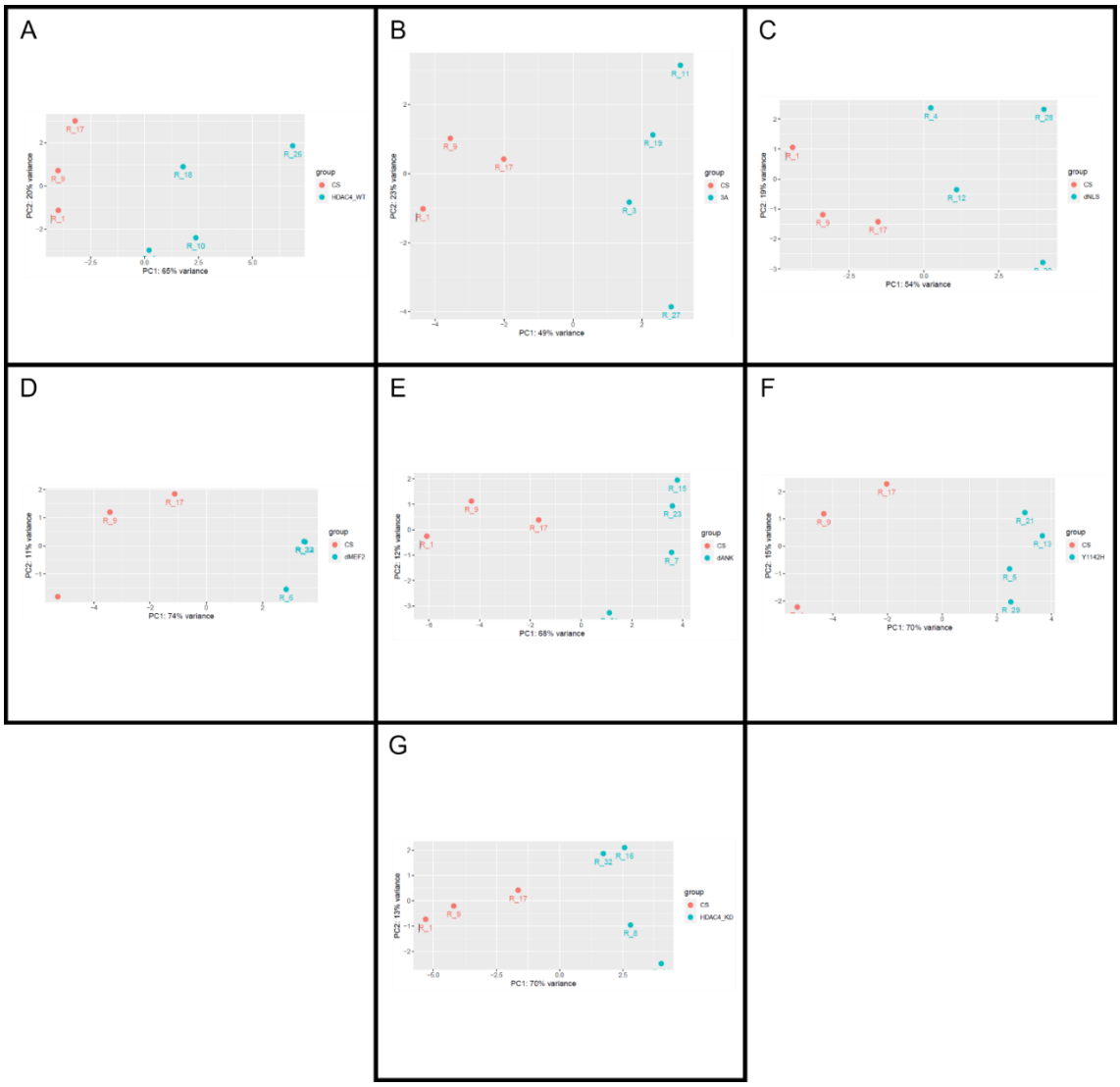

Figure 6.6: PCA analysis plot of the 50 most varying genes between CS control and the individual genotype treatment without outliers
Two-dimensional visualisation of samples' variances. The first principal component on the x-axis, PC1, spans the dimension of the largest variation between samples data and the second principal component on the y-axis, PC2, spans the dimension of the second largest variation.

6.3 Differential gene expression of pairwise comparison

Having examined the variances of the data, the next step was to identify differentially expressed genes based on the read counts comparison between the CS control and the individual treatment group. This pre-analysis was also performed by bioinformatician, Mauro Truglio. Normalisation of the read counts were performed with Salmon using the Transcripts Per Million (TPM) metric and DESeq2 was used to perform the statistical Wald test analysis on the pairwise comparisons with multiple test correction. Genes with a False Discovery Rate (FDR) (adjusted *p*-value) of <0.05 were deemed to be statistically significant in their differential expression. In order to analyse the extent of the differences between individual treatment compared to control in terms of read count, an MA plot was used visualise the distribution of differentially regulated genes based on their mean normalised read counts. The plots showed that for all pairwise comparison, much of the significantly expressed genes with a mean normalised count of at least 1e+01 had a $\log_2$ fold change below 2 or above -2 (**Figure 6.7A-G**). Traditionally, a $\log_2$ fold change of >2 or <-2 is used as a threshold to capture the most significant differentially expressed genes, however such standard fold change cut-offs limit the data interpretation and prevents the discovery of future biological questions which may exist from the genes beneath the fold change threshold (Dalman, Deeter, Nimishakavi, & Duan, 2012). Therefore, based on the narrow convergence in the plots which led to majority of the significant genes to be between the $\log_2$ fold change margin of 1 and -1, it was rationalised that genes that were situated between $\log_2$ fold change 1 and 2 or -1 and -2 have the potential to be involved in the biological interpretation. It was then decided to also include significant genes with $\log_2$ fold change of >1 or <-1 for all pairwise treatment comparisons.

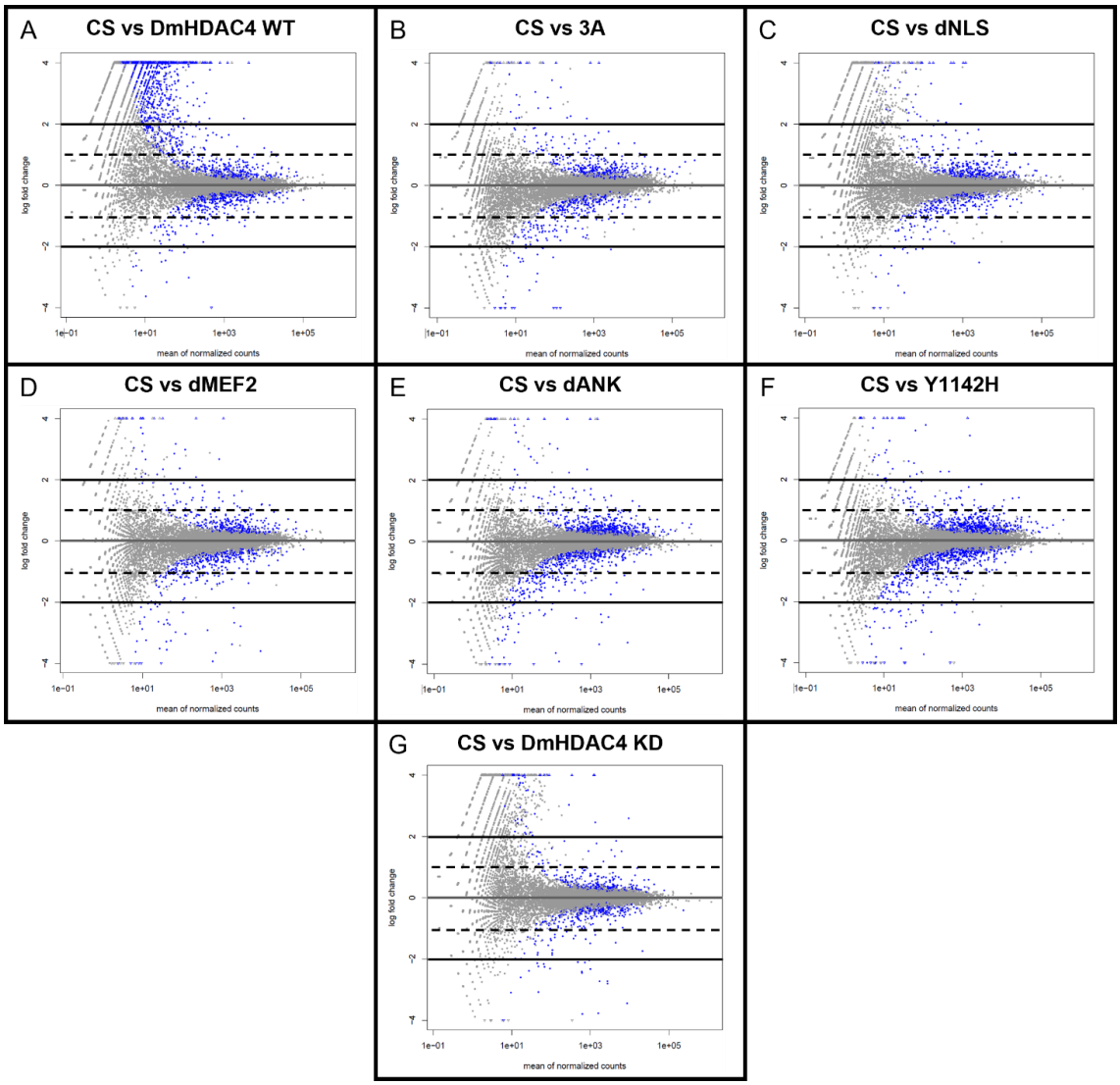

Figure 6.7: MA plot of pairwise comparisons between CS and individual treatment
Each data point in a plot represents a gene plotted against its mean of normalised counts (x-axis) and $\log_2$ fold change (y-axis). Blue dots represent genes that are significantly differentially expressed (FDR<0.05) while grey dots represent insignificant genes. Horizontal lines demarcate the $\log_2$ fold change of -2 and 2 while horizontal dotted lines demarcate -1 and 1.

Interestingly, pairwise comparison revealed that expression of *DmHDAC4*^{WT} resulted in a much higher number of more differentially expressed genes than all other genotypes (**Figure 6.8A-G & Table 6.2**). When comparing the number of differentially expressed genes between *DmHDAC4*^{WT} and *DmHDAC4* KD (**Figure 6.8A & G**), the lack of transcriptional changes in *DmHDAC4* KD suggests that repression of gene transcription by endogenous DmHDAC4 is minimal. However, not only did expression of *DmHDAC4*^{WT} not lead to a high level of downregulation (i.e., transcriptional repression), instead the opposite effect was observed, where 930 genes were reported to be

significantly differentially upregulated (**Figure 6.8A & Table 6.2**). Interestingly, none of the *DmHDAC4* variants induced the same level of differential expression with all resulting in between approximately 100 to 200 genes that were differentially up or downregulated (**Figure 6.8B-F & Table 6.2**).

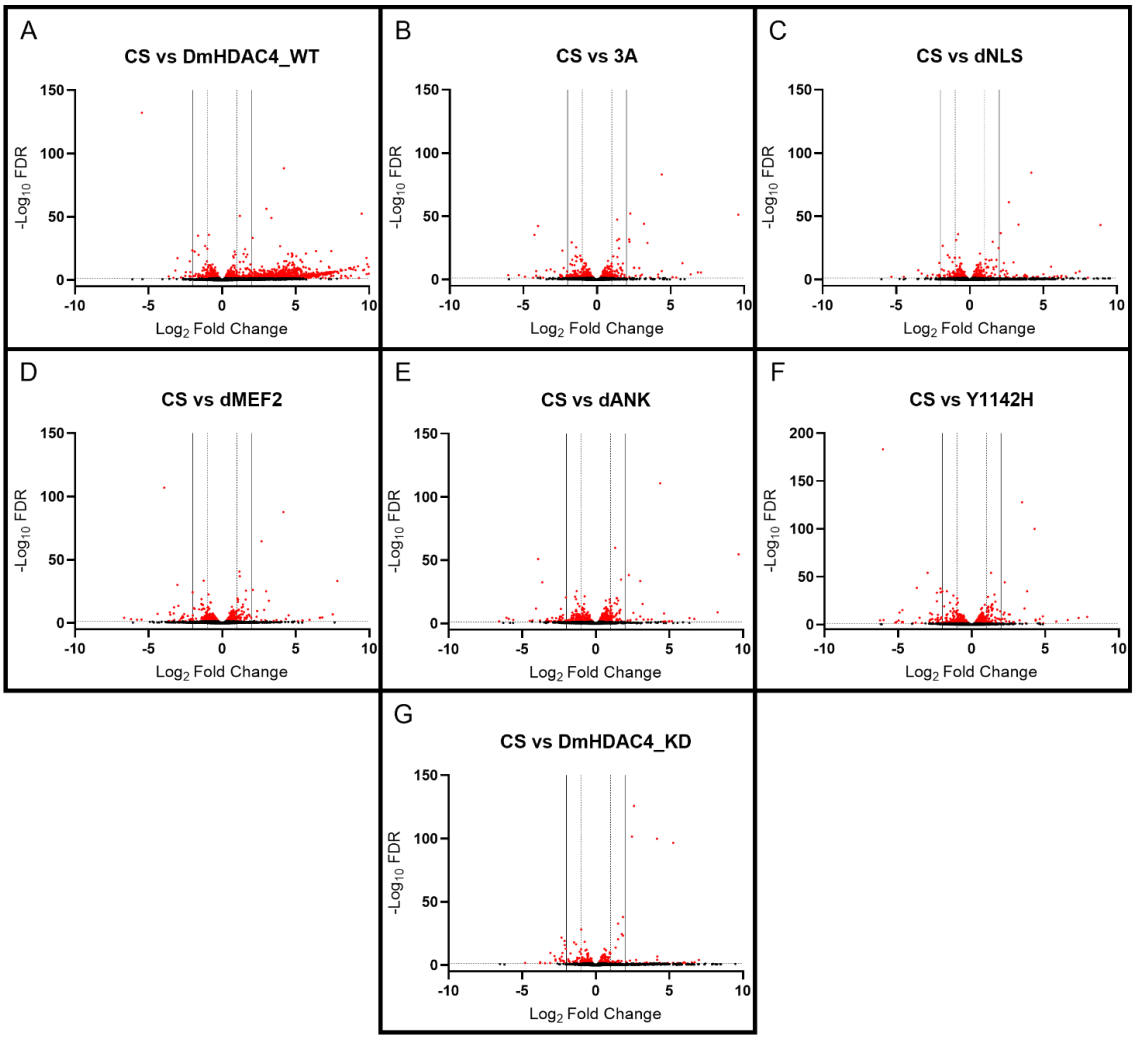

Figure 6.8: Volcano plot of pairwise comparisons between CS and individual treatment
Each data point in a plot represents a gene plotted against its $\log_2$ fold change (x-axis) and -$\log_{10}$ FDR (y-axis). Horizontal dotted line along the y-axis demarcates -$\log_{10}$ 0.05 which separates the statistically significant genes (red dots) (FDR<0.05) from the insignificant genes (black dots). Vertical lines demarcate the $\log_2$ fold change of -2 and 2 while vertical dotted lines demarcate -1 and 1.

CS vs DmHDAC4^{WT}	No. of genes
Upregulated	930
Downregulated	55
Total	985

CS vs 3A	No. of genes
Upregulated	63
Downregulated	86
Total	149

CS vs dNLS	No. of genes
Upregulated	66
Downregulated	44
Total	110

CS vs dMEF2	No. of genes
Upregulated	59
Downregulated	84
Total	143

CS vs dANK	No. of genes
Upregulated	62
Downregulated	126
Total	188

CS vs Y1142H	No. of genes
Upregulated	74
Downregulated	120
Total	194

CS vs DmHDAC4 KD	No. of genes
Upregulated	50
Downregulated	40
Total	90

Table 6.2: Number of significantly differentially up and downregulated genes for individual pairwise comparison
Number of genes that are significantly differentially expressed captured with a $\log_2$ fold change threshold of >1 or <-1.

6.4 Functional enrichment analysis of the differentially expressed genes

To provide further functional interpretation of the changes in gene expression that were identified, the Database for Analysis, Visualisation, and Integrated Discovery (DAVID), an online bioinformatic tool, was utilised to perform an enrichment analysis of gene function on the sets of differentially expressed genes for each genotype. The databases selected to annotate the genes for their roles and functions were from the Gene Ontology (GO) resource and Kyoto Encyclopaedia of Genes and Genomes (KEGG) which comprised of machine-readable curated information on gene function that can be utilised for functional analysis of large gene datasets. The GO database is essentially split into three categories namely Biological Process, Cellular Components and Molecular Function. A list of all significant processes identified from gene sets were listed into annotation charts by DAVID (**Supplementary Table 9.1-9.13**), however, to provide further confidence as to whether a process has significant impact, annotation cluster analysis was carried out. This analysis groups the terms/processes displayed in the charts

based on a defined percentage of genes that are similar between sets and filters out sets of genes that are not highly enriched for terms/processes. Ideally clusters that are enriched with terms/processes deriving from similar set of genes should be closely related in terms of function, hence further implicating the role of the genes. The terms and cluster filtering approach was set to be more stringent compared to the default set-up. The degree of similarity between terms/processes was set to be at least having 75% similar number of genes overlap and accepting only categories with *p*-value of <0.05. Clusters with enrichment score of at least 2.0 was deemed as the cut-off for acceptance but at least one annotation within the cluster should have an FDR of <0.05.

6.4.1 Analysis of overexpression and KD of *DmHDAC4*

6.4.1.1 Annotation cluster analysis of pairwise comparison: *CS* versus $DmHDAC4^{WT}$

For *CS* versus $DmHDAC4^{WT}$ comparison, the differential gene expression resulting from expression of $DmHDAC4^{WT}$ yielded 9 clusters of enriched terms among which a few clusters contain terms/processes that are suggestive of the genes' role within the cluster (**Table 6.3**). Among the enriched term/process clusters that have a score of >2.0, Annotation Cluster 1, 2 and 4 indicate changes to genes affecting reproduction, biosynthesis of antibiotics and mating and egg laying behaviour respectively. However, these terms/processes do not appear to be relevant in the context of this project. Annotation Cluster 6 suggest a process that enriched for genes involved in glycolysis and gluconeogenesis while genes from Annotation Cluster 9 are implicated in starch and sucrose metabolism and α-1,4-glucosidase, an enzyme that is known to breakdown glycogen to glucose. Therefore, these two clusters suggest that glucose/sugar metabolism may have been impacted. Annotation Cluster 8 implicates the tricarboxylic acid (TCA) cycle which is an important process for generating reduced nicotinamide adenine dinucleotide (NADH) and reduced flavin adenine dinucleotide (FADH2) which are crucial electron donor for electron transfer in the electron transport chain that results in the generation of ATP. In Annotation Cluster 6, glycolysis is a process that converts glucose to pyruvate which is then required by the TCA cycle to generate NADH and FADH2. Hence, these clusters could potentially suggest a strong association between the

expression of *DmHDAC4*^{WT} with glucose metabolism and mitochondrial energy production.

When considering the remaining clusters, Annotation Cluster 3 contained genes enriched for enzymatic activities by aminopeptidase which are ubiquitous enzyme that are involved in amino acid retrieval from proteins which plays many roles in biological process including memory and also diseases which includes diabetes (Mucha, Drag, Dalton, & Kafarski, 2010). Additionally, fatty acid elongation from Annotation Cluster 7, a reverse process of β-oxidation which is the breaking down of fatty acid in the mitochondria to produce acetyl-CoA, NADH and FADH2 further suggests that an increase in HDAC4 impacts cellular energy production (Houten & Wanders, 2010; Kemp et al., 2005).

CS vs DmHDAC4 WT:

Cluster #	Category	Term	Count	%	*p*-value	Fold Enrichment	FDR
Annotation Cluster 1 Enrichment Score: 29.7	GOTERM_BP_DIRECT	Multicellular Organism Reproduction	73	7.315	5.411E-36	5.848	3.052E-33
	GOTERM_CC_DIRECT	Extracellular Space	94	9.419	7.023E-25	3.217	1.208E-22
Annotation Cluster 2 Enrichment Score: 6.94	KEGG_PATHWAY	Carbon Metabolism	22	2.204	2.857E-09	4.600	1.828E-07
	KEGG_PATHWAY	Biosynthesis Of Antibiotics	23	2.305	4.588E-06	2.939	9.788E-05
Annotation Cluster 3 Enrichment Score: 5.57	GOTERM_MF_DIRECT	Aminopeptidase Activity	11	1.102	8.767E-07	7.445	3.025E-04
	GOTERM_MF_DIRECT	Metalloexopeptidase Activity	8	0.802	2.111E-06	1.122	3.641E-04
	GOTERM_MF_DIRECT	Manganese Ion Binding	8	0.802	1.046E-05	9.237	1.203E-03
Annotation Cluster 4 Enrichment Score: 4.53	GOTERM_BP_DIRECT	Post-Mating Behaviour	7	0.701	3.179E-07	1.809	4.984E-05
	GOTERM_BP_DIRECT	Oviposition	5	0.501	2.711E-03	7.950	1.136E-01
Annotation Cluster 5 Enrichment Score: 3.72	GOTERM_BP_DIRECT	Chitin Metabolic Process	16	1.603	7.475E-05	3.340	7.027E-03
	GOTERM_MF_DIRECT	Chitin Binding	17	1.703	4.760E-04	2.713	2.053E-02
Annotation Cluster 6 Enrichment Score: 3.51	KEGG_PATHWAY	Glycolysis / Gluconeogenesis	11	1.102	6.142E-05	4.774	6.615E-04
	GOTERM_BP_DIRECT	Glycolytic Process	7	0.701	1.530E-03	5.359	8.631E-02
Annotation Cluster 7 Enrichment Score: 3.10	GOTERM_MF_DIRECT	3-Oxo-Arachidoyl-CoA Synthase Activity	7	0.701	3.519E-04	6.870	1.735E-02
	GOTERM_MF_DIRECT	3-Oxo-Cerotoyl-CoA Synthase Activity	7	0.701	3.519E-04	6.870	1.735E-02
	GOTERM_MF_DIRECT	3-Oxo-Lignoceronyl-CoA Synthase Activity	7	0.701	3.519E-04	6.870	1.735E-02
	GOTERM_MF_DIRECT	Fatty Acid Elongase Activity	6	0.601	2.135E-03	6.198	7.174E-02
	GOTERM_BP_DIRECT	Fatty Acid Elongation	6	0.601	3.423E-03	5.637	1.136E-01
Annotation Cluster 8 Enrichment Score: 3.04	KEGG_PATHWAY	Citrate Cycle (TCA Cycle)	10	1.002	6.202E-05	5.349	6.615E-04
	GOTERM_BP_DIRECT	Tricarboxylic Acid Cycle	7	0.701	1.314E-02	3.529	2.851E-01
Annotation Cluster 9 Enrichment Score: 2.54	KEGG_PATHWAY	Starch And Sucrose Metabolism	7	0.701	1.717E-03	5.194	1.221E-02
	GOTERM_MF_DIRECT	Maltose Alpha-Glucosidase Activity	5	0.501	3.266E-03	7.549	8.668E-02
	GOTERM_MF_DIRECT	Alpha-1,4-Glucosidase Activity	5	0.501	4.391E-03	7.010	1.082E-01

Table 6.3: DAVID annotation cluster analysis of pairwise comparison: *CS* versus *DmHDAC4*^{WT}

The annotated clusters that have an enrichment score of ≥2.0 and at least one annotated term with FDR≤0.05 (5.0E-02) are shown. Genes were annotated using databases from GO Term Biological Processes (GOTERM_BP_DIRECT), Cellular Components (GOTERM_CC_DIRECT), Molecular Function (GOTERM_MF_DIRECT) and KEGG pathway database (KEGG_PATHWAY). Count column indicates the number of genes from the list of significantly differentially expressed genes that are implicated in the corresponding terms. Percentage column refers to the percentage of genes from the list that are annotated with the term. *P*-value column is derived from a Modified Fisher's Exact test of the number genes from the list that are involved in a term against the database list. Fold enrichment column indicates the number of fold that the term is expected to happen as opposed to being due to random occurrence. FDR column is the adjusted *p*-value.

6.4.1.2 Annotation cluster analysis of pairwise comparison: *CS* versus *DmHDAC4* KD

The first three clusters that were identified to be enriched in KD of *DmHDAC4* (**Table 6.4**) suggest changes in expression of genes involved in immune responses such as humoral immune response, defense response to gram-positive bacterium and innate immune response, indicating DmHDAC4 is required in *Drosophila* innate immunity. Annotation Cluster 4 suggests changes in expression of genes involved in environmental stress response along with processing of protein and pre-mRNA (spliceosome). As both *CS* and *DmHDAC4* KD flies underwent the same heat shock treatment, it is interesting to discover that KD of *DmHDAC4* elicits a differential gene expression cluster that includes response to stressors such as heat and hypoxia, and splicing and endoplasmic reticulum protein processing was also enriched in this cluster. These findings may suggest that DmHDAC4 is required for regulation of thermotolerance genes that could result in pre or posttranslational processing.

CS vs DmHDAC4 KD:

Cluster #	Category	Term	Count	%	*p*-value	Fold Enrichment	FDR
Annotation Cluster 1 Enrichment Score: 7.72	GOTERM_BP_DIRECT	Humoral Immune Response	7	6.931	6.578E-09	4.517	4.034E-07
	GOTERM_BP_DIRECT	Defense Response To Gram-Positive Bacterium	8	7.921	5.645E-08	2.212	1.400E-06
Annotation Cluster 2 Enrichment Score: 7.20	GOTERM_BP_DIRECT	Antibacterial Humoral Response	8	7.921	7.045E-11	5.387	8.735E-09
	GOTERM_BP_DIRECT	Response To Bacterium	8	7.921	1.370E-08	2.693	4.247E-07
	GOTERM_BP_DIRECT	Innate Immune Response	9	8.911	2.837E-07	1.340	5.863E-06
	GOTERM_BP_DIRECT	Defense Response	5	4.950	6.047E-05	2.278	6.930E-04
Annotation Cluster 3 Enrichment Score: 5.81	GOTERM_BP_DIRECT	Antibacterial Humoral Response	8	7.921	7.045E-11	5.387	8.735E-09
	GOTERM_BP_DIRECT	Defense Response To Gram-Negative Bacterium	7	6.931	6.147E-05	1.004	6.930E-04
	GOTERM_BP_DIRECT	Defense Response To Bacterium	5	4.950	8.533E-04	1.156	8.140E-03
Annotation Cluster 4 Enrichment Score: 4.36	GOTERM_BP_DIRECT	Response To Heat	9	8.911	9.759E-09	2.050	4.034E-07
	GOTERM_BP_DIRECT	Response To Hypoxia	6	5.941	2.181E-06	2.733	3.863E-05
	GOTERM_BP_DIRECT	Heat Shock-Mediated Polytene Chromosome Puffing	4	3.960	8.491E-06	8.850	1.316E-04
	GOTERM_BP_DIRECT	Response To Unfolded Protein	4	3.960	2.019E-05	6.883	2.782E-04
	KEGG_PATHWAY	Protein Processing In Endoplasmic Reticulum	6	5.941	2.736E-04	8.689	6.293E-03
	GOTERM_CC_DIRECT	Microtubule Associated Complex	8	7.921	1.987E-03	4.383	2.848E-02
	KEGG_PATHWAY	Endocytosis	5	4.950	2.349E-03	7.732	2.227E-02
	KEGG_PATHWAY	Spliceosome	5	4.950	2.905E-03	7.299	2.227E-02

Table 6.4: DAVID annotation cluster analysis of pairwise comparison: *CS* versus *DmHDAC4* KD

The annotated clusters that have an enrichment score of ≥2.0 and at least one annotated term with FDR≤0.05 (5.0E-02) are shown. Genes were annotated using databases from GO Term Biological Processes (GOTERM_BP_DIRECT), Cellular Components (GOTERM_CC_DIRECT) and KEGG pathway database (KEGG_PATHWAY). Count column indicates the number of genes from the list of significantly differentially expressed genes that are implicated in the corresponding terms. Percentage column refers to the percentage of genes from the list that are annotated with the term. *P*-value column is derived from a Modified Fisher's Exact test of the number genes from the list that are involved in a term against the database list. Fold enrichment column indicates the number of fold that the term is expected to happen as opposed to being due to random occurrence. FDR column is the adjusted *p*-value.

6.4.2 Analysis of overexpression of subcellular mutant variants

6.4.2.1 Annotation cluster analysis of pairwise comparison: *CS* versus *3A* or *dNLS*

Curiously, the cluster analysis of *CS* versus *3A* is only enriched for genes involved in the structural makeup of chitin and chitin development which is surprising as all RNA samples were obtained from fully developed adult heads (**Table 6.5**). This could perhaps be an indication of unexplored process of genes in post-developmental fly heads that are also involved in chitin processes. It should also be noted that Annotation Cluster 5 in *CS* versus $DmHDAC4^{WT}$ (**Table 6.3**) is enriched for genes involved in chitin binding and metabolism. As expression of *3A* was shown in previous chapters to result in a more severe developmental phenotype and also impairs memory formation in the courtship suppression assay (Main et al., 2021), genes listed in these chitin-based terms/processes were further assessed for potential candidates that could be involved in brain function. Among the list of genes annotated, Annotation Cluster 5 of *CS* versus $DmHDAC4^{WT}$ revealed a candidate gene, *Tequila* (**Supplementary Table 9.14**), a neurotrypsin ortholog which has been reported to regulate LTM formation in *Drosophila* (Chen et al., 2012; Didelot et al., 2006). The remaining annotated genes in the cluster did not suggest any relevance to any neuronal or related cellular function. Although cluster reporting of *CS* versus *3A* did not reveal *Tequila* in the gene list (**Supplementary Table 9.14**), heatmap analysis revealed *Tequila* to be among the top 50 significantly differentially expressed genes (**Supplementary Figure 9.10**). The scenario of this analysis trend suggests that while cluster analysis provides a mean to assess for process or pathways implicated due to the differential gene expression, the variances that exist between samples could potentially lead to lower cluster enrichment which could exclude key results or information. Therefore, while *CS* versus *3A* comparison did not reveal a similar chitin-based cluster as observed for $DmHDAC4^{WT}$, individual gene identification did reveal a degree of similarity. Despite the identification of a gene that relates to memory formation, it is still unclear how *3A* could have a more severe phenotype compared to $DmHDAC4^{WT}$. Perhaps, the formation DmHDAC4 into puncta aggregates could impede other nuclear process or even its own functions in the nucleus resulting in low transcriptional changes. However, it is still unknown whether these aggregates are neurotoxic, therefore, these aggregates in combination with *Tequila* function could be the source of phenotype exacerbation in *CS* versus *3A*.

CS vs 3A:

Cluster #	Category	Term	Count	%	*p*-value	Fold Enrichment	FDR
Annotation Cluster 1 Enrichment Score: 2.81	GOTERM_MF_DIRECT	Structural Constituent Of Chitin-Based Larval Cuticle	7	4.575	5.186E-04	6.812	5.756E-02
	GOTERM_CC_DIRECT	Extracellular Matrix	7	4.575	1.120E-03	5.884	2.912E-02
	GOTERM_BP_DIRECT	Chitin-Based Cuticle Development	7	4.575	2.376E-03	5.096	4.943E-01
	GOTERM_MF_DIRECT	Structural Constituent Of Cuticle	6	3.922	4.339E-03	5.526	1.606E-01

Table 6.5: DAVID annotation cluster analysis of pairwise comparison: *CS* versus *3A*
The annotated cluster that has an enrichment score of ≥2.0 and at least one annotated term with FDR≤0.05 (5.0E-02) are shown. Genes were annotated using databases from GO Term Biological Processes (GOTERM_BP_DIRECT), Cellular Components (GOTERM_CC_DIRECT) and Molecular Function (GOTERM_MF_DIRECT). Count column indicates the number of genes from the list of significantly differentially expressed genes that are implicated in the corresponding terms. Percentage column refers to the percentage of genes from the list that are annotated with the term. *P*-value column is derived from a Modified Fisher's Exact test of the number genes from the list that are involved in a term against the database list. Fold enrichment column indicates the number of fold that the term is expected to happen as opposed to being due to random occurrence. FDR column is the adjusted *p*-value.

For the cytoplasmic mutant, dNLS, although the annotation chart analysis revealed a few significant GO and KEGG terms (**Supplementary Table 9.3**), there were no cluster enrichment detected. This is consistent with its restriction to the cytoplasm, thus having less impact on transcriptional regulation and any other potential nuclear activities.

6.4.2.2 Annotation cluster analysis of pairwise comparison: *CS* versus *dMEF2*

Although dMEF2 is predominantly cytoplasmic like dNLS, comparison of *CS* versus *dMEF2* resulted in clusters which appear to be similar in terms/processes as those resulting from KD of *DmHDAC4*. Clusters that implicate the genes in stress response, protein processing and immune response were also identified (**Table 6.6**).

CS vs dMEF2:

Cluster #	Category	Term	Count	%	*p*-value	Fold Enrichment	FDR
Annotation Cluster 1 Enrichment Score: 3.80	GOTERM_BP_DIRECT	Response To Heat	9	5.921	2.093E-07	13.994	2.636E-05
	GOTERM_BP_DIRECT	Heat Shock-Mediated Polytene Chromosome Puffing	5	3.289	2.487E-07	75.522	2.636E-05
	GOTERM_BP_DIRECT	Response To Hypoxia	6	3.947	1.467E-05	18.658	7.773E-04
	GOTERM_BP_DIRECT	Response To Unfolded Protein	4	2.632	6.436E-05	46.991	2.002E-03
	KEGG_PATHWAY	Protein Processing In Endoplasmic Reticulum	6	3.947	2.143E-03	5.924	6.308E-02
	KEGG_PATHWAY	Endocytosis	5	3.289	1.112E-02	5.272	8.133E-02
	KEGG_PATHWAY	Spliceosome	5	3.289	1.355E-02	4.976	8.133E-02
	GOTERM_CC_DIRECT	Microtubule Associated Complex	8	5.263	2.478E-02	2.756	6.196E-01
Annotation Cluster 2 Enrichment Score: 3.20	GOTERM_BP_DIRECT	Antibacterial Humoral Response	5	3.289	5.607E-05	22.985	2.002E-03
	GOTERM_BP_DIRECT	Response To Bacterium	6	3.947	6.609E-05	13.791	2.002E-03
	GOTERM_BP_DIRECT	Innate Immune Response	7	4.605	4.218E-04	7.116	1.118E-02
	GOTERM_BP_DIRECT	Defense Response To Bacterium	5	3.289	3.541E-03	7.890	8.201E-02
	GOTERM_BP_DIRECT	Defense Response To Gram-Negative Bacterium	5	3.289	1.852E-02	4.895	3.021E-01

Table 6.6: DAVID annotation cluster analysis of pairwise comparison: *CS* versus *dMEF2*

The annotated clusters that have an enrichment score of ≥2.0 and at least one annotated term with FDR≤0.05 (5.0E-02) are shown. Genes were annotated using databases from GO Term Biological Processes (GOTERM_BP_DIRECT), Cellular Components (GOTERM_CC_DIRECT) and Molecular Function (GOTERM_MF_DIRECT). Count column indicates the number of genes from the list of significantly differentially expressed genes that are implicated in the corresponding terms. Percentage column refers to the percentage of genes from the list that are annotated with the term. *P*-value column is derived from a Modified Fisher's Exact test of the number genes from the list that are involved in a term against the database list. Fold enrichment column indicates the number of fold that the term is expected to happen as opposed to being due to random occurrence. FDR column is the adjusted *p*-value.

6.4.2.3 Annotation cluster analysis of pairwise comparison: *DmHDAC4^{WT}* versus *3A*, *dNLS* or *dMEF2*

As expression of the subcellular-restricted variants, *3A*, *dNLS* and *dMEF2* resulted in very few differentially regulated genes when compared to *DmHDAC4^{WT}*, this suggests these mutations might each impair the full transcriptional regulation function of *DmHDAC4^{WT}*. Therefore, each of the three variants were directly compared to *DmHDAC4^{WT}* to uncover the clusters that are regulated by *DmHDAC4^{WT}*.

Most of the clusters identified were the same as those observed in the *CS* versus *DmHDAC4^{WT}* comparison (**Table 6.3**), however there were some differences for *DmHDAC4^{WT}* versus *3A* and *DmHDAC4^{WT}* versus *dMEF2*. For *DmHDAC4* versus *3A* (**Table 6.7**), the clusters that involved chitin metabolic process, fatty acid elongation and starch and sucrose metabolism were not present, however there was enrichment of a cluster comprising of malate metabolic process and pyruvate metabolism (Annotation Cluster 6) which are part of the extended processes that feeds into the TCA cycle. This suggests that 3A mutation may affect energy production perhaps through influencing pathways relating to pyruvate metabolism.

DmHDAC4 WT vs 3A:

Cluster #	Category	Term	Count	%	*p*-value	Fold Enrichment	FDR
Annotation Cluster 1 Enrichment Score: 27.7	GOTERM_BP_DIRECT	Multicellular Organism Reproduction	76	7.329	2.825E-38	5.976	1.684E-35
	GOTERM_CC_DIRECT	Extracellular Space	85	8.197	1.724E-18	2.803	3.120E-16
Annotation Cluster 2 Enrichment Score: 8.80	KEGG_PATHWAY	Carbon Metabolism	25	2.411	8.468E-12	5.227	4.911E-10
	KEGG_PATHWAY	Biosynthesis Of Antibiotics	25	2.411	2.986E-07	3.194	6.433E-06
Annotation Cluster 3 Enrichment Score: 5.54	GOTERM_MF_DIRECT	Aminopeptidase Activity	11	1.061	9.473E-07	7.383	3.334E-04
	GOTERM_MF_DIRECT	Metalloexopeptidase Activity	8	0.771	2.234E-06	11.122	3.932E-04
	GOTERM_MF_DIRECT	Manganese Ion Binding	8	0.771	1.106E-05	9.159	1.298E-03
Annotation Cluster 4 Enrichment Score: 5.02	GOTERM_BP_DIRECT	Post-Mating Behavior	7	0.675	3.552E-07	17.752	7.056E-05
	GOTERM_BP_DIRECT	Oviposition	6	0.579	2.619E-04	9.364	1.561E-02
Annotation Cluster 5 Enrichment Score: 4.92	KEGG_PATHWAY	Citrate Cycle (TCA Cycle)	12	1.157	1.073E-06	6.419	1.557E-05
	GOTERM_BP_DIRECT	Tricarboxylic Acid Cycle	10	0.964	1.347E-04	4.948	1.265E-02
Annotation Cluster 6 Enrichment Score: 3.43	GOTERM_BP_DIRECT	Malate Metabolic Process	6	0.579	2.619E-04	9.364	1.561E-02
	KEGG_PATHWAY	Pyruvate Metabolism	9	0.868	5.311E-04	4.600	5.134E-03
Annotation Cluster 7 Enrichment Score: 2.78	KEGG_PATHWAY	Glycolysis / Gluconeogenesis	9	0.868	1.635E-03	3.906	1.355E-02
	GOTERM_BP_DIRECT	Glycolytic Process	7	0.675	1.684E-03	5.260	6.273E-02
Annotation Cluster 8 Enrichment Score: 2.66	GOTERM_BP_DIRECT	Negative Regulation Of Female Receptivity, Post-Mating	7	0.675	7.235E-05	8.876	8.624E-03
	GOTERM_MF_DIRECT	Hormone Activity	5	0.482	6.515E-02	3.244	6.949E-01

Table 6.7: DAVID annotation cluster analysis of pairwise comparison: *DmHDAC4^{WT}* versus *3A*

The annotated clusters that have an enrichment score of ≥2.0 and at least one annotated term with FDR≤0.05 (5.0E-02) are shown. Genes were annotated using databases from GO Term Biological Processes (GOTERM_BP_DIRECT), Cellular Components (GOTERM_CC_DIRECT) and Molecular Function (GOTERM_MF_DIRECT). Count column indicates the number of genes from the list of significantly differentially expressed genes that are implicated in the corresponding terms. Percentage column refers to the percentage of genes from the list that are annotated with the term. *P*-value column is derived from a Modified Fisher's Exact test of the number genes from the list that are involved in a term against the database list. Fold enrichment column indicates the number of fold that the term is expected to happen as opposed to being due to random occurrence. FDR column is the adjusted *p*-value.

DmHDAC4^{WT} versus *dMEF2* (**Table 6.8**) lacks the cluster that was involved in fatty acid elongation but has a cluster involved in lipase activity (Annotation Cluster 10). Fatty acid elongation could suggest an increase in lipid formation which could potentially be offset by lipase activity. As excess lipid formation that results in increased formation of lipid droplet organelles by neurons with mitochondrial defect has been known to contribute towards neurodegeneration (Liu et al., 2015), perhaps this could be applied to neurodevelopment where there is a potential increase in lipid droplet formation by fatty acid elongation which could contribute to MB development impairment caused by *DmHDAC4^{WT}* whereas *dMEF2* is able to rescue phenotype due to the presence of the lipase activity, which as the name implies, breaking down of lipid.

DmHDAC4 WT vs dMEF2:

Cluster #	Category	Term	Count	%	*p*-value	Fold Enrichment	FDR
Annotation Cluster 1 Enrichment Score: 29.7	GOTERM_BP_DIRECT	Multicellular Organism Reproduction	76	7.488	5.709E-39	6.112	2.706E-36
	GOTERM_CC_DIRECT	Extracellular Space	90	8.867	7.992E-22	3.020	1.255E-19
Annotation Cluster 2 Enrichment Score: 8.27	KEGG_PATHWAY	Carbon Metabolism	25	2.463	3.142E-11	4.937	1.885E-09
	KEGG_PATHWAY	Biosynthesis Of Antibiotics	25	2.463	9.216E-07	3.017	1.843E-05
Annotation Cluster 3 Enrichment Score: 5.58	GOTERM_MF_DIRECT	Aminopeptidase Activity	11	1.084	8.598E-07	7.461	2.872E-04
	GOTERM_MF_DIRECT	Metalloexopeptidase Activity	8	0.788	2.081E-06	11.240	3.475E-04
	GOTERM_MF_DIRECT	Manganese Ion Binding	8	0.788	1.032E-05	9.256	1.149E-03
Annotation Cluster 4 Enrichment Score: 4.54	GOTERM_BP_DIRECT	Post-Mating Behaviour	7	0.690	3.109E-07	18.154	4.912E-05
	GOTERM_BP_DIRECT	Oviposition	5	0.493	2.674E-03	7.980	6.525E-02
Annotation Cluster 5 Enrichment Score: 4.02	KEGG_PATHWAY	Citrate Cycle (TCA Cycle)	11	1.084	1.464E-05	5.557	2.197E-04
	GOTERM_BP_DIRECT	Tricarboxylic Acid Cycle	9	0.887	6.369E-04	4.554	2.744E-02
Annotation Cluster 6 Enrichment Score: 3.47	GOTERM_BP_DIRECT	Glycolytic Process	8	0.788	2.193E-04	6.147	1.040E-02
	KEGG_PATHWAY	Glycolysis / Gluconeogenesis	10	0.985	5.214E-04	4.099	4.469E-03
Annotation Cluster 7 Enrichment Score: 3.46	GOTERM_BP_DIRECT	Heat Shock-Mediated Polytene Chromosome Puffing	6	0.591	4.901E-06	17.783	4.646E-04
	GOTERM_BP_DIRECT	Response To Unfolded Protein	6	0.591	2.712E-05	13.831	2.143E-03
	GOTERM_BP_DIRECT	Response To Heat	10	0.985	5.050E-03	3.051	1.041E-01
	GOTERM_BP_DIRECT	Response To Hypoxia	6	0.591	2.218E-02	3.661	2.695E-01
Annotation Cluster 8 Enrichment Score: 2.86	KEGG_PATHWAY	Starch And Sucrose Metabolism	8	0.788	3.683E-04	5.606	3.683E-03
	KEGG_PATHWAY	Galactose Metabolism	8	0.788	6.718E-04	5.111	5.039E-03
	GOTERM_MF_DIRECT	Maltose Alpha-Glucosidase Activity	5	0.493	3.241E-03	7.565	1.203E-01
	GOTERM_MF_DIRECT	Alpha-1,4-Glucosidase Activity	5	0.493	4.358E-03	7.025	1.323E-01
Annotation Cluster 9 Enrichment Score: 2.71	GOTERM_MF_DIRECT	Chitin Binding	16	1.576	1.360E-03	2.559	9.086E-02
	GOTERM_BP_DIRECT	Chitin Metabolic Process	13	1.281	2.753E-03	2.724	6.525E-02
Annotation Cluster 10 Enrichment Score: 2.55	GOTERM_MF_DIRECT	Lipase Activity	8	0.788	6.077E-04	5.245	5.074E-02
	GOTERM_BP_DIRECT	Lipid Catabolic Process	8	0.788	1.295E-02	3.132	1.711E-01

Table 6.8: DAVID annotation cluster analysis of pairwise comparison: *DmHDAC4^{WT}* versus *dMEF2*

The annotated clusters that have an enrichment score of ≥2.0 and at least one annotated term with FDR≤0.05 (5.0E-02) are shown. Genes were annotated using databases from GO Term Biological Processes (GOTERM_BP_DIRECT), Cellular Components (GOTERM_CC_DIRECT) and Molecular Function (GOTERM_MF_DIRECT). Count column indicates the number of genes from the list of significantly differentially expressed genes that are implicated in the corresponding terms. Percentage column refers to the percentage of genes from the list that are annotated with the term. *P*-value column is derived from a Modified Fisher's Exact test of the number genes from the list that are involved in a term against the database list. Fold enrichment column indicates the number of fold that the term is expected to happen as opposed to being due to random occurrence. FDR column is the adjusted *p*-value.

6.4.2.4 Annotation cluster analysis of pairwise comparison: dMEF2 versus 3A

In the RNA-Seq analysis of *Drosophila* brain conducted by Main et al. (2021), the cytoplasmic-restricted hHDAC4 mutant, *L175A* (which carries a mutation in the MEF2-binding site) was compared to the human *3A* variant, as a comparison between nuclear and cytoplasmic pools of HDAC4 to ideally identify transcriptional changes resulting from nuclear accumulation of HDAC4. This analysis revealed differential regulation of a small set of cytochrome P450 genes that are involved in processes including of monooxygenase activity and oxidoreductase activity. Such activities have been known for their roles in substrate oxidation through electron transfer in the mitochondria which could implicate the formation of reactive oxygen species (ROS) that are harmful to cells (Veith & Moorthy, 2018)

dMEF2 vs 3A:

Cluster #	Category	Term	Count	%	*p*-value	Fold Enrichment	FDR
Annotation Cluster 1 Enrichment Score: 2.92	GOTERM_MF_DIRECT	Iron Ion Binding	5	16.667	1.595E-04	16.508	4.465E-03
	GOTERM_CC_DIRECT	Organelle Membrane	4	13.333	5.654E-04	23.075	6.785E-03
	GOTERM_MF_DIRECT	Monooxygenase Activity	4	13.333	6.058E-04	22.211	6.237E-03
	GOTERM_MF_DIRECT	Oxidoreductase Activity, Acting On Paired Donors, With Incorporation Or Reduction Of Molecular Oxygen	4	13.333	6.682E-04	21.478	6.237E-03
	GOTERM_MF_DIRECT	Heme Binding	4	13.333	1.961E-03	14.807	1.373E-02
	GOTERM_BP_DIRECT	Oxidation-Reduction Process	5	16.667	4.812E-03	6.672	1.445E-01
	GOTERM_CC_DIRECT	Endoplasmic Reticulum Membrane	4	13.333	1.048E-02	8.248	6.289E-02

Table 6.9: DAVID annotation cluster analysis of pairwise comparison: *dMEF2* versus *3A*

The annotated cluster that has an enrichment score of ≥2.0 and at least one annotated term with FDR≤0.05 (5.0E-02) are shown. Genes were annotated using databases from GO Term Biological Processes (GOTERM_BP_DIRECT), Cellular Components (GOTERM_CC_DIRECT) and Molecular Function (GOTERM_MF_DIRECT). Count column indicates the number of genes from the list of significantly differentially expressed genes that are implicated in the corresponding terms. Percentage column refers to the percentage of genes from the list that are annotated with the term. *P*-value column is derived from a Modified Fisher's Exact test of the number genes from the list that are involved in a term against the database list. Fold enrichment column indicates the number of fold that the term is expected to happen as opposed to being due to random occurrence. FDR column is the adjusted *p*-value.

Interestingly, the dMEF2 and 3A comparison from this study displayed a single cluster which also includes monooxygenase and oxidoreductase activities and oxidation-reduction process which confirms the similarity between human and *Drosophila* variants (**Table 6.9**). This could potentially emphasize a difference in impact to mitochondrial energy production and ROS production between nuclear and cytoplasmic DmHDAC4.

6.4.3 Analysis of overexpression of *dANK* and *Y1142H*

6.4.3.1 Annotation cluster analysis of pairwise comparison: *CS* versus *dANK* and *DmHDAC4^{WT}* versus *dANK*

Expression of *dANK* resulted in enrichment of gene cluster relating to chitin cuticle development (Annotation Cluster 4) (**Table 6.10**). *Tequila* was also listed in the heatmap analysis of top 50 most significantly differentially expressed genes (not shown).

CS vs dANK:

Cluster #	Category	Term	Count	%	*p*-value	Fold Enrichment	FDR
Annotation Cluster 1 Enrichment Score: 5.38	GOTERM_BP_DIRECT	Response To Heat	11	5.446	7.102E-09	13.374	1.761E-06
	GOTERM_CC_DIRECT	Microtubule Associated Complex	11	5.446	2.459E-03	3.142	5.410E-02
Annotation Cluster 2 Enrichment Score: 4.02	GOTERM_BP_DIRECT	Heat Shock-Mediated Polytene Chromosome Puffing	5	2.475	6.754E-07	59.055	5.583E-05
	GOTERM_BP_DIRECT	Response To Unfolded Protein	5	2.475	2.386E-06	45.931	1.352E-04
	GOTERM_BP_DIRECT	Response To Hypoxia	7	3.465	2.725E-06	17.022	1.352E-04
	KEGG_PATHWAY	Protein Processing In Endoplasmic Reticulum	7	3.465	2.016E-03	4.905	7.460E-02
	KEGG_PATHWAY	Endocytosis	6	2.970	8.203E-03	4.489	9.377E-02
	KEGG_PATHWAY	Spliceosome	6	2.970	1.042E-02	4.238	9.377E-02
Annotation Cluster 3 Enrichment Score: 3.12	GOTERM_MF_DIRECT	Odorant Binding	8	3.960	6.927E-04	5.348	4.572E-02
	GOTERM_BP_DIRECT	Sensory Perception Of Chemical Stimulus	7	3.465	8.186E-04	6.291	3.384E-02
Annotation Cluster 4 Enrichment Score: 2.63	GOTERM_MF_DIRECT	Structural Constituent Of Cuticle	8	3.960	6.927E-04	5.348	4.572E-02
	GOTERM_CC_DIRECT	Extracellular Matrix	8	3.960	1.272E-03	4.828	4.199E-02
	GOTERM_MF_DIRECT	Structural Constituent Of Chitin-Based Larval Cuticle	7	3.465	2.777E-03	4.944	1.222E-01
	GOTERM_BP_DIRECT	Chitin-Based Cuticle Development	7	3.465	1.223E-02	3.640	2.528E-01

Table 6.10: DAVID annotation cluster analysis of pairwise comparison: *CS* versus *dANK*

The annotated clusters that have an enrichment score of ≥2.0 and at least one annotated term with FDR≤0.05 (5.0E-02) are shown. Genes were annotated using databases from GO Term Biological Processes (GOTERM_BP_DIRECT), Cellular Components (GOTERM_CC_DIRECT) and Molecular Function (GOTERM_MF_DIRECT). Count column indicates the number of genes from the list of significantly differentially expressed genes that are implicated in the corresponding terms. Percentage column refers to the percentage of genes from the list that are annotated with the term. *P*-value column is derived from a Modified Fisher's Exact test of the number genes from the list that are involved in a term against the database list. Fold enrichment column indicates the number of fold that the term is expected to happen as opposed to being due to random occurrence. FDR column is the adjusted *p*-value.

Comparison between *DmHDAC4*^{WT} and *dANK* (**Table 6.11**) included most of the clusters shown in *CS* versus *DmHDAC4*^{WT} (**Table 6.3**), however, there were additional clusters such as Annotation Cluster 8 that includes malate metabolic process and pyruvate metabolism which was also observed in *DmHDAC4*^{WT} versus *3A* (**Table 6.7**). Since *dANK* was also shown to be required in MB development similar to *3A*, this cluster could perhaps provide an insight into the pathways through which *3A* and *dANK* cause MB developmental impairment. It should be noted that although there are other clusters (Annotation Cluster 6, 9 and 11) that could also contribute to the dANK-induced developmental impairments, the main focus was on processes that relates to mitochondrial energy production as they were the main processes found in *CS* versus *DmHDAC4*^{WT} that have the most relevance to neuronal function.

DmHDAC4 WT vs dANK:

Cluster #	Category	Term	Count	%	*p*-value	Fold Enrichment	FDR
Annotation Cluster 1 Enrichment Score: 32.2	GOTERM_BP_DIRECT	Multicellular Organism Reproduction	87	6.861	1.866E-41	5.493	1.198E-38
	GOTERM_CC_DIRECT	Extracellular Space	108	8.517	2.215E-24	2.864	4.630E-22
Annotation Cluster 2 Enrichment Score: 7.84	KEGG_PATHWAY	Carbon Metabolism	27	2.129	6.446E-11	4.391	4.512E-09
	KEGG_PATHWAY	Biosynthesis Of Antibiotics	27	2.129	3.180E-06	2.683	5.565E-05
Annotation Cluster 3 Enrichment Score: 5.13	GOTERM_MF_DIRECT	Manganese Ion Binding	9	0.710	4.461E-06	8.111	1.481E-03
	GOTERM_MF_DIRECT	Aminopeptidase Activity	11	0.868	8.273E-06	5.811	1.481E-03
	GOTERM_MF_DIRECT	Metalloexopeptidase Activity	8	0.631	1.105E-05	8.754	1.481E-03
Annotation Cluster 4 Enrichment Score: 4.79	KEGG_PATHWAY	Citrate Cycle (TCA Cycle)	13	1.025	1.920E-06	5.408	5.565E-05
	GOTERM_BP_DIRECT	Tricarboxylic Acid Cycle	11	0.868	1.383E-04	4.371	9.867E-03
Annotation Cluster 5 Enrichment Score: 4.51	GOTERM_BP_DIRECT	Post-Mating Behavior	7	0.552	1.307E-06	14.254	2.097E-04
	GOTERM_BP_DIRECT	Oviposition	6	0.473	7.257E-04	7.519	3.106E-02
Annotation Cluster 6 Enrichment Score: 3.55	GOTERM_BP_DIRECT	Heat Shock-Mediated Polytene Chromosome Puffing	6	0.473	1.615E-05	13.963	2.073E-03
	GOTERM_BP_DIRECT	Response To Unfolded Protein	6	0.473	8.734E-05	10.860	7.009E-03
	GOTERM_BP_DIRECT	Response To Hypoxia	7	0.552	1.600E-02	3.354	2.446E-01
Annotation Cluster 7 Enrichment Score: 3.23	GOTERM_MF_DIRECT	Chitin Binding	20	1.577	3.570E-04	2.491	3.588E-02
	GOTERM_BP_DIRECT	Chitin Metabolic Process	16	1.262	9.682E-04	2.633	3.656E-02
Annotation Cluster 8 Enrichment Score: 3.17	KEGG_PATHWAY	Pyruvate Metabolism	10	0.789	6.266E-04	3.975	6.266E-03
	GOTERM_BP_DIRECT	Malate Metabolic Process	6	0.473	7.257E-04	7.519	3.106E-02
Annotation Cluster 9 Enrichment Score: 2.88	GOTERM_MF_DIRECT	Fatty-Acyl-CoA Reductase (Alcohol-Forming) Activity	7	0.552	4.969E-04	6.308	3.995E-02
	GOTERM_BP_DIRECT	Long-Chain Fatty-Acyl-CoA Metabolic Process	6	0.473	2.111E-03	6.109	5.894E-02
	GOTERM_BP_DIRECT	Wax Biosynthetic Process	6	0.473	2.111E-03	6.109	5.894E-02
Annotation Cluster 10 Enrichment Score: 2.85	GOTERM_BP_DIRECT	Glycolytic Process	8	0.631	9.498E-04	4.827	3.656E-02
	KEGG_PATHWAY	Glycolysis / Gluconeogenesis	10	0.789	2.138E-03	3.375	1.667E-02
Annotation Cluster 11 Enrichment Score: 2.29	GOTERM_CC_DIRECT	Eukaryotic Translation Initiation Factor 4F Complex	6	0.473	8.919E-04	7.185	3.728E-02
	GOTERM_MF_DIRECT	RNA Cap Binding	5	0.394	2.732E-03	7.660	1.569E-01
	GOTERM_MF_DIRECT	Eukaryotic Initiation Factor 4G Binding	4	0.315	1.204E-02	7.660	2.548E-01
	GOTERM_MF_DIRECT	RNA 7-Methylguanosine Cap Binding	4	0.315	2.340E-02	6.128	3.244E-01
Annotation Cluster 12 Enrichment Score: 2.24	KEGG_PATHWAY	Galactose Metabolism	8	0.631	2.143E-03	4.209	1.667E-02
	KEGG_PATHWAY	Starch And Sucrose Metabolism	7	0.552	6.151E-03	4.039	4.306E-02
	GOTERM_MF_DIRECT	Maltose Alpha-Glucosidase Activity	5	0.394	7.949E-03	5.892	2.394E-01
	GOTERM_MF_DIRECT	Alpha-1,4-Glucosidase Activity	5	0.394	1.056E-02	5.471	2.548E-01

Table 6.11: DAVID annotation cluster analysis of pairwise comparison: *DmHDAC4^{WT}* versus *dANK*
The annotated clusters that have an enrichment score of ≥2.0 and at least one annotated term with FDR≤0.05 (5.0E-02) are shown. Genes were annotated using databases from GO Term Biological Processes (GOTERM_BP_DIRECT), Cellular Components (GOTERM_CC_DIRECT) and Molecular Function (GOTERM_MF_DIRECT). Count column indicates the number of genes from the list of significantly differentially expressed genes that are implicated in the corresponding terms. Percentage column refers to the percentage of genes from the list that are annotated with the term. *P*-value column is derived from a Modified Fisher's Exact test of the number genes from the list that are involved in a term against the database list. Fold enrichment column indicates the number of fold that the term is expected to happen as opposed to being due to random occurrence. FDR column is the adjusted *p*-value.

6.4.3.3 Annotation cluster analysis of pairwise comparison: *CS* versus *Y1142H* and *DmHDAC4^{WT}* versus *Y1142H*

Expression of *Y1142H* resulted in enrichment of genes that are also involved in chitin cuticle development (*Tequila* also present in top 50 genes heatmap analysis) (**Table 6.12**). When *Y1142H* was compared to *DmHDAC4^{WT}* (**Table 6.13**), malate metabolic process and pyruvate metabolism was once again a cluster of significance (Annotation Cluster 6). Although expression of *Y1142H* did not impair MB development (**Figure 4.17**), it did however lead to a reduction in eye impairment not exhibited by other variants (not

including *dMEF2*) when compared to *DmHDAC4*^{WT} (**Figure 4.9**). Therefore, while it is uncertain of the process involved, it is possible that DmHDAC4 could also be mediating transcriptional changes via its deacetylase domain that targets only specific genes such as the ones relating to pyruvate metabolism.

CS vs Y1142H:

Cluster #	Category	Term	Count	%	*p*-value	Fold Enrichment	FDR
Annotation Cluster 1 Enrichment Score: 4.27	GOTERM_MF_DIRECT	Structural Constituent Of Cuticle	11	5.392	1.939E-06	7.413	2.695E-04
	GOTERM_MF_DIRECT	Structural Constituent Of Chitin-Based Larval Cuticle	9	4.412	7.271E-05	6.409	5.053E-03
	GOTERM_CC_DIRECT	Extracellular Matrix	9	4.412	1.331E-04	5.884	3.326E-03
	GOTERM_BP_DIRECT	Chitin-Based Cuticle Development	9	4.412	4.507E-04	4.940	3.440E-02
Annotation Cluster 2 Enrichment Score: 3.61	GOTERM_BP_DIRECT	Humoral Immune Response	5	2.451	1.418E-04	18.181	3.304E-02
	GOTERM_BP_DIRECT	Defense Response To Gram-Positive Bacterium	6	2.941	4.209E-04	9.350	3.440E-02
Annotation Cluster 3 Enrichment Score: 2.79	GOTERM_MF_DIRECT	Odorant Binding	8	3.922	6.597E-04	5.391	2.293E-02
	GOTERM_BP_DIRECT	Sensory Perception Of Chemical Stimulus	6	2.941	3.918E-03	5.692	1.304E-01

Table 6.12: DAVID annotation cluster analysis of pairwise comparison: *CS* versus *Y1142H*
The annotated clusters that have an enrichment score of ≥2.0 and at least one annotated term with FDR≤0.05 (5.0E-02) are shown. Genes were annotated using databases from GO Term Biological Processes (GOTERM_BP_DIRECT), Cellular Components (GOTERM_CC_DIRECT) and Molecular Function (GOTERM_MF_DIRECT). Count column indicates the number of genes from the list of significantly differentially expressed genes that are implicated in the corresponding terms. Percentage column refers to the percentage of genes from the list that are annotated with the term. *P*-value column is derived from a Modified Fisher's Exact test of the number genes from the list that are involved in a term against the database list. Fold enrichment column indicates the number of fold that the term is expected to happen as opposed to being due to random occurrence. FDR column is the adjusted *p*-value.

DmHDAC4 WT vs Y1142H:

Cluster #	Category	Term	Count	%	*p*-value	Fold Enrichment	FDR
Annotation Cluster 1 Enrichment Score: 31.2	GOTERM_BP_DIRECT	Multicellular Organism Reproduction	83	6.998	7.431E-40	5.580	4.607E-37
	GOTERM_CC_DIRECT	Extracellular Space	103	8.685	5.071E-24	2.932	9.989E-22
Annotation Cluster 2 Enrichment Score: 7.68	KEGG_PATHWAY	Carbon Metabolism	25	2.108	5.258E-10	4.350	3.313E-08
	KEGG_PATHWAY	Biosynthesis Of Antibiotics	27	2.277	8.164E-07	2.871	1.444E-05
Annotation Cluster 3 Enrichment Score: 5.38	GOTERM_MF_DIRECT	Manganese Ion Binding	9	0.759	2.563E-06	8.730	8.197E-04
	GOTERM_MF_DIRECT	Aminopeptidase Activity	11	0.927	4.281E-06	6.255	8.197E-04
	GOTERM_MF_DIRECT	Metalloexopeptidase Activity	8	0.675	6.779E-06	9.423	8.655E-04
Annotation Cluster 4 Enrichment Score: 4.70	KEGG_PATHWAY	Citrate Cycle (TCA Cycle)	13	1.096	9.165E-07	5.786	1.444E-05
	GOTERM_BP_DIRECT	Tricarboxylic Acid Cycle	10	0.843	4.359E-04	4.230	3.003E-02
Annotation Cluster 5 Enrichment Score: 4.65	GOTERM_BP_DIRECT	Post-Mating Behaviour	7	0.590	9.014E-07	15.176	1.220E-04
	GOTERM_BP_DIRECT	Oviposition	6	0.506	5.436E-04	8.005	3.064E-02
Annotation Cluster 6 Enrichment Score: 3.34	KEGG_PATHWAY	Pyruvate Metabolism	10	0.843	3.773E-04	4.253	3.962E-03
	GOTERM_BP_DIRECT	Malate Metabolic Process	6	0.506	5.436E-04	8.005	3.064E-02
Annotation Cluster 7 Enrichment Score: 2.65	KEGG_PATHWAY	Glycolysis / Gluconeogenesis	10	0.843	1.322E-03	3.611	9.253E-03
	GOTERM_BP_DIRECT	Glycolytic Process	7	0.590	3.718E-03	4.497	1.356E-01

Table 6.13: DAVID annotation cluster analysis of pairwise comparison: *DmHDAC4*^{WT} versus *Y1142H*
The annotated clusters that have an enrichment score of ≥2.0 and at least one annotated term with FDR≤0.05 (5.0E-02) are shown. Genes were annotated using databases from GO Term Biological Processes (GOTERM_BP_DIRECT), Cellular Components (GOTERM_CC_DIRECT) and Molecular Function (GOTERM_MF_DIRECT). Count column indicates the number of genes from the list of significantly differentially expressed genes that are implicated in the corresponding terms. Percentage column refers to the percentage of genes from the list that are annotated with the term. *P*-value column is derived from a Modified Fisher's Exact test of the number genes from the list that are involved in a

term against the database list. Fold enrichment column indicates the number of fold that the term is expected to happen as opposed to being due to random occurrence. FDR column is the adjusted *p*-value.

6.5 Overview of the functional cluster analysis

The annotation cluster analysis of the differentially expressed genes between pairwise comparison of *CS* and *DmHDAC4*^{WT} was shown to have the greatest number of genes clusters that were enriched. It is a logical conclusion that the clusters that were observed for *DmHDAC4*^{WT} but are lacking for each of the variants indicate that the respective functional domains are required for regulation of genes under those terms/processes. While this is a rational assumption, the variance among data is an important consideration to the interpretation of the cluster analysis. Therefore, clusters that are present or absent should be carefully considered as enrichment analysis serves only to distil the information from the differential gene expression data and is not necessarily a full representation of all the term processes impacted by differential gene expression.

Among the annotation clusters from *CS* versus *DmHDAC4*^{WT}, terms that relates to glucose metabolism and mitochondrial energy production pathway were identified as processes that have the potential to influence neuronal function. One of the processes under glucose metabolism was glycolysis, which breaks down glucose to pyruvate that is required by the TCA cycle in mitochondria to generate compounds required in the electron transport chain to produce ATP. ATP then provides the needed energy to the physiological functions of organs throughout the body including the brain. Diseases that affect glucose metabolism such as diabetes has also been associated with the progression of AD and cognitive impairment (Mergenthaler, Lindauer, Dienel, & Meisel, 2013). As for the processes relating to mitochondrial energy production, dysregulation of such processes could lead to not just impaired ATP production but also increase production of ROS which are harmful to cellular function (Kausar, Wang, & Cui, 2018). In fact, mitochondrial dysfunction has also been implicated as a major contributor to the development of neurodegenerative diseases that arise from diabetes (Cheng et al., 2019)

To determine whether expression of each mutant impacted pathways related to glucose metabolism and mitochondrial energy production, pairwise comparison between *DmHDAC4*^{WT} and each variant were performed and assessed for their significant term clusters in relation to *CS* versus *DmHDAC4*^{WT}. Most of these pairwise comparison (except

with *dNLS*) displayed term clusters relating to glucose metabolism and mitochondrial energy production, which means that these processes were no longer enriched on expression of the variant, therefore suggesting that the functional domains (that were mutated in the variants) are important for DmHDAC4 to induce transcriptional changes in genes involved in these processes. There was also the presence of new clusters in some instances such as those relating to pyruvate metabolism, which arises from comparisons between *DmHDAC4*^{WT} versus *3A*, *dANK* and *Y1142H*. In another pairwise comparison between *dMEF2* and *3A*, it was revealed to be enriched for a cluster of genes that relates to oxidative processes that are known to impact ROS production. Upon closer examination of the differentially expressed genes in the cluster, they belong to an enzymatic family of cytochrome P450. While cytochrome P450 is most widely known for its role in drug and xenobiotic metabolism, it has also been known to play a role in oxidation and has been involved in the generation of ROS (Veith & Moorthy, 2018). This could suggest oxidative stress being a strong influence on neuronal function caused by overexpression of DmHDAC4 and that the subcellular distribution of DmHDAC4 could play a role in differentially regulating those genes. In fact, *CS* versus *3A* was also enriched for clusters (>2.0) expressing the cytochrome P450 genes (not shown) but was excluded due to the terms FDR being >0.05.

6.5.1 Identification of candidate genes from cluster analysis

Cluster analysis allows the filtering of the large number of differentially expressed genes down to the most significantly relevant ones, though this could potentially exclude some genes depending on the type of stringency applied to the analysis. As the *CS* versus *DmHDAC4*^{WT} comparison yielded the greatest number of significantly differentially expressed genes and clusters, candidate genes for further analysis were identified from this pairwise comparison. For comparison of *DmHDAC4*^{WT} versus the variants, only the genes from the cluster involved in pyruvate metabolism and malate metabolic processes was included due to its recurring enrichment in *DmHDAC4*^{WT} versus 3A, dANK or Y1142H. Genes from the enriched clusters were assessed individually for terms/processes relating to glucose metabolism and mitochondrial energy production using an annotated function table generated from DAVID (**Supplementary Table 9.15 & 9.16**) after which

selected genes were further assessed for functional relevance using compiled gene information from FlyBase.

FBGN0034356	**CG10924 gene product from transcript CG10924-RA(Pepck2)**
	Log2 Fold Change: 1.713, Adjusted p-value: 7.22E-21
GOTERM_BP_DIRECT	gluconeogenesis,
GOTERM_CC_DIRECT	mitochondrion,
GOTERM_MF_DIRECT	phosphoenolpyruvate carboxykinase (GTP) activity, GTP binding,
KEGG_PATHWAY	Glycolysis / Gluconeogenesis, Citrate cycle (TCA cycle), Pyruvate metabolism, Metabolic pathways, Biosynthesis of antibiotics, FoxO signaling pathway, Insulin resistance,
FBGN0023479	**CG4821 gene product from transcript CG4821-RG(Tequila)**
	Log2 Fold Change: 1.210, Adjusted p-value: 2.83E-51
GOTERM_BP_DIRECT	chitin metabolic process, proteolysis, short-term memory, long-term memory, glucose homeostasis, regulation of insulin-like growth factor receptor signaling pathway,
GOTERM_CC_DIRECT	extracellular region, membrane,
GOTERM_MF_DIRECT	serine-type endopeptidase activity, scavenger receptor activity, chitin binding,
FBGN0261575	**target of brain insulin(tobi)**
	Log2 Fold Change: 2.179, Adjusted p-value: 6.08E-09
GOTERM_BP_DIRECT	carbohydrate metabolic process,
GOTERM_MF_DIRECT	hydrolase activity, hydrolyzing O-glycosyl compounds, alpha-1,4-glucosidase activity, maltose alpha-glucosidase activity,
KEGG_PATHWAY	Galactose metabolism, Starch and sucrose metabolism, Metabolic pathways,

Table 6.14: GO and KEGG terms annotation of selected candidate genes
Table shows the annotation of three gene candidates selected from the list of 73 genes derived from the cluster analysis of *CS* versus *DmHDAC4*^{WT} and cluster that displayed pyruvate metabolism and malate metabolic processes

From the list of 73 genes derived from the enriched clusters (**Supplementary Table 9.15 & 9.16**), three genes were selected for further analysis based on their relevance to glucose metabolism or cellular energy production and genetic tools that are already available (**Table 6.14**). When checking the genes against the *Drosophila* gene expression database, FlyAtlas 2, expression data suggests that the genes were minimally expressed in the adult fly brain. However, a literature review on each of the genes suggests that they may play a role in neuronal function:

Pepck2

Phosphoenolpyruvate carboxykinase 2 (*Pepck2*) is an enzyme that is orthologous to the human *phosphoenolpyruvate carboxykinase 2-mitochondrial* (*Pck2*) which converts oxaloacetate to phosphoenolpyruvate

during gluconeogenesis and is distributed across the cytoplasm and in the mitochondria. *Pepck* in *Drosophila* is mostly reported to be expressed in the adipose tissue (Chatterjee & Perrimon, 2021) while *Pck2* is expressed in a range of tissues including adipose tissue, liver, kidney, pancreatic β-cells and even neurons (Méndez-Lucas et al., 2013; Méndez-Lucas, Hyroššová, Novellasdemunt, Viñals, & Perales, 2014). A study in the mouse demonstrated that overexpression of *Pepck* led to a reduction in the ability of insulin to suppress gluconeogenic gene expression, leading to increased glucose production in the liver (Sun et al., 2002). Although, this was not directly linked to insulin resistance in Type II diabetes mellitus, glycaemia in diabetic mice was reduced when *Pepck* was silenced through intravenous administration of vector-based RNAi to the liver (Gomez-Valades et al., 2006). The further investigation of the role of *Pck2*/*Pepck2* in HDAC4-mediated neuronal dysfunction is also of wider relevance as diabetes has been associated with the progression of AD and cognitive impairment (Mergenthaler et al., 2013).

Tequila

Annotation cluster analyses identified genes relating to chitin binding and chitin metabolic processes, however a closer examination of the list of genes in the cluster identified the gene, *Tequila*, in which the biological processes listed from GO terms suggest it is also involved in STM, LTM, glucose homeostasis and regulation of insulin-like growth factor receptor signalling pathway (**Table 6.14**). Tequila is an orthologue of the neurotrypsin human serine protease 12 (PRSS12) (Ross, Jiang, Kanost, & Wang, 2003). Mutations to *PRSS12* have been reported in nonsyndromic mental retardation (Molinari et al., 2002). *Tequila* KD in the adult *Drosophila* MB results in reduced STM in the T-maze odour learning and memory paradigm (Colomb, Kaiser, Chabaud, & Preat, 2009). In another study with similar paradigm, deficits in LTM but not STM were observed (Didelot et al., 2006). In relation to glucose homeostasis, homozygous *Tequila* mutant flies displayed higher circulating glucose in hemolymph which suggest an impairment in glucose clearance. *Drosophila* insulin-like peptide was also reduced in this mutant (Huang et al., 2015). This decrease in insulin production seems to suggest a phenotype that is similar to Type 2 diabetes mellitus. However, Tequila is differentially upregulated in flies

expressing *DmHDAC4*^{WT}, while KD of *DmHDAC4* did not display a statistically significant reduction of the gene. Whether overexpression of this gene has an impact on neuronal function is currently unknown, therefore, it is also of interest to further investigate the genetic interaction between increased expression of *DmHDAC4* and KD of *Tequila* to determine the extent in which overexpression of *DmHDAC4* affects neuronal impairment when *Tequila* is reduced.

tobi

The *target of brain insulin* (*tobi*) gene is highly conserved with mammalian *α-1,4-glucosidase*, which encodes an enzyme that breaks down glycogen to glucose (Adeva-Andany, González-Lucán, Donapetry-García, Fernández-Fernández, & Ameneiros-Rodríguez, 2016; Buch, Melcher, Bauer, Katzenberger, & Pankratz, 2008). Overexpression of *tobi* in *Drosophila* led to a reduction in glycogen, which further suggests a conserve function and, just as the name implies, the gene is a target of insulin signaling. Ablation of insulin producing cells in the *Drosophila* brain led to a decrease in *tobi* expression (Buch et al., 2008). Since insulin is most commonly known to control glucose level, perhaps *tobi* could be a link between diabetes and AD. In humans, clinical studies that observed diabetic patients having increased amount of brain amyloid deposition (Janson et al., 2004), and AD patients having a higher blood glucose level (Razay, Vreugdenhil, & Wilcock, 2007) when compared to control patients, have linked diabetes and AD (Akter et al., 2011). Some of the possible causes may include insulin processing where insulin in the brain can bind to insulin receptor to potentially interact with phosphatidylinositol 3-kinase to induce β-amyloid dependent memory loss (Chiang, Wang, Xie, Yau, & Zhong, 2010). Mitochondrial dysfunction and oxidative stress is another potential cause, as a rat model of Type 2 diabetes exhibited impairments in the electron transport chain in brain mitochondria (Moreira, Santos, Moreno, Seiça, & Oliveira, 2003). Therefore, this impact to ATP production can potentially deprive neurons of energy which can lead to neurodegeneration (Akter et al., 2011). However, the mechanism underpinning these correlations is largely unknown. In a recent study involving a *Drosophila* model of AD, it was discovered that accumulation of β-amyloid led to an increase in *Drosophila*

insulin-like peptide which also increased tobi expression. Mutations to the insulin receptor alleviated the phenotypes associated with AD, hence insulin signaling maybe a downstream effector contributing to the disease phenotype (Huang, Wan, Wang, & Zhou, 2019).

Although the 10 genes from the cluster displaying pyruvate metabolism and malate metabolic processes contained many relevant processes relating to mitochondrial energy production (**Supplementary Table 9.16)**, none of the genes were selected due to the lack of genetic tools in Flybase, however these genes can be reserved for future analysis to determine whether they are specifically regulated by the variants (*3A*, *dANK* or *Y1142H*).

6.5.1.1 The effects of *Pepck2*, *Tequila* or *tobi* KD on MB development

Having identified potential gene candidates, a preliminary test was first carried out to determine whether any of these genes are important for neuronal function in *Drosophila*. Although the RNA-Seq data were derived from samples of post-developmental adult heads, due to time constraints (refer to **Appendix 9.6: Explanation of COVID-19 Impacts DRC Form**), only their role in MB development was able to be investigated. F1 flies derived from *OK107GAL4;tubGAL80^{ts}* females crossed to males with RNAi inverted repeats that target *Pepck2, Tequila,* or *tobi* were raised at 30°C (**Figure 6.9A**) and 18°C (**Figure 6.9B**) and analysed for deficits in axon morphogenesis in the MB. KD of all three genes resulted a range of severe morphological deficits and the levels of penetrance compared to the control were highly significant, therefore *Pepck2*, *Tequila* and *tobi* are all required in KCs for normal axon morphogenesis.

To determine whether these genes are downstream targets of *DmHDAC4*, the RNAi will be co-expressed with *DmHDAC4* to determine whether KD of any of the genes can alleviate MB phenotype caused by overexpression of *DmHDAC4^{WT}* and thus interact in the same pathway as HDAC4 to impair MB formation.

A

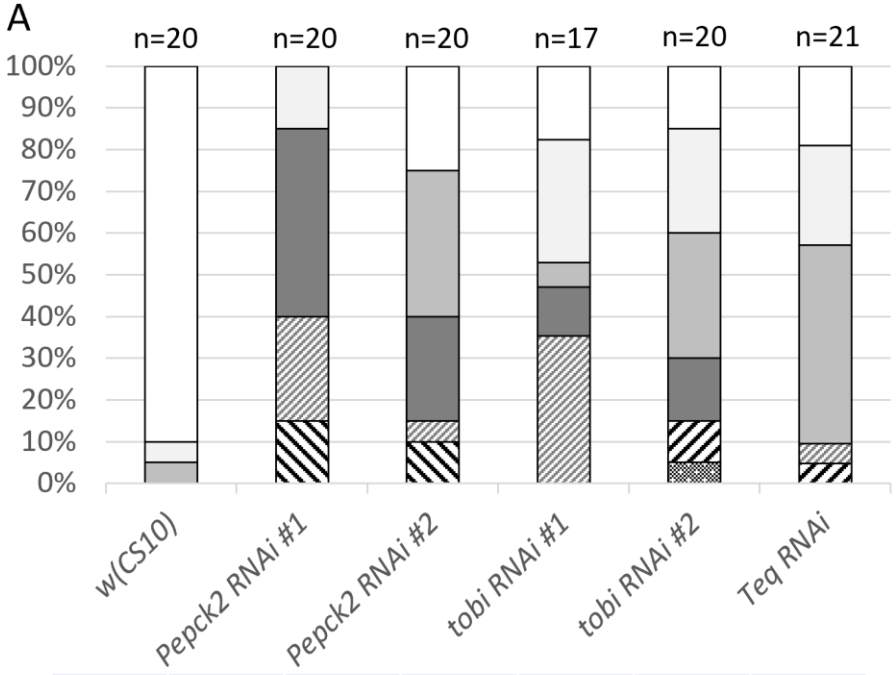

Genotype:	*w(CS10)*	*Pepck2 RNAi #1*	*Pepck2 RNAi #2*	*tobi RNAi #1*	*tobi RNAi #2*	*Teq RNAi*
Normal	19	0	0	4	18	0
Abnormal	0	33	20	15	1	18

One-tailed Fisher's exact test:

w(CS10) vs *Pepck2 RNAi #1* – ***p<0.001
w(CS10) vs *Pepck2 RNAi #2* – ***p<0.001
w(CS10) vs *tobi RNAi #1* – ***p<0.001
w(CS10) vs *tobi RNAi #2* – ***p<0.001
w(CS10) vs *Teq RNAi* – ***p<0.001

B

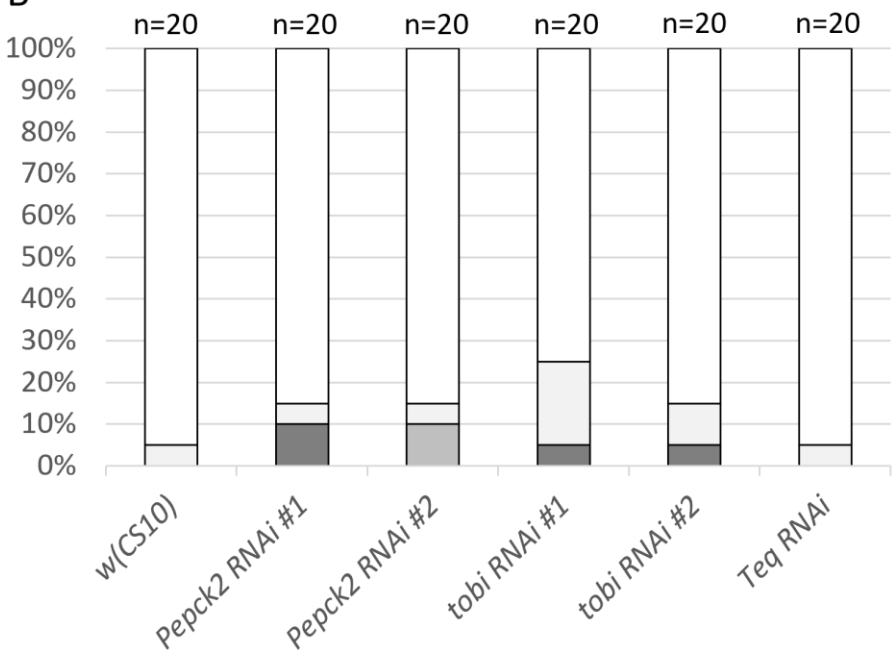

Continue next page ->

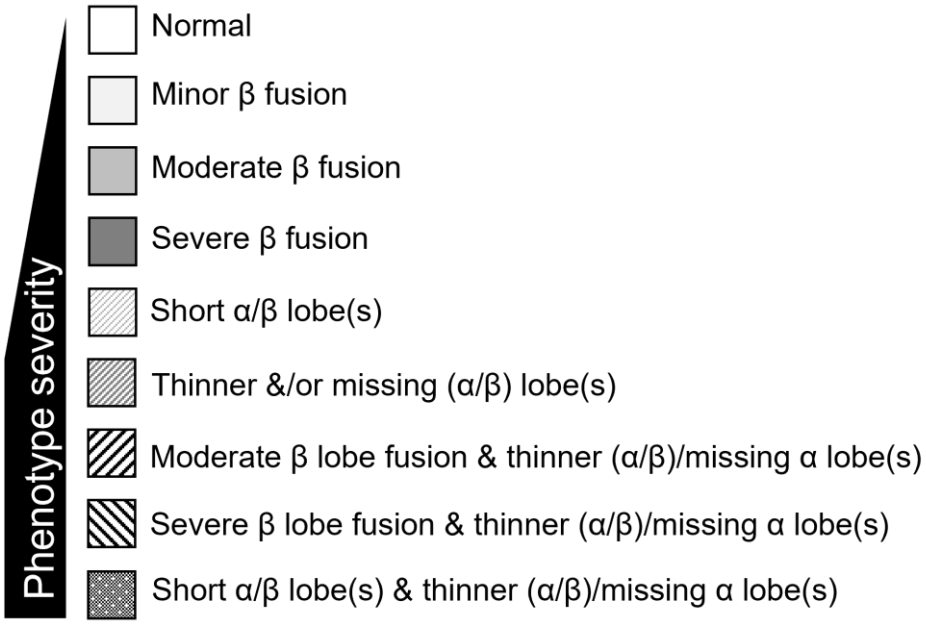

Figure 6.9: MB deficits resulting from KD of *Pepck2, Tequila* and *tobi*
Each bar represents the percentage of phenotypic distribution of a genotype. The x-axis represents genotype of the control or RNAi lines with the pan-MB (OK107GAL5; tubGAL80^{ts}) driver raised at (A) 30°C and (B) 18°C The sample size for each genotype is indicated above each bar. Table displays the number of samples with normal or abnormal (combination of all phenotypes within treatment) from variant expression driven by *OK107GAL4; tubGAL80^{ts}*. One-tailed Fisher's exact test was used for significance testing between comparison of interest.

6.5.2 Preliminary tests for oxidative stress

From the annotation table of 73 genes (**Supplementary Table 9.15 & 9.16**), a number of genes were present that are classified with terms/processes relating to mitochondrial energy production such as the TCA cycle, mitochondrial electron transport, mitochondrial respiratory chain complex II and oxidoreductase activity. Mitochondrial dysfunction that affects the electron transport chain can contribute to increase in ROS. In the pairwise comparison between dMEF2 and 3A (**Table 6.9**), the enriched gene cluster also included oxidoreductase activity as one of the processes which could suggest that different subcellular DmHDAC4 can regulate ROS production since the cytochrome P450 genes within the cluster were either differentially up or down regulated (not shown). As mentioned in Section 6.4.2.4, a parallel analysis performed in this lab by Main et al. (2021) comparing the RNA-Seq data of human 3A and human L175A (cytoplasmic-restricted mutant through mutation of MEF2-binding site) also revealed an enrichment for oxidoreductase activity through differential regulation of cytochrome P450 genes. Although cytochrome P450 was reported mostly as a drug metabolizing enzyme in the

liver, many subfamilies have also been identified in the brain (Miksys & Tyndale, 2002). It is involved in substrate oxidation and has also been known to be involved in ROS production (Veith & Moorthy, 2018). Since ROS has also been implicated in cytoskeletal regulation through redox modification of actin (Dalle-Donne, Rossi, Milzani, Di Simplicio, & Colombo, 2001), this could potentially impact the growth cone pathfinding capability of developing neurons (Oswald, Garnham, Sweeney, & Landgraf, 2018). Therefore, based on the data of this project, it was hypothesised that increased expression of *DmHDAC4* may impair development through the elevation of ROS such as superoxide ion which is formed when electrons leaked from the transport chain and reduces oxygen molecules. One of the methods available for detecting ROS is via dihydroethidium (DHE) staining which in the presence of superoxide, oxidises to form 2-hydroxyethidium which emits red fluorescent signal and tends to intercalate with DNA in the nucleus. Whole fly brains with pan-neuronal expression of $DmHDAC4^{WT}$ and the variant *3A*, *dNLS* and *dMEF2*, were assessed for DHE fluorescent intensity in comparison to the driver only control. However, whole brain DHE intensity appeared the same among all samples and did not appear different compared to control (**Figure 6.10A-E**). The DHE intensity in a supposed positive control via RNAi KD of the gene *nebula* also did not show intensity difference when compared to CS control (not shown). This could be due to the fact that a hypomorphic *nebula* mutant was used in the reported study instead of RNAi KD (Chang & Min, 2005) and due to time constraints, the efficacy of the RNAi has not yet been validated. In an unrelated experiment that tested for DHE intensity in the retina via RNAi KD of *Coenzyme Q8*, a *Drosophila* homologue to human *Coenzyme Q8A* which plays a role in oxidative phosphorylation in the electron transport chain. It revealed a significant increase in DHE intensity in the retina albeit not just within the nucleus (**Supplementary Figure 9.13**), thus suggesting an increase in ROS formation. While this suggests that the DHE assay is detecting ROS, optimisation needs to be carried out.

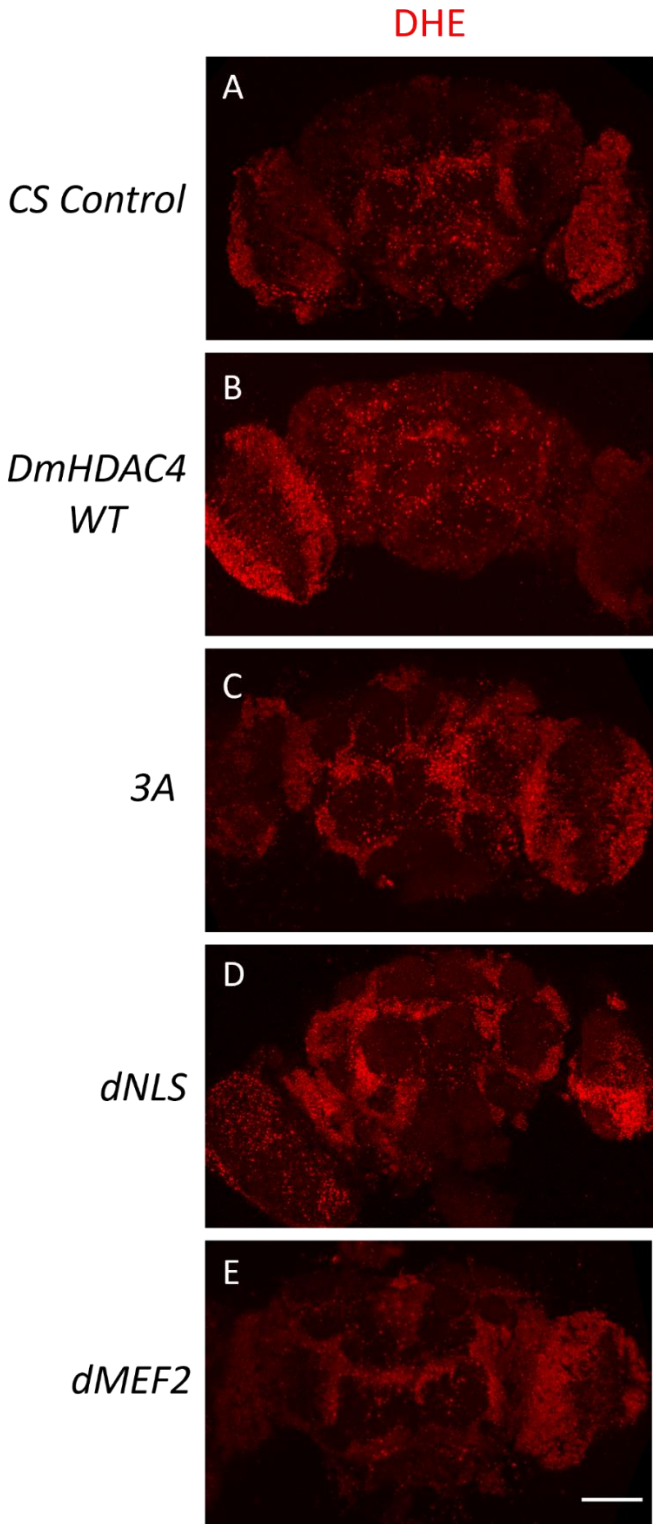

Figure 6.10: Assessing for ROS using DHE
Figure shows representative images of *Drosophila* whole brain DHE staining between control and treatments. Each genotype was derived from F1s of elavGAL4 crossed to respective UAS variant genotype which were raised at 25°C. Scale bar=100μm.

Another test for oxidative stress was also carried out by assessing for lipid droplet accumulation in the glial cells of retina. The increase in ROS has recently been associated with increase in lipogenesis which led to the accumulation of lipids in the form of large lipid droplet organelles in neighbouring glial cells of afflicted neurons (**Figure 6.11G**). The uptake of harmful peroxidated lipids by the glial cells was deemed to be a protective mechanism in which ROS induces lipid production, and the lipids are shuttled to neighbouring glial cells (Liu, MacKenzie, Putluri, Maletić-Savatić, & Bellen, 2017; Liu et al., 2015). An assay for glial lipid droplets was performed on flies expressing *DmHDAC4*^{WT} or *3A* in the retina via the *GMR-GAL4* driver. As the developmental impairment of the retina resulting from expression of *DmHDAC4*^{WT} and *3A* could affect visualisation of lipid droplets, flies were first raised at 18°C to minimise structural developmental defects followed by three days of post-developmental 30°C incubation to induce expression. Nile Red staining, which targets lipids, was used to highlight lipid rich tissues and to detect lipid droplets. Lipid droplets were not detected in retina expressing either *DmHDAC4*^{WT} or *3A* (**Figure 6.11A-F**). During the assessment of the rough eye phenotype assay in Chapter 4 (**Figure 4.9**), necrotic patches devoid of any pigment were detected on the retina of freshly eclosed *3A*-expressing flies, suggesting that the degeneration process initiates during development. It was speculated that perhaps excess lipid accumulation in glia could cause the cells to rupture, resulting in the loss of glial pigment. This could potentially release the peroxidated lipids back onto the neurons which then results in neurodegeneration. Additionally, apoptosis induced proliferation occurs during normal development of *Drosophila* photoreceptors as well as other brain regions and extracellular ROS have recently been implicated in driving the process (Fogarty et al., 2016). Therefore, it will be interesting to analyse the eye imaginal disc of developing larva for lipid droplets to determine whether the defects observed from the rough eye screen could be a result of aberrant ROS production during eye development.

The preliminary experiments for ROS detection suggest that increased expression of *DmHDAC4*^{WT} does not impact ROS production despite the RNA-Seq data revealing genes that play a role in mitochondrial related processes, therefore it could be that the impacted processes do not affect the electron transport chain enough to influence significant change in the level of ROS.

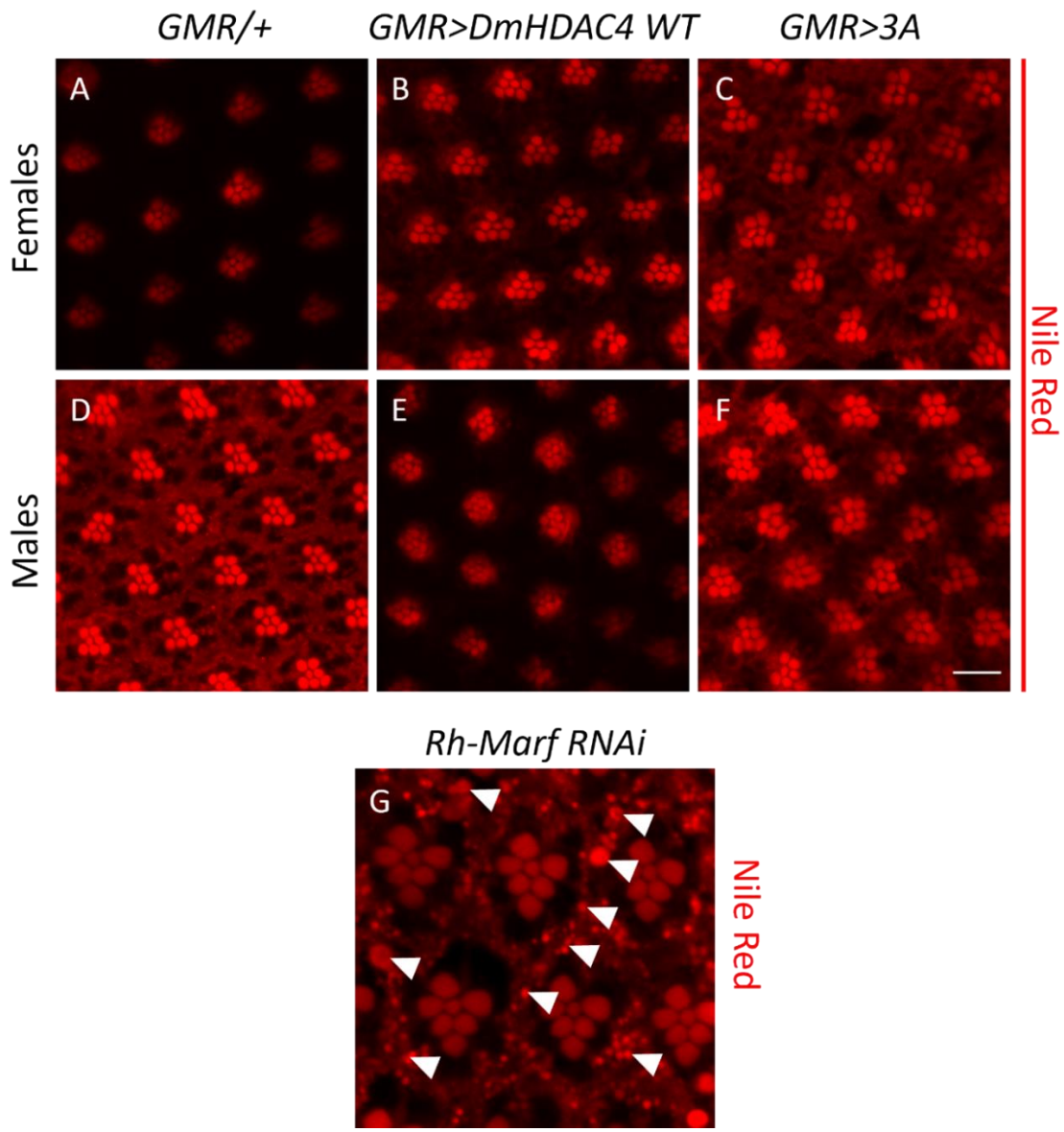

Figure 6.11: Assessing for lipid droplets using Nile Red staining
(A-F) shows representative images Nile Red staining of rhabdomeres and glial cells in *Drosophila* retina. Each genotype was derived from F1s of GMR-GAL4 crossed to CS control, *UAS-DmHDAC4 WT* or *UAS-3A* which were raised at 18°C and incubated at 30°C post-developmentally for 3 days. (G) Representative image of Nile Red staining of lipid droplets in glial cells with Rhodopsin promoter driven *Marf* RNAi KD (Liu et al., 2015). Arrowheads indicate clusters of lipid droplets lining the pigment glia. Image used under CC BY-NC-ND 4.0 (http://creativecommons.org/licenses/by-nc-nd/4.0). Scale bar=10μm.

6.6 Discussion

6.6.1 The DmHDAC4 variants display a reduced capacity to regulate gene expression

The RNA-Seq data of *Drosophila* whole brain RNA extract have provided some insights into the role of DmHDAC4 in transcriptional regulation of neuronal processes. A previous RNA-Seq analysis of transcriptional changes resulting from *DmHDAC4* overexpression in the *Drosophila* brain revealed only 26 significantly differentially expressed genes (Schwartz et al., 2016). The small number of genes was initially thought to be due to DmHDAC4 being present in only a subset number of KC nuclei which led to minimal alteration in transcription. However, the current RNA-Seq data in this project revealed almost 985 significantly differentially expressed genes. A cut-off for genes at >2 or <-2 $\log_2$ fold change still includes around 860 significantly differentially expressed genes. This major difference between two RNA-Seq dataset of the same genotype could likely be due to sample variances. PCA analysis from this current dataset revealed distinct cluster separation between control and *DmHDAC4*^{WT} along PC1, however the variance analysis data from the original study was not available.

Although *DmHDAC4*^{WT} was revealed to have a high number of differentially expressed genes, 930 genes were upregulated and only 55 genes were downregulated. This does not suggest global repression of transcription but rather predominantly a role promoting gene transcription. The same could not be said for the rest of the pairwise comparison of all of the variants, none of which exhibited the same high number of transcriptional changes. PCA analysis of each variant samples were shown to cluster separately from the control, which then indicate no overlap of variance along PC1, therefore suggesting that this low number of transcriptional changes are not due to variance overlap between genotypes. These data suggest that the motifs that facilitate subcellular shuttling as well as ankyrin-binding and deacetylase activity are all required for DmHDAC4 to regulate gene expression.

A recent RNA-Seq study by Main et al. (2021) analysed the transcriptional changes resulting from expression of nuclear and cytoplasmically-restricted mutants hHDAC4. Expression of the cytoplasmic *L175A* mutant resulted in 374 upregulated and 236 downregulated genes while expression of the nuclear *3A* mutant resulted in only 101

upregulated and 39 downregulated genes, which appeared to suggest a role of cytoplasmic hHDAC4 in gene regulation, particularly in gene upregulation. However, in this current study, expression of *3A* revealed a total of 149 differentially expressed genes and cytoplasmic-restricted DmHDAC4 mutants *dNLS* and *dMEF2* only had a total of 110 and 143 differentially expressed genes, respectively. While the difference in number of differentially expressed genes from the cytoplasmic HDAC4 could be due to the difference between the species of hHDAC4 and DmHDAC4, the cause of this difference is still unclear. Additionally, the low number of upregulated differentially expressed genes resulting from KD of *DmHDAC4* suggests that the main role of DmHDAC4 is not of a transcriptional repressor. Therefore, the transcriptional changes caused by *DmHDAC4* overexpression could be the result of a novel DmHDAC4 interaction with other proteins that leads predominantly to upregulation of gene targets. This may include non-histone targets in which deacetylation to repressors via histone deacetylation activates specific transcription factors to promote gene transcription. Alternatively, the gene upregulation could also be the result of an indirect pathway such as the alteration of activity or distribution of a protein that is required to regulate transcription factor and that DmHDAC4 binding to such protein could give way to more transcriptional activity.

The *dANK* mutant also facilitated approximately five-fold fewer changes in gene expression than $DmHDAC4^{WT}$, suggesting the ankyrin-binding site is important in this role. In a study by McKinsey et al. (2006), the ankyrin repeat-containing proteins ANKRA2 and RFXANK were shown to interact with Class II HDACs which led to repression of MHC II genes expression in mouse embryonic cells. This could suggest DmHDAC4 is potentially forming complex(es) with ankyrin repeat-containing protein(s) to target repression of specific genes. However, as mentioned, the 930 genes upregulated by $DmHDAC4^{WT}$ comparison is not indicative of gene repression. From an unpublished data mentioned by McKinsey et al. (2006), HDAC5, which is another Class IIa HDAC, forms a complex with RFXANK and is able to translocate out of the nucleus via 14-3-3ζ binding. Therefore, if DmHDAC4 is able to repress gene transcription to a certain degree, an increase in cellular DmHDAC4 abundance (UAS overexpression) could also potentially lead to increase chances of more putative DmHDAC4/Ankyrin complex being exported out of the nucleus which could explain the increase in upregulated gene from $DmHDAC4^{WT}$ overexpression. In *Drosophila*, the *RFXANK/ANKRA2* homologue is *CG5846* which is still uncharacterised and has no known function. The study of *CG5846*

can potentially uncover new function of the role of ankyrin repeat-containing proteins in *Drosophila* neurobiology, and is currently the focus of another PhD student's research as described in the previous chapter.

Heads expressing *Y1142H* also displayed a reduced number of differentially expressed genes compared to *DmHDAC4*^{WT} suggesting that the deacetylase activity of DmHDAC4 is required for its role in impairing eye development. However, it is unclear whether this occurs via the traditional deacetylation of histone lysine residues to prevent transcription factor access or whether it deacetylates non-histone targets. Although vertebrate HDAC4 is known to be catalytically inactive, HDAC4 has been reported in an *in vitro* study to be able to directly reduce the acetylation of the transcription factor, hypoxia-inducible factor 1 α, which results in the reduction of protein stability and affects the response of cancer cell under hypoxic condition (Geng et al., 2011). In *Drosophila*, while HDAC4 deacetylase domain appears to be functional, memory formation is independent of its deacetylase activity (Fitzsimons et al., 2013) as is the impairment to MB development, which was shown in the results of Chapter 4. However, it appears to have a role in eye development. Therefore, this evidence could suggest that the role of HDAC4 deacetylase domain could likely extend beyond its commonly perceived role as a gene repressor. As the number of upregulated genes in *CS* versus *DmHDAC4*^{WT} makes the process of gene repression via deacetylation seems counter-intuitive, perhaps the deacetylation could be indirectly upregulating transcription by regulating non-histone proteins that are required for repressing transcription.

6.6.2 DmHDAC4 regulates genes involved in energy production and glucose metabolism

In order to better understand the processes that are affected as a result of overexpression of DmHDAC4 and each variant, the differentially expressed genes were annotated and clustered together with reference to the GO and KEGG databases. Having extensively analysed the annotation clusters of the different pairwise comparison and to reduce the complexity in interpreting the information, the terms/processes from annotated clusters of *CS* versus *DmHDAC4*^{WT} were the primary focus due to the highest number of transcriptional changes. Among the 9 clusters identified, some clusters which include terms/processes such as multicellular organism reproduction, biosynthesis of antibiotics,

post-mating behaviour and chitin metabolic process were deemed to be irrelevant to the nature of this project, however it was also noted that the clusters in which the genes reside in does not fully represent the genes capability and function and each gene could have other roles that are not suggested by the cluster.

In the interest of better identifying for terms/processes that could potentially affect neuronal functions, clusters that include terms/processes such as TCA cycle and glycolysis were recognised as potential processes that are important to mitochondrial energy production and glucose metabolism, respectively, which are also important to neuronal function (Kausar et al., 2018; Mergenthaler et al., 2013). A related cluster that implicates fatty acid elongation is also a process that is present in the mitochondria and fatty acid, alongside pyruvate, are both energy sources that feeds into the TCA cycle (Kastaniotis et al., 2017; Nemani et al., 2020). Another related cluster which implicates α-1, 4-glucosidase activity is an important process that breaks down glycogen to glucose (Adeva-Andany et al., 2016) (**Figure 6.12**). When pairwise comparison between *DmHDAC4*^{WT} and the variants were made, the TCA cycle and glycolysis clusters were also present which suggest the mutations alter how DmHDAC4 regulates these processes. However, *DmHDAC4*^{WT} versus *3A*, *dANK* and *Y1142H* also displayed an additional cluster of genes involved in pyruvate metabolism and malate metabolic processes, both of which are important in the TCA cycle. Pyruvate is converted from glucose through glycolysis which then oxidises to form acetyl-CoA. Acetyl-CoA is required by the TCA cycle and combines with the cycle's end product, oxaloacetate to form citrate which is the start of the cycle. Malate metabolic processes comprise of enzymatic genes that are fumarase and malate dehydrogenase which converts fumarate to malate and malate to oxaloacetate respectively (Martínez-Reyes & Chandel, 2020) (**Figure 6.12**). The differential downregulation of genes relating to this process further implies an impact on cellular energy production. While the presence of the pyruvate metabolism and malate metabolic processes cluster may suggest that the differential expression of these gene clusters are what sets *3A* and *dANK* apart from *DmHDAC4*^{WT} in terms of their functional domain requirements in MB development and Y1142H in terms of its deacetylase domain requirement in eye development, this cluster was not enriched when comparison to *CS* versus *3A*, *dANK* and *Y1142H* were made. Therefore, even though the fumarase and malate dehydrogenase genes were differentially regulated in the *CS* comparison, they were not statistically significant. Despite this, the differential changes could perhaps have

an impact on neurodevelopment as fumarase deficiency has been known to result in developmental encephalopathy and intellectual disability (Bayley, Launonen, & Tomlinson, 2008; Kerrigan, Aleck, Tarby, Bird, & Heidenreich, 2000). Alternatively, the limited transcriptional changes in *CS* versus *3A*, *dANK* and *Y1142H* could also mean that the requirements of the mutants on development are not dependent on the effect of transcriptional changes but rather more on non-transcriptional process such as targeting of non-histone proteins such as tubulin (Paroni et al., 2008) to affect morphological changes.

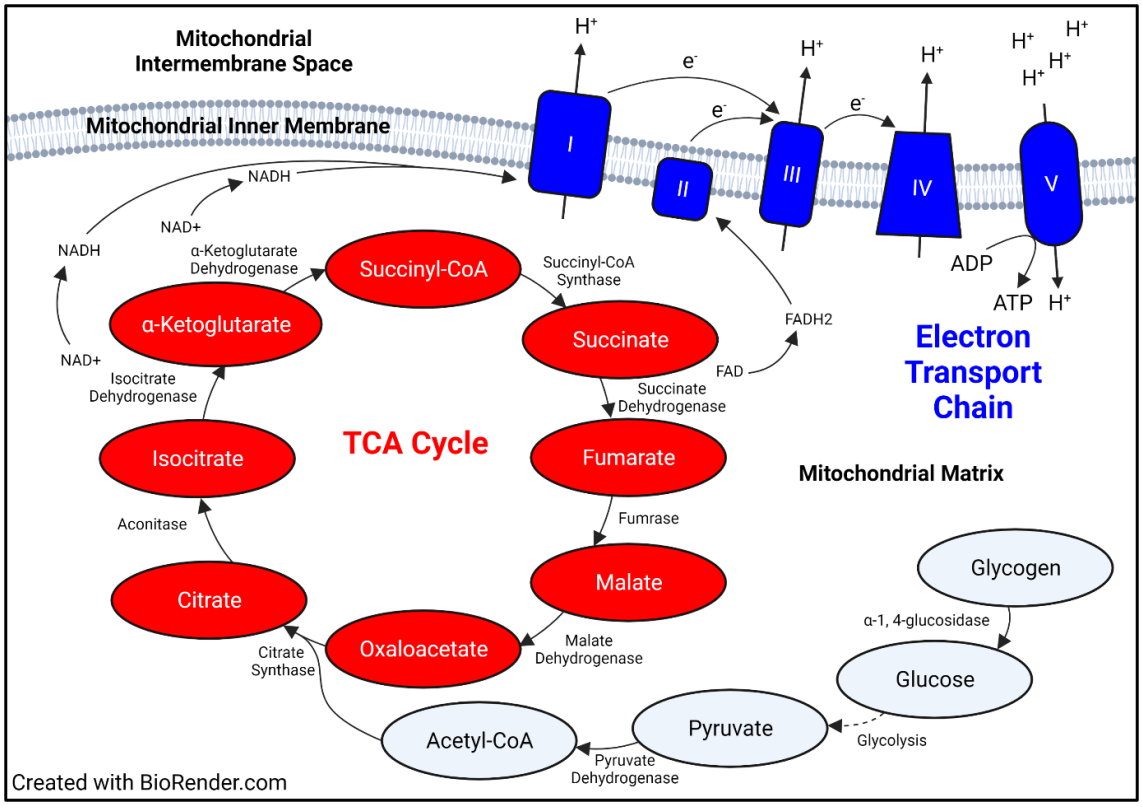

Figure 6.12: Simplified diagram of the TCA cycle and the electron transport chain
Glycogen store is converted to glucose by α-1,4-glucosidase after which it undergoes glycolysis to produce pyruvate. Pyruvate is then converted to Acetyl-CoA by pyruvate dehydrogenase. Acetyl-Coa combines with oxaloacetate to form citrate which is catalysed by citrate synthase. Citrate is isomerise into isocitrate by aconitase. Isocitrate is oxidise into α-ketoglutarate by isocitrate dehydrogenase and this reaction is followed by a reduction of an NAD molecule into NADH which is able to transfer its electron to complex I of the electron transport chain. This enables complex I to pump H^+ from the mitochondrial intermembrane space into the mitochondrial matrix. α-Ketoglutarate is converted into succinyl-CoA by α-ketoglutarate dehydrogenase which also reduces a molecule of NAD into NADH. Succinyl-CoA is converted into succinate by succinyl-CoA synthase. Succinate is converted to fumarate by succinate dehydrogenase which then reduces a molecule of FAD to FADH2. FADH2 can also transfer an electron over to complex II. Fumarate is converted to malate by fumrase and the final reaction of the cycle is malate conversion to oxaloacetate by malate dehydrogenase. Electrons transferred onto complex I and II of the electron transport chain are then transferred to complex III and IV which also acts to pump more H^+ into the matrix. Complex V which is an ATP synthase that converts ADP to ATP is activated by the mitochondrial membrane potential generated from the funnelling of matrix H^+ through

complex V into the intermembrane space as a result of H^+ concentration gradient. This figure is an original artwork created with referenced to Martínez-Reyes and Chandel (2020).

The potential for HDAC4 to impact glucose metabolism and energy production suggests that there could be a disruption to these processes when DmHDAC4 is overexpressed. As such, this presents a new perspective towards how HDAC4 can affect neuronal function. The brain is one of the most energy demanding organ compared to other tissues and glucose is an essential substrate for producing ATP. Approximately 25% of glucose in the human body is required for basal brain function and almost 70% of the energy produced is spent on neuronal signalling which includes processes such as maintaining resting potential, generating action potential, and transporting post synaptic receptors (Han, Liang, & Zhou, 2021). Additionally, there has also been increasing evidence of a correlation between glucose or mitochondrial dysfunction and neurodegenerative diseases such as AD, PD, ALS and HD (Han et al., 2021).

Although the result of glucose metabolism and energy production influence was based on post developmental brain samples, it could also potentially be the source for the developmental defects observed in MB phenotype. There have also been studies that has correlated neurodevelopmental diseases with dysfunction in energy metabolism; such as autism with impaired mitochondrial function, Down syndrome with increase in oxidative stress and reduced ATP production, fragile X syndrome with increase in ROS and reduced ATP production (Oyarzábal, Musokhranova, Barros, & García-Cazorla, 2021). Additionally, the comparison of dMEF2 versus 3A revealed both up and down regulation of a group of cytochrome P450 genes that are involved in monooxygenase and oxidoreductase activity. This differential expression was also observed between hHDAC4 of L175A versus 3A (Main et al., 2021). In humans, cytochrome P450 is traditionally known to be present in mitochondria of liver cells and metabolise drugs and xenobiotics to enable the foreign substrate to be excreted out of the body. However, subfamilies of cytochrome P450 have also been found to be present in the brain (Miksys & Tyndale, 2002). Its most common reaction is its role in substrate oxidation, in which there are a few stages in its enzymatic cycle which has been known to be a source for ROS production (Veith & Moorthy, 2018). The differential expression of cytochrome P450 genes in the *Drosophila* brain between dMEF2 and 3A could suggest a difference in cytoplasmic and nuclear regulation of ROS and an importance of the MEF2-binding site in regulating cytochrome P450 genes. Since, hHDAC4 3A overexpression has

exacerbated phenotype in both MB development as well as courtship memory impairment (Main et al., 2021) and ROS has also been associated with neurodegeneration (Kausar et al., 2018), the impact of ROS on MB development severity could also be considered as another potential cause. In fact, increasing amount of evidence have suggests that ROS could act as a second messengers that regulate neurodevelopmental processes such as neuronal polarity and growth cone behaviour. An example of ROS impact on neurodevelopment is the development of the parvalbumin-expressing inhibitory interneurons (PVIs) which are crucial for regulating neuronal excitation and inhibition within the cortical network (Oswald et al., 2018). These neurons were thought to be highly sensitive to ROS and are protected by the perineuronal nets from oxidative stress (Cabungcal et al., 2013). Hence, dysregulation to ROS was thought to affect the development of cortical network which could impair neuronal performance and leads to neurological disorder (Do, Cuenod, & Hensch, 2015). Analysis of post-mortem brain tissue of patients with autism exhibited reduction in PVIs and additionally a correlation of increased oxidative stress and reduced PVIs integrity was also observed in mouse model with autism related chromosomal deletion (Hashemi, Ariza, Rogers, Noctor, & Martínez-Cerdeño, 2017; Steullet et al., 2017). Therefore, this highlights the importance of ROS assessment in this study.

The impact of DmHDAC4 on ROS production was assessed using DHE, however no significant changes in DHE intensity were detected in post developmental brain samples between control and the pan-neuronal expression of $DmHDAC4^{WT}$ and the variants. This result was puzzling as mitochondria are known to be the major source of ROS production in mammalian cells (Cui, Kong, & Zhang, 2012), and it was thought that any perturbation to mitochondrial processes caused by overexpression of DmHDAC4 should elicit a change in ROS. Many studies have shown the ability for ROS to damage mitochondrial DNA (mtDNA) which can affect ageing via apoptosis (de la Asuncion et al., 1996; Mecocci et al., 1993; Yamaguchi & Perkins, 2009). mtDNA are the blueprints for mitochondrial machineries required in the electron transport chain, therefore, mutations to these machineries could potentially lead to a vicious cycle in which the oxidative damage to mtDNA could result in impaired protein formation or function required for respiratory chain, hence, leading to more ROS production and further damage to mtDNA (Cui et al., 2012). However, this theory has also been challenged as it was noted that not all mutations will lead to production in superoxide (Bandy & Davison, 1990; Hiona &

Leeuwenburgh, 2008). In fact, ageing mice with increased mtDNA mutations did not exhibit increase in ROS production (Kujoth et al., 2005; Trifunovic et al., 2004). This suggest that ROS may not be the sole mediator of phenotypes. Therefore, while the effect of DmHDAC4 overexpression on mitochondrial energy production may not affect ROS production, how it can impact neuronal function is still a question that requires further study. It should be noted that the test for ROS using DHE should also be investigated in the larva model since this study focused mostly on improper neurodevelopment. Additionally, a different approach of assaying with DHE could also be performed such as using fresh live neuronal cultures as opposed to dissecting for brain tissue which has the potential to cause cellular damage and result in premature ROS production prior to analysis which could potentially mask any significant difference.

Another preliminary test for potential ROS involvement was also carried out in the *Drosophila* photoreceptor in the form of a lipid droplet assay. Lipid droplets are organelles that store fat and are derived from the endoplasmic reticulum. They are mostly present in the liver and fat tissue (Murphy, 2001), however, cancerous cells have also been implicated with lipogenesis where the lipid droplets were thought to provide energy for the cells to proliferate (Bozza & Viola, 2010). Additionally, ROS induced lipid droplets formation in glial cells have recently been associated with neurodegeneration in *Drosophila* photoreceptor which can be delayed by reducing the accumulation of lipid droplets. The neurodegenerative cause of lipid droplets is most likely due to the elevated ROS which also led to lipids being peroxidated which are then harmful to neurons when overabundance of peroxidated lipids are released from the glia back on to the neurons (Liu et al., 2015). In the rough eye phenotype assessment (**Figure 4.9**), it was noticed that one of the phenotypes observed is the lack of red pigment which could suggest the absence of pigment glia and also some genotypes displayed additional necrotic features. Initially, it was rationalised that this could be due to excessive lipid uptake by glia which could eventually result in the destruction of glia which then in turn led to the release of harmful lipids, resulting in necrosis of surrounding cells which include photoreceptor neurons. However, lipid droplets were not observed when $DmHDAC4^{WT}$ or *3A* was post-developmentally expressed. Despite this negative result, it should be noted that the lipid droplet assay should also be carried out in developing neurons as the sterol regulatory element binding protein (SREBP) which is required for the biogenesis of lipid droplets is also known to be required in larva growth. Larvae with mutant SREBP are lethal but is

able to survive to adulthood with the aid of fatty acids supplementation to its diet (Kunte, Matthews, & Rawson, 2006). Therefore, while the potential impact of DmHDAC4 on ROS production does not seem to affect post developmental *Drosophila* brain, more investigations are still required to determine its changes during development.

6.6.3 Transcriptional targets of HDAC4 are required for MB development

The annotation cluster analysis has provided a direction to explore the mechanism through which increased accumulation of HDAC4 impacts neuronal function, therefore three genes were selected from among the clusters discussed above to determine whether they represent potential targets through which HDAC4 acts to impair MB development. The genes selected were *Pepck2*, *Tequila* and *tobi*, whose functions were briefly described in Section 6.5.1. Although each of the genes were shown to be required in the proper development of the MB via a KD approach, genetic interactions between these genes and DmHDAC4 are currently still being tested. As these genes were upregulated on expression of $DmHDAC4^{WT}$, it was rationalised that a concurrent overexpression of $DmHDAC4^{WT}$ and KD of these genes could allow a better understanding of the extent in which they can impact MB development.

With the potential of these three genes being a genetic interactor, future experiments to better characterise the role of *DmHDAC4* with these gene candidates includes by first confirming the KD of the genes via RT-qPCR after which it will be necessary to determine the expression pattern of each gene in the brain and whether if they are expressed in the same region as DmHDAC4. It will also be interesting to determine their role in memory performance by conducting courtship suppression assay on flies with KD of the genes. Additionally, to determine how DmHDAC4 can regulate the genes, chromatin immunoprecipitation can also be done to see if DmHDAC4 is present at the promoter of the genes or perhaps to identify for the genes transcription factors so as to determine whether if HDAC4 upregulate the genes indirectly by interacting with repressors to derepress gene transcription.

6.6.4 Limitations of bulk neuronal RNA-Seq

The method of bulk RNA-Seq has provided some degree of insights to the processes involved, the limitation is evident when trying to reconcile what was observed from the differential expression pattern data to phenotypic data that are cell or tissue specific as it has been shown that there are differences in developmental requirements of *DmHDAC4* between the eye and MB, particularly when involving the MEF2-binding site. Additionally, obtaining RNA samples from whole head also means that any changes are an average across the brain and any differences between the retina and other brain region such as the MB could be hidden. On top of that, the large number of brains required per replicates add to the genetic heterogeneity of the sample which also likely contribute to the variances between replicates of the same genotype. Therefore, it will be useful for any future RNA-Seq experiment to focus on isolating a neuronal type such as the KCs and performing single cell RNA-Seq on those cell type can likely produce a better resolution of transcriptional profile. Nevertheless, apart from $DmHDAC4^{WT}$, this analysis shows that the variants do not appear to facilitate large changes in expression.

7. SUMMARY

The work presented in this thesis has increased understanding of the mechanisms through which increased abundance of HDAC4 impairs neuronal development, the main findings of which are highlighted below.

7.1 Intact serine phosphorylation sites and an intact ankyrin-binding site of DmHDAC4 are required for normal MB formation

Both expression of *DmHDAC4*^{WT} and mutant variants in the presence of endogenous HDAC4, or in a background of depleted endogenous HDAC4, impaired normal MB development, which highlights the requirement of serine phosphorylation sites and ankyrin-binding site. The phenotypic penetrance was suppressed by the introduction of mutations into the MEF2-binding site, which restricted the variants to the cytoplasm. This may indicate that increased abundance of nuclear DmHDAC4 could lead to over suppression of MEF2 target genes. In fact, expression of *3A* and *dANK* in the MB resulted in reduced expression of FasII, which is a cell adhesion molecule important for MB axon morphogenesis that has been reported to be targeted by MEF2 (Sivachenko et al., 2013) and Ank2 (Pielage et al., 2008). It remains to be determined whether HDAC4 regulates MEF2-dependent transcription of FasII and also whether while in the cytoplasm, DmHDAC4 also interacts with ankyrin repeat-containing proteins to stabilise FasII. However, the role of DmHDAC4 in the cytoplasm is still not completely understood. While expression of dNLS impaired MB development, dMEF2 (which is also cytoplasmically-restricted) did not. This could potentially be due to dNLS not being completely restricted to the cytoplasm as some protein remained in the nucleus, however this seems unlikely as majority of dNLS appeared cytoplasmic. It will therefore be important to verify whether the difference in phenotype between dNLS and dMEF2 is a result of the increased efficacy of dMEF2 to shuttle out of the nucleus to reduce nuclear activity or is due to it not being able to interact with binding partners in the cytoplasm that rely on the MEF2-binding site, and identification of cytoplasmic binding partners will be a key future direction.

7.2 An active deacetylase domain is required for the HDAC4-induced impairment of eye development, but the MEF2-binding site is not

In the *Drosophila* eye, expression of *DmHDAC*^{WT} and all variants except *Y1142H* also resulted in significant disruption to development. The lack of phenotype resulting from expression of *Y1142H* further suggests a cell-specific role of HDAC4 and it remains to be determined whether this is via alterations to gene expression via deacetylation of histones or involves deacetylation of non-histone targets to affect developmental changes in the eye. Expression of *3A* and *dANK* exhibited more severe phenotypes than *DmHDAC4*^{WT}, however, unlike in the eye, these phenotypes were not reduced on mutation of MEF2-binding site. The *dANK_dMEF2* mutant, which was also shown to be cytoplasmically-restricted still exhibited an unchanged phenotype severity when compared to *dANK*. This along with the severe phenotype resulting from *dNLS* indicates that increased cytoplasmic HDAC4 impairs eye development and it will be of interest to identify proteins that interact with cytoplasmic HDAC4, including those that interact with the ankyrin repeat-binding domain to constrain the detrimental effects of increased cytoplasmic HDAC4.

7.3 RNA-Seq analysis provide insights into potential disruption to cellular energy production

Pan-neuronally expressed *DmHDAC4*^{WT} was shown to result in the highest number of transcriptional changes compared to the other *DmHDAC4* variants. The analysis of the differentially expressed genes suggest that processes relating to mitochondrial energy production were affected. Therefore, it is possible that abnormal mitochondrial processes could potentially affect neuronal function since the brain requires energy to maintain resting membrane potential and to generate action potentials. However, there was no clear correlation between phenotypic severity in the eye or MB with the transcriptional changes observed for each of the variants. Moreover, the low transcriptional changes exhibited by the *DmHDAC4* variants could also suggest that non-transcriptional processes may be

involved or that significant changes are occurring in a small number of neurons that require techniques such as single cell PCR in order to identify them.

7.4 Conclusion

The work described in this thesis has provided new insights such as how subcellular activities of HDAC4 impact neuronal development as well as the importance of the MEF2-binding site, ankyrin repeat-binding site and the deacetylase domain. Additionally, it was also discovered that the HDAC4 acts through varying mechanism(s) depending on the cell type, as was demonstrated by the requirements of MEF2-binding site in inducing the MB phenotype but not the eye and the requirements of active deacetylase domain in eye phenotype manifestation but not the MB. Transcriptional changes from genes identified from expression of *DmHDAC*^{WT} that are known to be involved in mitochondrial energy production also indicate the potential transcriptional role HDAC4 may have on neuronal function, however the low number of differential gene expression in *DmHDAC4* variants could also suggest non-transcriptional roles. Together, these findings potentially open up new avenues of investigation into how altered expression of HDAC4 impacts neurodevelopmental and neurodegenerative disease. A significant example is the finding that in the brain, expression of dMEF2 has almost no phenotype, therefore strategies to block the MEF2-binding site would be worth investigating to reduce the detrimental effects of increased nuclear and cytoplasmic HDAC4.

8. REFERENCES

Abel, T., & Lattal, K. M. (2001). Molecular mechanisms of memory acquisition, consolidation and retrieval. *Current Opinion in Neurobiology, 11*(2), 180-187. https://doi.org/10.1016/S0959-4388(00)00194-X

Abel, T., & Zukin, R. S. (2008). Epigenetic targets of HDAC inhibition in neurodegenerative and psychiatric disorders. *Current opinion in pharmacology, 8*(1), 57-64. 10.1016/j.coph.2007.12.002

Adeva-Andany, M. M., González-Lucán, M., Donapetry-García, C., Fernández-Fernández, C., & Ameneiros-Rodríguez, E. (2016). Glycogen metabolism in humans. *BBA clinical, 5*, 85-100. 10.1016/j.bbacli.2016.02.001

Agis-Balboa, R. C., Pavelka, Z., Kerimoglu, C., & Fischer, A. (2013). Loss of HDAC5 impairs memory function: implications for Alzheimer's disease. *J Alzheimers Dis, 33*(1), 35-44. 10.3233/jad-2012-121009

Akalal, D.-B. G., Wilson, C. F., Zong, L., Tanaka, N. K., Ito, K., & Davis, R. L. (2006). Roles for Drosophila mushroom body neurons in olfactory learning and memory. *Learning & memory (Cold Spring Harbor, N.Y.), 13*(5), 659-668. 10.1101/lm.221206

Akter, K., Lanza, E. A., Martin, S. A., Myronyuk, N., Rua, M., & Raffa, R. B. (2011). Diabetes mellitus and Alzheimer's disease: shared pathology and treatment? *British journal of clinical pharmacology, 71*(3), 365-376. 10.1111/j.1365-2125.2010.03830.x

Alarcon, J. M., Malleret, G., Touzani, K., Vronskaya, S., Ishii, S., Kandel, E. R., & Barco, A. (2004). Chromatin acetylation, memory, and LTP are impaired in CBP+/- mice: a model for the cognitive deficit in Rubinstein-Taybi syndrome and its amelioration. *Neuron, 42*(6), 947-959. 10.1016/j.neuron.2004.05.021

Anderson, K. W., Chen, J., Wang, M., Mast, N., Pikuleva, I. A., & Turko, I. V. (2015). Quantification of histone deacetylase isoforms in human frontal cortex, human retina, and mouse brain. *PLoS One, 10*(5), e0126592. 10.1371/journal.pone.0126592

Androschuk, A., Al-Jabri, B., & Bolduc, F. V. (2015). From Learning to Memory: What Flies Can Tell Us about Intellectual Disability Treatment. *Frontiers in psychiatry, 6*, 85-85. 10.3389/fpsyt.2015.00085

Anney, R. J. L., Ripke, S., Anttila, V., Grove, J., Holmans, P., Huang, H., . . . The Autism Spectrum Disorders Working Group of The Psychiatric Genomics, C. (2017). Meta-analysis of GWAS of over 16,000 individuals with autism spectrum

disorder highlights a novel locus at 10q24.32 and a significant overlap with schizophrenia. *Molecular Autism, 8*(1), 21. 10.1186/s13229-017-0137-9

Aso, Y., Grubel, K., Busch, S., Friedrich, A. B., Siwanowicz, I., & Tanimoto, H. (2009). The mushroom body of adult Drosophila characterized by GAL4 drivers. *J Neurogenet, 23*(1-2), 156-172. 10.1080/01677060802471718

Aso, Y., Hattori, D., Yu, Y., Johnston, R. M., Iyer, N. A., Ngo, T.-T. B., . . . Rubin, G. M. (2014). The neuronal architecture of the mushroom body provides a logic for associative learning. *eLife, 3*, e04577. 10.7554/eLife.04577

Assali, A., Harrington, A. J., & Cowan, C. W. (2019). Emerging roles for MEF2 in brain development and mental disorders. *Current Opinion in Neurobiology, 59*, 49-58. 10.1016/j.conb.2019.04.008

Backs, J., Song, K., Bezprozvannaya, S., Chang, S., & Olson, E. N. (2006). CaM kinase II selectively signals to histone deacetylase 4 during cardiomyocyte hypertrophy. *J Clin Invest, 116*(7), 1853-1864. 10.1172/JCI27438

Bahari-Javan, S., Maddalena, A., Kerimoglu, C., Wittnam, J., Held, T., Bahr, M., . . . Sananbenesi, F. (2012). HDAC1 regulates fear extinction in mice. *J Neurosci, 32*(15), 5062-5073. 10.1523/jneurosci.0079-12.2012

Baker, N. E., Li, K., Quiquand, M., Ruggiero, R., & Wang, L.-H. (2014). Eye development. *Methods (San Diego, Calif.), 68*(1), 252-259. 10.1016/j.ymeth.2014.04.007

Bandy, B., & Davison, A. J. (1990). Mitochondrial mutations may increase oxidative stress: implications for carcinogenesis and aging? *Free Radic Biol Med, 8*(6), 523-539. 10.1016/0891-5849(90)90152-9

Barbosa, A. C., Kim, M.-S., Ertunc, M., Adachi, M., Nelson, E. D., McAnally, J., . . . Olson, E. N. (2008). MEF2C, a transcription factor that facilitates learning and memory by negative regulation of synapse numbers and function. *Proceedings of the National Academy of Sciences, 105*(27), 9391.

Barco, A., Bailey, C. H., & Kandel, E. R. (2006). Common molecular mechanisms in explicit and implicit memory. *J Neurochem, 97*(6), 1520-1533. 10.1111/j.1471-4159.2006.03870.x

Bayley, J.-P., Launonen, V., & Tomlinson, I. P. M. (2008). The FH mutation database: an online database of fumarate hydratase mutations involved in the MCUL (HLRCC) tumor syndrome and congenital fumarase deficiency. *BMC medical genetics, 9*, 20-20. 10.1186/1471-2350-9-20

Beckingham, K. M., Armstrong, J. D., Texada, M. J., Munjaal, R., & Baker, D. A. (2005). Drosophila melanogaster--the model organism of choice for the complex biology of multi-cellular organisms. *Gravit Space Biol Bull, 18*(2), 17-29.

Bennett, V., & Baines, A. J. (2001). Spectrin and ankyrin-based pathways: metazoan inventions for integrating cells into tissues. *Physiol Rev, 81*(3), 1353-1392. 10.1152/physrev.2001.81.3.1353

Berdeaux, R., Goebel, N., Banaszynski, L., Takemori, H., Wandless, T., Shelton, G. D., & Montminy, M. (2007). SIK1 is a class II HDAC kinase that promotes survival of skeletal myocytes. *Nat Med, 13*(5), 597-603. 10.1038/nm1573

Bi, C., Wu, J., Jiang, T., Liu, Q., Cai, W., Yu, P., . . . Sun, Z. S. (2012). Mutations of ANK3 identified by exome sequencing are associated with autism susceptibility. *Hum Mutat, 33*(12), 1635-1638. 10.1002/humu.22174

Bolduc, F. V., & Tully, T. (2009). Fruit flies and intellectual disability. *Fly, 3*(1), 91-104. 10.4161/fly.3.1.7812

Bolger, T. A., Zhao, X., Cohen, T. J., Tsai, C.-C., & Yao, T.-P. (2007). The Neurodegenerative Disease Protein Ataxin-1 Antagonizes the Neuronal Survival Function of Myocyte Enhancer Factor-2*. *Journal of Biological Chemistry, 282*(40), 29186-29192. https://doi.org/10.1074/jbc.M704182200

Borghi, S., Molinari, S., Razzini, G., Parise, F., Battini, R., & Ferrari, S. (2001). The nuclear localization domain of the MEF2 family of transcription factors shows member-specific features and mediates the nuclear import of histone deacetylase 4. *J Cell Sci, 114*(Pt 24), 4477-4483.

Borrelli, E., Nestler, E. J., Allis, C. D., & Sassone-Corsi, P. (2008). Decoding the epigenetic language of neuronal plasticity. *Neuron, 60*(6), 961-974. 10.1016/j.neuron.2008.10.012

Bottomley, M. J., Lo Surdo, P., Di Giovine, P., Cirillo, A., Scarpelli, R., Ferrigno, F., . . . Carfi, A. (2008). Structural and functional analysis of the human HDAC4 catalytic domain reveals a regulatory structural zinc-binding domain. *J Biol Chem, 283*(39), 26694-26704. 10.1074/jbc.M803514200

Bozza, P. T., & Viola, J. P. (2010). Lipid droplets in inflammation and cancer. *Prostaglandins Leukot Essent Fatty Acids, 82*(4-6), 243-250. 10.1016/j.plefa.2010.02.005

Brand, A. H., & Perrimon, N. (1993). Targeted gene expression as a means of altering cell fates and generating dominant phenotypes. *Development, 118*(2), 401-415.

Brandl, A., Heinzel, T., & Kramer, O. H. (2009). Histone deacetylases: salesmen and customers in the post-translational modification market. *Biol Cell, 101*(4), 193-205. 10.1042/bc20080158

Broide, R. S., Redwine, J. M., Aftahi, N., Young, W., Bloom, F. E., & Winrow, C. J. (2007). Distribution of histone deacetylases 1-11 in the rat brain. *J Mol Neurosci, 31*(1), 47-58.

Bruserud, O., Stapnes, C., Ersvaer, E., Gjertsen, B. T., & Ryningen, A. (2007). Histone deacetylase inhibitors in cancer treatment: a review of the clinical toxicity and the modulation of gene expression in cancer cell. *Curr Pharm Biotechnol, 8*(6), 388-400.

Buch, S., Melcher, C., Bauer, M., Katzenberger, J., & Pankratz, M. J. (2008). Opposing Effects of Dietary Protein and Sugar Regulate a Transcriptional Target of Drosophila Insulin-like Peptide Signaling. *Cell Metabolism, 7*(4), 321-332. https://doi.org/10.1016/j.cmet.2008.02.012

Burli, R. W., Luckhurst, C. A., Aziz, O., Matthews, K. L., Yates, D., Lyons, K. A., . . . Dominguez, C. (2013). Design, synthesis, and biological evaluation of potent and selective class IIa histone deacetylase (HDAC) inhibitors as a potential therapy for Huntington's disease. *J Med Chem, 56*(24), 9934-9954. 10.1021/jm4011884

Busson, D., & Pret, A. M. (2007). GAL4/UAS targeted gene expression for studying Drosophila Hedgehog signaling. *Methods Mol Biol, 397*, 161-201. 10.1007/978-1-59745-516-9_13

Cabungcal, J.-H., Steullet, P., Morishita, H., Kraftsik, R., Cuenod, M., Hensch, T. K., & Do, K. Q. (2013). Perineuronal nets protect fast-spiking interneurons against oxidative stress. *Proceedings of the National Academy of Sciences, 110*(22), 9130. 10.1073/pnas.1300454110

Caldeira, M. V., Melo, C. V., Pereira, D. B., Carvalho, R., Correia, S. S., Backos, D. S., . . . Duarte, C. B. (2007). Brain-derived neurotrophic factor regulates the expression and synaptic delivery of alpha-amino-3-hydroxy-5-methyl-4-isoxazole propionic acid receptor subunits in hippocampal neurons. *J Biol Chem, 282*(17), 12619-12628. 10.1074/jbc.M700607200

Campbell, R. A. A., & Turner, G. C. (2010). The mushroom body. *Current Biology, 20*(1), R11-R12. https://doi.org/10.1016/j.cub.2009.10.031

Cao, J., Sun, L., Aramsangtienchai, P., Spiegelman, N. A., Zhang, X., Huang, W., . . . Lin, H. (2019). HDAC11 regulates type I interferon signaling through defatty-acylation of SHMT2. *Proceedings of the National Academy of Sciences, 116*(12), 5487. 10.1073/pnas.1815365116

Cao, W., Song, H. J., Gangi, T., Kelkar, A., Antani, I., Garza, D., & Konsolaki, M. (2008). Identification of novel genes that modify phenotypes induced by Alzheimer's beta-amyloid overexpression in Drosophila. *Genetics*, *178*(3), 1457-1471. 10.1534/genetics.107.078394

Caussinus, E., Kanca, O., & Affolter, M. (2011). Fluorescent fusion protein knockout mediated by anti-GFP nanobody. *Nat Struct Mol Biol*, *19*(1), 117-121. 10.1038/nsmb.2180

Champagne, F. A., & Curley, J. P. (2009). Epigenetic mechanisms mediating the long-term effects of maternal care on development. *Neurosci Biobehav Rev*, *33*(4), 593-600. 10.1016/j.neubiorev.2007.10.009

Chang, K. T., & Min, K. T. (2005). Drosophila melanogaster homolog of Down syndrome critical region 1 is critical for mitochondrial function. *Nat Neurosci*, *8*(11), 1577-1585. 10.1038/nn1564

Chang, S., Bezprozvannaya, S., Li, S., & Olson, E. N. (2005). An expression screen reveals modulators of class II histone deacetylase phosphorylation. *Proc Natl Acad Sci U S A*, *102*(23), 8120-8125. 10.1073/pnas.0503275102

Chatterjee, N., & Perrimon, N. (2021). What fuels the fly: Energy metabolism in Drosophila and its application to the study of obesity and diabetes. *Science Advances*, *7*(24), eabg4336. 10.1126/sciadv.abg4336

Chawla, S., Vanhoutte, P., Arnold, F. J. L., Huang, C. L. H., & Bading, H. (2003). Neuronal activity-dependent nucleocytoplasmic shuttling of HDAC4 and HDAC5. *Journal of Neurochemistry*, *85*(1), 151-159. 10.1046/j.1471-4159.2003.01648.x

Chen, B., & Cepko, C. L. (2009). HDAC4 regulates neuronal survival in normal and diseased retinas. *Science*, *323*(5911), 256-259. 10.1126/science.1166226

Chen, C.-C., Wu, J.-K., Lin, H.-W., Pai, T.-P., Fu, T.-F., Wu, C.-L., . . . Chiang, A.-S. (2012). Visualizing Long-Term Memory Formation in Two Neurons of the Drosophila Brain. *Science*, *335*(6069), 678-685. doi:10.1126/science.1212735

Cheng, H., Gang, X., Liu, Y., Wang, G., Zhao, X., & Wang, G. (2019). Mitochondrial dysfunction plays a key role in the development of neurodegenerative diseases in diabetes. *American Journal of Physiology-Endocrinology and Metabolism*, *318*(5), E750-E764. 10.1152/ajpendo.00179.2019

Cheng, Y., Endo, K., Wu, K., Rodan, A. R., Heberlein, U., & Davis, R. L. (2001). Drosophila fasciclinII Is Required for the Formation of Odor Memories and for Normal Sensitivity to Alcohol. *Cell*, *105*(6), 757-768. https://doi.org/10.1016/S0092-8674(01)00386-5

Chiang, H. C., Wang, L., Xie, Z., Yau, A., & Zhong, Y. (2010). PI3 kinase signaling is involved in Abeta-induced memory loss in Drosophila. *Proc Natl Acad Sci U S A, 107*(15), 7060-7065. 10.1073/pnas.0909314107

Chiaradonna, F., Cirulli, C., Palorini, R., Votta, G., & Alberghina, L. (2015). New Insights into the Connection Between Histone Deacetylases, Cell Metabolism, and Cancer. *Antioxidants & redox signaling, 23*(1), 30-50. 10.1089/ars.2014.5854

Cho, Richard W., Buhl, Lauren K., Volfson, D., Tran, A., Li, F., Akbergenova, Y., & Littleton, J. T. (2015). Phosphorylation of Complexin by PKA Regulates Activity-Dependent Spontaneous Neurotransmitter Release and Structural Synaptic Plasticity. *Neuron, 88*(4), 749-761. https://doi.org/10.1016/j.neuron.2015.10.011

Cho, Y., Griswold, A., Campbell, C., & Min, K. T. (2005). Individual histone deacetylases in Drosophila modulate transcription of distinct genes. *Genomics, 86*(5), 606-617. 10.1016/j.ygeno.2005.07.007

Chuang, D.-M., Leng, Y., Marinova, Z., Kim, H.-J., & Chiu, C.-T. (2009). Multiple roles of HDAC inhibition in neurodegenerative conditions. *Trends in neurosciences, 32*(11), 591-601. 10.1016/j.tins.2009.06.002

Cohen, S., & Greenberg, M. E. (2008). Communication between the synapse and the nucleus in neuronal development, plasticity, and disease. *Annu Rev Cell Dev Biol, 24*, 183-209. 10.1146/annurev.cellbio.24.110707.175235

Cohen, T. J., Barrientos, T., Hartman, Z. C., Garvey, S. M., Cox, G. A., & Yao, T. P. (2009). The deacetylase HDAC4 controls myocyte enhancing factor-2-dependent structural gene expression in response to neural activity. *Faseb j, 23*(1), 99-106. 10.1096/fj.08-115931

Cohen, T. J., Waddell, D. S., Barrientos, T., Lu, Z., Feng, G., Cox, G. A., . . . Yao, T. P. (2007). The histone deacetylase HDAC4 connects neural activity to muscle transcriptional reprogramming. *J Biol Chem, 282*(46), 33752-33759. 10.1074/jbc.M706268200

Colomb, J., Kaiser, L., Chabaud, M. A., & Preat, T. (2009). Parametric and genetic analysis of Drosophila appetitive long-term memory and sugar motivation. *Genes, Brain and Behavior, 8*(4), 407-415. https://doi.org/10.1111/j.1601-183X.2009.00482.x

Craig, T. J., & Henley, J. M. (2012). Protein SUMOylation in spine structure and function. *Curr Opin Neurobiol, 22*(3), 480-487. 10.1016/j.conb.2011.10.017

Crittenden, J. R., Skoulakis, E. M. C., Goldstein, E. S., & Davis, R. L. (2018). Drosophila mef2 is essential for normal mushroom body and wing development. *Biol Open, 7*(9) 10.1242/bio.035618

Cui, H., Kong, Y., & Zhang, H. (2012). Oxidative Stress, Mitochondrial Dysfunction, and Aging. *Journal of Signal Transduction, 2012*, 646354. 10.1155/2012/646354

Dalle-Donne, I., Rossi, R., Milzani, A., Di Simplicio, P., & Colombo, R. (2001). The actin cytoskeleton response to oxidants: from small heat shock protein phosphorylation to changes in the redox state of actin itself. *Free Radic Biol Med, 31*(12), 1624-1632. 10.1016/s0891-5849(01)00749-3

Dalman, M. R., Deeter, A., Nimishakavi, G., & Duan, Z.-H. (2012). Fold change and p-value cutoffs significantly alter microarray interpretations. *BMC Bioinformatics, 13*(2), S11. 10.1186/1471-2105-13-S2-S11

Darcy, M. J., Calvin, K., Cavnar, K., & Ouimet, C. C. (2010). Regional and subcellular distribution of HDAC4 in mouse brain. *J Comp Neurol, 518*(5), 722-740. 10.1002/cne.22241

Davis, F. J., Gupta, M., Camoretti-Mercado, B., Schwartz, R. J., & Gupta, M. P. (2003). Calcium/calmodulin-dependent protein kinase activates serum response factor transcription activity by its dissociation from histone deacetylase, HDAC4. Implications in cardiac muscle gene regulation during hypertrophy. *J Biol Chem, 278*(22), 20047-20058. 10.1074/jbc.M209998200

Day, J. J., & Sweatt, J. D. (2011). Epigenetic mechanisms in cognition. *Neuron, 70*(5), 813-829. 10.1016/j.neuron.2011.05.019

de la Asuncion, J. G., Millan, A., Pla, R., Bruseghini, L., Esteras, A., Pallardo, F. V., . . . Viña, J. (1996). Mitochondrial glutathione oxidation correlates with age-associated oxidative damage to mitochondrial DNA. *Faseb j, 10*(2), 333-338. 10.1096/fasebj.10.2.8641567

Dequiedt, F., Martin, M., Von Blume, J., Vertommen, D., Lecomte, E., Mari, N., . . . Kettmann, R. (2006). New role for hPar-1 kinases EMK and C-TAK1 in regulating localization and activity of class IIa histone deacetylases. *Mol Cell Biol, 26*(19), 7086-7102. 10.1128/mcb.00231-06

Didelot, G., Molinari, F., Tchénio, P., Comas, D., Milhiet, E., Munnich, A., . . . Preat, T. (2006). Tequila, a Neurotrypsin Ortholog, Regulates Long-Term Memory Formation in Drosophila</em&gt. *Science, 313*(5788), 851. 10.1126/science.1127215

Dietzl, G., Chen, D., Schnorrer, F., Su, K.-C., Barinova, Y., Fellner, M., . . . Dickson, B. J. (2007). A genome-wide transgenic RNAi library for conditional gene inactivation in Drosophila. *Nature, 448*(7150), 151-156. 10.1038/nature05954

Do, K. Q., Cuenod, M., & Hensch, T. K. (2015). Targeting Oxidative Stress and Aberrant Critical Period Plasticity in the Developmental Trajectory to Schizophrenia. *Schizophr Bull, 41*(4), 835-846. 10.1093/schbul/sbv065

Dompierre, J. P., Godin, J. D., Charrin, B. C., Cordelières, F. P., King, S. J., Humbert, S., & Saudou, F. (2007). Histone Deacetylase 6 Inhibition Compensates for the Transport Deficit in Huntington's Disease by Increasing Tubulin Acetylation. *The Journal of Neuroscience, 27*(13), 3571. 10.1523/JNEUROSCI.0037-07.2007

Drazic, A., Myklebust, L. M., Ree, R., & Arnesen, T. (2016). The world of protein acetylation. *Biochim Biophys Acta, 1864*(10), 1372-1401. 10.1016/j.bbapap.2016.06.007

Duffy, J. B. (2002). GAL4 system in Drosophila: a fly geneticist's Swiss army knife. *Genesis, 34*(1-2), 1-15. 10.1002/gene.10150

Dulac, C. (2010). Brain function and chromatin plasticity. *Nature, 465*, 728. 10.1038/nature09231

Edwards, T. N., & Meinertzhagen, I. A. (2010). The functional organisation of glia in the adult brain of Drosophila and other insects. *Prog Neurobiol, 90*(4), 471-497. 10.1016/j.pneurobio.2010.01.001

Enneking, E. M., Kudumala, S. R., Moreno, E., Stephan, R., Boerner, J., Godenschwege, T. A., & Pielage, J. (2013). Transsynaptic coordination of synaptic growth, function, and stability by the L1-type CAM Neuroglian. *PLoS Biol, 11*(4), e1001537. 10.1371/journal.pbio.1001537

Etkin, A., Alarcón, J. M., Weisberg, S. P., Touzani, K., Huang, Y. Y., Nordheim, A., & Kandel, E. R. (2006). A role in learning for SRF: deletion in the adult forebrain disrupts LTD and the formation of an immediate memory of a novel context. *Neuron, 50*(1), 127-143. 10.1016/j.neuron.2006.03.013

Ewert, J.-P. (2013). cAMP and Memory. In A. L. C. Runehov & L. Oviedo (Eds.), *Encyclopedia of Sciences and Religions* (pp. 305-305). Dordrecht: Springer Netherlands. 10.1007/978-1-4020-8265-8_200145

Federspiel, J. D., Greco, T. M., Lum, K. K., & Cristea, I. M. (2019). Hdac4 Interactions in Huntington's Disease Viewed Through the Prism of Multiomics. *Mol Cell Proteomics, 18*(8 suppl 1), S92-s113. 10.1074/mcp.RA118.001253

Fischle, W., Dequiedt, F., Hendzel, M. J., Guenther, M. G., Lazar, M. A., Voelter, W., & Verdin, E. (2002). Enzymatic activity associated with class II HDACs is dependent on a multiprotein complex containing HDAC3 and SMRT/N-CoR. *Mol Cell, 9*(1), 45-57.

Fitzsimons, H. L. (2015). The Class IIa histone deacetylase HDAC4 and neuronal function: Nuclear nuisance and cytoplasmic stalwart? *Neurobiol Learn Mem, 123*, 149-158. 10.1016/j.nlm.2015.06.006

Fitzsimons, H. L., Schwartz, S., Given, F. M., & Scott, M. J. (2013). The histone deacetylase HDAC4 regulates long-term memory in Drosophila. *PLoS One, 8*(12), e83903. 10.1371/journal.pone.0083903

Flavell, S. W., Cowan, C. W., Kim, T. K., Greer, P. L., Lin, Y., Paradis, S., . . . Greenberg, M. E. (2006). Activity-dependent regulation of MEF2 transcription factors suppresses excitatory synapse number. *Science, 311*(5763), 1008-1012. 10.1126/science.1122511

Fogarty, C. E., Diwanji, N., Lindblad, J. L., Tare, M., Amcheslavsky, A., Makhijani, K., . . . Bergmann, A. (2016). Extracellular Reactive Oxygen Species Drive Apoptosis-Induced Proliferation via Drosophila Macrophages. *Current biology : CB, 26*(5), 575-584. 10.1016/j.cub.2015.12.064

Freeman, M. (1996). Reiterative use of the EGF receptor triggers differentiation of all cell types in the Drosophila eye. *Cell, 87*(4), 651-660. 10.1016/s0092-8674(00)81385-9

Freymuth, P. S., & Fitzsimons, H. L. (2017). The ERM protein Moesin is essential for neuronal morphogenesis and long-term memory in Drosophila. *Mol Brain, 10*(1), 41. 10.1186/s13041-017-0322-y

Fushima, K., & Tsujimura, H. (2007). Precise control of fasciclin II expression is required for adult mushroom body development in Drosophila. *Dev Growth Differ, 49*(3), 215-227. 10.1111/j.1440-169X.2007.00922.x

Gao, L., Cueto, M. A., Asselbergs, F., & Atadja, P. (2002). Cloning and functional characterization of HDAC11, a novel member of the human histone deacetylase family. *J Biol Chem, 277*(28), 25748-25755. 10.1074/jbc.M111871200

Gee, H. Y., Zhang, F., Ashraf, S., Kohl, S., Sadowski, C. E., Vega-Warner, V., . . . Hildebrandt, F. (2015). KANK deficiency leads to podocyte dysfunction and nephrotic syndrome. *The Journal of clinical investigation, 125*(6), 2375-2384. 10.1172/JCI79504

Geng, H., Harvey, C. T., Pittsenbarger, J., Liu, Q., Beer, T. M., Xue, C., & Qian, D. Z. (2011). HDAC4 protein regulates HIF1α protein lysine acetylation and cancer cell response to hypoxia. *J Biol Chem, 286*(44), 38095-38102. 10.1074/jbc.M111.257055

Glozak, M. A., Sengupta, N., Zhang, X., & Seto, E. (2005). Acetylation and deacetylation of non-histone proteins. *Gene, 363*, 15-23. 10.1016/j.gene.2005.09.010

Gomez-Valades, A. G., Vidal-Alabro, A., Molas, M., Boada, J., Bermudez, J., Bartrons, R., & Perales, J. C. (2006). Overcoming diabetes-induced hyperglycemia through inhibition of hepatic phosphoenolpyruvate carboxykinase (GTP) with RNAi. *Mol Ther, 13*(2), 401-410. 10.1016/j.ymthe.2005.08.026

Gomez, T. M., & Letourneau, P. C. (2014). Actin dynamics in growth cone motility and navigation. *Journal of Neurochemistry, 129*(2), 221-234. 10.1111/jnc.12506

Govindarajan, N., Rao, P., Burkhardt, S., Sananbenesi, F., Schlüter, O. M., Bradke, F., . . . Fischer, A. (2013). Reducing HDAC6 ameliorates cognitive deficits in a mouse model for Alzheimer's disease. *EMBO Mol Med, 5*(1), 52-63. 10.1002/emmm.201201923

Gräff, J., Rei, D., Guan, J.-S., Wang, W.-Y., Seo, J., Hennig, K. M., . . . Tsai, L.-H. (2012). An epigenetic blockade of cognitive functions in the neurodegenerating brain. *Nature, 483*(7388), 222-226. 10.1038/nature10849

Greer, P. L., & Greenberg, M. E. (2008). From synapse to nucleus: calcium-dependent gene transcription in the control of synapse development and function. *Neuron, 59*(6), 846-860. 10.1016/j.neuron.2008.09.002

Gregoire, S., & Yang, X. J. (2005). Association with class IIa histone deacetylases upregulates the sumoylation of MEF2 transcription factors. *Mol Cell Biol, 25*(6), 2273-2287. 10.1128/MCB.25.6.2273-2287.2005

Groth, A. C., Fish, M., Nusse, R., & Calos, M. P. (2004). Construction of transgenic Drosophila by using the site-specific integrase from phage phiC31. *Genetics, 166*(4), 1775-1782. 10.1534/genetics.166.4.1775

Guan, J. S., Haggarty, S. J., Giacometti, E., Dannenberg, J. H., Joseph, N., Gao, J., . . . Tsai, L. H. (2009). HDAC2 negatively regulates memory formation and synaptic plasticity. *Nature, 459*(7243), 55-60. 10.1038/nature07925

Guo, L., Han, A., Bates, D. L., Cao, J., & Chen, L. (2007). Crystal structure of a conserved N-terminal domain of histone deacetylase 4 reveals functional insights into glutamine-rich domains. *Proceedings of the National Academy of Sciences, 104*(11), 4297.

Haberland, M., Montgomery, R. L., & Olson, E. N. (2009). The many roles of histone deacetylases in development and physiology: implications for disease and therapy. *Nat Rev Genet, 10*(1), 32-42. 10.1038/nrg2485

Han, R., Liang, J., & Zhou, B. (2021). Glucose Metabolic Dysfunction in Neurodegenerative Diseases-New Mechanistic Insights and the Potential of Hypoxia as a Prospective Therapy Targeting Metabolic Reprogramming. *International journal of molecular sciences, 22*(11) 10.3390/ijms22115887

Harrington, A. J., Raissi, A., Rajkovich, K., Berto, S., Kumar, J., Molinaro, G., . . . Cowan, C. W. (2016). MEF2C regulates cortical inhibitory and excitatory synapses and behaviors relevant to neurodevelopmental disorders. *eLife, 5* 10.7554/eLife.20059

Hashemi, E., Ariza, J., Rogers, H., Noctor, S. C., & Martínez-Cerdeño, V. (2017). The Number of Parvalbumin-Expressing Interneurons Is Decreased in the Prefrontal Cortex in Autism. *Cereb Cortex, 27*(3), 1931-1943. 10.1093/cercor/bhw021

Hattori, D., Demir, E., Kim, H. W., Viragh, E., Zipursky, S. L., & Dickson, B. J. (2007). Dscam diversity is essential for neuronal wiring and self-recognition. *Nature, 449*(7159), 223-227. 10.1038/nature06099

Hawkins, R. D., Kandel, E. R., & Bailey, C. H. (2006). Molecular mechanisms of memory storage in Aplysia. *Biol Bull, 210*(3), 174-191. 10.2307/4134556

Heger, D. A. (2015). *An Introduction to Artificial Neural Networks (ANN)-Methods , Abstraction , and Usage*.

Hiona, A., & Leeuwenburgh, C. (2008). The role of mitochondrial DNA mutations in aging and sarcopenia: implications for the mitochondrial vicious cycle theory of aging. *Exp Gerontol, 43*(1), 24-33. 10.1016/j.exger.2007.10.001

Hobara, T., Uchida, S., Otsuki, K., Matsubara, T., Funato, H., Matsuo, K., . . . Watanabe, Y. (2010). Altered gene expression of histone deacetylases in mood disorder patients. *J Psychiatr Res, 44*(5), 263-270. 10.1016/j.jpsychires.2009.08.015

Hoshino, M., Tagawa, K., Okuda, T., Murata, M., Oyanagi, K., Arai, N., . . . Okazawa, H. (2003). Histone deacetylase activity is retained in primary neurons expressing mutant huntingtin protein. *J Neurochem, 87*(1), 257-267. 10.1046/j.1471-4159.2003.01991.x

Houten, S. M., & Wanders, R. J. A. (2010). A general introduction to the biochemistry of mitochondrial fatty acid β-oxidation. *Journal of inherited metabolic disease, 33*(5), 469-477. 10.1007/s10545-010-9061-2

Huang, C.-W., Wang, H.-D., Bai, H., Wu, M.-S., Yen, J.-H., Tatar, M., . . . Wang, P.-Y. (2015). Tequila Regulates Insulin-Like Signaling and Extends Life Span in Drosophila melanogaster. *The Journals of Gerontology: Series A, 70*(12), 1461-1469. 10.1093/gerona/glv094

Huang, Y., Wan, Z., Wang, Z., & Zhou, B. (2019). Insulin signaling in Drosophila melanogaster mediates Aβ toxicity. *Communications Biology, 2*(1), 13. 10.1038/s42003-018-0253-x

Iga, J., Ueno, S., Yamauchi, K., Numata, S., Kinouchi, S., Tayoshi-Shibuya, S., . . . Ohmori, T. (2007). Altered HDAC5 and CREB mRNA expressions in the peripheral leukocytes of major depression. *Prog Neuropsychopharmacol Biol Psychiatry, 31*(3), 628-632. 10.1016/j.pnpbp.2006.12.014

Janson, J., Laedtke, T., Parisi, J. E., O'Brien, P., Petersen, R. C., & Butler, P. C. (2004). Increased Risk of Type 2 Diabetes in Alzheimer Disease. *Diabetes, 53*(2), 474-481. 10.2337/diabetes.53.2.474

Jayathilaka, N., Han, A., Gaffney, K. J., Dey, R., Jarusiewicz, J. A., Noridomi, K., . . . Chen, L. (2012). Inhibition of the function of class IIa HDACs by blocking their interaction with MEF2. *Nucleic Acids Res, 40*(12), 5378-5388. 10.1093/nar/gks189

Jia, H., Wang, Y., Morris, C. D., Jacques, V., Gottesfeld, J. M., Rusche, J. R., & Thomas, E. A. (2016). The Effects of Pharmacological Inhibition of Histone Deacetylase 3 (HDAC3) in Huntington's Disease Mice. *PLoS One, 11*(3), e0152498. 10.1371/journal.pone.0152498

Jiang, L., Schlesinger, F., Davis, C. A., Zhang, Y., Li, R., Salit, M., . . . Oliver, B. (2011). Synthetic spike-in standards for RNA-seq experiments. *Genome Res, 21*(9), 1543-1551. 10.1101/gr.121095.111

Josling, G. A., Selvarajah, S. A., Petter, M., & Duffy, M. F. (2012). The role of bromodomain proteins in regulating gene expression. *Genes, 3*(2), 320-343. 10.3390/genes3020320

Kandel, E. R. (2001). The molecular biology of memory storage: a dialogue between genes and synapses. *Science, 294*(5544), 1030-1038. 10.1126/science.1067020

Kandel, E. R. (2012). The molecular biology of memory: cAMP, PKA, CRE, CREB-1, CREB-2, and CPEB. *Mol Brain, 5*(1), 14. 10.1186/1756-6606-5-14

Kandel, E. R., Schwartz, J. H., & Jessell, T. M. (2000). *Principles of neural science* (4th Edition ed.). Health Professions Division: New York: McGraw-Hill.

Kastaniotis, A. J., Autio, K. J., Kerätär, J. M., Monteuuis, G., Mäkelä, A. M., Nair, R. R., . . . Hiltunen, J. K. (2017). Mitochondrial fatty acid synthesis, fatty acids and mitochondrial physiology. *Biochimica et Biophysica Acta (BBA) - Molecular and Cell Biology of Lipids, 1862*(1), 39-48. https://doi.org/10.1016/j.bbalip.2016.08.011

Kausar, S., Wang, F., & Cui, H. (2018). The Role of Mitochondria in Reactive Oxygen Species Generation and Its Implications for Neurodegenerative Diseases. *Cells, 7*(12), 274. 10.3390/cells7120274

Kelly, S. M., Elchert, A., & Kahl, M. (2017). Dissection and Immunofluorescent Staining of Mushroom Body and Photoreceptor Neurons in Adult Drosophila melanogaster Brains. *Journal of visualized experiments : JoVE*(129), 56174. 10.3791/56174

Kemp, S., Valianpour, F., Denis, S., Ofman, R., Sanders, R. J., Mooyer, P., . . . Wanders, R. J. (2005). Elongation of very long-chain fatty acids is enhanced in X-linked

adrenoleukodystrophy. *Mol Genet Metab, 84*(2), 144-151. 10.1016/j.ymgme.2004.09.015

Kerrigan, J. F., Aleck, K. A., Tarby, T. J., Bird, C. R., & Heidenreich, R. A. (2000). Fumaric aciduria: Clinical and imaging features. *Annals of Neurology, 47*(5), 583-588. https://doi.org/10.1002/1531-8249(200005)47:5<583::AID-ANA5>3.0.CO;2-Y

Kim, M. S., Akhtar, M. W., Adachi, M., Mahgoub, M., Bassel-Duby, R., Kavalali, E. T., . . . Monteggia, L. M. (2012). An essential role for histone deacetylase 4 in synaptic plasticity and memory formation. *J Neurosci, 32*(32), 10879-10886. 10.1523/JNEUROSCI.2089-12.2012

Kim, S., Kim, J., Park, S., Park, J.-J., & Lee, S. (2021). Drosophila Graf regulates mushroom body β-axon extension and olfactory long-term memory. *Mol Brain, 14*(1), 73. 10.1186/s13041-021-00782-x

Kim, Y. Z. (2014). Altered histone modifications in gliomas. *Brain tumor research and treatment, 2*(1), 7-21. 10.14791/btrt.2014.2.1.7

King, I., Tsai, L. T. Y., Pflanz, R., Voigt, A., Lee, S., Jäckle, H., . . . Heberlein, U. (2011). Drosophila tao controls mushroom body development and ethanol-stimulated behavior through par-1. *The Journal of neuroscience : the official journal of the Society for Neuroscience, 31*(3), 1139-1148. 10.1523/JNEUROSCI.4416-10.2011

Kong, Q., Hao, Y., Li, X., Wang, X., Ji, B., & Wu, Y. (2018). HDAC4 in ischemic stroke: mechanisms and therapeutic potential. *Clin Epigenetics, 10*(1), 117. 10.1186/s13148-018-0549-1

Korzus, E., Rosenfeld, M. G., & Mayford, M. (2004). CBP histone acetyltransferase activity is a critical component of memory consolidation. *Neuron, 42*(6), 961-972. 10.1016/j.neuron.2004.06.002

Kottler, B., & van Swinderen, B. (2014). Taking a new look at how flies learn. *eLife, 3*, e03978. 10.7554/eLife.03978

Kristiansen, L. V., Velasquez, E., Romani, S., Baars, S., Berezin, V., Bock, E., . . . Garcia-Alonso, L. (2005). Genetic analysis of an overlapping functional requirement for L1- and NCAM-type proteins during sensory axon guidance in Drosophila. *Molecular and Cellular Neuroscience, 28*(1), 141-152. https://doi.org/10.1016/j.mcn.2004.09.003

Kujoth, G. C., Hiona, A., Pugh, T. D., Someya, S., Panzer, K., Wohlgemuth, S. E., . . . Prolla, T. A. (2005). Mitochondrial DNA mutations, oxidative stress, and apoptosis in mammalian aging. *Science, 309*(5733), 481-484. 10.1126/science.1112125

Kunte, A. S., Matthews, K. A., & Rawson, R. B. (2006). Fatty acid auxotrophy in Drosophila larvae lacking SREBP. *Cell Metab, 3*(6), 439-448. 10.1016/j.cmet.2006.04.011

Kurusu, M., Awasaki, T., Masuda-Nakagawa, L. M., Kawauchi, H., Ito, K., & Furukubo-Tokunaga, K. (2002). Embryonic and larval development of the Drosophila mushroom bodies: concentric layer subdivisions and the role of fasciclin II. *Development, 129*(2), 409-419. 10.1242/dev.129.2.409

Lahm, A., Paolini, C., Pallaoro, M., Nardi, M. C., Jones, P., Neddermann, P., . . . Gallinari, P. (2007). Unraveling the hidden catalytic activity of vertebrate class IIa histone deacetylases. *Proceedings of the National Academy of Sciences of the United States of America, 104*(44), 17335-17340. 10.1073/pnas.0706487104

Larkin, A., Marygold, S. J., Antonazzo, G., Attrill, H., dos Santos, G., Garapati, P. V., . . . Consortium, F. (2020). FlyBase: updates to the Drosophila melanogaster knowledge base. *Nucleic Acids Research, 49*(D1), D899-D907. 10.1093/nar/gkaa1026

Le, T. N., Williams, S. R., Alaimo, J. T., & Elsea, S. H. (2019). Genotype and phenotype correlation in 103 individuals with 2q37 deletion syndrome reveals incomplete penetrance and supports HDAC4 as the primary genetic contributor. *Am J Med Genet A, 179*(5), 782-791. 10.1002/ajmg.a.61089

Lee, P. T., Zirin, J., Kanca, O., Lin, W.-W., Schulze, K. L., Li-Kroeger, D., . . . Bellen, H. J. (2018). A gene-specific T2A-GAL4 library for Drosophila. *eLife, 7*, e35574. 10.7554/eLife.35574

Lee, T., Lee, A., & Luo, L. (1999). Development of the Drosophila mushroom bodies: sequential generation of three distinct types of neurons from a neuroblast. *Development, 126*(18), 4065-4076.

Levenson, J. M., O'Riordan, K. J., Brown, K. D., Trinh, M. A., Molfese, D. L., & Sweatt, J. D. (2004). Regulation of histone acetylation during memory formation in the hippocampus. *J Biol Chem, 279*(39), 40545-40559. 10.1074/jbc.M402229200

Li, F., Lindsey, J. W., Marin, E. C., Otto, N., Dreher, M., Dempsey, G., . . . Rubin, G. M. (2020). The connectome of the adult Drosophila mushroom body provides insights into function. *eLife, 9*, e62576. 10.7554/eLife.62576

Li, J., Chen, J., Ricupero, C. L., Hart, R. P., Schwartz, M. S., Kusnecov, A., & Herrup, K. (2012). Nuclear accumulation of HDAC4 in ATM deficiency promotes neurodegeneration in ataxia telangiectasia. *Nat Med, 18*(5), 783-790. 10.1038/nm.2709

Li, J., Ding, Y., & Zheng, L. (2014). Chapter 9 - Histone-Mediated Transgenerational Epigenetics. In T. Tollefsbol (Ed.), *Transgenerational Epigenetics* (pp. 87-103). Oxford: Academic Press. https://doi.org/10.1016/B978-0-12-405944-3.00009-X

Li, W. Z., Li, S. L., Zheng, H. Y., Zhang, S. P., & Xue, L. (2012). A broad expression profile of the GMR-GAL4 driver in Drosophila melanogaster. *Genet Mol Res, 11*(3), 1997-2002. 10.4238/2012.August.6.4

Lin, D. M., Fetter, R. D., Kopczynski, C., Grenningloh, G., & Goodman, C. S. (1994). Genetic analysis of Fasciclin II in Drosophila: defasciculation, refasciculation, and altered fasciculation. *Neuron, 13*(5), 1055-1069. 10.1016/0896-6273(94)90045-0

Liu, L., MacKenzie, K. R., Putluri, N., Maletić-Savatić, M., & Bellen, H. J. (2017). The Glia-Neuron Lactate Shuttle and Elevated ROS Promote Lipid Synthesis in Neurons and Lipid Droplet Accumulation in Glia via APOE/D. *Cell Metabolism, 26*(5), 719-737.e716. https://doi.org/10.1016/j.cmet.2017.08.024

Liu, L., Zhang, K., Sandoval, H., Yamamoto, S., Jaiswal, M., Sanz, E., . . . Bellen, H. J. (2015). Glial lipid droplets and ROS induced by mitochondrial defects promote neurodegeneration. *Cell, 160*(1-2), 177-190. 10.1016/j.cell.2014.12.019

Liu, S. S., Wu, F., Jin, Y. M., Chang, W. Q., & Xu, T.-M. (2020). HDAC11: a rising star in epigenetics. *Biomedicine & Pharmacotherapy, 131*, 110607. https://doi.org/10.1016/j.biopha.2020.110607

Liu, Y., Peng, L., Seto, E., Huang, S., & Qiu, Y. (2012). Modulation of histone deacetylase 6 (HDAC6) nuclear import and tubulin deacetylase activity through acetylation. *The Journal of biological chemistry, 287*(34), 29168-29174. 10.1074/jbc.M112.371120

Loriol, C., Khayachi, A., Poupon, G., Gwizdek, C., & Martin, S. (2013). Activity-dependent regulation of the sumoylation machinery in rat hippocampal neurons. *Biol Cell, 105*(1), 30-45. 10.1111/boc.201200016

Lu, J., McKinsey, T. A., Zhang, C. L., & Olson, E. N. (2000). Regulation of skeletal myogenesis by association of the MEF2 transcription factor with class II histone deacetylases. *Mol Cell, 6*(2), 233-244.

Luan, H., Peabody, N. C., Vinson, C. R., & White, B. H. (2006). Refined spatial manipulation of neuronal function by combinatorial restriction of transgene expression. *Neuron, 52*(3), 425-436. 10.1016/j.neuron.2006.08.028

Lubin, F. D., Roth, T. L., & Sweatt, J. D. (2008). Epigenetic regulation of BDNF gene transcription in the consolidation of fear memory. *J Neurosci, 28*(42), 10576-10586. 10.1523/jneurosci.1786-08.2008

Maddox, S. A., Kilaru, V., Shin, J., Jovanovic, T., Almli, L. M., Dias, B. G., . . . Smith, A. K. (2018). Estrogen-dependent association of HDAC4 with fear in female mice and women with PTSD. *Mol Psychiatry, 23*(3), 658-665. 10.1038/mp.2016.250

Main, P., Tan, W. J., Wheeler, D., & Fitzsimons, H. L. (2021). Increased Abundance of Nuclear HDAC4 Impairs Neuronal Development and Long-Term Memory. *Front Mol Neurosci, 14*(48) 10.3389/fnmol.2021.616642

Maness, P. F., & Schachner, M. (2007). Neural recognition molecules of the immunoglobulin superfamily: signaling transducers of axon guidance and neuronal migration. *Nat Neurosci, 10*(1), 19-26. 10.1038/nn1827

Martin, M., Kettmann, R., & Dequiedt, F. (2007). Class IIa histone deacetylases: regulating the regulators. *Oncogene, 26*(37), 5450-5467. 10.1038/sj.onc.1210613

Martin, M., Potente, M., Janssens, V., Vertommen, D., Twizere, J. C., Rider, M. H., . . . Dequiedt, F. (2008). Protein phosphatase 2A controls the activity of histone deacetylase 7 during T cell apoptosis and angiogenesis. *Proc Natl Acad Sci U S A, 105*(12), 4727-4732. 10.1073/pnas.0708455105

Martin, S., Wilkinson, K. A., Nishimune, A., & Henley, J. M. (2007). Emerging extranuclear roles of protein SUMOylation in neuronal function and dysfunction. *Nat Rev Neurosci, 8*(12), 948-959. 10.1038/nrn2276

Martínez-Reyes, I., & Chandel, N. S. (2020). Mitochondrial TCA cycle metabolites control physiology and disease. *Nature Communications, 11*(1), 102. 10.1038/s41467-019-13668-3

McBride, S. M., Giuliani, G., Choi, C., Krause, P., Correale, D., Watson, K., . . . Siwicki, K. K. (1999). Mushroom body ablation impairs short-term memory and long-term memory of courtship conditioning in Drosophila melanogaster. *Neuron, 24*(4), 967-977.

McGuire, S. E., Deshazer, M., & Davis, R. L. (2005). Thirty years of olfactory learning and memory research in Drosophila melanogaster. *Prog Neurobiol, 76*(5), 328-347. 10.1016/j.pneurobio.2005.09.003

McGuire, S. E., Le, P. T., Osborn, A. J., Matsumoto, K., & Davis, R. L. (2003). Spatiotemporal rescue of memory dysfunction in Drosophila. *Science, 302*(5651), 1765-1768. 10.1126/science.1089035

McGuire, S. E., Mao, Z., & Davis, R. L. (2004). Spatiotemporal gene expression targeting with the TARGET and gene-switch systems in Drosophila. *Sci STKE, 2004*(220), pl6. 10.1126/stke.2202004pl6

McKinsey, T. A., Kuwahara, K., Bezprozvannaya, S., & Olson, E. N. (2006). Class II histone deacetylases confer signal responsiveness to the ankyrin-repeat proteins

ANKRA2 and RFXANK. *Mol Biol Cell, 17*(1), 438-447. 10.1091/mbc.e05-07-0612

McKinsey, T. A., Zhang, C. L., & Olson, E. N. (2000). Activation of the myocyte enhancer factor-2 transcription factor by calcium/calmodulin-dependent protein kinase-stimulated binding of 14-3-3 to histone deacetylase 5. *Proceedings of the National Academy of Sciences of the United States of America, 97*(26), 14400-14405. 10.1073/pnas.260501497

McKinsey, T. A., Zhang, C. L., & Olson, E. N. (2001). Identification of a Signal-Responsive Nuclear Export Sequence in Class II Histone Deacetylases. *Molecular and Cellular Biology, 21*(18), 6312-6321. 10.1128/mcb.21.18.6312-6321.2001

McKinsey, T. A., Zhang, C. L., & Olson, E. N. (2002). MEF2: a calcium-dependent regulator of cell division, differentiation and death. *Trends Biochem Sci, 27*(1), 40-47.

McQuown, S. C., Barrett, R. M., Matheos, D. P., Post, R. J., Rogge, G. A., Alenghat, T., . . . Wood, M. A. (2011). HDAC3 is a critical negative regulator of long-term memory formation. *J Neurosci, 31*(2), 764-774. 10.1523/JNEUROSCI.5052-10.2011

Mecocci, P., Macgarvey, U., Kaufman, A. E., Koontz, D. A., Shoffner, J. M., Wallace, D. C., & Beal, M. F. (1993). Oxidative damage to mitochondrial DNA shows marked ag… dependent increases in human brain. *Annals of Neurology, 34*

Méndez-Lucas, A., Duarte, J. A. G., Sunny, N. E., Satapati, S., He, T., Fu, X., . . . Perales, J. C. (2013). PEPCK-M expression in mouse liver potentiates, not replaces, PEPCK-C mediated gluconeogenesis. *Journal of hepatology, 59*(1), 105-113. 10.1016/j.jhep.2013.02.020

Méndez-Lucas, A., Hyroššová, P., Novellasdemunt, L., Viñals, F., & Perales, J. C. (2014). Mitochondrial phosphoenolpyruvate carboxykinase (PEPCK-M) is a pro-survival, endoplasmic reticulum (ER) stress response gene involved in tumor cell adaptation to nutrient availability. *The Journal of biological chemistry, 289*(32), 22090-22102. 10.1074/jbc.M114.566927

Mergenthaler, P., Lindauer, U., Dienel, G. A., & Meisel, A. (2013). Sugar for the brain: the role of glucose in physiological and pathological brain function. *Trends in neurosciences, 36*(10), 587-597. 10.1016/j.tins.2013.07.001

Michel, C. I., Kraft, R., & Restifo, L. L. (2004). Defective neuronal development in the mushroom bodies of Drosophila fragile X mental retardation 1 mutants. *J Neurosci, 24*(25), 5798-5809. 10.1523/jneurosci.1102-04.2004

Mielcarek, M., Landles, C., Weiss, A., Bradaia, A., Seredenina, T., Inuabasi, L., . . . Bates, G. P. (2013). HDAC4 reduction: a novel therapeutic strategy to target cytoplasmic

huntingtin and ameliorate neurodegeneration. *PLoS Biol, 11*(11), e1001717. 10.1371/journal.pbio.1001717

Mihaylova, M. M., Vasquez, D. S., Ravnskjaer, K., Denechaud, P. D., Yu, R. T., Alvarez, J. G., . . . Shaw, R. J. (2011). Class IIa histone deacetylases are hormone-activated regulators of FOXO and mammalian glucose homeostasis. *Cell, 145*(4), 607-621. 10.1016/j.cell.2011.03.043

Miksys, S. L., & Tyndale, R. F. (2002). Drug-metabolizing cytochrome P450s in the brain. *Journal of psychiatry & neuroscience : JPN, 27*(6), 406-415.

Miller, C. A., & Sweatt, J. D. (2007). Covalent modification of DNA regulates memory formation. *Neuron, 53*(6), 857-869. 10.1016/j.neuron.2007.02.022

Miska, E. A., Karlsson, C., Langley, E., Nielsen, S. J., Pines, J., & Kouzarides, T. (1999). HDAC4 deacetylase associates with and represses the MEF2 transcription factor. *The EMBO Journal, 18*(18), 5099-5107. 10.1093/emboj/18.18.5099

Miska, E. A., Langley, E., Wolf, D., Karlsson, C., Pines, J., & Kouzarides, T. (2001). Differential localization of HDAC4 orchestrates muscle differentiation. *Nucleic Acids Research, 29*(16), 3439-3447. 10.1093/nar/29.16.3439

Mohler, P. J., Gramolini, A. O., & Bennett, V. (2002). The ankyrin-B C-terminal domain determines activity of ankyrin-B/G chimeras in rescue of abnormal inositol 1,4,5-trisphosphate and ryanodine receptor distribution in ankyrin-B (-/-) neonatal cardiomyocytes. *J Biol Chem, 277*(12), 10599-10607. 10.1074/jbc.M110958200

Molinari, F., Rio, M., Meskenaite, V., Encha-Razavi, F., Augé, J., Bacq, D., . . . Colleaux, L. (2002). Truncating Neurotrypsin Mutation in Autosomal Recessive Nonsyndromic Mental Retardation. *Science, 298*(5599), 1779-1781. 10.1126/science.1076521

Moreira, P. I., Santos, M. S., Moreno, A. n. M., Seiça, R., & Oliveira, C. R. (2003). Increased Vulnerability of Brain Mitochondria in Diabetic (Goto-Kakizaki) Rats With Aging and Amyloid-β Exposure. *Diabetes, 52*(6), 1449-1456. 10.2337/diabetes.52.6.1449

Morris, B., Etoubleau, C., Bourthoumieu, S., Reynaud-Perrine, S., Laroche, C., Lebbar, A., . . . Elsea, S. H. (2012). Dose dependent expression of HDAC4 causes variable expressivity in a novel inherited case of brachydactyly mental retardation syndrome. *Am J Med Genet A, 158A*(8), 2015-2020. 10.1002/ajmg.a.35463

Morris, M. J., & Monteggia, L. M. (2013). Unique functional roles for class I and class II histone deacetylases in central nervous system development and function. *Int J Dev Neurosci, 31*(6), 370-381. 10.1016/j.ijdevneu.2013.02.005

Morrison, B. E., Majdzadeh, N., & D'Mello, S. R. (2007). Histone deacetylases: focus on the nervous system. *Cell Mol Life Sci, 64*(17), 2258-2269. 10.1007/s00018-007-7035-9

Mucha, A., Drag, M., Dalton, J. P., & Kafarski, P. (2010). Metallo-aminopeptidase inhibitors. *Biochimie, 92*(11), 1509-1529. 10.1016/j.biochi.2010.04.026

Murphy, D. J. (2001). The biogenesis and functions of lipid bodies in animals, plants and microorganisms. *Prog Lipid Res, 40*(5), 325-438. 10.1016/s0163-7827(01)00013-3

Murphy, M. P., & LeVine, H., 3rd. (2010). Alzheimer's disease and the amyloid-beta peptide. *J Alzheimers Dis, 19*(1), 311-323. 10.3233/JAD-2010-1221

Nardone, S., Sams, D. S., Reuveni, E., Getselter, D., Oron, O., Karpuj, M., & Elliott, E. (2014). DNA methylation analysis of the autistic brain reveals multiple dysregulated biological pathways. *Transl Psychiatry, 4*, e433. 10.1038/tp.2014.70

Nemani, N., Dong, Z., Daw, C. C., Madaris, T. R., Ramachandran, K., Enslow, B. T., . . . Madesh, M. (2020). Mitochondrial pyruvate and fatty acid flux modulate MICU1-dependent control of MCU activity. *Science signaling, 13*(628), eaaz6206. 10.1126/scisignal.aaz6206

Nériec, N., & Desplan, C. (2016). From the Eye to the Brain: Development of the Drosophila Visual System. *Curr Top Dev Biol, 116*, 247-271. 10.1016/bs.ctdb.2015.11.032

New Zealand framework for dementia care. (2013). Wellington: Ministry of Health.

Ortega-Martínez, S. (2015). A new perspective on the role of the CREB family of transcription factors in memory consolidation via adult hippocampal neurogenesis. *Front Mol Neurosci, 8*(46) 10.3389/fnmol.2015.00046

Oswald, M. C. W., Garnham, N., Sweeney, S. T., & Landgraf, M. (2018). Regulation of neuronal development and function by ROS. *FEBS letters, 592*(5), 679-691. 10.1002/1873-3468.12972

Our Annual Story: The 2017 Report of Alzheimers NZ. (2017). (Vol. 2018). Alzheimers New Zealand: Alzheimers New Zealand.

Oyarzábal, A., Musokhranova, U., Barros, L., & García-Cazorla, A. (2021). Energy metabolism in childhood neurodevelopmental disorders. *EBioMedicine, 69*, 103474. 10.1016/j.ebiom.2021.103474

Pang, P. T., & Lu, B. (2004). Regulation of late-phase LTP and long-term memory in normal and aging hippocampus: role of secreted proteins tPA and BDNF. *Ageing Research Reviews, 3*(4), 407-430. https://doi.org/10.1016/j.arr.2004.07.002

Park, S.-Y., & Kim, J.-S. (2020). A short guide to histone deacetylases including recent progress on class II enzymes. *Experimental & Molecular Medicine, 52*(2), 204-212. 10.1038/s12276-020-0382-4

Paroni, G., Cernotta, N., Dello Russo, C., Gallinari, P., Pallaoro, M., Foti, C., . . . Brancolini, C. (2008). PP2A regulates HDAC4 nuclear import. *Mol Biol Cell, 19*(2), 655-667. 10.1091/mbc.e07-06-0623

Paroni, G., Mizzau, M., Henderson, C., Del Sal, G., Schneider, C., & Brancolini, C. (2004). Caspase-dependent Regulation of Histone Deacetylase 4 Nuclear-Cytoplasmic Shuttling Promotes Apoptosis. *Molecular Biology of the Cell, 15*(6), 2804-2818. 10.1091/mbc.e03-08-0624

Patterson, C. (2018). *World Alzheimer Report 2018 - The state of the art of dementia research: New frontiers*: Alzheimer's Disease International.

Peixoto, L., & Abel, T. (2013). The role of histone acetylation in memory formation and cognitive impairments. *Neuropsychopharmacology, 38*(1), 62-76. 10.1038/npp.2012.86

Petronis, A. (2010). Epigenetics as a unifying principle in the aetiology of complex traits and diseases. *Nature, 465*, 721. 10.1038/nature09230

Pielage, J., Cheng, L., Fetter, R. D., Carlton, P. M., Sedat, J. W., & Davis, G. W. (2008). A presynaptic giant ankyrin stabilizes the NMJ through regulation of presynaptic microtubules and transsynaptic cell adhesion. *Neuron, 58*(2), 195-209. 10.1016/j.neuron.2008.02.017

Pigna, E., Simonazzi, E., Sanna, K., Bernadzki, K. M., Proszynski, T., Heil, C., . . . Moresi, V. (2019). Histone deacetylase 4 protects from denervation and skeletal muscle atrophy in a murine model of amyotrophic lateral sclerosis. *EBioMedicine, 40*, 717-732. 10.1016/j.ebiom.2019.01.038

Poe, A. R., Wang, B., Sapar, M. L., Ji, H., Li, K., Onabajo, T., . . . Han, C. (2019). Robust CRISPR/Cas9-Mediated Tissue-Specific Mutagenesis Reveals Gene Redundancy and Perdurance in Drosophila. *Genetics, 211*(2), 459-472. 10.1534/genetics.118.301736

Rashid, A. J., Cole, C. J., & Josselyn, S. A. (2014). Emerging roles for MEF2 transcription factors in memory. *Genes Brain Behav, 13*(1), 118-125. 10.1111/gbb.12058

Raun, N., Jones, S., & Kramer, J. M. (2021). Conditioned courtship suppression in Drosophila melanogaster. *J Neurogenet*, 1-27. 10.1080/01677063.2021.1873323

Razay, G., Vreugdenhil, A., & Wilcock, G. (2007). The metabolic syndrome and Alzheimer disease. *Arch Neurol, 64*(1), 93-96. 10.1001/archneur.64.1.93

Renthal, W., & Nestler, E. J. (2008). Epigenetic mechanisms in drug addiction. *Trends Mol Med, 14*(8), 341-350. 10.1016/j.molmed.2008.06.004

Rogge, G. A., Singh, H., Dang, R., & Wood, M. A. (2013). HDAC3 is a negative regulator of cocaine-context-associated memory formation. *J Neurosci, 33*(15), 6623-6632. 10.1523/JNEUROSCI.4472-12.2013

Ross, J., Jiang, H., Kanost, M. R., & Wang, Y. (2003). Serine proteases and their homologs in the Drosophila melanogaster genome: an initial analysis of sequence conservation and phylogenetic relationships. *Gene, 304*, 117-131. https://doi.org/10.1016/S0378-1119(02)01187-3

Sando, R., III, Gounko, N., Pieraut, S., Liao, L., Yates, J., 3rd, & Maximov, A. (2012). HDAC4 governs a transcriptional program essential for synaptic plasticity and memory. *Cell, 151*(4), 821-834. 10.1016/j.cell.2012.09.037

Sang, T. K., & Jackson, G. R. (2005). Drosophila models of neurodegenerative disease. *NeuroRx, 2*(3), 438-446. 10.1602/neurorx.2.3.438

Scheschonka, A., Tang, Z., & Betz, H. (2007). Sumoylation in neurons: nuclear and synaptic roles? *Trends Neurosci, 30*(3), 85-91. 10.1016/j.tins.2007.01.003

Schmitt, M., & Matthies, H. (1979). Biochemical studies on histones of the central nervous system. III. Incorporation of carbon14-acetate into the histones of different rat brain regions during a learning experiment. *Acta Biol Med Ger, 38*(4), 683-689.

Schwartz, S. (2016). *Investigating the role of histone deacetylase HDAC4 in long-term memory formation : a thesis presented in partial fulfilment of the requirements for the degree of Doctor of Philosophy in Genetics at Massey University, Manawatu, New Zealand.* (Doctor of Philosophy (PhD) Doctoral), Massey University, Retrieved from http://hdl.handle.net/10179/11504

Schwartz, S., Truglio, M., Scott, M. J., & Fitzsimons, H. L. (2016). Long-Term Memory in Drosophila Is Influenced by Histone Deacetylase HDAC4 Interacting with SUMO-Conjugating Enzyme Ubc9. *Genetics, 203*(3), 1249-1264. 10.1534/genetics.115.183194

Schwartz, S., Wilson, S. J., Hale, T. K., & Fitzsimons, H. L. (2021). Ankyrin2 is required for neuronal morphogenesis and long-term memory and interacts genetically with HDAC4. *bioRxiv*, 2021.2007.2018.452850. 10.1101/2021.07.18.452850

Sen, A., Nelson, T. J., & Alkon, D. L. (2015). ApoE4 and Abeta Oligomers Reduce BDNF Expression via HDAC Nuclear Translocation. *J Neurosci, 35*(19), 7538-7551. 10.1523/jneurosci.0260-15.2015

Sen, T., & Sen, N. (2016). Isoflurane-induced inactivation of CREB through histone deacetylase 4 is responsible for cognitive impairment in developing brain. *Neurobiol Dis, 96*, 12-21. 10.1016/j.nbd.2016.08.005

Seo, H. W., Kim, E. J., Na, H., & Lee, M. O. (2009). Transcriptional activation of hypoxia-inducible factor-1alpha by HDAC4 and HDAC5 involves differential recruitment of p300 and FIH-1. *FEBS Lett, 583*(1), 55-60. 10.1016/j.febslet.2008.11.044

Shalizi, A., Gaudilliere, B., Yuan, Z., Stegmuller, J., Shirogane, T., Ge, Q., . . . Bonni, A. (2006). A calcium-regulated MEF2 sumoylation switch controls postsynaptic differentiation. *Science, 311*(5763), 1012-1017. 10.1126/science.1122513

Shen, X., Chen, J., Li, J., Kofler, J., & Herrup, K. (2016). Neurons in Vulnerable Regions of the Alzheimer's Disease Brain Display Reduced ATM Signaling. *eNeuro, 3*(1) 10.1523/eneuro.0124-15.2016

Shu, G., Kramár, E. A., López, A. J., Huynh, G., Wood, M. A., & Kwapis, J. L. (2018). Deleting HDAC3 rescues long-term memory impairments induced by disruption of the neuron-specific chromatin remodeling subunit BAF53b. *Learning & memory (Cold Spring Harbor, N.Y.), 25*(3), 109-114. 10.1101/lm.046920.117

Siegenthaler, D., Enneking, E. M., Moreno, E., & Pielage, J. (2015). L1CAM/Neuroglian controls the axon-axon interactions establishing layered and lobular mushroom body architecture. *J Cell Biol, 208*(7), 1003-1018. 10.1083/jcb.201407131

Sivachenko, A., Li, Y., Abruzzi, K. C., & Rosbash, M. (2013). The transcription factor Mef2 links the Drosophila core clock to Fas2, neuronal morphology, and circadian behavior. *Neuron, 79*(2), 281-292. 10.1016/j.neuron.2013.05.015

Sokolowski, M. B. (2001). Drosophila: Genetics meets behaviour. *Nature Reviews Genetics, 2*(11), 879-890. 10.1038/35098592

Spindler, S. R., & Hartenstein, V. (2010). The Drosophila neural lineages: a model system to study brain development and circuitry. *Development genes and evolution, 220*(1-2), 1-10. 10.1007/s00427-010-0323-7

Stefanko, D. P., Barrett, R. M., Ly, A. R., Reolon, G. K., & Wood, M. A. (2009). Modulation of long-term memory for object recognition via HDAC inhibition. *Proceedings of the National Academy of Sciences of the United States of America, 106*(23), 9447-9452. 10.1073/pnas.0903964106

Steullet, P., Cabungcal, J. H., Coyle, J., Didriksen, M., Gill, K., Grace, A. A., . . . Do, K. Q. (2017). Oxidative stress-driven parvalbumin interneuron impairment as a common mechanism in models of schizophrenia. *Mol Psychiatry, 22*(7), 936-943. 10.1038/mp.2017.47

Stocker, R. F. (1994). The organization of the chemosensory system in Drosophila melanogaster: a rewiew. *Cell and Tissue Research, 275*(1), 3-26. 10.1007/BF00305372

Sun, L., Telles, E., Karl, M., Cheng, F., Luetteke, N., Sotomayor, E. M., . . . Seto, E. (2018). Loss of HDAC11 ameliorates clinical symptoms in a multiple sclerosis mouse model. *Life science alliance, 1*(5), e201800039-e201800039. 10.26508/lsa.201800039

Sun, Y., Liu, S., Ferguson, S., Wang, L., Klepcyk, P., Yun, J. S., & Friedman, J. E. (2002). Phosphoenolpyruvate carboxykinase overexpression selectively attenuates insulin signaling and hepatic insulin sensitivity in transgenic mice. *J Biol Chem, 277*(26), 23301-23307. 10.1074/jbc.M200964200

Sung, Y. M., Lee, T., Yoon, H., DiBattista, A. M., Song, J. M., Sohn, Y., . . . Hoe, H. S. (2013). Mercaptoacetamide-based class II HDAC inhibitor lowers Abeta levels and improves learning and memory in a mouse model of Alzheimer's disease. *Exp Neurol, 239*, 192-201. 10.1016/j.expneurol.2012.10.005

Sweatt, J. D. (2013). The emerging field of neuroepigenetics. *Neuron, 80*(3), 624-632. 10.1016/j.neuron.2013.10.023

Takahashi-Fujigasaki, J., & Fujigasaki, H. (2006). Histone deacetylase (HDAC) 4 involvement in both Lewy and Marinesco bodies. *Neuropathol Appl Neurobiol, 32*(5), 562-566. 10.1111/j.1365-2990.2006.00733.x

Tang, H., Macpherson, P., Marvin, M., Meadows, E., Klein, W. H., Yang, X. J., & Goldman, D. (2009). A histone deacetylase 4/myogenin positive feedback loop coordinates denervation-dependent gene induction and suppression. *Mol Biol Cell, 20*(4), 1120-1131. 10.1091/mbc.E08-07-0759

Tessier, C. R., & Broadie, K. (2009). Activity-dependent modulation of neural circuit synaptic connectivity. *Front Mol Neurosci, 2*, 8. 10.3389/neuro.02.008.2009

Thul, P. J., Åkesson, L., Wiking, M., Mahdessian, D., Geladaki, A., Ait Blal, H., . . . Lundberg, E. (2017). A subcellular map of the human proteome. *Science, 356*(6340), eaal3321. 10.1126/science.aal3321

Trazzi, S., Fuchs, C., Viggiano, R., De Franceschi, M., Valli, E., Jedynak, P., . . . Ciani, E. (2016). HDAC4: a key factor underlying brain developmental alterations in CDKL5 disorder. *Hum Mol Genet, 25*(18), 3887-3907. 10.1093/hmg/ddw231

Trifunovic, A., Wredenberg, A., Falkenberg, M., Spelbrink, J. N., Rovio, A. T., Bruder, C. E., . . . Larsson, N. G. (2004). Premature ageing in mice expressing defective mitochondrial DNA polymerase. *Nature, 429*(6990), 417-423. 10.1038/nature02517

Uhlén, M., Fagerberg, L., Hallström, B. M., Lindskog, C., Oksvold, P., Mardinoglu, A., . . . Pontén, F. (2015). Tissue-based map of the human proteome. *Science, 347*(6220), 1260419. 10.1126/science.1260419

van der Voet, M., Nijhof, B., Oortveld, M. A., & Schenck, A. (2014). Drosophila models of early onset cognitive disorders and their clinical applications. *Neurosci Biobehav Rev, 46 Pt 2*, 326-342. 10.1016/j.neubiorev.2014.01.013

Vecsey, C. G., Hawk, J. D., Lattal, K. M., Stein, J. M., Fabian, S. A., Attner, M. A., . . . Wood, M. A. (2007). Histone deacetylase inhibitors enhance memory and synaptic plasticity via CREB:CBP-dependent transcriptional activation. *J Neurosci, 27*(23), 6128-6140. 10.1523/jneurosci.0296-07.2007

Vega, R. B., Matsuda, K., Oh, J., Barbosa, A. C., Yang, X., Meadows, E., . . . Olson, E. N. (2004). Histone deacetylase 4 controls chondrocyte hypertrophy during skeletogenesis. *Cell, 119*(4), 555-566. 10.1016/j.cell.2004.10.024

Veith, A., & Moorthy, B. (2018). Role of Cytochrome P450s in the Generation and Metabolism of Reactive Oxygen Species. *Current opinion in toxicology, 7*, 44-51. 10.1016/j.cotox.2017.10.003

Verdin, E., Dequiedt, F., & Kasler, H. G. (2003). Class II histone deacetylases: versatile regulators. *Trends Genet, 19*(5), 286-293. 10.1016/s0168-9525(03)00073-8

Verdone, L., Caserta, M., & Di Mauro, E. (2005). Role of histone acetylation in the control of gene expression. *Biochem Cell Biol, 83*(3), 344-353. 10.1139/o05-041

Villavicencio-Lorini, P., Klopocki, E., Trimborn, M., Koll, R., Mundlos, S., & Horn, D. (2013). Phenotypic variant of Brachydactyly-mental retardation syndrome in a family with an inherited interstitial 2q37.3 microdeletion including HDAC4. *Eur J Hum Genet, 21*(7), 743-748. 10.1038/ejhg.2012.240

Voglis, G., & Tavernarakis, N. (2006). The role of synaptic ion channels in synaptic plasticity. *EMBO reports, 7*(11), 1104-1110. 10.1038/sj.embor.7400830

Volmar, C.-H., & Wahlestedt, C. (2015). Histone deacetylases (HDACs) and brain function. *Neuroepigenetics, 1*, 20-27. https://doi.org/10.1016/j.nepig.2014.10.002

Wakeling, E., McEntagart, M., Bruccoleri, M., Shaw-Smith, C., Stals, K. L., Wakeling, M., . . . Caswell, R. C. (2021). Missense substitutions at a conserved 14-3-3 binding site in HDAC4 cause a novel intellectual disability syndrome. *Human Genetics and Genomics Advances, 2*(1), 100015. https://doi.org/10.1016/j.xhgg.2020.100015

Wang, A. H., Gregoire, S., Zika, E., Xiao, L., Li, C. S., Li, H., . . . Yang, X. J. (2005). Identification of the ankyrin repeat proteins ANKRA and RFXANK as novel

partners of class IIa histone deacetylases. *J Biol Chem, 280*(32), 29117-29127. 10.1074/jbc.M500295200

Wang, A. H., Kruhlak, M. J., Wu, J., Bertos, N. R., Vezmar, M., Posner, B. I., . . . Yang, X. J. (2000). Regulation of histone deacetylase 4 by binding of 14-3-3 proteins. *Mol Cell Biol, 20*(18), 6904-6912.

Wang, A. H., & Yang, X. J. (2001). Histone Deacetylase 4 Possesses Intrinsic Nuclear Import and Export Signals. *Molecular and Cellular Biology, 21*(17), 5992-6005. 10.1128/mcb.21.17.5992-6005.2001

Wang, B., Moya, N., Niessen, S., Hoover, H., Mihaylova, M. M., Shaw, R. J., . . . Montminy, M. (2011). A hormone-dependent module regulating energy balance. *Cell, 145*(4), 596-606. 10.1016/j.cell.2011.04.013

Wang, W. H., Cheng, L. C., Pan, F. Y., Xue, B., Wang, D. Y., Chen, Z., & Li, C. J. (2011). Intracellular trafficking of histone deacetylase 4 regulates long-term memory formation. *Anat Rec (Hoboken), 294*(6), 1025-1034. 10.1002/ar.21389

Weeks, K. L., Ranieri, A., Karaś, A., Bernardo, B. C., Ashcroft, A. S., Molenaar, C., . . . Avkiran, M. (2017). β-Adrenergic Stimulation Induces Histone Deacetylase 5 (HDAC5) Nuclear Accumulation in Cardiomyocytes by B55α-PP2A-Mediated Dephosphorylation. *Journal of the American Heart Association, 6*(4), e004861. 10.1161/JAHA.116.004861

Williams, S. R., Aldred, M. A., Der Kaloustian, V. M., Halal, F., Gowans, G., McLeod, D. R., . . . Elsea, S. H. (2010). Haploinsufficiency of HDAC4 causes brachydactyly mental retardation syndrome, with brachydactyly type E, developmental delays, and behavioral problems. *Am J Hum Genet, 87*(2), 219-228. 10.1016/j.ajhg.2010.07.011

Wilson, S. J. (2021). *Teasing apart the interaction between HDAC4 and Ankyrin2 in Drosophila neuronal function : a thesis presented in partial fulfilment of the requirements for the degree of Master of Science in Biochemistry, School of Fundamental Sciences, Massey University, Manawatu, New Zealand.* (Master of Science (MSc) Masters), Massey University, Retrieved from http://hdl.handle.net/10179/16298

Wu, Q., Yang, X., Zhang, L., Zhang, Y., & Feng, L. (2017). Nuclear Accumulation of Histone Deacetylase 4 (HDAC4) Exerts Neurotoxicity in Models of Parkinson's Disease. *Mol Neurobiol, 54*(9), 6970-6983. 10.1007/s12035-016-0199-2

Wu, Y., Hou, F., Wang, X., Kong, Q., Han, X., & Bai, B. (2016). Aberrant Expression of Histone Deacetylases 4 in Cognitive Disorders: Molecular Mechanisms and a Potential Target. *Front Mol Neurosci, 9*, 114-114. 10.3389/fnmol.2016.00114

Xu, C., Jin, J., Bian, C., Lam, R., Tian, R., Weist, R., . . . Min, J. (2012). Sequence-specific recognition of a PxLPxI/L motif by an ankyrin repeat tumbler lock. *Science signaling, 5*(226), ra39. 10.1126/scisignal.2002979

Yamaguchi, R., & Perkins, G. (2009). Dynamics of mitochondrial structure during apoptosis and the enigma of Opa1. *Biochimica et biophysica acta, 1787*(8), 963-972. 10.1016/j.bbabio.2009.02.005

Yang, X.-J., & Grégoire, S. (2005). Class II histone deacetylases: from sequence to function, regulation, and clinical implication. *Molecular and Cellular Biology, 25*(8), 2873-2884. 10.1128/MCB.25.8.2873-2884.2005

Yao, Y. L., & Yang, W. M. (2011). Beyond histone and deacetylase: an overview of cytoplasmic histone deacetylases and their nonhistone substrates. *J Biomed Biotechnol, 2011*, 146493. 10.1155/2011/146493

Yu, Y. T. (1996). Distinct domains of myocyte enhancer binding factor-2A determining nuclear localization and cell type-specific transcriptional activity. *J Biol Chem, 271*(40), 24675-24683.

Zhang, C. L., McKinsey, T. A., Lu, J. R., & Olson, E. N. (2001). Association of COOH-terminal-binding protein (CtBP) and MEF2-interacting transcription repressor (MITR) contributes to transcriptional repression of the MEF2 transcription factor. *The Journal of biological chemistry, 276*(1), 35-39. 10.1074/jbc.m007364200

Zhang, P., Sun, Q., Zhao, C., Ling, S., Li, Q., Chang, Y. Z., & Li, Y. (2014). HDAC4 protects cells from ER stress induced apoptosis through interaction with ATF4. *Cell Signal, 26*(3), 556-563. 10.1016/j.cellsig.2013.11.026

Zhao, S., Guo, J., Zhao, Y., Fei, C., Zheng, Q., Li, X., & Chang, C. (2016). Chidamide, a novel histone deacetylase inhibitor, inhibits the viability of MDS and AML cells by suppressing JAK2/STAT3 signaling. *Am J Transl Res, 8*(7), 3169-3178.

Zhao, X., Lenek, D., Dag, U., Dickson, B. J., & Keleman, K. (2018). Persistent activity in a recurrent circuit underlies courtship memory in Drosophila. *eLife, 7*, e31425. 10.7554/eLife.31425

Zhou, X., Richon, V. M., Wang, A. H., Yang, X. J., Rifkind, R. A., & Marks, P. A. (2000). Histone deacetylase 4 associates with extracellular signal-regulated kinases 1 and 2, and its cellular localization is regulated by oncogenic Ras. *Proc Natl Acad Sci U S A, 97*(26), 14329-14333. 10.1073/pnas.250494697

Zhu, X., Wang, S., Yu, L., Jin, J., Ye, X., Liu, Y., & Xu, Y. (2017). HDAC3 negatively regulates spatial memory in a mouse model of Alzheimer's disease. *Aging cell, 16*(5), 1073-1082. 10.1111/acel.12642

Zhu, Y., Huang, M., Bushong, E., Phan, S., Uytiepo, M., Beutter, E., . . . Maximov, A. (2019). Class IIa HDACs regulate learning and memory through dynamic experience-dependent repression of transcription. *Nature Communications, 10*(1), 3469. 10.1038/s41467-019-11409-0

Ziemka-Nalecz, M., Jaworska, J., Sypecka, J., & Zalewska, T. (2018). Histone Deacetylase Inhibitors: A Therapeutic Key in Neurological Disorders? *J Neuropathol Exp Neurol, 77*(10), 855-870. 10.1093/jnen/nly073

9. APPENDICES

9.1 Sequence of *DmHDAC4*^{WT} and variants

5′

```
gcggccgccaacatgtctagtcccgacgatagaataccaatacacgatctgccatcagaa
             M  S  S  P  D  D  R  I  P  I  H  D  L  P  S  E
gccggaagcgatgagcgattgctgcacataacgccggccactctgacattggacttcaag
 A  G  S  D  E  R  L  L  H  I  T  P  A  T  L  T  L  D  F  K
ccccatcccgccgtggatatcgatcagcagatcatggagctcaagaagagccaggagctg
 P  H  P  A  V  D  I  D  Q  Q  I  M  E  L  K  K  S  Q  E  L
caaaagcagcggcttatcaactcgtttcaggagcaatcgaagcaaatggaattggagcat
 Q  K  Q  R  L  I  N  S  F  Q  E  Q  S  K  Q  M  E  L  E  H
aaacttcaattggagcacaagtatcaatttgcggtgaattcacatggcgctttccaggaa
 K  L  Q  L  E  H  K  Y  Q  F  A  V  N  S  H  G  A  F  Q  E
ttgcgaaacgagagcatggtgacagccgccgctgctgcggtggctcaggagcaacatcgc
 L  R  N  E  S  M  V  T  A  A  A  A  A  V  A  Q  E  Q  H  R
caacagttgcatcaacagcagcagcaacatcagcagcagcagcagcagcaacatcaa
 Q  Q  L  H  Q  Q  Q  Q  Q  H  Q  Q  Q  Q  Q  Q  Q  Q  H  Q
cagcagcagcagcagcaacaggcacgcggcagggatggcatgaaactcaagcagaactgt
 Q  Q  Q  Q  Q  Q  Q  A  R  G  R  D  G  M  K  L  K  Q  N  C
agtgccaatgccagtcccgaggtcaaacagattctcaactgcttcatcctgagcagaaag
 S  A  N  A  S  P  E  V  K  Q  I  L  N  C  F  I  L  S  R  K
tcccaggcggcggcatcgaatggcacaacgacaacgtcgccctacaggaatcgcggcgtg
 S  Q  A  A  A  S  N  G  T  T  T  T  S  P  Y  R  N  R  G  V
gtgaagagctcctcgggcgaatccctcccagctggaaccgtgaccagtgcgcatccgtac
 V  K  S  S  S  G  E  S  L  P  A  G  T  V  T  S  A  H  P  Y
aaaatacctcagccgccaccctcactgctcaaatatgaatctgattttccgctgaggaag
 K  I  P  Q  P  P  P  S  L  L  K  Y  E  S  D  F  P  L  R  K
acagcatccgaaccgaacctgctgaagatccggctgaagcagagcgtcatcgagcgcaag
 T  A  S  E  P  N  L  L  K  I  R  L  K  Q  S  V  I  E  R  K
gcccgcatcggaggaccggcgggagccggcgccacgaacgactcctccaggcggcgcag
 A  R  I  G  G  P  A  G  A  R  R  H  E  R  L  L  Q  A  A  Q
cgtaggcagcaaaagaactcggttctcacaaactgcaacagtacaccggattctggaccc
 R  R  Q  Q  K  N  S  V  L  T  N  C  N  S  T  P  D  S  G  P
aattcaccgccctcggcagctgcgttggcggtgggcgtggtcggtagccgtggatcaccg
 N  S  P  P  S  A  A  A  L  A  V  G  V  V  G  S  R  G  S  P
acaagtgcacccattcaggaggaaaacgaggagggcagccaatatcagccgggccagagg
 T  S  A  P  I  Q  E  E  N  E  E  G  S  Q  Y  Q  P  G  Q  R
agcagcatcaacgatttgccattgttcagttcaccatcgctgccgaatatttcgctcggg
 S  S  I  N  D  L  P  L  F  S  S  P  S  L  P  N  I  S  L  G
cgaccgcatttacccaactcggcgcaggcgcatgcccaggtgaatgcccaggttgctgcc
 R  P  H  L  P  N  S  A  Q  A  H  A  Q  V  N  A  Q  V  A  A
caggctcaggcacaggcccaggcacaggcacaggcgcatgccatgttcgcggcactggct
 Q  A  Q  A  Q  A  Q  A  Q  A  Q  A  H  A  M  F  A  A  L  A
gccgcccagggtggctgcggacagccgggctactataatccactgggcatggcattcgtt
 A  A  Q  G  G  C  G  Q  P  G  Y  Y  N  P  L  G  M  A  F  V
ggccggcaaccagcaccgctggccatgattccggccacggggatagcaccgcagcaaccg
 G  R  Q  P  A  P  L  A  M  I  P  A  T  G  I  A  P  Q  Q  P
tcgccggtggtgcgcagtgcatcggccacttcgacatcgtcgtcgcaggcctcgctggtg
 S  P  V  V  R  S  A  S  A  T  S  T  S  S  S  Q  A  S  L  V
```

```
ggcgatgtggcgccaccgcaggctcatgccgcctccaccattctgccctcgtcatcgtcc
 G  D  V  A  P  P  Q  A  H  A  A  S  T  I  L  P  S  S  S  S
tacatgcagcaactgggcagtgtggccggttcgggtgttaatctccatgccgccgccgtt
 Y  M  Q  Q  L  G  S  V  A  G  S  G  V  N  L  H  A  A  A  V
gctgcagcggcagcagcagccgccgccggttcactgccaccgaccaatagccatggt
 A  A  A  A  A  A  A  A  A  A  G  S  L  P  P  T  N  S  H  G
cacggacacggttcccacgcacatccacatccacatgcccatggacacgggcatggccat
 H  G  H  G  S  H  A  H  P  H  P  H  A  H  G  H  G  H  G  H
ggccatggtatctacgctggccaccagcacaatgtgcccataacggacgcccaggtggcg
 G  H  G  I  Y  A  G  H  Q  H  N  V  P  I  T  D  A  Q  V  A
caggtgcatctgcacaaacagggccatcggccgctgggacgaacgcagtcggcaccactg
 Q  V  H  L  H  K  Q  G  H  R  P  L  G  R  T  Q  S  A  P  L
ccccttggacatccgatgctaaccggagctgtgcaactgaatgtggtccaaacgcactac
 P  L  G  H  P  M  L  T  G  A  V  Q  L  N  V  V  Q  T  H  Y
gagaatagtgaggcggagcgccaggcgtacgagcaccaggtggtgaaccagaaagtccgc
 E  N  S  E  A  E  R  Q  A  Y  E  H  Q  V  V  N  Q  K  V  R
cagaccgtcctgactcgcagcggagctgctgcagcagccgctgctgccgccggcgtgagc
 Q  T  V  L  T  R  S  G  A  A  A  A  A  A  A  A  A  G  V  S
gtggtgcgtgaggcacagttgaaggaggaggatgacgactcggccgccgaggtgatggac
 V  V  R  E  A  Q  L  K  E  E  D  D  D  S  A  A  E  V  M  D
ctcacagataagaaaaaaccgccgaagacggtgctaaccagcacgatagccaccagtacg
 L  T  D  K  K  K  P  P  K  T  V  L  T  S  T  I  A  T  S  T
tcccagaatctgcccgaagctttggcggcggcggcggcggcagccgcctaccgtgccccg
 S  Q  N  L  P  E  A  L  A  A  A  A  A  A  A  A  Y  R  A  P
cacaacgcgtccagtaactccgcctccgccacaaagtccggtattaagctgcgggaccag
 H  N  A  S  S  N  S  A  S  A  T  K  S  G  I  K  L  R  D  Q
gagtatttgcaacagcagcgggagcaactattgctccttcagcaggaggaggaactggcg
 E  Y  L  Q  Q  Q  R  E  Q  L  L  L  L  Q  Q  E  E  E  L  A
aagagcctaatgcgtccgctatcgcgaacgcttagcagtccgctggtgccgctggggcca
 K  S  L  M  R  P  L  S  R  T  L  S  S  P  L  V  P  L  G  P
catggtcttagtcagattcccgacactggacaacagccggcaccgatagccacatcctcg
 H  G  L  S  Q  I  P  D  T  G  Q  Q  P  A  P  I  A  T  S  S
tcggccgatcatataccgcccgttaacctctcgctgccgcatcgccagcaccgccagcta
 S  A  D  H  I  P  P  V  N  L  S  L  P  H  R  Q  H  R  Q  L
atgagcacactatacgccagccaattgcgtaaccaccagccatcggcgagtggttcaccg
 M  S  T  L  Y  A  S  Q  L  R  N  H  Q  P  S  A  S  G  S  P
ccgcacaaggtcaccaccggtttggcctacgatccgcttatgctgaagcattcgtgtatt
 P  H  K  V  T  T  G  L  A  Y  D  P  L  M  L  K  H  S  C  I
tgcggagacaatgcccagcatccggagcacagtggtcgactgcagagcgtgtgggcacgg
 C  G  D  N  A  Q  H  P  E  H  S  G  R  L  Q  S  V  W  A  R
ttaaatgaaacggatctggtgaagcgttgcgatcgcctgcgcgctcgcaaggcgacacag
 L  N  E  T  D  L  V  K  R  C  D  R  L  R  A  R  K  A  T  Q
gaggagctgcagactgtgcacaccgaagcgcatgccatgctcttcggttcgaatcagtgc
 E  E  L  Q  T  V  H  T  E  A  H  A  M  L  F  G  S  N  Q  C
cagctcagcaggcccaagttggaaaacacgttgtcggccagctttgtgcgtttgtcgtgc
 Q  L  S  R  P  K  L  E  N  T  L  S  A  S  F  V  R  L  S  C
ggcggcttgggtgtggatctggataccacgtggaatgagcaccatacggcaaccgctgca
 G  G  L  G  V  D  L  D  T  T  W  N  E  H  H  T  A  T  A  A
cgaatggcagccggttgtgttatcgatttggcactgaagacggccaagggtgacctgcgg
 R  M  A  A  G  C  V  I  D  L  A  L  K  T  A  K  G  D  L  R
aatggctttgccgttgtccggccgccgggccatcatgcggaggccaatttggccatgggc
 N  G  F  A  V  V  R  P  P  G  H  H  A  E  A  N  L  A  M  G
ttttgtttcttcaattcgatagccattgcggccaagctgctgcgtcagcggatgcccgag
 F  C  F  F  N  S  I  A  I  A  A  K  L  L  R  Q  R  M  P  E
gtgcggcgcatcctgatcgtcgattgggatgtgcatcacggcaatggcacacagcaagca
 V  R  R  I  L  I  V  D  W  D  V  H  H  G  N  G  T  Q  Q  A
```

ttctaccaaagtcccgacattctatatctttccatacatcgacacgatgacggtaacttc
F Y Q S P D I L Y L S I H R H D D G N F
tttcccggcacaggtggacccacagagtgcggctccggtgctggtctcggctttaacgtg
F P G T G G P T E C G S G A G L G F N V
aacatctcatggtctggggcacttaatccgccactgggcgacgccgagtatatcgctgca
N I S W S G A L N P P L G D A E Y I A A
ttccgtaccgttgtgatgcccatcgcgcggagctttaatccggacattgtgctggtatcc
F R T V V M P I A R S F N P D I V L V S
tccggcttcgatgcggccaccggccatccggcaccgctgggtggctaccatgtctctccg
S G F D A A T G H P A P L G G Y H V S P
gcctgctttgggttcatgacccgcgaactccttcagttggccaacggcaaagtggtgctg
A C F G F M T R E L L Q L A N G K V V L
gccctcgagggcggctacgatctggccgccatctgtgattccgcccaggagtgtgtgcgg
A L E G G Y D L A A I C D S A Q E C V R
gcgctgctcggcgatcccgctgctcccattgccaaggccgagctggagcgcccgccttgc
A L L G D P A A P I A K A E L E R P P C
cagaatgccatcaatacgctccagaagacgatagccatacagcaaacgcattggccctgc
Q N A I N T L Q K T I A I Q Q T H W P C
gtgaggatgctggagcacacggttggcttgtctgcgctggagacgctcaaggtggagcac
V R M L E H T V G L S A L E T L K V E H
gacgagtccgagacgatcaacgccatggctggcctctcgatgcagtcgatgcacagaact
D E S E T I N A M A G L S M Q S M H R T
ctatcccgcgatgattccgaggagccgatggatcaggatgaaaccaaa**ggcggaggcgag**
L S R D D S E E P M D Q D E T K **G G G E**
caaaagctcatttctgaagaggacttgaatgaaatg**gagcaaaagctcatttctgaagag**
Q K L I S E E D L N E M **E Q K L I S E E**
gacttgaatgaaatg**gagcaaaagctcatttctgaagaggacttg**aatgaaatg**gagcaa**
D L N E M **E Q K L I S E E D L** N E M **E Q**
aagctcatttctgaagaggacttgaatgaaatg**gagcaaaagctcatttctgaagaggac**
K L I S E E D L N E M **E Q K L I S E E D**
ttgaatgaaatggagagcttgggcgacctcaccatg**gagcaaaagctcatttctgaagag**
L N E M E S L G D L T M **E Q K L I S E E**
gacttgtag**tctaga**
D L -

3’

Supplementary Figure 9.1: Sequence of *DmHDAC^{WT}-myc* with highlighted residues of interest for generation of mutant variants

The *Not*I (bold blue) and *Xba*I (bold green) restriction sites flank the nucleotide sequence of *DmHDAC4^{WT}-myc* (nucleotides accompanied with amino acids) at the 5’ and 3’ ends respectively, which were used for insertion into *Not*I and *Xba*I of the pUASTattB plasmid. A Kozak sequence was also included in the sequence (bold red). At the 3’ end, a 3x glycine linker sequence (underlined black bold) is followed by the 6x myc sequence (black bold). The nucleotides and amino acids that are highlighted represent nucleotides and corresponding amino acids that were mutated to generate the different DmHDAC4 variants: 3A-myc (cyan), dNLS-myc (green), dMEF2-myc (yellow), dANK-myc (magenta) and Y1142H-myc (red). Residues were all mutated to alanine except for Y1142H-myc in which the tyrosine was mutated to histidine.

9.2 Sequence of *DmMEF2 T148A* mutant

5′

```
gcggccgccaacatgggccgcaaaaaaattcaaatatcacgcatcaccgatgaacgcaat
            M  G  R  K  K  I  Q  I  S  R  I  T  D  E  R  N
cggcaggtgaccttcaacaagcgcaagttcggcgtgatgaagaaggcctacgagctgtcc
 R  Q  V  T  F  N  K  R  K  F  G  V  M  K  K  A  Y  E  L  S
gtgctctgcgactgcgagatcgccctgatcatcttctcgtcgagcaacaagctgtaccag
 V  L  C  D  C  E  I  A  L  I  I  F  S  S  S  N  K  L  Y  Q
tacgccagcaccgacatggatcgcgtcctgctcaagtacaccgagtacaacgagccccac
 Y  A  S  T  D  M  D  R  V  L  L  K  Y  T  E  Y  N  E  P  H
gagtccctcaccaacaagaacatcatcgagaaggagaacaagaacggcgtgatgtcgccg
 E  S  L  T  N  K  N  I  I  E  K  E  N  K  N  G  V  M  S  P
gactcgcccgaagccgaaacggactacacactcactccgcgaacggaggccaagtacaac
 D  S  P  E  A  E  T  D  Y  T  L  T  P  R  T  E  A  K  Y  N
aagatcgacgaggagttccagaacatgatgcagcgcaaccagatggccatcggcggtgcg
 K  I  D  E  E  F  Q  N  M  M  Q  R  N  Q  M  A  I  G  G  A
ggtgcccctcgccagcttccaaacagcagctacgccctgcccgtttctgttccggtgccg
 G  A  P  R  Q  L  P  N  S  S  Y  A  L  P  V  S  V  P  V  P
ggatcttacggcgacaacctgctgcaggccagtccacagatgtcccacaccaacatcagc
 G  S  Y  G  D  N  L  L  Q  A  S  P  Q  M  S  H  T  N  I  S
ccccgtccatcgagttcggagacggattcaggtgggatgtccctgataatttatccatcg
 P  R  P  S  S  S  E  T  D  S  G  G  M  S  L  I  I  Y  P  S
ggttccatgctggagatgtcgaacggctatccgcattcacactcgccgcttgtgggatca
 G  S  M  L  E  M  S  N  G  Y  P  H  S  H  S  P  L  V  G  S
ccgagtccgggtcccagtcctggcatagcccaccatttgtccattaagcagcagtcgccg
 P  S  P  G  P  S  P  G  I  A  H  H  L  S  I  K  Q  Q  S  P
ggcagccagaacggacgagcttccaatctaagggtcgtcataccgcccacaattgccccc
 G  S  Q  N  G  R  A  S  N  L  R  V  V  I  P  P  T  I  A  P
ataccgcccaatatgtcagcgccggatgatgtgggatatgcagatcaacgacagagccag
 I  P  P  N  M  S  A  P  D  D  V  G  Y  A  D  Q  R  Q  S  Q
acatcgcttaacacgccagtggtcacgctgcagacgccgattcccgccctcacgagctat
 T  S  L  N  T  P  V  V  T  L  Q  T  P  I  P  A  L  T  S  Y
tcctttggggcgcaggacttctcctcctccggcgtaatgaacagcgcggatatcatgagc
 S  F  G  A  Q  D  F  S  S  S  G  V  M  N  S  A  D  I  M  S
ctcaacacctggcatcagggcctggtgccgcactctagtctctcgcacctggctgtctcg
 L  N  T  W  H  Q  G  L  V  P  H  S  S  L  S  H  L  A  V  S
aatagcacgccgccgcccgccacctcccccgtctccataaaggtcaaggctgagccgcag
 N  S  T  P  P  P  A  T  S  P  V  S  I  K  V  K  A  E  P  Q
tcgccgccgagagatctttccgccagcggtcatcagcagaatagcaatggttccacgggc
 S  P  P  R  D  L  S  A  S  G  H  Q  Q  N  S  N  G  S  T  G
agcggcggatccagcagcagcaccagtagcaacgccagcggaggagcaggaggcggtgga
 S  G  G  S  S  S  S  T  S  S  N  A  S  G  G  A  G  G  G  G
gccgtcagcgcagccaatgtcatcacgcacttgaacaacgtcagtgtcctggcgggaggt
 A  V  S  A  A  N  V  I  T  H  L  N  N  V  S  V  L  A  G  G
ccttcggggcagggaggaggaggcggaggcggcggcagcaacggaaatgtcgaacaggcc
 P  S  G  Q  G  G  G  G  G  G  G  G  S  N  G  N  V  E  Q  A
accaatcttagcgtactgagccacgcgcagcaacatcacctgggcatgcccaactcgcgt
 T  N  L  S  V  L  S  H  A  Q  Q  H  H  L  G  M  P  N  S  R
ccctcgtccacgggccacatcacacccactccaggtgcgccgagcagcgaccaggatgtg
 P  S  S  T  G  H  I  T  P  T  P  G  A  P  S  S  D  Q  D  V
cgtctggcagccgtcgccgtgcagcagcaacagcagcagccacatcagcaacagcaacta
 R  L  A  A  V  A  V  Q  Q  Q  Q  Q  Q  P  H  Q  Q  Q  Q  L
```

ggcgactacgatgcccccaaccacaaacggccgagaatatcgggcggatggggcacaggc
G D Y D A P N H K R P R I S G G W G T G
ggaggctacccatacgatgttcctgactatgcggctatccctatgacgtcccggactat
G G Y P Y D V P D Y A G Y P Y D V P D Y
gcaggatcctatccatatgacgttccagattacgcttagtctaga
A G S Y P Y D V P D Y A –

3′

Supplementary Figure 9.2: Sequence of *DmMEF2 T148A-HA*
The *Not*I (bold blue) and *Xba*I (bold green) restriction sites flank the nucleotide sequence of *DmMEF2 T148A-HA* (nucleotides accompanied with amino acids) at the 5' and 3' ends respectively, which were used for insertion into *Not*I and *Xba*I of the pUASTattB plasmid. A Kozak sequence was also included (bold red). At the 3' end, a 3x glycine linker sequence (underlined black bold) is followed by 3x HA tag sequence (black bold). Mutation of the tyrosine residue to alanine is highlighted in red.

9.3 Genetic crosses

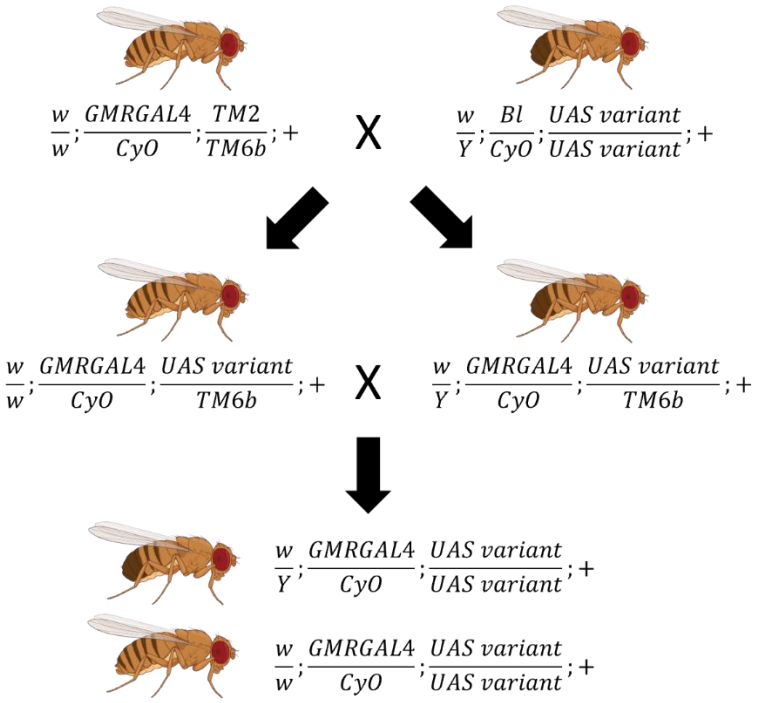

Supplementary Figure 9.3: Crossing scheme to generate *GMRGAL4* flies with two copies of *UAS variant*
Balancer chromosomes (Cyo, TM2 & TM6b) were used to follow transgene transmission through each generation.

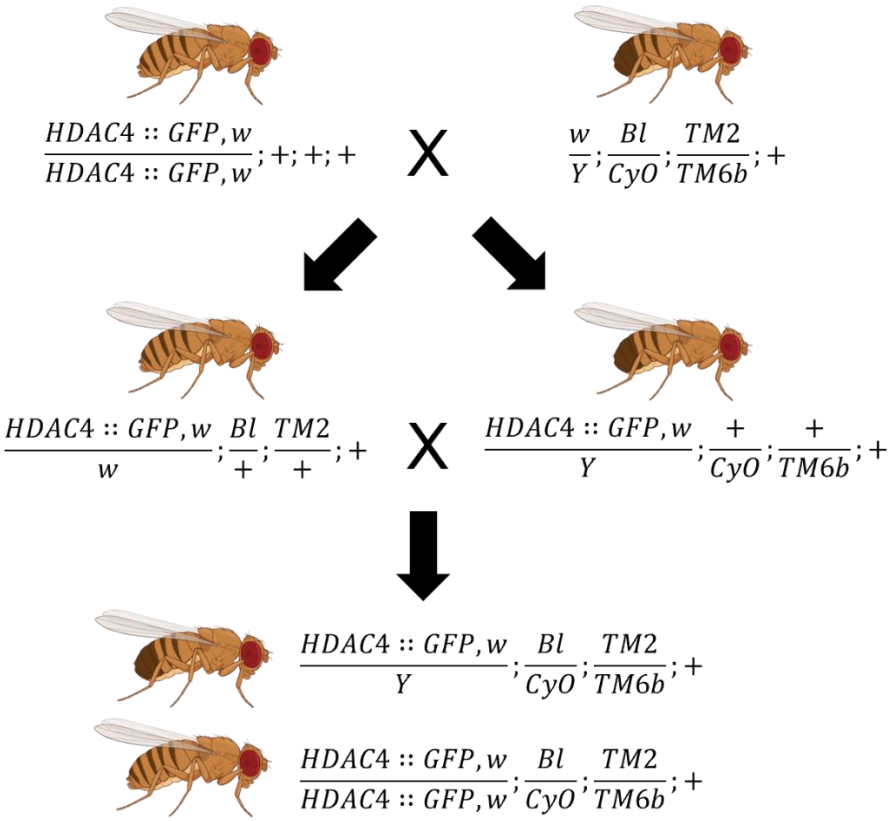

Supplementary Figure 9.4: Crossing scheme that was carried out to generate a hemi/homozygous *HDAC4::GFP* line with double balanced 2nd and 3rd chromosome

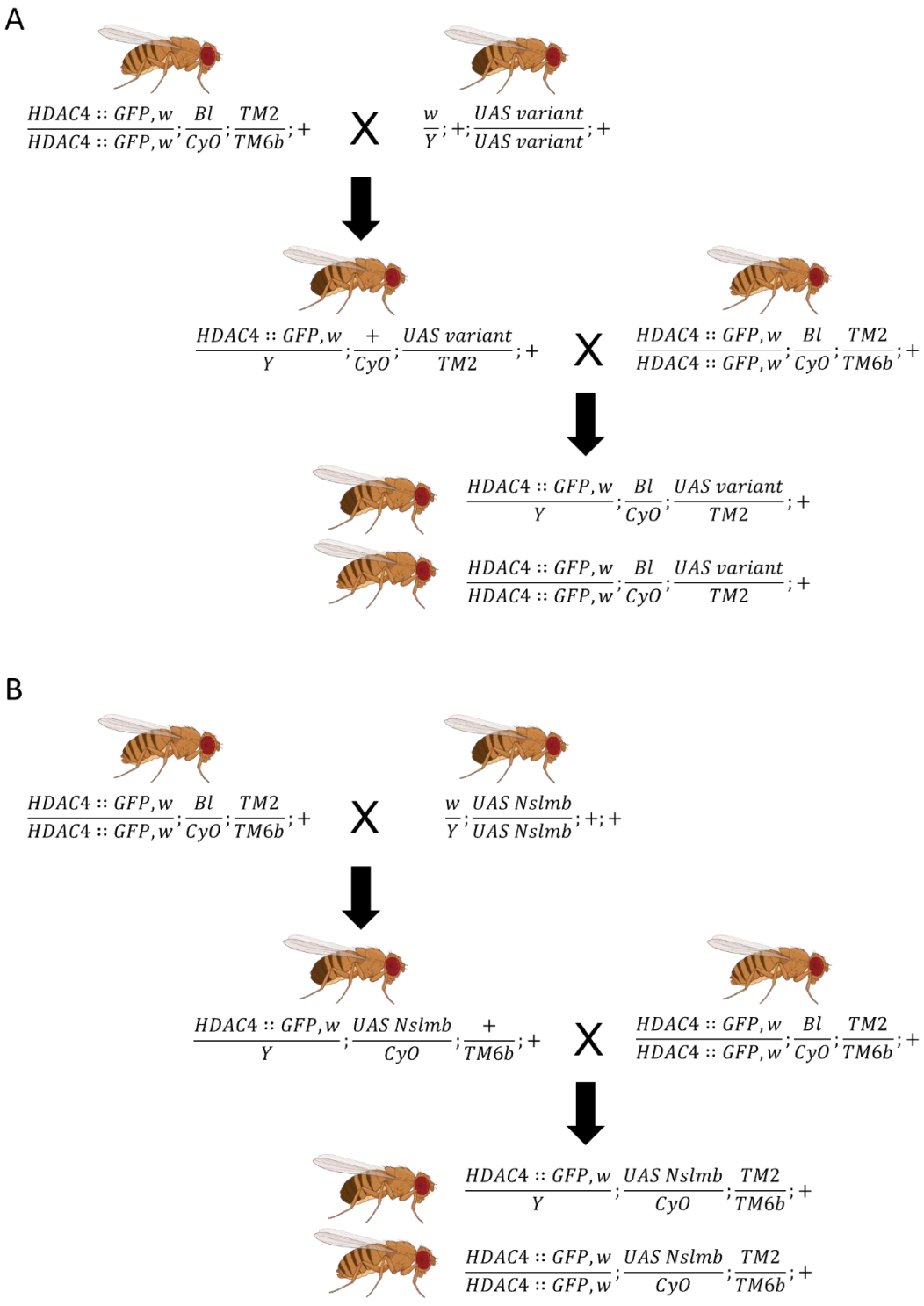

Supplementary Figure 9.5: Crossing schemes that was carried out to generate a *HDAC4::GFP* line with a balanced *UAS variant* or *a UAS Nslmb* (deGradFP)
(A) Crossing scheme to generate a transgenic line of a balanced *HDAC4::GFP* with *UAS variant*. (B) Crossing scheme to generate a transgenic line of a balanced *HDAC4::GFP* with *UAS Nslmb*.

A

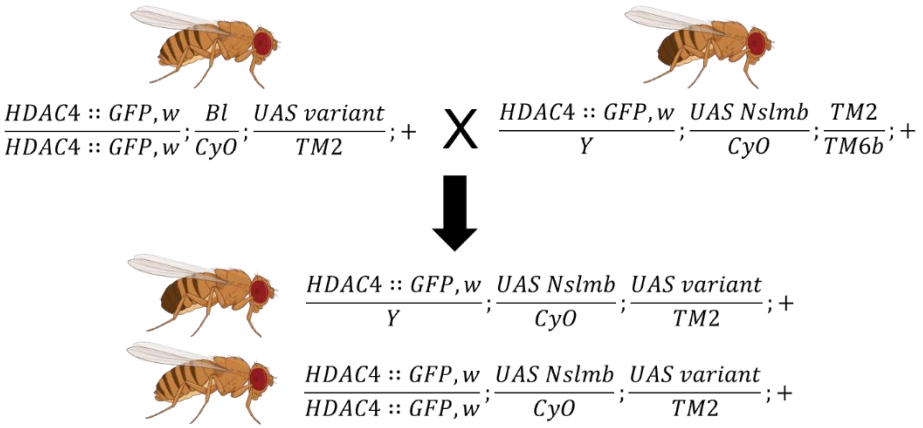

B

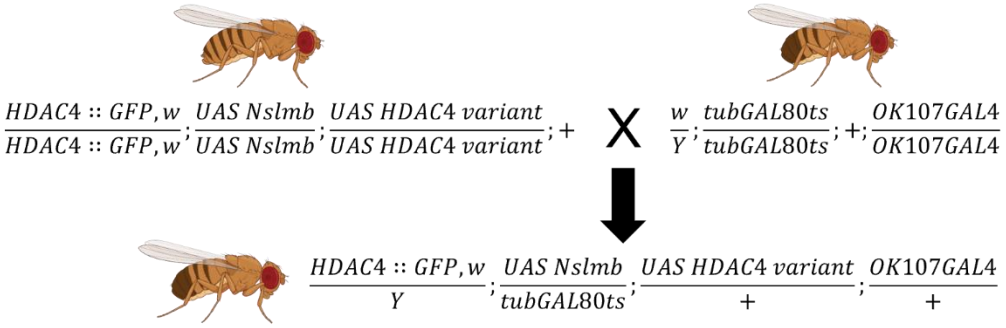

Supplementary Figure 9.6: Crossing schemes that was carried out to generate a line with endogenous *HDAC4::GFP* KD and expressing variant at the MB
(A) Crossing scheme to combine balanced *HDAC4::GFP* with *UAS variant* with balanced *HDAC4::GFP* with *UAS Nslmb*. (B) Female flies from crossing scheme A were crossed to *OK107GAL4; tubGAL80^{ts}* male flies. Only F1 male progenies were selected.

9.4 Supplementary Data

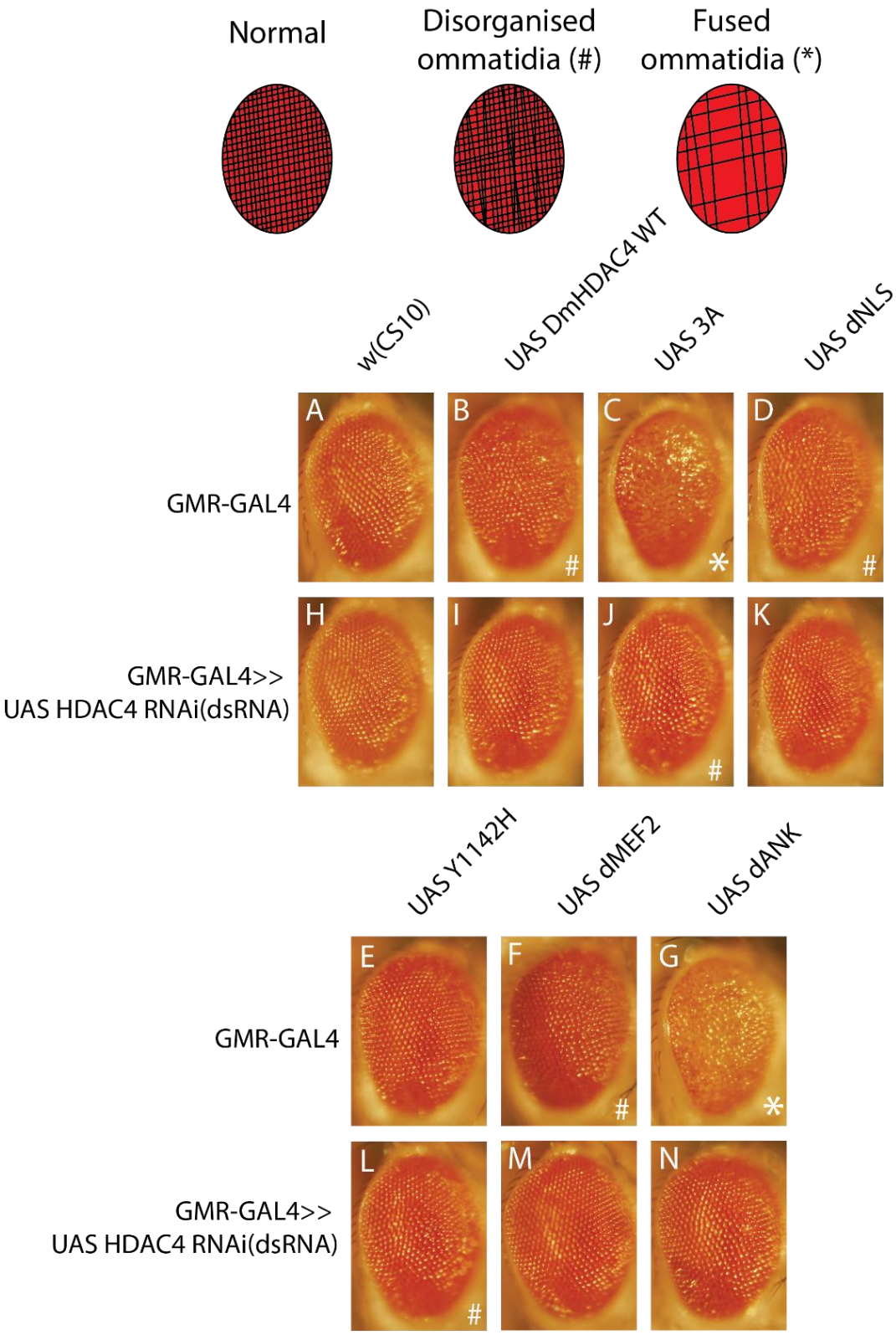

Supplementary Figure 9.7: Eye phenotypes from OE and KD of *DmHDAC4* in the retina

Representative images of *Drosophila* retina morphology of a control (*w(CS10)*) and each *UAS DmHDAC4* variant driven by *GMR-GAL4* in the presence and absence of a *UAS HDAC4*

RNAi. Hash (#) denotes subtle disorganisation of ommatidia while asterisk (*) denotes a more severe phenotype with multiple fused ommatidia. Each image is a representative image of n=12 retina.

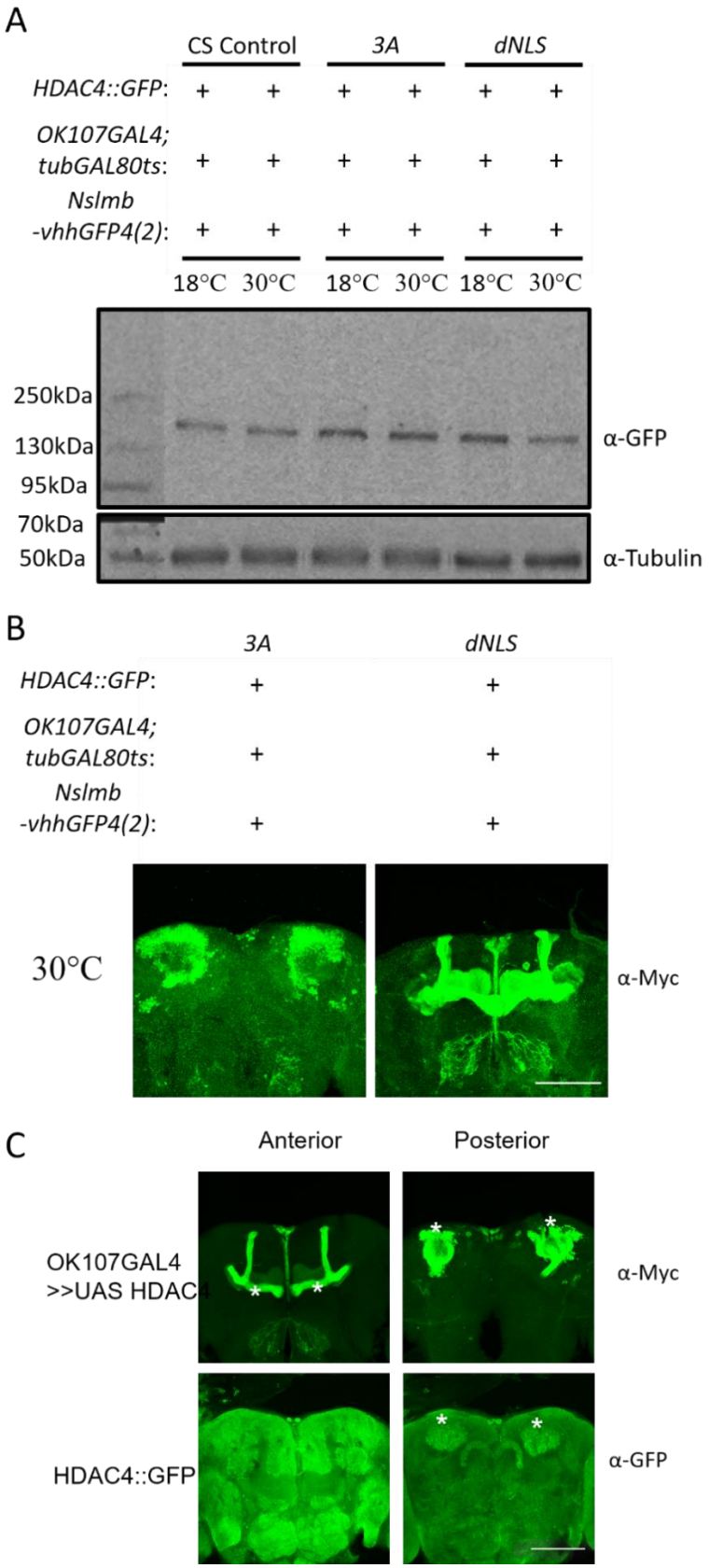

Supplementary Figure 9.8: Verification of transgene presence in *HDAC4::GFP* brains expressing *3A* or *dNLS* driven by *OK107GAL4;*tubGAL80^{ts}
(A) Western blot detection of GFP was carried out on the whole brain lysates (n=50) of the indicated genotypes to confirm the presence of HDAC4::GFP. (B) Immunohistochemical detection of Myc tagged 3A in nuclei and dNLS in the MB lobes, with the Myc antibody. (C) Immunohistochemistry on whole brains of the indicated genotypes. Asterisk (*) indicates the presence of endogenous HDAC4::GFP in the MB lobes located at anterior of the brain and the KCs and calyx at the posterior of the brain. Scale bar = 100μm.

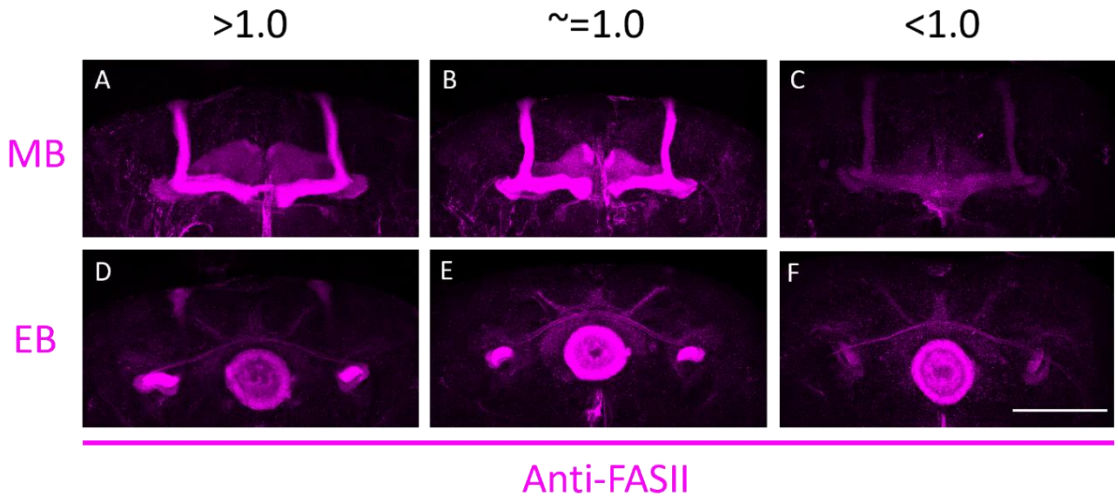

Supplementary Figure 9.9: FasII expression in the MB and EB
Confocal images represents the different FasII intensity observed in MB or EB. Indicated integer is an example of the expected value when the FasII intensity of MB is normalised to EB. Scale bar = 100 μm

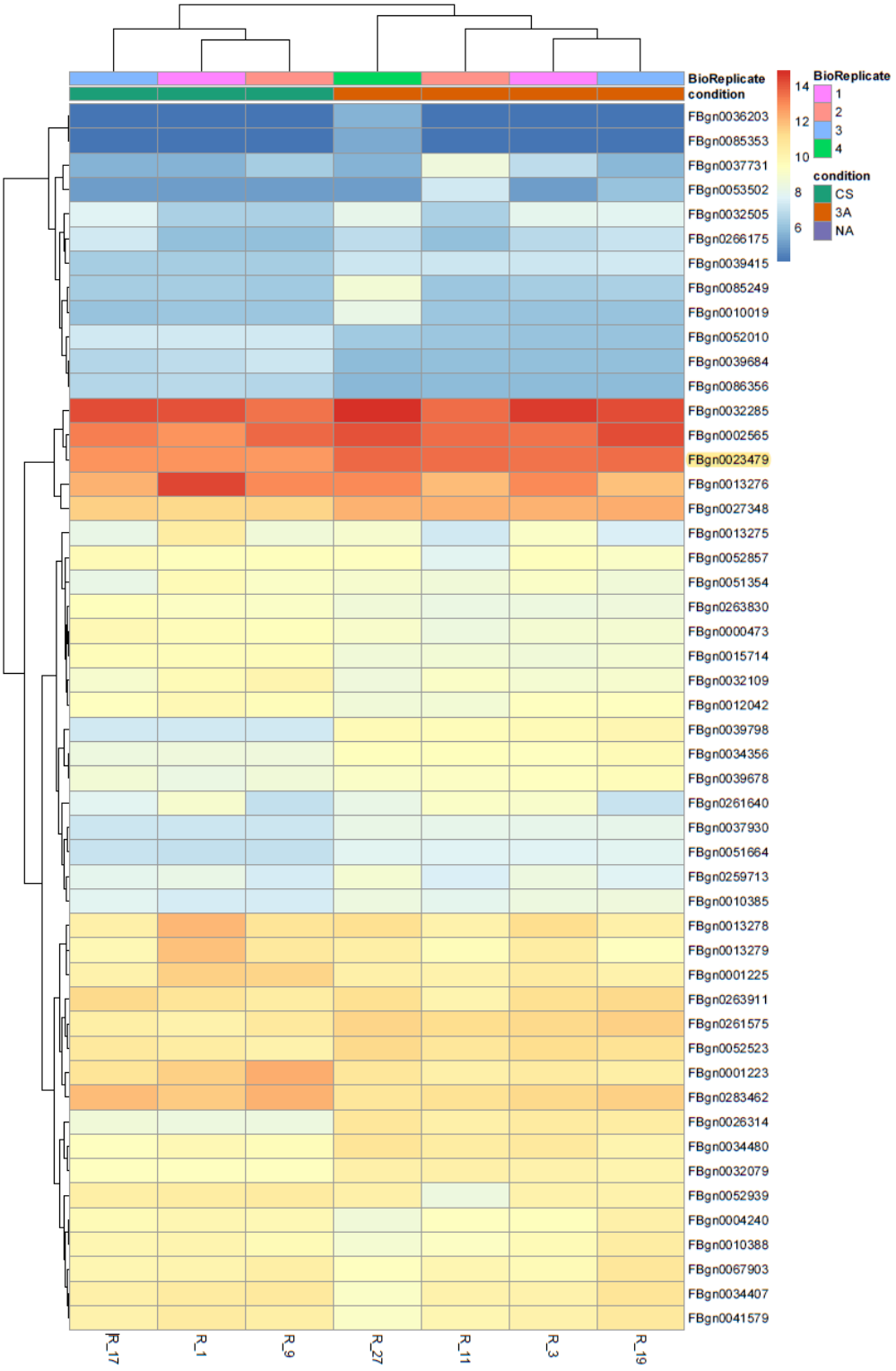

Supplementary Figure 9.10: Heatmap of top 50 most differentially expressed genes of CS versus 3A

FlyBase gene ID are indicated on the right side of the heatmap. Dendrogram on top and left side of the heatmap indicates hierarchical clustering. Each row indicates the differential expression of the gene across different conditions and replicates. FlyBase gene ID is indicated on the right side of the heatmap. Highlighted gene is *Tequila*.

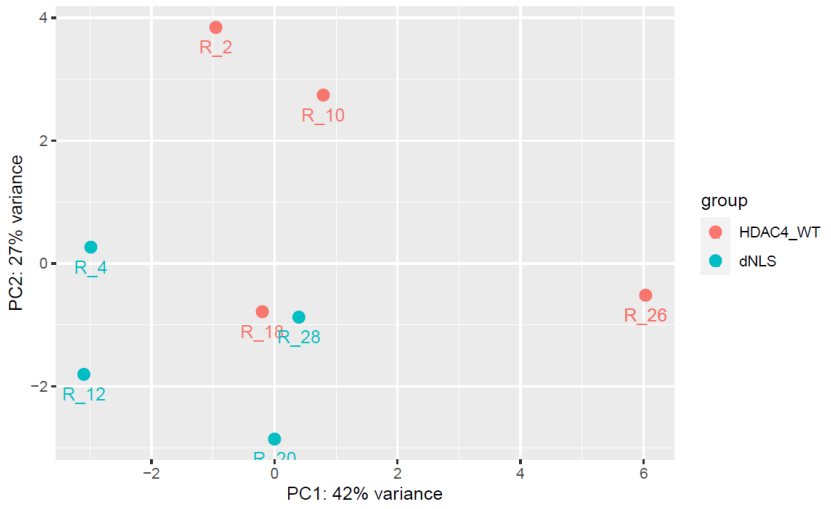

Supplementary Figure 9.11: PCA analysis plot of the 50 most varying genes between DmHDAC4^{WT} and dNLS
Two-dimensional visualisation of samples' variances. The first principal component on the x-axis, PC1, spans the dimension of the largest variation between samples data and the second principal component on the y-axis, PC2, spans the dimension of the second largest variation.

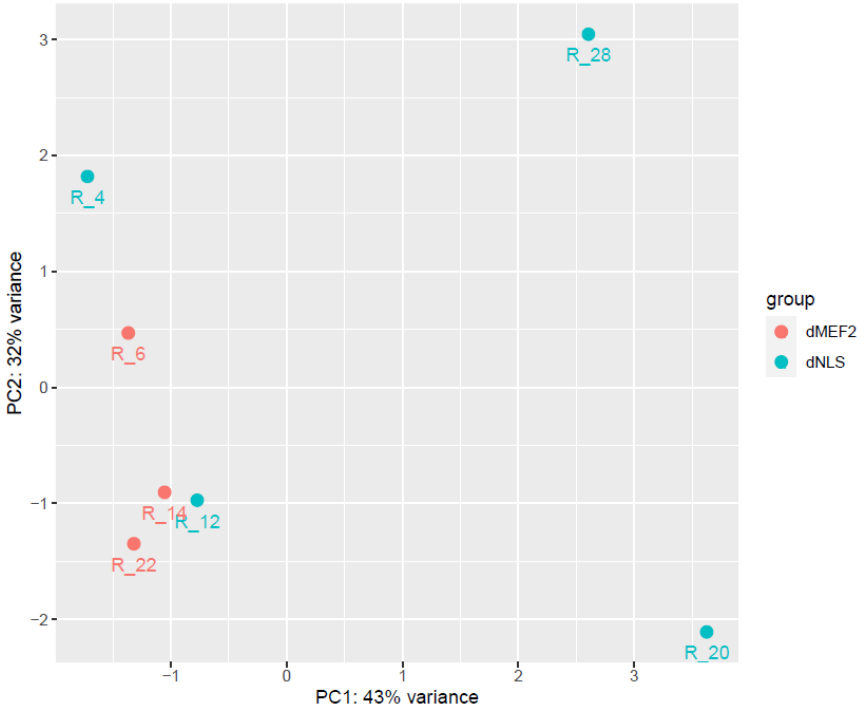

Supplementary Figure 9.12: PCA analysis plot of the 50 most varying genes between dMEF2 and dNLS
Two-dimensional visualisation of samples' variances. The first principal component on the x-axis, PC1, spans the dimension of the largest variation between samples data and the second principal component on the y-axis, PC2, spans the dimension of the second largest variation.

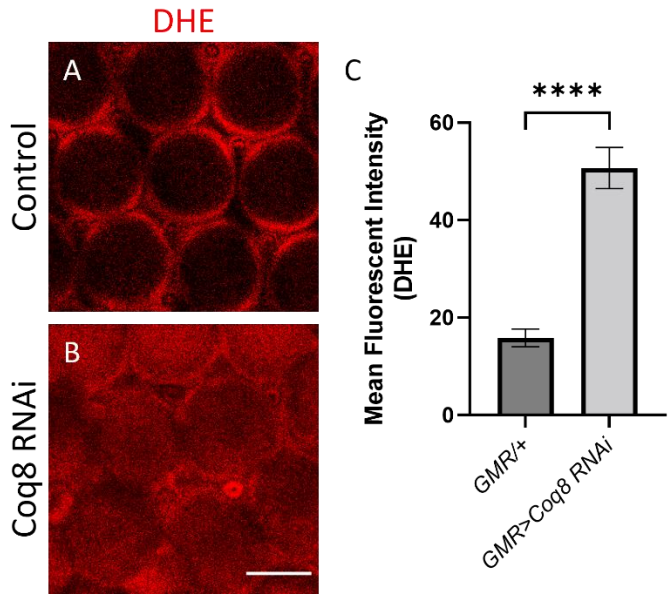

Supplementary Figure 9.13: Detection of ROS in retina of *Drosophila* with *Coenzyme Q8* KD using DHE

(A & B) Confocal images show DHE stained adult *Drosophila* retina. (C) Each bar represents the mean ± SEM fluorescent intensity of DHE for the indicated genotypes (*GMR/+*: n=6, *GMR>Coq8 RNAi*: n=7) (*t*-test $t_{(11)} = 7.117$, ****p<0.0001).

9.5 Supplementary Tables

CS vs DmHDAC4 WT:

GO Terms for Biological Process	Gene Count	%	*p*-value	Fold Enrichment	FDR
Multicellular Organism Reproduction	73	7.314629259	5.41E-36	5.848254357	3.05E-33
Sperm Competition	11	1.102204409	6.74E-08	9.473370927	1.90E-05
Post-Mating Behavior	7	0.701402806	3.18E-07	18.08552632	4.98E-05
Proteolysis	50	5.01002004	3.53E-07	2.175702414	4.98E-05
Microtubule-Based Movement	15	1.503006012	4.42E-05	3.690923738	0.004984358
Chitin Metabolic Process	16	1.603206413	7.48E-05	3.340472393	0.007026678
Behavior	5	0.501002004	1.67E-04	14.76369495	0.013493791
Glucose Metabolic Process	6	0.601202405	7.22E-04	7.75093985	0.045239497
Negative Regulation Of Female Receptivity, Post-Mating	6	0.601202405	7.22E-04	7.75093985	0.045239497
GO Terms for Cellular Components					
Extracellular Space	94	9.418837675	7.02E-25	3.217487786	1.21E-22
Extracellular Region	54	5.410821643	2.98E-06	1.951399201	2.56E-04
Sperm Flagellum	6	0.601202405	2.73E-04	9.273315862	0.01567982
Microtubule	12	1.20240481	9.91E-04	3.25819206	0.042600556
GO Terms for Molecular Function					
Aminopeptidase Activity	11	1.102204409	8.77E-07	7.445068164	3.02E-04
Metalloexopeptidase Activity	8	0.801603206	2.11E-06	11.21594684	3.64E-04
Manganese Ion Binding	8	0.801603206	1.05E-05	9.236662107	0.00120336
Serine-Type Endopeptidase Inhibitor Activity	14	1.402805611	2.02E-04	3.392477749	0.017345772
3-Oxo-Lignoceronyl-CoA Synthase Activity	7	0.701402806	3.52E-04	6.869767442	0.017345772
3-Oxo-Cerotoyl-CoA Synthase Activity	7	0.701402806	3.52E-04	6.869767442	0.017345772
3-Oxo-Arachidoyl-CoA Synthase Activity	7	0.701402806	3.52E-04	6.869767442	0.017345772
Chitin Binding	17	1.703406814	4.76E-04	2.712800151	0.020528108
KEGG Pathway					
Carbon Metabolism	22	2.204408818	2.86E-09	4.6	1.83E-07
Metabolic Pathways	69	6.913827655	1.50E-08	1.761376249	4.81E-07
Biosynthesis Of Antibiotics	23	2.304609218	4.59E-06	2.938888889	9.79E-05
Galactose Metabolism	10	1.002004008	8.01E-06	6.764705882	1.28E-04
Glycolysis / Gluconeogenesis	11	1.102204409	6.14E-05	4.773584906	6.62E-04
Citrate Cycle (TCA Cycle)	10	1.002004008	6.20E-05	5.348837209	6.62E-04
Biosynthesis Of Amino Acids	11	1.102204409	2.79E-04	4.015873016	0.002552099
Pyruvate Metabolism	9	0.901803607	5.31E-04	4.6	0.004248696
Starch And Sucrose Metabolism	7	0.701402806	0.001717049	5.193548387	0.012210126

Supplementary Table 9.1: DAVID annotation chart analysis of pairwise comparison: *CS* versus *DmHDAC4^{WT}*

Genes were annotated using databases from GO Term Biological Processes (GOTERM_BP_DIRECT), Cellular Components (GOTERM_CC_DIRECT) and Molecular Function (GOTERM_MF_DIRECT). Count column indicates the number of genes from the list of significantly differentially expressed genes that are implicated in the corresponding terms. Percentage column refers to the percentage of genes from the list that are annotated with the term. *P*-value column is derived from a Modified Fisher's Exact test of the number genes from the list that are involved in a term against the database list. Fold enrichment column indicates the number of fold that the term is expected to happen as opposed to being due to random occurrence. FDR column is the adjusted *p*-value.

CS vs 3A:

GO Terms for Cellular Components	Gene Count	%	*p*-value	Fold Enrichment	FDR
Extracellular Region	15	9.803921569	1.68E-04	3.220066804	0.008752796
Extracellular Matrix	7	4.575163399	0.001120151	5.883802817	0.029123922
GO Terms for Molecular Function					
Structural Constituent Of Chitin-Based Larval Cuticle	7	4.575163399	5.19E-04	6.812159329	0.047562163

Supplementary Table 9.2: DAVID annotation chart analysis of pairwise comparison: *CS* versus *3A*

Genes were annotated using databases from GO Term Biological Processes (GOTERM_BP_DIRECT), Cellular Components (GOTERM_CC_DIRECT) and Molecular Function (GOTERM_MF_DIRECT). Count column indicates the number of genes from the list of significantly differentially expressed genes that are implicated in the corresponding terms. Percentage column refers to the percentage of genes from the list that are annotated with the term. *P*-value column is derived from a Modified Fisher's Exact test of the number genes from the list that are involved in a term against the database list. Fold enrichment column indicates the number of fold that the term is expected to happen as opposed to being due to random occurrence. FDR column is the adjusted *p*-value.

CS vs dNLS:

GO Terms for Cellular Components	Gene Count	%	*p*-value	Fold Enrichment	FDR
Extracellular Region	12	10.34482759	2.91E-04	3.667601512	0.010752359
KEGG Pathway					
Glycosaminoglycan Degradation	3	2.586206897	0.002799381	34.2125	0.048778015
Metabolic Pathways	11	9.482758621	0.003562304	2.227672956	0.048778015

Supplementary Table 9.3: DAVID annotation chart analysis of pairwise comparison: *CS* versus *dNLS*

Genes were annotated using databases from GO Term Biological Processes (GOTERM_BP_DIRECT), Cellular Components (GOTERM_CC_DIRECT) and Molecular Function (GOTERM_MF_DIRECT). Count column indicates the number of genes from the list of significantly differentially expressed genes that are implicated in the corresponding terms. Percentage column refers to the percentage of genes from the list that are annotated with the term. *P*-value column is derived from a Modified Fisher's Exact test of the number genes from the list that are involved in a term against the database list. Fold enrichment column indicates the number of fold that the term is expected to happen as opposed to being due to random occurrence. FDR column is the adjusted *p*-value.

CS vs dMEF2:

GO Terms for Biological Process	Gene Count	%	*p*-value	Fold Enrichment	FDR
Response To Heat	9	5.921052632	2.09E-07	13.99377828	2.64E-05
Heat Shock-Mediated Polytene Chromosome Puffing	5	3.289473684	2.49E-07	75.52197802	2.64E-05
Chaperone-Mediated Protein Folding	5	3.289473684	9.16E-06	35.24358974	6.47E-04
Response To Hypoxia	6	3.947368421	1.47E-05	18.65837104	7.77E-04
Antibacterial Humoral Response	5	3.289473684	5.61E-05	22.98494983	0.00200166
Response To Unfolded Protein	4	2.631578947	6.44E-05	46.99145299	0.00200166
Response To Bacterium	6	3.947368421	6.61E-05	13.7909699	0.00200166
Innate Immune Response	7	4.605263158	4.22E-04	7.116494083	0.011177079
GO Terms for Cellular Components					
Extracellular Region	19	12.5	4.44E-06	3.532114515	2.22E-04

Supplementary Table 9.4: DAVID annotation chart analysis of pairwise comparison: *CS* versus *dMEF2*

Genes were annotated using databases from GO Term Biological Processes (GOTERM_BP_DIRECT), Cellular Components (GOTERM_CC_DIRECT) and Molecular Function (GOTERM_MF_DIRECT). Count column indicates the number of genes from the list of significantly differentially expressed genes that are implicated in the corresponding terms. Percentage column refers to the percentage of genes from the list that are annotated with the term. *P*-value column is derived from a Modified Fisher's Exact test of the number genes from the list that are involved in a term against the database list. Fold enrichment column indicates the number of fold that the term is expected to happen as opposed to being due to random occurrence. FDR column is the adjusted *p*-value.

CS vs dANK:

GO Terms for Biological Process	Gene Count	%	*p*-value	Fold Enrichment	FDR
Response To Heat	11	5.445544554	7.10E-09	13.37417072	1.76E-06
Chaperone-Mediated Protein Folding	6	2.97029703	6.30E-07	33.07067669	5.58E-05
Heat Shock-Mediated Polytene Chromosome Puffing	5	2.475247525	6.75E-07	59.05477981	5.58E-05
Response To Unfolded Protein	5	2.475247525	2.39E-06	45.93149541	1.35E-04
Response To Hypoxia	7	3.465346535	2.73E-06	17.02167183	1.35E-04
Sensory Perception Of Chemical Stimulus	7	3.465346535	8.19E-04	6.290617849	0.033835376
Proteolysis	15	7.425742574	0.00166787	2.610842897	0.05909024
GO Terms for Cellular Components					
Extracellular Region	21	10.3960396	5.09E-06	3.236579967	3.36E-04
Extracellular Matrix	8	3.96039604	0.001272398	4.827735645	0.041989118
Microtubule Associated Complex	11	5.445544554	0.002459314	3.142051282	0.054104919
GO Terms for Molecular Function					
Odorant Binding	8	3.96039604	6.93E-04	5.347926267	0.045717726
Structural Constituent Of Cuticle	8	3.96039604	6.93E-04	5.347926267	0.045717726

Supplementary Table 9.5: DAVID annotation chart analysis of pairwise comparison: *CS* versus *dANK*

Genes were annotated using databases from GO Term Biological Processes (GOTERM_BP_DIRECT), Cellular Components (GOTERM_CC_DIRECT) and Molecular Function (GOTERM_MF_DIRECT). Count column indicates the number of genes from the list of significantly differentially expressed genes that are implicated in the corresponding terms. Percentage column refers to the percentage of genes from the list that are annotated with the term. *P*-value column is derived from a Modified Fisher's Exact test of the number genes from the list that are involved in a term against the database list. Fold enrichment column indicates the number of fold that the term is expected to happen as opposed to being due to random occurrence. FDR column is the adjusted *p*-value.

CS vs Y1142H:

GO Terms for Biological Process	Gene Count	%	*p*-value	Fold Enrichment	FDR
Humoral Immune Response	5	2.450980392	1.42E-04	18.18121693	0.033037701
Defense Response To Gram-Positive Bacterium	6	2.941176471	4.21E-04	9.350340136	0.034396714
Chitin-Based Cuticle Development	9	4.411764706	4.51E-04	4.939802336	0.034396714
Chaperone-Mediated Protein Folding	4	1.960784314	5.91E-04	23.27195767	0.034396714
Oxidation-Reduction Process	14	6.862745098	8.05E-04	2.965480043	0.037494891
GO Terms for Cellular Components					
Extracellular Region	21	10.29411765	1.38E-06	3.506294964	6.92E-05
Extracellular Matrix	9	4.411764706	1.33E-04	5.883802817	0.003326457
GO Terms for Molecular Function					
Structural Constituent Of Cuticle	11	5.392156863	1.94E-06	7.413182346	2.70E-04
Structural Constituent Of Chitin-Based Larval Cuticle	9	4.411764706	7.27E-05	6.408651634	0.00505333
Carbohydrate Binding	8	3.921568627	1.20E-04	7.103969393	0.005576016
Odorant Binding	8	3.921568627	6.60E-04	5.391405343	0.022926032
KEGG Pathway					
Metabolic Pathways	23	11.2745098	2.58E-07	2.495283019	1.34E-05

Supplementary Table 9.6: DAVID annotation chart analysis of pairwise comparison: *CS* versus *Y1142H*

Genes were annotated using databases from GO Term Biological Processes (GOTERM_BP_DIRECT), Cellular Components (GOTERM_CC_DIRECT) and Molecular Function (GOTERM_MF_DIRECT). Count column indicates the number of genes from the list of significantly differentially expressed genes that are implicated in the corresponding terms. Percentage column refers to the percentage of genes from the list that are annotated with the term. *P*-value column is derived from a Modified Fisher's Exact test of the number genes from the list that are involved in a term against the database list. Fold enrichment column indicates the number of fold that the term is expected to happen as opposed to being due to random occurrence. FDR column is the adjusted *p*-value.

CS vs DmHDAC4 Knockdown:

GO Terms for Biological Process	Gene Count	%	*p*-value	Fold Enrichment	FDR
Antibacterial Humoral Response	8	7.920792079	7.04E-11	53.86895285	8.74E-09
Humoral Immune Response	7	6.930693069	6.58E-09	45.1713615	4.03E-07
Response To Heat	9	8.910891089	9.76E-09	20.49792875	4.03E-07
Response To Bacterium	8	7.920792079	1.37E-08	26.93447642	4.25E-07
Defense Response To Gram-Positive Bacterium	8	7.920792079	5.65E-08	22.12474849	1.40E-06
Innate Immune Response	9	8.910891089	2.84E-07	13.40249187	5.86E-06
Response To Hypoxia	6	5.940594059	2.18E-06	27.33057167	3.86E-05
Heat Shock-Mediated Polytene Chromosome Puffing	4	3.96039604	8.49E-06	88.49899396	1.32E-04
Response To Unfolded Protein	4	3.96039604	2.02E-05	68.83255086	2.78E-04
Defense Response	5	4.95049505	6.05E-05	22.77547639	6.93E-04
Defense Response To Gram-Negative Bacterium	7	6.930693069	6.15E-05	10.03808033	6.93E-04
Chaperone-Mediated Protein Folding	4	3.96039604	1.06E-04	41.29953052	0.001099705
Defense Response To Bacterium	5	4.95049505	8.53E-04	11.55770444	0.008139574
Cold Acclimation	3	2.97029703	0.00109124	58.07746479	0.00966527
GO Terms for Cellular Components					
Extracellular Region	21	20.79207921	2.82E-11	6.207866494	1.21E-09
Extracellular Space	12	11.88118812	6.26E-04	3.360013405	0.013451408
Microtubule Associated Complex	8	7.920792079	0.001986765	4.38295082	0.028476967
KEGG Pathway					
Protein Processing In Endoplasmic Reticulum	6	5.940594059	2.74E-04	8.688888889	0.006293108
Endocytosis	5	4.95049505	0.00234911	7.731638418	0.022273376
Spliceosome	5	4.95049505	0.002905223	7.298666667	0.022273376

Supplementary Table 9.7: DAVID annotation chart analysis of pairwise comparison: *CS* versus *DmHDAC4* KD

Genes were annotated using databases from GO Term Biological Processes (GOTERM_BP_DIRECT), Cellular Components (GOTERM_CC_DIRECT) and Molecular Function (GOTERM_MF_DIRECT). Count column indicates the number of genes from the list of significantly differentially expressed genes that are implicated in the corresponding terms. Percentage column refers to the percentage of genes from the list that are annotated with the term. *P*-value column is derived from a Modified Fisher's Exact test of the number genes from the list that are involved in a term against the database list. Fold enrichment column indicates the number of fold that the term is expected to happen as opposed to being due to random occurrence. FDR column is the adjusted *p*-value.

DmHDAC4 WT vs 3A:

GO Terms for Biological Process	Gene Count	%	*p*-value	Fold Enrichment	FDR
Multicellular Organism Reproduction	76	7.328833173	2.83E-38	5.976257902	1.68E-35
Sperm Competition	11	1.06075217	8.03E-08	9.298585486	2.39E-05
Post-Mating Behavior	7	0.675024108	3.55E-07	17.75184502	7.06E-05
Microtubule-Based Movement	15	1.446480231	5.41E-05	3.622825514	0.008066701
Negative Regulation Of Female Receptivity, Post-Mating	7	0.675024108	7.23E-05	8.875922509	0.0086239
Tricarboxylic Acid Cycle	10	0.964320154	1.35E-04	4.948249482	0.012645441
Cilium Movement	8	0.771456123	1.49E-04	6.492103321	0.012645441
Behavior	5	0.482160077	1.80E-04	14.49130206	0.01341616
Oviposition	6	0.578592093	2.62E-04	9.363610559	0.015611062
Malate Metabolic Process	6	0.578592093	2.62E-04	9.363610559	0.015611062
Spermatogenesis, Exchange Of Chromosomal Proteins	5	0.482160077	5.99E-04	11.27101271	0.032449086
Sperm Individualization	10	0.964320154	8.74E-04	3.9015044	0.043388581
Spermatogenesis	19	1.832208293	0.00101228	2.379436017	0.045117022
Sperm Motility	6	0.578592093	0.001068834	7.160408075	0.045117022
Proteolysis	40	3.857280617	0.001135496	1.708448242	0.045117022
GO Terms for Cellular Components					
Extracellular Space	85	8.196721311	1.72E-18	2.802713884	3.12E-16
Sperm Flagellum	6	0.578592093	3.26E-04	8.933174933	0.02204589
Microtubule	13	1.253616201	3.65E-04	3.400240008	0.02204589
Extracellular Region	47	4.532304725	9.27E-04	1.636142052	0.035176476
Axoneme	6	0.578592093	9.72E-04	7.258204633	0.035176476
GO Terms for Molecular Function					
Aminopeptidase Activity	11	1.06075217	9.47E-07	7.382635726	3.33E-04
Metalloexopeptidase Activity	8	0.771456123	2.23E-06	11.12189278	3.93E-04
Manganese Ion Binding	8	0.771456123	1.11E-05	9.159205821	0.001297882
Microtubule Binding	18	1.735776278	2.48E-05	3.30509078	0.002178855
KEGG Pathway					
Carbon Metabolism	25	2.410800386	8.47E-12	5.227272727	4.91E-10
Biosynthesis Of Antibiotics	25	2.410800386	2.99E-07	3.194444444	6.43E-06
Metabolic Pathways	66	6.364513018	3.33E-07	1.684794673	6.43E-06
Citrate Cycle (TCA Cycle)	12	1.157184185	1.07E-06	6.418604651	1.56E-05
Biosynthesis Of Amino Acids	11	1.06075217	2.79E-04	4.015873016	0.003237976
Pyruvate Metabolism	9	0.867888139	5.31E-04	4.6	0.005133841
Glycolysis / Gluconeogenesis	9	0.867888139	0.001635069	3.905660377	0.013547715
Galactose Metabolism	7	0.675024108	0.002821322	4.735294118	0.020454585

Supplementary Table 9.8: DAVID annotation chart analysis of pairwise comparison: *DmHDAC4*^{WT} versus *3A*

Genes were annotated using databases from GO Term Biological Processes (GOTERM_BP_DIRECT), Cellular Components (GOTERM_CC_DIRECT) and Molecular Function (GOTERM_MF_DIRECT). Count column indicates the number of genes from the list of significantly differentially expressed genes that are implicated in the corresponding terms. Percentage column refers to the percentage of genes from the list that are annotated with the term. *P*-value column is derived from a Modified Fisher's Exact test of the number genes from the list that are involved in a term against the database list. Fold enrichment column indicates the number of fold that the term is expected to happen as opposed to being due to random occurrence. FDR column is the adjusted *p*-value.

DmHDAC4 WT vs dMEF2:

GO Terms for Biological Process	Gene Count	%	*p*-value	Fold Enrichment	FDR
Multicellular Organism Reproduction	76	7.487684729	5.71E-39	6.111569402	2.71E-36
Sperm Competition	11	1.083743842	6.50E-08	9.509119497	1.54E-05
Post-Mating Behavior	7	0.689655172	3.11E-07	18.15377358	4.91E-05
Proteolysis	48	4.729064039	1.82E-06	2.096556107	2.15E-04
Heat Shock-Mediated Polytene Chromosome Puffing	6	0.591133005	4.90E-06	17.78328841	4.65E-04
Response To Unfolded Protein	6	0.591133005	2.71E-05	13.83144654	0.002142686
Cilium Movement	8	0.78817734	1.29E-04	6.63909434	0.008691831
Sperm Individualization	11	1.083743842	1.55E-04	4.388824383	0.008691831
Behavior	5	0.492610837	1.65E-04	14.81940701	0.008691831
Glycolytic Process	8	0.78817734	2.19E-04	6.147309574	0.01039501
Tricarboxylic Acid Cycle	9	0.886699507	6.37E-04	4.554256788	0.027442557
Negative Regulation Of Female Receptivity, Post-Mating	6	0.591133005	7.10E-04	7.780188679	0.028028381
Protein Refolding	5	0.492610837	8.82E-04	10.37358491	0.032146587
Lipid Metabolic Process	12	1.18226601	0.001480043	3.112075472	0.050110029
GO Terms for Cellular Components					
Extracellular Space	90	8.866995074	7.99E-22	3.020051342	1.25E-19
Extracellular Region	59	5.812807882	9.12E-08	2.090196605	7.16E-06
Sperm Flagellum	6	0.591133005	3.00E-04	9.09112891	0.01570615
GO Terms for Molecular Function					
Aminopeptidase Activity	11	1.083743842	8.60E-07	7.460841613	2.87E-04
Metalloexopeptidase Activity	8	0.78817734	2.08E-06	11.23970944	3.48E-04
Manganese Ion Binding	8	0.78817734	1.03E-05	9.256231306	0.00114884
Lipase Activity	8	0.78817734	6.08E-04	5.24519774	0.050738983
KEGG Pathway					
Carbon Metabolism	25	2.463054187	3.14E-11	4.936868687	1.89E-09
Metabolic Pathways	69	6.798029557	3.33E-07	1.663522013	1.00E-05
Biosynthesis Of Antibiotics	25	2.463054187	9.22E-07	3.016975309	1.84E-05
Citrate Cycle (TCA Cycle)	11	1.083743842	1.46E-05	5.556847545	2.20E-04
Biosynthesis Of Amino Acids	12	1.18226601	9.42E-05	4.137566138	0.001130598
Starch And Sucrose Metabolism	8	0.78817734	3.68E-04	5.605734767	0.003682567
Glycolysis / Gluconeogenesis	10	0.985221675	5.21E-04	4.098532495	0.004469423
Galactose Metabolism	8	0.78817734	6.72E-04	5.111111111	0.005038644
Pyruvate Metabolism	9	0.886699507	7.83E-04	4.344444444	0.005221776
Oxidative Phosphorylation	16	1.57635468	0.001318869	2.50039968	0.007913211
Arginine And Proline Metabolism	8	0.78817734	0.004233662	3.777777778	0.023092699

Supplementary Table 9.9: DAVID annotation chart analysis of pairwise comparison: *DmHDAC4^{WT}* versus *dMEF2*

Genes were annotated using databases from GO Term Biological Processes (GOTERM_BP_DIRECT), Cellular Components (GOTERM_CC_DIRECT) and Molecular Function (GOTERM_MF_DIRECT). Count column indicates the number of genes from the list of significantly differentially expressed genes that are implicated in the corresponding terms. Percentage column refers to the percentage of genes from the list that are annotated with the term. *P*-value column is derived from a Modified Fisher's Exact test of the number genes from the list that are involved in a term against the database list. Fold enrichment column indicates the number of fold that the term is expected to happen as opposed to being due to random occurrence. FDR column is the adjusted *p*-value.

DmHDAC4 WT vs dANK:

GO Terms for Biological Process	Gene Count	%	*p*-value	Fold Enrichment	FDR
Multicellular Organism Reproduction	87	6.861198738	1.87E-41	5.493264427	1.20E-38
Sperm Competition	12	0.94637224	5.07E-08	8.145185185	1.63E-05
Proteolysis	59	4.652996845	3.00E-07	2.023435478	6.41E-05
Post-Mating Behavior	7	0.552050473	1.31E-06	14.25407407	2.10E-04
Heat Shock-Mediated Polytene Chromosome Puffing	6	0.47318612	1.61E-05	13.9631746	0.002073321
Negative Regulation Of Female Receptivity, Post-Mating	8	0.630914826	2.21E-05	8.145185185	0.002368455
Cilium Movement	9	0.70977918	8.12E-05	5.864533333	0.007008952
Response To Unfolded Protein	6	0.47318612	8.73E-05	10.86024691	0.007008952
Tricarboxylic Acid Cycle	11	0.867507886	1.38E-04	4.370587173	0.009867342
Protein Refolding	6	0.47318612	1.66E-04	9.774222222	0.010648851
Sperm Individualization	12	0.94637224	2.53E-04	3.759316239	0.014783391
Spermatogenesis	23	1.813880126	3.55E-04	2.312830361	0.018983156
Behavior	5	0.394321767	4.22E-04	11.63597884	0.02083192
Malate Metabolic Process	6	0.47318612	7.26E-04	7.518632479	0.031059275
Oviposition	6	0.47318612	7.26E-04	7.518632479	0.031059275
Glycolytic Process	8	0.630914826	9.50E-04	4.826776406	0.036563963
Chitin Metabolic Process	16	1.261829653	9.68E-04	2.632787131	0.036563963
Spermatogenesis, Exchange Of Chromosomal Proteins	5	0.394321767	0.00137513	9.050205761	0.049046303
Protein Targeting To Mitochondrion	8	0.630914826	0.001499919	4.493895275	0.050681488
Microtubule-Based Movement	14	1.104100946	0.001698293	2.715061728	0.053178875
Transmembrane Transport	32	2.523659306	0.001739496	1.79755811	0.053178875
Long-Chain Fatty-Acyl-CoA Metabolic Process	6	0.47318612	0.002111451	6.108888889	0.05893703
Wax Biosynthetic Process	6	0.47318612	0.002111451	6.108888889	0.05893703
GO Terms for Cellular Components					
Extracellular Space	108	8.517350158	2.22E-24	2.864359254	4.63E-22
Extracellular Region	61	4.810725552	4.05E-05	1.708035435	0.004228956
Microtubule	14	1.104100946	7.61E-04	2.945358402	0.037281181
Sperm Flagellum	6	0.47318612	8.92E-04	7.185379838	0.037281181
Eukaryotic Translation Initiation Factor 4F Complex	6	0.47318612	8.92E-04	7.185379838	0.037281181
Mitochondrial Outer Membrane	8	0.630914826	0.007044162	3.459627329	0.225760718
Inner Dynein Arm	4	0.315457413	0.007561364	8.896184561	0.225760718
Axoneme	5	0.394321767	0.016414033	4.865100932	0.428816607
Tricarboxylic Acid Cycle Enzyme Complex	3	0.23659306	0.022591761	11.67624224	0.5246309
GO Terms for Molecular Function					
Manganese Ion Binding	9	0.70977918	4.46E-06	8.110658125	0.001481249
Aminopeptidase Activity	11	0.867507886	8.27E-06	5.811084557	0.001481249
Metalloexopeptidase Activity	8	0.630914826	1.11E-05	8.75436115	0.001481249
Chitin Binding	20	1.577287066	3.57E-04	2.491078376	0.035877514
Fatty-Acyl-CoA Reductase (Alcohol-Forming) Activity	7	0.552050473	4.97E-04	6.308289652	0.039951578
KEGG Pathway					
Carbon Metabolism	27	2.129337539	6.45E-11	4.390909091	4.51E-09
Citrate Cycle (TCA Cycle)	13	1.025236593	1.92E-06	5.408268734	5.57E-05
Metabolic Pathways	78	6.151419558	2.45E-06	1.548649649	5.57E-05
Biosynthesis Of Antibiotics	27	2.129337539	3.18E-06	2.683333333	5.57E-05
Oxidative Phosphorylation	19	1.498422713	5.01E-04	2.445243805	0.006265666
Biosynthesis Of Amino Acids	12	0.94637224	5.40E-04	3.407407407	0.006265666
Pyruvate Metabolism	10	0.788643533	6.27E-04	3.975308642	0.006265666
Glycolysis / Gluconeogenesis	10	0.788643533	0.002137523	3.375262055	0.016667345
Galactose Metabolism	8	0.630914826	0.002142944	4.209150327	0.016667345
Starch And Sucrose Metabolism	7	0.552050473	0.006151344	4.039426523	0.043059405

Supplementary Table 9.10: DAVID annotation chart analysis of pairwise comparison: *DmHDAC4^{WT}* versus *dANK*

Genes were annotated using databases from GO Term Biological Processes (GOTERM_BP_DIRECT), Cellular Components (GOTERM_CC_DIRECT) and Molecular Function (GOTERM_MF_DIRECT). Count column indicates the number of genes from the list of significantly differentially expressed genes that are implicated in the corresponding terms. Percentage column refers to the percentage of genes from the list that are annotated with the term. *P*-value column is derived from a Modified Fisher's Exact test of the number genes from the list that are involved in a term against the database list. Fold enrichment column indicates the number of fold that the term is expected to happen as opposed to being due to random occurrence. FDR column is the adjusted *p*-value.

DmHDAC4 WT vs Y1142H:

GO Terms for Biological Process	Gene Count	%	*p*-value	Fold Enrichment	FDR
Multicellular Organism Reproduction	83	6.998313659	7.43E-40	5.579610202	4.61E-37
Proteolysis	61	5.143338954	5.45E-09	2.227315291	1.69E-06
Sperm Competition	11	0.927487352	3.50E-07	7.949263933	7.23E-05
Post-Mating Behavior	7	0.590219224	9.01E-07	15.17586751	1.22E-04
Negative Regulation Of Female Receptivity, Post-Mating	9	0.758853288	9.84E-07	9.755914826	1.22E-04
Sperm Storage	7	0.590219224	4.30E-05	9.338995389	0.004447281
Protein Refolding	6	0.505902192	1.23E-04	10.40630915	0.010899757
Behavior	5	0.42158516	3.31E-04	12.38846327	0.025658216
Tricarboxylic Acid Cycle	10	0.84317032	4.36E-04	4.230206971	0.030028607
Malate Metabolic Process	6	0.505902192	5.44E-04	8.004853191	0.030639454
Oviposition	6	0.505902192	5.44E-04	8.004853191	0.030639454
Sperm Individualization	11	0.927487352	6.53E-04	3.668891046	0.033727453
Microtubule-Based Movement	14	1.180438449	9.61E-04	2.89064143	0.045816436
Spermatogenesis, Exchange Of Chromosomal Proteins	5	0.42158516	0.00108595	9.635471434	0.048092084
GO Terms for Cellular Components					
Extracellular Space	103	8.6846543	5.07E-24	2.932078365	9.99E-22
Extracellular Region	64	5.396290051	4.89E-07	1.923453237	4.82E-05
Sperm Flagellum	6	0.505902192	6.44E-04	7.712307692	0.042314058
GO Terms for Molecular Function					
Manganese Ion Binding	9	0.758853288	2.56E-06	8.730122244	8.20E-04
Aminopeptidase Activity	11	0.927487352	4.28E-06	6.254915171	8.20E-04
Metalloexopeptidase Activity	8	0.674536256	6.78E-06	9.422989089	8.66E-04
Microtubule Binding	17	1.433389545	5.97E-04	2.644659674	0.057192633
Serine-Type Endopeptidase Activity	32	2.698145025	7.79E-04	1.884597818	0.059633255
KEGG Pathway					
Carbon Metabolism	25	2.107925801	5.26E-10	4.349968214	3.31E-08
Metabolic Pathways	82	6.913996627	1.11E-09	1.741918459	3.50E-08
Biosynthesis Of Antibiotics	27	2.276559865	8.16E-07	2.870979021	1.44E-05
Citrate Cycle (TCA Cycle)	13	1.096121417	9.17E-07	5.786469345	1.44E-05
Oxidative Phosphorylation	19	1.602023609	2.12E-04	2.616239875	0.002668445
Pyruvate Metabolism	10	0.84317032	3.77E-04	4.253302253	0.003961775
Starch And Sucrose Metabolism	8	0.674536256	8.03E-04	4.939318746	0.007222628
Biosynthesis Of Amino Acids	11	0.927487352	0.001230538	3.341880342	0.009253453
Glycolysis / Gluconeogenesis	10	0.84317032	0.001321922	3.611294366	0.009253453
Galactose Metabolism	7	0.590219224	0.007067929	3.940559441	0.044527954
Folate Biosynthesis	6	0.505902192	0.008015951	4.593566434	0.044642012
Arginine And Proline Metabolism	8	0.674536256	0.00850324	3.328671329	0.044642012

Supplementary Table 9.11: DAVID annotation chart analysis of pairwise comparison: *DmHDAC4^{WT}* versus *Y1142H*

Genes were annotated using databases from GO Term Biological Processes (GOTERM_BP_DIRECT), Cellular Components (GOTERM_CC_DIRECT) and Molecular Function (GOTERM_MF_DIRECT). Count column indicates the number of genes from the list of significantly differentially expressed genes that are implicated in the corresponding terms. Percentage column refers to the percentage of genes from the list that are annotated with the term. *P*-value column is derived from a Modified Fisher's Exact test of the number genes from the list that are involved in a term against the database list. Fold enrichment column indicates the number of fold that the term is expected to happen as opposed to being due to random occurrence. FDR column is the adjusted *p*-value.

dMEF2 vs 3A:

GO Terms for Cellular Components	Gene Count	%	*p*-value	Fold Enrichment	FDR
Organelle Membrane	4	13.33333333	5.65E-04	23.07479862	0.006784609
GO Terms for Molecular Function					
Iron Ion Binding	5	16.66666667	1.59E-04	16.50782361	0.004464663
Monooxygenase Activity	4	13.33333333	6.06E-04	22.21052632	0.006236968
Oxidoreductase Activity, Acting On Paired Donors, With Incorporation Or Reduction Of Molecular Oxygen	4	13.33333333	6.68E-04	21.47831116	0.006236968
Heme Binding	4	13.33333333	0.001960865	14.80701754	0.013726054

Supplementary Table 9.12: DAVID annotation chart analysis of pairwise comparison: *dMEF2* versus *3A*

Genes were annotated using databases from GO Term Biological Processes (GOTERM_BP_DIRECT), Cellular Components (GOTERM_CC_DIRECT) and Molecular Function (GOTERM_MF_DIRECT). Count column indicates the number of genes from the list of significantly differentially expressed genes that are implicated in the corresponding terms. Percentage column refers to the percentage of genes from the list that are annotated with the term. *P*-value column is derived from a Modified Fisher's Exact test of the number genes from the list that are involved in a term against the database list. Fold enrichment column indicates the number of fold that the term is expected to happen as opposed to being due to random occurrence. FDR column is the adjusted *p*-value.

dMEF2 vs dNLS:

GO Terms for Cellular Components	Gene Count	%	*p*-value	Fold Enrichment	FDR
Extracellular Region	4	44.44444444	0.002990557	10.30421377	0.023924452

Supplementary Table 9.13: DAVID annotation chart analysis of pairwise comparison: *dMEF2* versus *dNLS*

Genes were annotated using databases from GO Term Biological Processes (GOTERM_BP_DIRECT), Cellular Components (GOTERM_CC_DIRECT) and Molecular Function (GOTERM_MF_DIRECT). Count column indicates the number of genes from the list of significantly differentially expressed genes that are implicated in the corresponding terms. Percentage column refers to the percentage of genes from the list that are annotated with the term. *P*-value column is derived from a Modified Fisher's Exact test of the number genes from the list that are involved in a term against the database list. Fold enrichment column indicates the number of fold that the term is expected to happen as opposed to being due to random occurrence. FDR column is the adjusted *p*-value.

Comparison	Cluster #	FLYBASE_GENE_ID	Genes within Cluster
CS vs DmHDAC4 WT	Annotation Cluster 5	FBGN0040959	CG17814 gene product from transcript CG17814-RA(Peritrophin-15a)
		FBGN0085249	CG34220 gene product from transcript CG34220-RA(CG34220)
		FBGN0035933	CG13309 gene product from transcript CG13309-RA(CG13309)
		FBGN0023479	CG4821 gene product from transcript CG4821-RG(Tequila)
		FBGN0052656	Mucin 11A(Muc11A)
		FBGN0085353	CG34324 gene product from transcript CG34324-RA(CG34324)
		FBGN0030999	Mucin related 18B(Mur18B)
		FBGN0040687	CG14645 gene product from transcript CG14645-RA(CG14645)
		FBGN0051077	CG31077 gene product from transcript CG31077-RB(CG31077)
		FBGN0053265	Mucin 68E(Muc68E)
		FBGN0260430	CG42525 gene product from transcript CG42525-RB(CG42525)
		FBGN0085455	CG34426 gene product from transcript CG34426-RA(CG34426)
		FBGN0053258	CG33258 gene product from transcript CG33258-RB(CG33258)
		FBGN0259748	CG42397 gene product from transcript CG42397-RA(CG42397)
		FBGN0036203	Mucin 68D(Muc68D)
		FBGN0036232	CG14125 gene product from transcript CG14125-RB(CG14125)
CS vs 3A	Annotation Cluster 1	FBGN0020642	CG6956 gene product from transcript CG6956-RA(Lcp65Ac)
		FBGN0033942	Cuticular protein 51A(Cpr51A)
		FBGN0004782	CG1252 gene product from transcript CG1252-RA(Ccp84Ab)
		FBGN0085491	CG34462 gene product from transcript CG34462-RA(CG34462)
		FBGN0036879	Cuticular protein 76Bb(Cpr76Bb)
		FBGN0039480	Cuticular protein 97Ea(Cpr97Ea)
		FBGN0036881	Cuticular protein 76Bd(Cpr76Bd)

Supplementary Table 9.14: Comparison of genes within clusters involved in chitin-based processes
Annotation Cluster 5 of *CS* versus *DmHDAC4*^{WT}and Annotation Cluster 1 of *CS* versus *3A* includes chitin-based processes.

FBGN0036328	**CG10749 gene product from transcript CG10749-RA(CG10749)**
***CS* vs *DmHDAC4*^{WT}**	**Log_2 Fold Change: 5.146, Adjusted *p*-value: 1.50E-02**
GOTERM_BP_DIRECT	carbohydrate metabolic process, tricarboxylic acid cycle, malate metabolic process,
GOTERM_CC_DIRECT	mitochondrial matrix,
GOTERM_MF_DIRECT	L-malate dehydrogenase activity,
KEGG_PATHWAY	Citrate cycle (TCA cycle), Cysteine and methionine metabolism, Pyruvate metabolism, Glyoxylate and dicarboxylate metabolism, Metabolic pathways, Biosynthesis of antibiotics, Carbon metabolism,

FBGN0034356	**CG10924 gene product from transcript CG10924-RA(Pepck2)**
***CS* vs *DmHDAC4*^{WT}**	**Log_2 Fold Change: 1.713, Adjusted *p*-value: 7.22E-21**
GOTERM_BP_DIRECT	gluconeogenesis,
GOTERM_CC_DIRECT	mitochondrion,
GOTERM_MF_DIRECT	phosphoenolpyruvate carboxykinase (GTP) activity, GTP binding,
KEGG_PATHWAY	Glycolysis / Gluconeogenesis, Citrate cycle (TCA cycle), Pyruvate metabolism, Metabolic pathways, Biosynthesis of antibiotics, FoxO signaling pathway, Insulin resistance,

FBGN0037115	**CG11249 gene product from transcript CG11249-RA(CG11249)**
***CS* vs *DmHDAC4*^{WT}**	**Log_2 Fold Change: 4.765, Adjusted *p*-value: 1.34E-03**
GOTERM_BP_DIRECT	glycolytic process,

GOTERM_MF_DIRECT	magnesium ion binding, pyruvate kinase activity, potassium ion binding,
KEGG_PATHWAY	Glycolysis / Gluconeogenesis, Purine metabolism, Pyruvate metabolism, Metabolic pathways, Biosynthesis of antibiotics, Carbon metabolism, Biosynthesis of amino acids,

FBGN0035933	**CG13309 gene product from transcript CG13309-RA(CG13309)**
CS* vs *DmHDAC4^{WT}	**Log_2 Fold Change: 6.882, Adjusted *p*-value: 5.92E-05**
GOTERM_BP_DIRECT	chitin metabolic process, multicellular organism reproduction,
GOTERM_CC_DIRECT	extracellular region, extracellular space,
GOTERM_MF_DIRECT	chitin binding,

FBGN0036232	**CG14125 gene product from transcript CG14125-RB(CG14125)**
CS* vs *DmHDAC4^{WT}	**Log_2 Fold Change: 8.065, Adjusted *p*-value: 3.34E-02**
GOTERM_BP_DIRECT	chitin metabolic process,
GOTERM_CC_DIRECT	extracellular region,
GOTERM_MF_DIRECT	chitin binding,

FBGN0040687	**CG14645 gene product from transcript CG14645-RA(CG14645)**
CS* vs *DmHDAC4^{WT}	**Log_2 Fold Change: 9.299, Adjusted *p*-value: 2.23E-02**
GOTERM_BP_DIRECT	chitin metabolic process,
GOTERM_CC_DIRECT	extracellular region,
GOTERM_MF_DIRECT	chitin binding,

FBGN0037988	**CG14740 gene product from transcript CG14740-RA(CG14740)**
CS* vs *DmHDAC4^{WT}	**Log_2 Fold Change: 3.146, Adjusted *p*-value: 2.05E-03**
GOTERM_BP_DIRECT	tricarboxylic acid cycle,
GOTERM_CC_DIRECT	mitochondrial matrix,
GOTERM_MF_DIRECT	citrate (Si)-synthase activity, transferase activity, transferring acyl groups, acyl groups converted into alkyl on transfer,
KEGG_PATHWAY	Citrate cycle (TCA cycle), Glyoxylate and dicarboxylate metabolism, Metabolic pathways, Biosynthesis of antibiotics, Carbon metabolism, 2-Oxocarboxylic acid metabolism, Biosynthesis of amino acids,

FBGN0037763	**CG16904 gene product from transcript CG16904-RA(CG16904)**
CS* vs *DmHDAC4^{WT}	**Log_2 Fold Change: 7.841, Adjusted *p*-value: 2.46E-07**
GOTERM_BP_DIRECT	fatty acid elongation,
GOTERM_CC_DIRECT	integral component of membrane,
GOTERM_MF_DIRECT	fatty acid elongase activity, 3-oxo-arachidoyl-CoA synthase activity, 3-oxo-cerotoyl-CoA synthase activity, 3-oxo-lignoceronyl-CoA synthase activity,

FBGN0011270	**CG17645 gene product from transcript CG17645-RA(Pglym87)**
CS* vs *DmHDAC4^{WT}	**Log_2 Fold Change: 1.565, Adjusted *p*-value: 1.22E-02**
GOTERM_BP_DIRECT	gluconeogenesis, glycolytic process, regulation of pentose-phosphate shunt,

GOTERM_CC_DIRECT	cytosol,
GOTERM_MF_DIRECT	bisphosphoglycerate mutase activity, bisphosphoglycerate 2-phosphatase activity, phosphoglycerate mutase activity, 2,3-bisphosphoglycerate-dependent phosphoglycerate mutase activity,
KEGG_PATHWAY	Glycolysis / Gluconeogenesis, Glycine, serine and threonine metabolism, Metabolic pathways, Biosynthesis of antibiotics, Carbon metabolism, Biosynthesis of amino acids,

FBGN0040959	**CG17814 gene product from transcript CG17814-RA(Peritrophin-15a)**
***CS* vs *DmHDAC4*^{WT}**	**Log_2 Fold Change: 6.545, Adjusted *p*-value: 1.44E-03**
GOTERM_BP_DIRECT	chitin metabolic process,
GOTERM_CC_DIRECT	extracellular region, extracellular space,
GOTERM_MF_DIRECT	chitin binding,

FBGN0032969	**CG2528 gene product from transcript CG2528-RG(CG2528)**
***CS* vs *DmHDAC4*^{WT}**	**Log_2 Fold Change: 4.968, Adjusted *p*-value: 1.39E-05**
GOTERM_BP_DIRECT	proteolysis,
GOTERM_CC_DIRECT	cytoplasm,
GOTERM_MF_DIRECT	aminopeptidase activity, serine-type endopeptidase activity, serine-type exopeptidase activity,

FBGN0031462	**CG2964 gene product from transcript CG2964-RA(CG2964)**
***CS* vs *DmHDAC4*^{WT}**	**Log_2 Fold Change: 3.076, Adjusted *p*-value: 3.16E-02**
GOTERM_BP_DIRECT	pyruvate metabolic process, glycolytic process,
GOTERM_CC_DIRECT	cytoplasm, plasma membrane,
GOTERM_MF_DIRECT	magnesium ion binding, pyruvate kinase activity, kinase activity, potassium ion binding,
KEGG_PATHWAY	Glycolysis / Gluconeogenesis, Purine metabolism, Pyruvate metabolism, Metabolic pathways, Biosynthesis of antibiotics, Carbon metabolism, Biosynthesis of amino acids,

FBGN0050008	**CG30008 gene product from transcript CG30008-RA(CG30008)**
***CS* vs *DmHDAC4*^{WT}**	**Log_2 Fold Change: 3.231, Adjusted *p*-value: 9.99E-08**
GOTERM_BP_DIRECT	fatty acid elongation,
GOTERM_CC_DIRECT	integral component of membrane,
GOTERM_MF_DIRECT	fatty acid elongase activity, 3-oxo-arachidoyl-CoA synthase activity, 3-oxo-cerotoyl-CoA synthase activity, 3-oxo-lignoceronyl-CoA synthase activity,

FBGN0050293	**CG30293 gene product from transcript CG30293-RA(Cht12)**
***CS* vs *DmHDAC4*^{WT}**	**Log_2 Fold Change: 4.821, Adjusted *p*-value: 2.56E-04**
GOTERM_BP_DIRECT	carbohydrate metabolic process, chitin catabolic process, ecdysis, chitin-based cuticle, chitin-based cuticle development, wound healing,
GOTERM_CC_DIRECT	extracellular region,
GOTERM_MF_DIRECT	chitinase activity, chitin binding,

KEGG_PATHWAY	Amino sugar and nucleotide sugar metabolism,

FBGN0051077	**CG31077 gene product from transcript CG31077-RB(CG31077)**
CS* vs *DmHDAC4^{WT}	**Log_2 Fold Change: 6.401, Adjusted *p*-value: 6.44E-03**
GOTERM_BP_DIRECT	chitin metabolic process,
GOTERM_CC_DIRECT	extracellular region,
GOTERM_MF_DIRECT	chitin binding,

FBGN0051141	**CG31141 gene product from transcript CG31141-RA(CG31141)**
CS* vs *DmHDAC4^{WT}	**Log_2 Fold Change: 2.631, Adjusted *p*-value: 4.90E-02**
GOTERM_BP_DIRECT	fatty acid biosynthetic process, fatty acid elongation,
GOTERM_CC_DIRECT	integral component of membrane,
GOTERM_MF_DIRECT	fatty acid elongase activity, 3-oxo-arachidoyl-CoA synthase activity, 3-oxo-cerotoyl-CoA synthase activity, 3-oxo-lignoceronyl-CoA synthase activity,

FBGN0052026	**CG32026 gene product from transcript CG32026-RA(CG32026)**
CS* vs *DmHDAC4^{WT}	**Log_2 Fold Change: 3.459, Adjusted *p*-value: 6.19E-05**
GOTERM_BP_DIRECT	oxidation-reduction process,
GOTERM_CC_DIRECT	microtubule associated complex,
GOTERM_MF_DIRECT	magnesium ion binding, isocitrate dehydrogenase (NAD+) activity, oxidoreductase activity, acting on the CH-OH group of donors, NAD or NADP as acceptor, NAD binding,
KEGG_PATHWAY	Citrate cycle (TCA cycle), Metabolic pathways, Biosynthesis of antibiotics, Carbon metabolism, 2-Oxocarboxylic acid metabolism, Biosynthesis of amino acids,

FBGN0043783	**CG32444 gene product from transcript CG32444-RA(CG32444)**
CS* vs *DmHDAC4^{WT}	**Log_2 Fold Change: 1.001, Adjusted *p*-value: 2.65E-07**
GOTERM_BP_DIRECT	glucose metabolic process, hexose metabolic process, galactose catabolic process via UDP-galactose,
GOTERM_MF_DIRECT	aldose 1-epimerase activity, isomerase activity, carbohydrate binding,
KEGG_PATHWAY	Glycolysis / Gluconeogenesis, Galactose metabolism, Metabolic pathways, Biosynthesis of antibiotics,

FBGN0052445	**CG32445 gene product from transcript CG32445-RA(CG32445)**
CS* vs *DmHDAC4^{WT}	**Log_2 Fold Change: 4.338, Adjusted *p*-value: 2.89E-05**
GOTERM_BP_DIRECT	glucose metabolic process, hexose metabolic process, galactose catabolic process via UDP-galactose,
GOTERM_MF_DIRECT	aldose 1-epimerase activity, isomerase activity, carbohydrate binding,
KEGG_PATHWAY	Glycolysis / Gluconeogenesis, Galactose metabolism, Metabolic pathways, Biosynthesis of antibiotics,

FBGN0042710	**CG32849 gene product from transcript CG32849-RA(Hex-t2)**
CS* vs *DmHDAC4^{WT}	**Log_2 Fold Change: 5.101, Adjusted *p*-value: 1.68E-05**

GOTERM_BP_DIRECT	cellular glucose homeostasis, fructose metabolic process, glucose metabolic process, mannose metabolic process, glycolytic process, carbohydrate phosphorylation,
GOTERM_CC_DIRECT	cytosol,
GOTERM_MF_DIRECT	glucokinase activity, hexokinase activity, ATP binding, glucose binding, fructokinase activity, mannokinase activity,
KEGG_PATHWAY	Glycolysis / Gluconeogenesis, Fructose and mannose metabolism, Galactose metabolism, Starch and sucrose metabolism, Amino sugar and nucleotide sugar metabolism, Metabolic pathways, Biosynthesis of antibiotics, Carbon metabolism,

FBGN0053258	**CG33258 gene product from transcript CG33258-RB(CG33258)**
CS* vs *DmHDAC4^{WT}	**Log_2 Fold Change: 3.210, Adjusted *p*-value: 2.43E-03**
GOTERM_BP_DIRECT	chitin metabolic process,
GOTERM_CC_DIRECT	extracellular region,
GOTERM_MF_DIRECT	chitin binding,

FBGN0085249	**CG34220 gene product from transcript CG34220-RA(CG34220)**
CS* vs *DmHDAC4^{WT}	**Log_2 Fold Change: 3.768, Adjusted *p*-value: 1.39E-02**
GOTERM_BP_DIRECT	chitin metabolic process,
GOTERM_CC_DIRECT	extracellular region,
GOTERM_MF_DIRECT	chitin binding,

FBGN0085353	**CG34324 gene product from transcript CG34324-RA(CG34324)**
CS* vs *DmHDAC4^{WT}	**Log_2 Fold Change: 10.257, Adjusted *p*-value: 1.09E-02**
GOTERM_BP_DIRECT	chitin metabolic process,
GOTERM_CC_DIRECT	extracellular region,
GOTERM_MF_DIRECT	chitin binding,

FBGN0085455	**CG34426 gene product from transcript CG34426-RA(CG34426)**
CS* vs *DmHDAC4^{WT}	**Log_2 Fold Change: 5.460, Adjusted *p*-value: 3.47E-02**
GOTERM_BP_DIRECT	chitin metabolic process,
GOTERM_CC_DIRECT	extracellular region,
GOTERM_MF_DIRECT	chitin binding,

FBGN0035005	**CG3483 gene product from transcript CG3483-RA(CG3483)**
CS* vs *DmHDAC4^{WT}	**Log_2 Fold Change: 5.384, Adjusted *p*-value: 3.00E-03**
GOTERM_BP_DIRECT	oxidation-reduction process,
GOTERM_MF_DIRECT	magnesium ion binding, isocitrate dehydrogenase (NAD+) activity, oxidoreductase activity, acting on the CH-OH group of donors, NAD or NADP as acceptor, NAD binding,
KEGG_PATHWAY	Citrate cycle (TCA cycle), Metabolic pathways, Biosynthesis of antibiotics, Carbon metabolism, 2-Oxocarboxylic acid metabolism, Biosynthesis of amino acids,

FBGN0259748	**CG42397 gene product from transcript CG42397-RA(CG42397)**

***CS* vs *DmHDAC4*^{WT}**	**Log_2 Fold Change: 6.829, Adjusted *p*-value: 9.31E-03**
GOTERM_BP_DIRECT	chitin metabolic process,
GOTERM_CC_DIRECT	extracellular region,
GOTERM_MF_DIRECT	chitin binding,

FBGN0260430	**CG42525 gene product from transcript CG42525-RB(CG42525)**
***CS* vs *DmHDAC4*^{WT}**	**Log_2 Fold Change: 4.821, Adjusted *p*-value: 4.45E-02**
GOTERM_BP_DIRECT	chitin metabolic process,
GOTERM_CC_DIRECT	extracellular region,
GOTERM_MF_DIRECT	chitin binding,

FBGN0037862	**CG4706 gene product from transcript CG4706-RA(CG4706)**
***CS* vs *DmHDAC4*^{WT}**	**Log_2 Fold Change: 4.087, Adjusted *p*-value: 6.87E-04**
GOTERM_BP_DIRECT	tricarboxylic acid cycle, multicellular organism reproduction,
GOTERM_CC_DIRECT	extracellular space, mitochondrion,
GOTERM_MF_DIRECT	aconitate hydratase activity, metal ion binding, 4 iron, 4 sulfur cluster binding,
KEGG_PATHWAY	Citrate cycle (TCA cycle), Glyoxylate and dicarboxylate metabolism, Metabolic pathways, Biosynthesis of antibiotics, Carbon metabolism, 2-Oxocarboxylic acid metabolism, Biosynthesis of amino acids,

FBGN0259795	**CG4750 gene product from transcript CG4750-RC(loopin-1)**
***CS* vs *DmHDAC4*^{WT}**	**Log_2 Fold Change: 4.741, Adjusted *p*-value: 9.47E-22**
GOTERM_BP_DIRECT	proteolysis,
GOTERM_CC_DIRECT	cytoplasm,
GOTERM_MF_DIRECT	aminopeptidase activity, metalloexopeptidase activity, manganese ion binding,
KEGG_PATHWAY	Arginine and proline metabolism, Glutathione metabolism, Metabolic pathways,

FBGN0023479	**CG4821 gene product from transcript CG4821-RG(Tequila)**
***CS* vs *DmHDAC4*^{WT}**	**Log_2 Fold Change: 1.210, Adjusted *p*-value: 2.83E-51**
GOTERM_BP_DIRECT	chitin metabolic process, proteolysis, short-term memory, long-term memory, glucose homeostasis, regulation of insulin-like growth factor receptor signaling pathway,
GOTERM_CC_DIRECT	extracellular region, membrane,
GOTERM_MF_DIRECT	serine-type endopeptidase activity, scavenger receptor activity, chitin binding,

FBGN0032372	**CG4988 gene product from transcript CG4988-RA(CG4988)**
***CS* vs *DmHDAC4*^{WT}**	**Log_2 Fold Change: 3.930, Adjusted *p*-value: 4.45E-03**
GOTERM_BP_DIRECT	glucose metabolic process, hexose metabolic process, galactose catabolic process via UDP-galactose,
GOTERM_MF_DIRECT	aldose 1-epimerase activity, isomerase activity, carbohydrate binding,

KEGG_PATHWAY	Glycolysis / Gluconeogenesis, Galactose metabolism, Metabolic pathways, Biosynthesis of antibiotics,

FBGN0039425	**CG5432 gene product from transcript CG5432-RA(CG5432)**
***CS* vs *DmHDAC4*^{WT}**	**Log_2 Fold Change: 4.621, Adjusted *p*-value: 2.51E-06**
GOTERM_BP_DIRECT	glycolytic process,
GOTERM_MF_DIRECT	fructose-bisphosphate aldolase activity,
KEGG_PATHWAY	Glycolysis / Gluconeogenesis, Pentose phosphate pathway, Fructose and mannose metabolism, Metabolic pathways, Biosynthesis of antibiotics, Carbon metabolism, Biosynthesis of amino acids,

FBGN0036162	**CG6140 gene product from transcript CG6140-RB(CG6140)**
***CS* vs *DmHDAC4*^{WT}**	**Log_2 Fold Change: 5.167, Adjusted *p*-value: 5.94E-04**
GOTERM_BP_DIRECT	tricarboxylic acid cycle, fumarate metabolic process, malate metabolic process, protein tetramerization,
GOTERM_CC_DIRECT	cytoplasm, mitochondrion, cytosol, tricarboxylic acid cycle enzyme complex,
GOTERM_MF_DIRECT	fumarate hydratase activity,
KEGG_PATHWAY	Citrate cycle (TCA cycle), Pyruvate metabolism, Metabolic pathways, Biosynthesis of antibiotics, Carbon metabolism,

FBGN0038708	**CG6255 gene product from transcript CG6255-RA(CG6255)**
***CS* vs *DmHDAC4*^{WT}**	**Log_2 Fold Change: 3.551, Adjusted *p*-value: 4.93E-05**
GOTERM_BP_DIRECT	tricarboxylic acid cycle, succinyl-CoA metabolic process, succinate metabolic process, metabolic process, nucleoside triphosphate biosynthetic process, lateral inhibition,
GOTERM_CC_DIRECT	mitochondrial matrix,
GOTERM_MF_DIRECT	catalytic activity, succinate-CoA ligase (ADP-forming) activity, succinate-CoA ligase (GDP-forming) activity, ligase activity, cofactor binding,
KEGG_PATHWAY	Citrate cycle (TCA cycle), Propanoate metabolism, Metabolic pathways, Biosynthesis of antibiotics, Carbon metabolism,

FBGN0034121	**CG6262 gene product from transcript CG6262-RB(CG6262)**
***CS* vs *DmHDAC4*^{WT}**	**Log_2 Fold Change: 4.160, Adjusted *p*-value: 1.55E-09**
GOTERM_BP_DIRECT	trehalose metabolic process, trehalose catabolic process, metabolic process,
GOTERM_MF_DIRECT	alpha,alpha-trehalase activity,
KEGG_PATHWAY	Starch and sucrose metabolism, Metabolic pathways,

FBGN0037860	**CG6629 gene product from transcript CG6629-RA(CG6629)**
***CS* vs *DmHDAC4*^{WT}**	**Log_2 Fold Change: 6.004, Adjusted *p*-value: 1.44E-03**
GOTERM_BP_DIRECT	tricarboxylic acid cycle, mitochondrial electron transport, succinate to ubiquinone,

GOTERM_CC_DIRECT	mitochondrial respiratory chain complex II, succinate dehydrogenase complex (ubiquinone), integral component of membrane, succinate dehydrogenase complex,
GOTERM_MF_DIRECT	succinate dehydrogenase activity,
KEGG_PATHWAY	Citrate cycle (TCA cycle), Oxidative phosphorylation, Metabolic pathways, Biosynthesis of antibiotics, Carbon metabolism,

FBGN0039030	**CG6660 gene product from transcript CG6660-RA(CG6660)**
CS* vs *DmHDAC4^{WT}	**Log_2 Fold Change: 4.337, Adjusted *p*-value: 4.48E-03**
GOTERM_BP_DIRECT	fatty acid biosynthetic process,
GOTERM_CC_DIRECT	integral component of membrane,
GOTERM_MF_DIRECT	3-oxo-arachidoyl-CoA synthase activity, 3-oxo-cerotoyl-CoA synthase activity, 3-oxo-lignoceronyl-CoA synthase activity,

FBGN0038258	**CG7362 gene product from transcript CG7362-RB(CG7362)**
CS* vs *DmHDAC4^{WT}	**Log_2 Fold Change: 4.929, Adjusted *p*-value: 1.50E-05**
GOTERM_BP_DIRECT	glycolytic process, phagocytosis,
GOTERM_MF_DIRECT	magnesium ion binding, pyruvate kinase activity, potassium ion binding,
KEGG_PATHWAY	Glycolysis / Gluconeogenesis, Purine metabolism, Pyruvate metabolism, Metabolic pathways, Biosynthesis of antibiotics, Carbon metabolism, Biosynthesis of amino acids,

FBGN0028935	**CG7653 gene product from transcript CG7653-RB(CG7653)**
CS* vs *DmHDAC4^{WT}	**Log_2 Fold Change: 4.466, Adjusted *p*-value: 6.73E-03**
GOTERM_BP_DIRECT	proteolysis, peptide catabolic process,
GOTERM_CC_DIRECT	cytoplasm, plasma membrane,
GOTERM_MF_DIRECT	aminopeptidase activity, metallopeptidase activity, zinc ion binding, peptide binding, metalloaminopeptidase activity,

FBGN0038136	**CG8774 gene product from transcript CG8774-RB(CG8774)**
CS* vs *DmHDAC4^{WT}	**Log_2 Fold Change: 7.129, Adjusted *p*-value: 3.65E-05**
GOTERM_BP_DIRECT	proteolysis, peptide catabolic process,
GOTERM_CC_DIRECT	cytoplasm, plasma membrane, integral component of membrane,
GOTERM_MF_DIRECT	aminopeptidase activity, metallopeptidase activity, zinc ion binding, peptide binding, metalloaminopeptidase activity,

FBGN0034173	**CG9010 gene product from transcript CG9010-RA(CG9010)**
CS* vs *DmHDAC4^{WT}	**Log_2 Fold Change: 2.737, Adjusted *p*-value: 4.98E-02**
GOTERM_BP_DIRECT	glucose metabolic process, glycolytic process, oxidation-reduction process,
GOTERM_MF_DIRECT	glyceraldehyde-3-phosphate dehydrogenase (NAD+) (phosphorylating) activity, oxidoreductase activity, acting on the aldehyde or oxo group of donors, NAD or NADP as acceptor, NADP binding, NAD binding,
KEGG_PATHWAY	Glycolysis / Gluconeogenesis, Metabolic pathways, Biosynthesis of antibiotics, Carbon metabolism, Biosynthesis of amino acids,

FBGN0037765	**CG9458 gene product from transcript CG9458-RA(CG9458)**
CS* vs *DmHDAC4^{WT}	**Log_2 Fold Change: 4.238, Adjusted *p*-value: 3.70E-02**
GOTERM_BP_DIRECT	fatty acid elongation,
GOTERM_CC_DIRECT	integral component of membrane,
GOTERM_MF_DIRECT	fatty acid elongase activity, 3-oxo-arachidoyl-CoA synthase activity, 3-oxo-cerotoyl-CoA synthase activity, 3-oxo-lignoceronyl-CoA synthase activity,

FBGN0037764	**CG9459 gene product from transcript CG9459-RA(CG9459)**
CS* vs *DmHDAC4^{WT}	**Log_2 Fold Change: 6.013, Adjusted *p*-value: 3.46E-03**
GOTERM_BP_DIRECT	fatty acid elongation,
GOTERM_CC_DIRECT	integral component of membrane,
GOTERM_MF_DIRECT	fatty acid elongase activity, 3-oxo-arachidoyl-CoA synthase activity, 3-oxo-cerotoyl-CoA synthase activity, 3-oxo-lignoceronyl-CoA synthase activity,

FBGN0052072	**Elongase 68alpha(Elo68alpha)**
CS* vs *DmHDAC4^{WT}	**Log_2 Fold Change: 1.358, Adjusted *p*-value: 2.44E-02**
GOTERM_BP_DIRECT	fatty acid elongation, unsaturated fatty acid, fatty acid elongation, long-chain fatty acid biosynthetic process, pheromone biosynthetic process,
GOTERM_CC_DIRECT	integral component of membrane,
GOTERM_MF_DIRECT	fatty acid elongase activity, 3-oxo-arachidoyl-CoA synthase activity, 3-oxo-cerotoyl-CoA synthase activity, 3-oxo-lignoceronyl-CoA synthase activity,
KEGG_PATHWAY	Fatty acid elongation,

FBGN0002570	**Maltase A1(Mal-A1)**
CS* vs *DmHDAC4^{WT}	**Log_2 Fold Change: 1.218, Adjusted *p*-value: 3.00E-03**
GOTERM_BP_DIRECT	carbohydrate metabolic process,
GOTERM_MF_DIRECT	catalytic activity, alpha-1,4-glucosidase activity, maltose alpha-glucosidase activity,
KEGG_PATHWAY	Galactose metabolism, Starch and sucrose metabolism, Metabolic pathways,

FBGN0002569	**Maltase A2(Mal-A2)**
CS* vs *DmHDAC4^{WT}	**Log_2 Fold Change: 1.705, Adjusted *p*-value: 7.63E-03**
GOTERM_BP_DIRECT	carbohydrate metabolic process,
GOTERM_MF_DIRECT	catalytic activity, alpha-1,4-glucosidase activity, maltose alpha-glucosidase activity,
KEGG_PATHWAY	Galactose metabolism, Starch and sucrose metabolism, Metabolic pathways,

FBGN0033296	**Maltase A7(Mal-A7)**
CS* vs *DmHDAC4^{WT}	**Log_2 Fold Change: 8.890, Adjusted *p*-value: 4.26E-09**
GOTERM_BP_DIRECT	carbohydrate metabolic process,

GOTERM_MF_DIRECT	catalytic activity, alpha-1,4-glucosidase activity, maltose alpha-glucosidase activity,
KEGG_PATHWAY	Galactose metabolism, Starch and sucrose metabolism, Metabolic pathways,

FBGN0033297	**Maltase A8(Mal-A8)**
CS* vs *DmHDAC4^{WT}	**Log_2 Fold Change: 6.756, Adjusted *p*-value: 2.15E-06**
GOTERM_BP_DIRECT	carbohydrate metabolic process,
GOTERM_MF_DIRECT	catalytic activity, alpha-1,4-glucosidase activity, maltose alpha-glucosidase activity,
KEGG_PATHWAY	Galactose metabolism, Starch and sucrose metabolism, Metabolic pathways,

FBGN0052656	**Mucin 11A(Muc11A)**
CS* vs *DmHDAC4^{WT}	**Log_2 Fold Change: 3.633, Adjusted *p*-value: 1.37E-08**
GOTERM_BP_DIRECT	chitin metabolic process,
GOTERM_CC_DIRECT	extracellular region, extracellular matrix,
GOTERM_MF_DIRECT	extracellular matrix structural constituent, chitin binding,

FBGN0036203	**Mucin 68D(Muc68D)**
CS* vs *DmHDAC4^{WT}	**Log_2 Fold Change: 7.403, Adjusted *p*-value: 6.56E-05**
GOTERM_BP_DIRECT	chitin metabolic process,
GOTERM_CC_DIRECT	extracellular region, extracellular matrix,
GOTERM_MF_DIRECT	extracellular matrix structural constituent, chitin binding,

FBGN0053265	**Mucin 68E(Muc68E)**
CS* vs *DmHDAC4^{WT}	**Log_2 Fold Change: 4.237, Adjusted *p*-value: 9.36E-05**
GOTERM_BP_DIRECT	chitin metabolic process,
GOTERM_CC_DIRECT	extracellular region, extracellular matrix,
GOTERM_MF_DIRECT	extracellular matrix structural constituent, chitin binding,

FBGN0030999	**Mucin related 18B(Mur18B)**
CS* vs *DmHDAC4^{WT}	**Log_2 Fold Change: 7.248, Adjusted *p*-value: 3.42E-11**
GOTERM_BP_DIRECT	chitin metabolic process,
GOTERM_CC_DIRECT	extracellular region, extracellular matrix,
GOTERM_MF_DIRECT	extracellular matrix structural constituent, chitin binding,

FBGN0035915	**Sperm-Leucylaminopeptidase 1(S-Lap1)**
CS* vs *DmHDAC4^{WT}	**Log_2 Fold Change: 2.701, Adjusted *p*-value: 2.86E-11**
GOTERM_BP_DIRECT	proteolysis, mushroom body development,
GOTERM_CC_DIRECT	cytoplasm,
GOTERM_MF_DIRECT	aminopeptidase activity, metalloexopeptidase activity, manganese ion binding,
KEGG_PATHWAY	Arginine and proline metabolism, Glutathione metabolism, Metabolic pathways,

FBGN0052351	**Sperm-Leucylaminopeptidase 2(S-Lap2)**
CS* vs *DmHDAC4^{WT}	**Log_2 Fold Change: 3.874, Adjusted *p*-value: 9.68E-11**
GOTERM_BP_DIRECT	proteolysis,
GOTERM_CC_DIRECT	cytoplasm,
GOTERM_MF_DIRECT	aminopeptidase activity, metalloexopeptidase activity, manganese ion binding,
KEGG_PATHWAY	Arginine and proline metabolism, Glutathione metabolism, Metabolic pathways,

FBGN0045770	**Sperm-Leucylaminopeptidase 3(S-Lap3)**
CS* vs *DmHDAC4^{WT}	**Log_2 Fold Change: 5.042, Adjusted *p*-value: 1.69E-19**
GOTERM_BP_DIRECT	proteolysis,
GOTERM_CC_DIRECT	cytoplasm,
GOTERM_MF_DIRECT	aminopeptidase activity, metalloexopeptidase activity, manganese ion binding,

FBGN0052064	**Sperm-Leucylaminopeptidase 4(S-Lap4)**
CS* vs *DmHDAC4^{WT}	**Log_2 Fold Change: 5.112, Adjusted *p*-value: 3.75E-09**
GOTERM_BP_DIRECT	proteolysis,
GOTERM_CC_DIRECT	cytoplasm,
GOTERM_MF_DIRECT	aminopeptidase activity, metalloexopeptidase activity, manganese ion binding,
KEGG_PATHWAY	Arginine and proline metabolism, Glutathione metabolism, Metabolic pathways,

FBGN0033860	**Sperm-Leucylaminopeptidase 5(S-Lap5)**
CS* vs *DmHDAC4^{WT}	**Log_2 Fold Change: 7.509, Adjusted *p*-value: 9.09E-09**
GOTERM_BP_DIRECT	proteolysis, mesoderm development,
GOTERM_CC_DIRECT	cytoplasm,
GOTERM_MF_DIRECT	aminopeptidase activity, metalloexopeptidase activity, manganese ion binding,

FBGN0033868	**Sperm-Leucylaminopeptidase 7(S-Lap7)**
CS* vs *DmHDAC4^{WT}	**Log_2 Fold Change: 4.926, Adjusted *p*-value: 1.60E-07**
GOTERM_BP_DIRECT	proteolysis, multicellular organism reproduction,
GOTERM_CC_DIRECT	extracellular space, cytoplasm,
GOTERM_MF_DIRECT	aminopeptidase activity, metalloexopeptidase activity, manganese ion binding,

FBGN0034132	**Sperm-Leucylaminopeptidase 8(S-Lap8)**
CS* vs *DmHDAC4^{WT}	**Log_2 Fold Change: 4.761, Adjusted *p*-value: 7.76E-07**
GOTERM_BP_DIRECT	proteolysis,
GOTERM_CC_DIRECT	cytoplasm,
GOTERM_MF_DIRECT	aminopeptidase activity, metalloexopeptidase activity, manganese ion binding,
KEGG_PATHWAY	Arginine and proline metabolism, Glutathione metabolism, Metabolic pathways,

FBGN0030975	**Succinate dehydrogenase, subunit B (iron-sulfur)-like(SdhBL)**
CS* vs *DmHDAC4^{WT}	**Log_2 Fold Change: 2.783, Adjusted *p*-value: 6.87E-05**
GOTERM_BP_DIRECT	tricarboxylic acid cycle, mitochondrial electron transport, succinate to ubiquinone, aerobic respiration, respiratory electron transport chain,
GOTERM_CC_DIRECT	mitochondrial inner membrane, mitochondrial membrane, respiratory chain complex II,
GOTERM_MF_DIRECT	succinate dehydrogenase activity, succinate dehydrogenase (ubiquinone) activity, electron carrier activity, oxidoreductase activity, metal ion binding, 2 iron, 2 sulfur cluster binding, 3 iron, 4 sulfur cluster binding, 4 iron, 4 sulfur cluster binding,
KEGG_PATHWAY	Citrate cycle (TCA cycle), Oxidative phosphorylation, Metabolic pathways, Biosynthesis of antibiotics, Carbon metabolism,

FBGN0261575	**target of brain insulin(tobi)**
CS* vs *DmHDAC4^{WT}	**Log_2 Fold Change: 2.179, Adjusted *p*-value: 6.08E-09**
GOTERM_BP_DIRECT	carbohydrate metabolic process,
GOTERM_MF_DIRECT	hydrolase activity, hydrolyzing O-glycosyl compounds, alpha-1,4-glucosidase activity, maltose alpha-glucosidase activity,
KEGG_PATHWAY	Galactose metabolism, Starch and sucrose metabolism, Metabolic pathways,

Supplementary Table 9.15: List of 63 differentially expressed genes from the pairwise comparison of *CS* versus *DmHDAC4^{WT}*

FBGN0036328	**CG10749 gene product from transcript CG10749-RA(CG10749)**
DmHDAC4^{WT}* vs *3A	**Log_2 Fold Change: -5.928, Adjusted *p*-value: 1.68E-03**
DmHDAC4^{WT}* vs *dANK	**Log_2 Fold Change: -6.226, Adjusted *p*-value: 5.19E-04**
DmHDAC4^{WT}* vs *Y1142H	**Log_2 Fold Change: -6.129, Adjusted *p*-value: 6.83E-04**
GOTERM_BP_DIRECT	carbohydrate metabolic process, tricarboxylic acid cycle, malate metabolic process,
GOTERM_CC_DIRECT	mitochondrial matrix,
GOTERM_MF_DIRECT	L-malate dehydrogenase activity,
KEGG_PATHWAY	Citrate cycle (TCA cycle), Cysteine and methionine metabolism, Pyruvate metabolism, Glyoxylate and dicarboxylate metabolism, Metabolic pathways, Biosynthesis of antibiotics, Carbon metabolism,

FBGN0034356	**CG10924 gene product from transcript CG10924-RA(CG10924)**
DmHDAC4^{WT}* vs *3A	**N.A.**
DmHDAC4^{WT}* vs *dANK	**N.A.**
DmHDAC4^{WT}* vs *Y1142H	**Log_2 Fold Change: 1.707, Adjusted *p*-value: 1.37E-38**
GOTERM_BP_DIRECT	gluconeogenesis
GOTERM_CC_DIRECT	mitochondrion
GOTERM_MF_DIRECT	phosphoenolpyruvate carboxykinase (GTP) activity, GTP binding,
KEGG_PATHWAY	Glycolysis / Gluconeogenesis, Citrate cycle (TCA cycle), Pyruvate metabolism, Metabolic pathways, Biosynthesis of antibiotics, FoxO signaling pathway, Insulin resistance,

FBGN0037115	CG11249 gene product from transcript CG11249-RA(CG11249)
DmHDAC4^{WT} vs *3A*	**Log_2 Fold Change: -5.720, Adjusted *p*-value: 3.74E-05**
DmHDAC4^{WT} vs *dANK*	**Log_2 Fold Change: -4.711, Adjusted *p*-value: 4.79E-05**
DmHDAC4^{WT} vs *Y1142H*	**Log_2 Fold Change: -3.888, Adjusted *p*-value: 1.07E-04**
GOTERM_BP_DIRECT	glycolytic process,
GOTERM_MF_DIRECT	magnesium ion binding, pyruvate kinase activity, potassium ion binding,
KEGG_PATHWAY	Glycolysis / Gluconeogenesis, Purine metabolism, Pyruvate metabolism, Metabolic pathways, Biosynthesis of antibiotics, Carbon metabolism, Biosynthesis of amino acids,

FBGN0031462	CG2964 gene product from transcript CG2964-RA(CG2964)
DmHDAC4^{WT} vs *3A*	**Log_2 Fold Change: -4.884, Adjusted *p*-value: 1.62E-03**
DmHDAC4^{WT} vs *dANK*	**Log_2 Fold Change: -3.017, Adjusted *p*-value: 4.24E-03**
DmHDAC4^{WT} vs *Y1142H*	**Log_2 Fold Change: -2.136, Adjusted *p*-value: 3.66E-02**
GOTERM_BP_DIRECT	pyruvate metabolic process, glycolytic process,
GOTERM_CC_DIRECT	cytoplasm, plasma membrane,
GOTERM_MF_DIRECT	magnesium ion binding, pyruvate kinase activity, kinase activity, potassium ion binding,
KEGG_PATHWAY	Glycolysis / Gluconeogenesis, Purine metabolism, Pyruvate metabolism, Metabolic pathways, Biosynthesis of antibiotics, Carbon metabolism, Biosynthesis of amino acids,

FBGN0051874	CG31874 gene product from transcript CG31874-RA(CG31874)
DmHDAC4^{WT} vs *3A*	**Log_2 Fold Change: -1.545, Adjusted *p*-value: 1.21E-02**
DmHDAC4^{WT} vs *dANK*	**Log_2 Fold Change: -2.188, Adjusted *p*-value: 2.93E-02**
DmHDAC4^{WT} vs *Y1142H*	**Log_2 Fold Change: -2.529, Adjusted *p*-value: 5.75E-05**
GOTERM_BP_DIRECT	tricarboxylic acid cycle, fumarate metabolic process, malate metabolic process, protein tetramerization,
GOTERM_CC_DIRECT	mitochondrion, cytosol, tricarboxylic acid cycle enzyme complex,
GOTERM_MF_DIRECT	fumarate hydratase activity,
KEGG_PATHWAY	Citrate cycle (TCA cycle), Pyruvate metabolism, Metabolic pathways, Biosynthesis of antibiotics, Carbon metabolism,

FBGN0029890	CG4095 gene product from transcript CG4095-RA(CG4095)
DmHDAC4^{WT} vs *3A*	**Log_2 Fold Change: -1.404, Adjusted *p*-value: 1.83E-02**
DmHDAC4^{WT} vs *dANK*	**Log_2 Fold Change: -1.442, Adjusted *p*-value: 1.18E-02**
DmHDAC4^{WT} vs *Y1142H*	**Log_2 Fold Change: -1.591, Adjusted *p*-value: 7.74E-03**
GOTERM_BP_DIRECT	tricarboxylic acid cycle, fumarate metabolic process, malate metabolic process, protein tetramerization,
GOTERM_CC_DIRECT	cytoplasm, mitochondrion, cytosol, tricarboxylic acid cycle enzyme complex,
GOTERM_MF_DIRECT	fumarate hydratase activity,
KEGG_PATHWAY	Citrate cycle (TCA cycle), Pyruvate metabolism, Metabolic pathways, Biosynthesis of antibiotics, Carbon metabolism,

FBGN0036162	CG6140 gene product from transcript CG6140-RB(CG6140)
DmHDAC4^{WT} vs *3A*	**Log_2 Fold Change: -4.790, Adjusted *p*-value: 1.89E-04**
DmHDAC4^{WT} vs *dANK*	**Log_2 Fold Change: -6.422, Adjusted *p*-value: 4.38E-06**

DmHDAC4^{WT}* vs *Y1142H	**Log_2 Fold Change: -4.236, Adjusted *p*-value: 9.20E-05**
GOTERM_BP_DIRECT	tricarboxylic acid cycle, fumarate metabolic process, malate metabolic process, protein tetramerization,
GOTERM_CC_DIRECT	cytoplasm, mitochondrion, cytosol, tricarboxylic acid cycle enzyme complex,
GOTERM_MF_DIRECT	fumarate hydratase activity,
KEGG_PATHWAY	Citrate cycle (TCA cycle), Pyruvate metabolism, Metabolic pathways, Biosynthesis of antibiotics, Carbon metabolism,

FBGN0038258	**CG7362 gene product from transcript CG7362-RB(CG7362)**
DmHDAC4^{WT}* vs *3A	**Log_2 Fold Change: -3.452, Adjusted *p*-value: 1.53E-05**
DmHDAC4^{WT}* vs *dANK	**Log_2 Fold Change: -3.467, Adjusted *p*-value: 2.35E-07**
DmHDAC4^{WT}* vs *Y1142H	**Log_2 Fold Change: -4.626, Adjusted *p*-value: 2.64E-07**
GOTERM_BP_DIRECT	glycolytic process, phagocytosis,
GOTERM_MF_DIRECT	magnesium ion binding, pyruvate kinase activity, potassium ion binding,
KEGG_PATHWAY	Glycolysis / Gluconeogenesis, Purine metabolism, Pyruvate metabolism, Metabolic pathways, Biosynthesis of antibiotics, Carbon metabolism, Biosynthesis of amino acids,

FBGN0029154	**Malic enzyme like-1(Menl-1)**
DmHDAC4^{WT}* vs *3A	**Log_2 Fold Change: -3.092, Adjusted *p*-value: 2.99E-05**
DmHDAC4^{WT}* vs *dANK	**Log_2 Fold Change: -3.553, Adjusted *p*-value: 6.39E-04**
DmHDAC4^{WT}* vs *Y1142H	**Log_2 Fold Change: -2.943, Adjusted *p*-value: 2.70E-03**
GOTERM_BP_DIRECT	malate metabolic process, oxidation-reduction process,
GOTERM_CC_DIRECT	integral component of membrane,
GOTERM_MF_DIRECT	malate dehydrogenase (decarboxylating) (NAD+) activity, metal ion binding, NAD binding,
KEGG_PATHWAY	Pyruvate metabolism, Metabolic pathways, Carbon metabolism

FBGN0029153	**Malic enzyme like-2(Menl-2)**
DmHDAC4^{WT}* vs *3A	**Log_2 Fold Change: -6.760, Adjusted *p*-value: 2.73E-07**
DmHDAC4^{WT}* vs *dANK	**Log_2 Fold Change: -5.623, Adjusted *p*-value: 1.87E-05**
DmHDAC4^{WT}* vs *Y1142H	**Log_2 Fold Change: -4.219, Adjusted *p*-value: 1.22E-05**
GOTERM_BP_DIRECT	malate metabolic process, oxidation-reduction process,
GOTERM_MF_DIRECT	malate dehydrogenase (decarboxylating) (NAD+) activity, malate dehydrogenase (decarboxylating) (NADP+) activity, oxaloacetate decarboxylase activity, malate dehydrogenase (NADP+) activity, metal ion binding, NAD binding,
KEGG_PATHWAY	Pyruvate metabolism, Metabolic pathways, Carbon metabolism,

Supplementary Table 9.16: List of 10 differentially expressed genes from annotated cluster showing pyruvate metabolism and malate metabolic processes

#	Nomenclature	Chromosomal location	Genotype	Description / Source
1	*w(CS10)*		w[CS10]; +; +; +	Canton-S wild type / Ron Davis*

2	*HDAC4::GFP*	1st	y[1] w[*], P{w[+mC]=PTT-GA}HDAC4[CA07134]; +; +; +	GFP tagged HDAC4 / BDSC
3	*elavGAL4*	1st	w[CS10], P{w[+mW.hs]=GawBelav[C155]; +; +; +	Pan-neuronal GAL4 / BDSC
4	*elavGAL4, HDAC4::YFP*	1st	w[CS10], P{w[+mW.hs]=GawB}elav[C155], CPTI-000077 YFP tagged HDAC4 at 13174889 (intron); +; +; +	#3 recombined with YFP tagged HDAC4 / Helen Fitzsimons
5	*GMR-GAL4*	2nd	w[*]; P{w[+mC]=GAL4-ninaE.GMR}12; +; +	Eye-specific GAL4 / BDSC
6	*UAS-GFP*	2nd	w*; P{w+mC=UAS-2xEGFP}AH2; +; +	UAS driven GFP / BDSC
7	*UAS-HDAC4 RNAi(shRNA)*	2nd	w[1118]; P{VDRCsh330055}attP40; +; +	UAS driven HDAC4 RNAi (shRNA) / VDRC
8	*UAS-HDAC4 RNAi(dsRNA)*	3rd	w[CS10]; +; P{GD9446}v20522; +	UAS driven HDAC4 RNAi (dsRNA) / VDRC
9	*UAS-Nslmb-vhhGFP4(2)* OR *Nslmb-vhhGFP4(2)* OR *deGradFP(2)*	2nd	y[1] w[*]; P{w[+mC]=UAS-Nslmb-vhhGFP4}2; +; +	UAS driven GFP targeted protein ligase (deGradFP transgene on 2nd)/ BDSC
10	*UAS-Nslmb-vhhGFP4(3)* OR *Nslmb-vhhGFP4(3)* OR *deGradFP(3)*	3rd	w[*]; +; P{w[+mC]=UAS-Nslmb-vhhGFP4}3; +	UAS driven GFP targeted protein ligase (deGradFP transgene on 3rd)/ BDSC
11	*UAS-DmHDAC4^{WT}-myc* OR *DmHDAC4^{WT}*	3rd	w[CS10]; +; P{y[+t7.7]=CaryP}attP2, UAS-DmHDAC4(WT)-myc; +	UAS driven wild type DmHDAC4 / this study

12	*UAS-DmHDAC4-dNLS-myc* OR *dNLS*	3rd	w[CS10]; +; P{y[+t7.7]=CaryP}attP2, UAS-DmHDAC4-dNLS-myc; +	UAS driven cytoplasmic-restricted DmHDAC4 / this study
13	*UAS-DmHDAC4-3A-myc* OR *3A*	3rd	w[CS10]; +; P{y[+t7.7]=CaryP}attP2, UAS-DmHDAC4-3A-myc; +	UAS driven nuclear-restricted DmHDAC4 / this study
14	*UAS-DmHDAC4-Y1142H-myc* OR *Y1142H*	3rd	w[CS10]; +; P{y[+t7.7]=CaryP}attP2, UAS-DmHDAC4-Y1142H-myc; +	UAS driven catalytically inactive DmHDAC4 / this study
15	*UAS-DmHDAC4-dMEF2-myc* OR *dMEF2*	3rd	w[CS10]; +; P{y[+t7.7]=CaryP}attP2, UAS-DmHDAC4-dMEF2-myc; +	UAS driven MEF2-binding mutant DmHDAC4 / this study
16	*UAS-DmHDAC4-dANK-myc* OR *dANK*	3rd	w[CS10]; +; P{y[+t7.7]=CaryP}attP2, UAS-DmHDAC4-dANK)-myc; +	UAS driven ankyrin-binding mutant DmHDAC4 / this study
17	*UAS-DmHDAC4^{WT}-myc, UAS-HDAC4 RNAi(dsRNA)*	3rd	w[CS10]; +; P{y[+t7.7]=CaryP}attP2, UAS-DmHDAC4(WT)-myc, P{GD9446}v20522; +	#11 recombined with #8 on 3rd chromosome / Helen Fitzsimons
18	*UAS-DmHDAC-3A-myc, UAS-HDAC4 RNAi(dsRNA)*	3rd	w[CS10]; +; P{y[+t7.7]=CaryP}attP2, UAS-DmHDAC4-3A-myc, P{GD9446}v20522/TM3, Sb; +	#12 recombined with #8 on 3rd chromosome / Helen Fitzsimons
19	*UAS-DmHDAC-dNLS-myc, UAS-HDAC4 RNAi(dsRNA)*	3rd	w[CS10]; +; P{y[+t7.7]=CaryP}attP2, UAS-DmHDAC4-dNLS-myc, P{GD9446}v20522; +	#13 recombined with #8 on 3rd chromosome / Helen Fitzsimons
20	*UAS-DmHDAC-dMEF2-myc, UAS-HDAC4 RNAi(dsRNA)*	3rd	w[CS10]; +; P{y[+t7.7]=CaryP}attP2, UAS-DmHDAC4-dMEF2-myc, P{GD9446}v20522/TM3, Sb; +	#14 recombined with #8 on 3rd chromosome / Helen Fitzsimons
21	*UAS-DmHDAC-Y1142H-myc,*	3rd	w[CS10]; +; P{y[+t7.7]=CaryP}attP2,	#15 recombined with #8 on 3rd chromosome / Helen Fitzsimons

	UAS-HDAC4 RNAi(dsRNA)		UAS-DmHDAC4-Y1142H-myc, P{GD9446}v20522; +	
22	*UAS-DmHDAC-dANK-myc, UAS-HDAC4 RNAi(dsRNA)*	3rd	w[CS10]; +; P{y[+t7.7]=CaryP}attP2, UAS-DmHDAC4-dANK)-myc, P{GD9446}v20522; +	#16 recombined with #8 on 3rd chromosome / Helen Fitzsimons
23	*elavGAL4;tubGAL80^{ts}*	1st; 2nd	w[CS10], P{w[+mW.hs]=GawB}sdelav[C155]; P{w+mC=tubP-GAL80ts}10; +; +	#3 with tubulin driven temperature sensitive GAL80 (TARGET) / Helen Fitzsimons
24	*OK107GAL4;tubGAL80^{ts}*	4th; 2nd	w(CS10); P{w+mC=tubP-GAL80^{ts}}10; +; P{w+mW.hs=GawB}OK107	Pan-MB GAL4 with tubulin driven temperature sensitive GAL80 (TARGET) / Helen Fitzsimons
25	*α/β lobes Split GAL4* OR *α/β Split GAL4*	2nd; 3rd	w[1118]; P{y[+t7.7] w[+mC]=R13F02-p65.AD}attP40; P{y[+t7.7] w[+mC]=R44E04-GAL4.DBD}attP2; +	α/β lobes-specific MB GAL4 / BDSC
26	*γ lobes Split GAL4* OR *γ Split GAL4*	2nd; 3rd	w[1118]; P{y[+t7.7] w[+mC]=R13F02-p65.AD}attP40/CyO; P{y[+t7.7] w[+mC]=R45H04-GAL4.DBD}attP2; +	γ lobes-specific MB GAL4 / BDSC
27	*α'/β' lobes Spilt GAL4* OR *α'/β' Spilt GAL4*	2nd; 3rd	w[1118]; P{y[+t7.7] w[+mC]=R13F02-p65.AD}attP40/CyO; P{y[+t7.7] w[+mC]=R34A03-GAL4.DBD}attP2; +	α'/β' lobes-specific MB GAL4 / BDSC
28	*Balancer*	2nd; 3rd	w[1118]/Dp(1;Y)y[+]; CyO/Bl[1]; TM2/TM6B, Tb[1]	Balancer chromosomes on 2nd and 3rd chromosome / BDSC
29	*UAS- DmHDAC4-dNLS_dMEF2-myc* OR *dNLS_dMEF2*	3rd	y[1] w[67c23]; +; P{y[+t7.7]=CaryP}attP2, UAS-DmHDAC4-dNLS-dMEF2-myc. Insert into P2:(3L) 68A4; +	UAS driven DmHDAC4 with cytoplasmic-restricted and MEF2-binding mutations / this study
30	*UAS- DmHDAC4-3A_dMEF2-myc* OR *3A_dMEF2*	3rd	y[1] w[67c23]; +; P{y[+t7.7]=CaryP}attP2, UAS-DmHDAC4-3A-dMEF2-myc. Insert into P2:(3L) 68A4; +	UAS driven DmHDAC4 with nuclear-restricted and MEF2-binding mutations / this study

31	*UAS- DmHDAC4-dANK_dMEF2-myc* OR *dANK_dMEF2*	3rd	y[1] w[67c23]; +; P{y[+t7.7]=CaryP}attP2, UAS-DmHDAC4-dAnk-dMEF2-myc. Insert into P2:(3L) 68A4; +	UAS driven DmHDAC4 with ankyrin-binding and MEF2-binding mutation / this study
32	*UAS-DmMEF2-T148A-HA* OR *T148A*	2nd	w[1118]; PBac{y+-attP-3B}VK22, UAS-DmMEF2-T148A-HA. Insert into VK22(2R) 57F5; +; +	UAS driven DmMEF2 with T148A mutation / this study
33	*UAS Pepck RNAi #1* OR *Pepck2 RNAi #1*	2nd	w1118; P{GD5767} +; +	UAS driven Pepck2 RNAi / VDRC
34	*UAS Pepck RNAi #2* OR *Pepck2 RNAi #2*	2nd	w1118; P{KK103240}VIE-260B; +; +	UAS driven Pepck2 RNAi / VDRC
35	*UAS tobi RNAi #1* OR *tobi RNAi #1*	3rd	w1118; +; P{GD6263}v14734; +	UAS driven tobi RNAi / VDRC
36	*UAS tobi RNAi #2* OR *tobi RNAi #2*	2nd	w1118; P{KK100897}VIE-260B; +; +	UAS driven tobi RNAi / VDRC
37	*UAS Teq RNAi* OR *Teq RNAi*	2nd	w1118; P{GD4757}v45232; +; +	UAS driven Teq RNAi / VDRC
38	*UAS nebula RNAi* OR *nebula RNAi*	3rd	y[1] v[1]; +; P{y[+t7.7] v[+t1.8]=TRiP.JF02557}attP2; +	UAS driven nebula RNAi / BDSC
39	*Rh-Marf RNAi*	3rd	w*; +; P{ninaE-Marf-GD11094}3; +	Marf RNAi driven by rhodopsin promoter / BDSC

Supplementary Table 9.17: List of *Drosophila* transgenic lines used in experimental crosses

Bloomington *Drosophila* Stock Center (BDSC). Vienna *Drosophila* Resource Center (VDRC). (;) denotes separation of the chromosome between each transgene. (/) denotes the separation of the two alleles within the chromosome. (*) Ron Davis, Scripps Institute, Jupiter, FL, USA.

9.6 Explanation of COVID-19 Impacts DRC Form

MASSEY UNIVERSITY
TE KUNENGA KI PŪREHUROA
UNIVERSITY OF NEW ZEALAND

GRADUATE RESEARCH SCHOOL

Note for Examiners of Doctoral Theses
Explanation of COVID-19 Impacts

The Doctoral Research Committee recognises the impacts of Covid-19 on research, particularly for doctoral candidates, and we appreciate the efforts made by supervisors and candidates to ensure timely completion of the doctoral thesis. We know that in some cases this has meant the project has needed to be changed in some way, including its final presentation. For students whose work has been impacted, we invite supervisors to provide a note for examiners explaining the circumstances.

Instructions for Supervisors:

The note is designed to enable you to communicate to examiners your desire for them to take account of certain factors in their assessment of a thesis to address delays and disruptions experienced by a thesis student as a result of the Covid-19 pandemic.

The attached form should be used to provide **an explanation** to the examiners on what to consider in their evaluation. It should detail how the project was altered or how the final product of the thesis has been affected as a result of the disruption. Statements should be clear and succinct for the benefit of the examiners and in fairness to the student and others in the student cohort.

The form should be signed by the student, the supervisor and the Head of Academic Unit, or nominee, and included in the information that is sent out with the thesis.

For doctoral candidates, the completed form should be inserted into the front of the thesis before the abstract by the candidate when submitting their digital thesis for examination in the Student Portal. At the completion of the examination, the amended form which excludes any confidential comments to the examiners, should be included in the appendices.

Please be sure to indicate whether a student has received a suspension of studies due to Covid-19 and/or an extension, as it is important to note if students have already had some special consideration.

Approved by DRC 10/Feb/2021
DRC 21/02/03

MASSEY UNIVERSITY
TE KUNENGA KI PŪREHUROA
UNIVERSITY OF NEW ZEALAND

GRADUATE RESEARCH SCHOOL

Note for Examiners
Explanation of COVID-19 Impacts

Thank you for taking the time to examine this thesis, which has been undertaken during the Covid-19 pandemic. The New Zealand Government's response to Covid-19 includes a system of Alert Levels which have impacted upon researchers. Our University's pandemic plan applied the Government's expectations to our research environment to ensure the health and safety of our researchers, however, research was impacted by restrictions and disruptions, as outlined below.

For a six-week period from March 26 to April 27 2020, New Zealand was placed under very strict lockdown conditions (Level 4 – Lockdown), with students and staff unable to physically access University facilities, unless they were involved in essential research related to Covid-19. All field work ceased and data collection with humans was restricted to online methods, if appropriate. The restrictions were partially lifted on April 27, but students and staff were not generally allowed back into University facilities until May 13.

Ongoing disruptions have also been encountered for some students due to uncertainties over the potential for future Covid-19-related restrictions on activities, and a Covid-19 cluster outbreak based in Auckland in New Zealand on 12 August 2020 led to the imposition of rolling Level 2 (Reduce) and Level 3 (Restrict) conditions until 23 September 2020. Auckland campus based students remained on Level 2 until 7 October 2020. This Alert Level system continues to be utilised throughout 2021.

These changing Alert Levels have meant that some research students had experimental, clinical, laboratory, field work, and/or data collection or analysis interrupted, and consequently may have had to adjust their research plans. For some students, the impacts of Covid-19 stretched far beyond the lockdown period in April/May 2020, as they may have had to significantly revise their research plans.

Overseas travel is not permitted by the University and restrictions have been placed on the New Zealand borders which are closed to non-New Zealand citizens and permanent residents. This meant that international students who were based offshore at the time of lockdown, were unable to return to New Zealand. A small number of offshore students were provided permission to return to New Zealand in early 2021. Many students have also suffered from anxiety and stress-related issues, and have had financial impacts, meaning their research progress has been significantly delayed.

This form, as completed by the supervisor and student, outlines the extent that the research has been affected by Covid-19 conditions.

Approved by DRC 10/Feb/2021
DRC 21/02/03

Please consider the factors listed below in your assessment of the work.

This statement has been prepared by the candidate's supervisor in consultation with the student and has been endorsed by the relevant Head of Academic Unit.

Student Name:	Wei Jun Tan	ID Number:	18041825
Supervisor Name:	Helen Fitzsimons	Date:	21-Feb-22
Thesis title:	Investigating the role of HDAC4 in Drosophila neuronal function		

Considerations to be taken into account. Note: This statement will remain in the final copy of the thesis which will be available from the Massey University Library following the examination process.
[*Enter key considerations here for the examiners. This can include but is not limited to change of scope, scale, topic, focus; limitations in relation to data collection, access to necessary literature or archival materials, laboratories, field sites; disruptions as a result of lockdown and various alert levels, medical or health considerations etc*]

Wei was unable to enter the laboratory for two periods of approximately seven weeks in 2020 and three weeks in 2021, as outlined above. The ramifications of the university closures were not limited to the periods stated as all fly crosses generated prior to lockdown had to be abandoned and recommenced upon the university reopening, which led to a further delay of approximately eight weeks. This included balancing of the deGradFP lines over several generations, and expansion and crosses of fly stocks for the RNA-sequencing, which required RNA isolation from eight genotypes in quadruplicate.

Additionally, overseas courier services and supply chains were also impacted, which led to delayed delivery of reagents and transgenic lines. Some of the fly lines did not survive the extended period of transit and had to be reordered. As a consequence, due to time constraints, parts of some of the objectives were unable to be completed. This included:

Objective 1: Memory assessment using the courtship suppression assay was not carried out and RT-qPCR has not yet been performed to estimate the level of knockdown following deGradFP-mediated RNAi knockdown of HDAC4.

Objective 3: The delays to RNA-seq and delivery of the RNAi lines for this objective prevented more extensive analysis of the phenotypes resulting from knockdown of FasII, tequila and Pepck2, and RT-qPCR has not yet been carried out to confirm efficient knockdown.

Approved by DRC 10/Feb/2021
DRC 21/02/03

Confidential for Examiners Only: [*Please enter any other considerations which are confidential for examiners only and should not be placed in the final thesis version submitted to Library following the examination process]*

Signed, confirming this is a fair reflection of the impact of Covid-19 on this research.

Student	Wei Jun Tan	Digitally signed by Wei Jun Tan Date: 2022.02.21 13:00:54 +13'00'
Supervisor	Fitzsimons, Helen	Digitally signed by Fitzsimons, Helen Date: 2022.02.22 13:53:54 +13'00'
Head of Academic Unit (or nominee)	Catherine Whitby	Digitally signed by Catherine Whitby DN: cn=Catherine Whitby, c=NZ, o=Massey University, ou=School of Natural Sciences, email=c.p.whitby@massey.ac.nz Date: 2022.02.22 14:05:45 +13'00'

Approved by DRC 10/Feb/2021
DRC 21/02/03